

**Novel Expanded Porphyrin analogues: Syntheses,
conformation, aromaticity and Structural diversity.**

By
ARINDAM GHOSH
CHEM 11201204003

**National Institute of Science Education and Research,
Bhubaneswar, Odisha**

*A thesis submitted to the
Board of Studies in Chemical Sciences
In partial fulfillment of requirements
for the Degree of*

DOCTOR OF PHILOSOPHY
of
HOMI BHABHA NATIONAL INSTITUTE

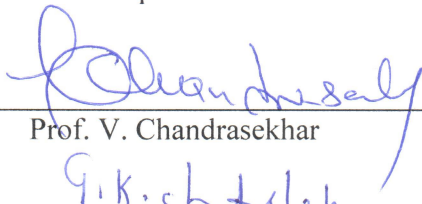
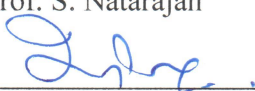
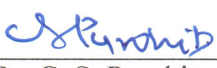


January, 2018

Homi Bhabha National Institute¹

Recommendations of the Viva Voce Committee

As members of the Viva Voce Committee, we certify that we have read the dissertation prepared by **Arindam Ghosh** "Novel Expanded Porphyrin analogues: Syntheses, conformation, aromaticity and Structural diversity" and recommend that it may be accepted as fulfilling the thesis requirement for the award of Degree of Doctor of Philosophy.

Chairman –	 Prof. V. Chandrasekhar	25/1/18 Date:
Guide-	 Prof. T. K. Chandrashekar	25/1/18 Date:
Co-guide –	 Prof. A. Srinivasan	25.1.18 Date:
External Member-	 Prof. S. Natarajan	25/1/18 Date:
Member 1-	 Dr. J. N. Behera	25/1/18 Date:
Member 2-	 Dr. C. S. Purohit	Date: 25/1/18
Member 3-	 Dr. P. V. Alone	25/1/2018 Date:

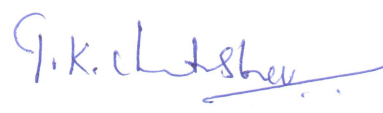
We hereby certify that we have read this thesis prepared under our direction and recommend that it may be accepted as fulfilling the thesis requirement.

Date: 25/01/18

Place: Satni


(Prof. A. Srinivasan)

Co-guide


(Prof. T. K. Chandrashekar)

Guide

STATEMENT BY AUTHOR

This dissertation has been submitted in partial fulfillment of requirements for an advanced degree at Homi Bhabha National Institute (HBNI) and is deposited in the Library to be made available to borrowers under rules of the HBNI.

Brief quotations from this dissertation are allowable without special permission, provided that accurate acknowledgement of source is made. Requests for permission for extended quotation from or reproduction of this manuscript in whole or in part may be granted by the Competent Authority of HBNI when in his or her judgment the proposed use of the material is in the interests of scholarship. In all other instances, however, permission must be obtained from the author.

Arindam Ghosh

DECLARATION

I, hereby declare that the investigation presented in the thesis has been carried out by me.
The work is original and has not been submitted earlier as a whole or in part for a degree
/ diploma at this or any other Institution / University.

Arindam Ghosh

List of Publications arising from the thesis

a. Published

- *1. **Arindam Ghosh**, Arvind Chaudhary, A. Srinivasan, C. H. Suresh and T. K. Chandrashekar "[32] π Fused Core-Modified Heptaphyrin with Möbius Aromaticity", *Chem. Eur. J.* **2016**, *22*, 3942-3946.
- *2. **Arindam Ghosh**, A. Srinivasan, C. H. Suresh, T. K. Chandrashekar "[40] π Fused and non-fused Core-modified nonaphyrins: Syntheses and structural Diversity", *Chem.Eur.J.* **2016**, *22*, 11152-11155.
3. Ganesan Karthik, W.-Y. Cha, **Arindam Ghosh**, T. Kim, A. Srinivasan, D. Kim, T. K. Chandrashekar. "Phenylene-Bridged Core-modified Planer Aromatic Octaphyrin: Aromaticity, Photophysical and Anion receptor properties", *Chem. Asian. J.* **2016**, *11*, 1447-1453.
- *4. W.-Y. Cha, T. Kim, **Aindam Ghosh**, Z. Zhang, V. M. Lynch, W. Kim, S. Lee, R. Ali, J. Jung, S. Fukuzumi, J. Park, J. L. Sessler, T. K. Chandrashekar, D. Kim. "Bicyclic Baird-type Aromaticity", *Nat. Chem.* **2017**, *9*, 1243-1248.

b. Communicated:

- *1. **Arindam Ghosh**, A. Srinivasan and T. K. Chandrashekar. "Octaphyrin with dual Conformers. (Communicated).

c. Manuscript under preparation:

- *1. **Arindam Ghosh**, A. Srinivasan and T. K. Chandrashekar. "Newly Synthesized [2.1.1.1.1] Pentaphyrin and [2.1.1.0.1.1] Hexaphyrin: with structural diversity", (Manuscript under preparation).

-
- *2. **Arindam Ghosh**, A. Srinivasan and T. K. Chandrashekar. "Highly planer [34] π Octaphyrin and its binding towards metal ion. ", (Manuscript under preparation).

* Pertaining to this thesis

Arindam Ghosh

Conferences

1. Applications in Materials and Catalysis, February 24-26th, 2014 organized at School of Chemical Sciences, NISER, Bhubaneswar.
2. “[32] π Fused Core-Modified Heptaphyrin with Möbius Aromaticity”- Arindam Ghosh, A. Srinivasan, T. K. Chandrashekar* in International Symposium on Modern Trends in Inorganic Chemistry-XVI (MTIC-XVI), December 3-5th, 2015 Organized by Department of Chemistry, Jadavpur University, Jadavpur, Kolkata. (**Poster Presentation**).
3. “[40] π Fused Core-Modified Nonaphyrin: Synthesis and structural diversity.”- Arindam Ghosh, A. Srinivasan, T. K. Chandrashekar* in 5th Symposium on Advance Biological Inorganic Chemistry (SABIC-2017), January 7-11th 2017 Organized by Tata Institute of Fundamental Research at Kolkata. (**Poster Presentation**).
4. “**Core-Modified Octaphyrin with dual conformation.**”- Arindam Ghosh in Inter-IISER Chemistry Meet 2017 (ICM-2017), January 20-22th 2017 Organized by IISER Bhopal. (**Oral Presentation**)

Arindam Ghosh

Dedicated to....

My Parents

&

Mrs. Asha Chandrashekar

ACKNOWLEDGEMENTS

First of all, “Thanks to Almighty”. The Goddess “**Durga**” for her blessing and giving me strength to complete the Doctoral degree.

I would like to express my gratitude to my thesis supervisor **Prof. T. K. Chandrashekar** for his valuable guidance, constant support, motivation and giving me freedom to think.

I am also indebted to madam (**Mrs. Asha Chandrashekar**) for her care.

It gives an immense pleasure to work with **Prof. A. Srinivasan**, my thesis co-supervisor.

I wish to express my gratitude for his unforgettable guidance, constant support and valuable suggestions throughout my PhD. This work might not have been possible without his encouragement. I also express my sincere thanks to madam (**Mrs. Meenapriya Srinivasan**).

I would like to express my gratefulness to **Prof. V. Chandrasekhar**, former Director of NISER and my thesis chairman for providing me infrastructure and all facilities in the laboratory which helps me to complete my research work without any obstacle.

I would like to thank the doctoral committee members, **Dr. J. N. Behera**, **Dr. C. S. Purohit** and all other faculty in School of Chemical Sciences, NISER for their valuable suggestions and useful discussions.

I am very much thankful to **Dr. S. Peruncheralathan**, **Dr. V. Krishnan** and **Dr. Arun Kumar** for their help at various levels of my research career.

My sincere thanks to my collaborator **Dr. C. H. Suresh**, NIIST, Trivandrum for his contributions towards theoretical studies described in the thesis.

I wish to express my gratitude to **Prof. Dongho Kim** and his group members, **Won-Young Cha** and **Taeyeon Kim**, Yonsei University, Korea for photophysical and theoretical studies described in the thesis.

*My sincere thanks to the technical staff, **Mr. Dipak, Mr. Sanjaya, Mr. Amit and Mr. Rajkumar** for collecting single crystal X-ray data, recording NMR and Mass analysis.*

*My special thanks to **Dr. Nemaï Tiwari** (Katwa College) for inspiring me towards Organic Synthesis.*

*I would like to thank my seniors, **Dr. G. Karthik and Dr. Arvind Chaudhury** for their help at my early career of research and my junior **Ms. Syamasrit Dash** for her support in various stages of my research work.*

*I would like to thank my present lab members **Dr. M. Murugavel. Dr. Narasingha Rao,** juniors (**Mainak, Sangya, Subhashree and Mahaprasad**) and past lab members (**Rishabh, Gourav, Khushboo and Prerna**), for providing a friendly environment throughout my research career.*

*I also thank some of my special friends, **Dr. Adinarayana B, Manas, Tanmay, Sourav, Pankaj** (NISER), **Abhijit** (Visva-Bharati) and **Debnath** (ISM Dhanbad) for their help and constant support and useful discussions.*

*Last but foremost, I wish to express my thankfulness to **Maa, Baba, Bhai (Achin)** for their sacrifice and constant support. They always stood behind me and supported me to reach this level. I express the deepest respect to my grandparents (**Late Bhrishnupada Ghosh and Late Yosodabala Ghosh**) who's blessing always gave me mental and moral support throughout my career.*

Arindam Ghosh

CONTENTS

	Page No.
Synopsis	xii-xxiii
List of Tables	xxv
List of Schemes	xxvi-xxvii
List of Figures	xxviii-xxxiv
List of Abbreviations	xxxv-xxxvi
Chapter 1	3-35
Chapter 2	37-58
Chapter 3	61-92
Chapter 4	95-129
Chapter 5	133-180
Chapter 6	183-214
Summary	215

SYNOPSIS

A porphyrin skeleton which nature has chosen for diverse biological functions is a simple cyclic tetrapyrrolic macrocycle containing four methine bridges. It is a 18π conjugated system which has a rich electronic spectra in the visible region. Taking clue from nature, synthetic chemists have modified porphyrin skeleton in different ways to create new macrocyclic systems with altered electronic structure. The modification include; (a) expansion of ring, (b) contraction of ring, (c) isomer formation by changing links and (d) core-modification by replacing one or two pyrrole rings by other heterocyclic rings such as thiophene, selenophene and tellurophene. ^[1-3] (**Chart-1**).

In this thesis, an attempt has been made to synthesise a range of core-modified expanded porphyrins, from pentaphyrins to nonaphyrins and their properties in terms of conformational changes,⁴ structural diversity,⁵ Hückel-Möbius aromatic switch⁶ over and electronic structure have been probed to understand the optical, electrochemical, photochemical and excited state properties.

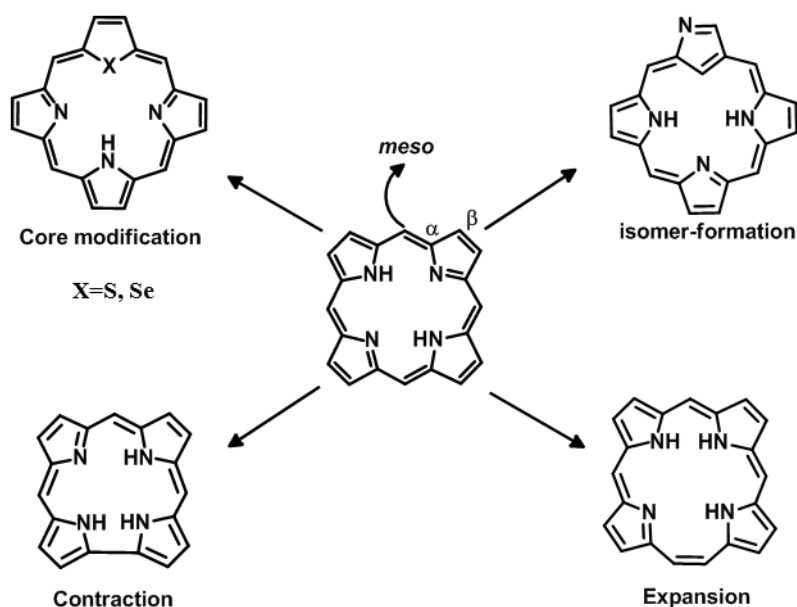


Chart-1: Porphyrin modifications.

Organization of the thesis:

This thesis is mainly divided into five chapters and a brief description of each chapter is given below:

Chapter 1: General introduction.

Chapter 2: General experimental methods.

Chapter 3: Core-modified Pentaphyrin and Hexaphyrins: Syntheses and structural diversity.

Chapter 4: Core-modified $[4n]\pi$ Heptaphyrins: Möbius aromaticity in freebase and protonated state.

Chapter 5: Core-modified $[4n+2]\pi$ Octaphyrins: Structural diversity & 3-dimensional aromaticity.

Chapter 6: Core-modified $[4n]\pi$ Nonaphyrins: Transformation from figure-eight to open conformation.

Chapter 1: General introduction

This chapter describes a general introduction to expanded porphyrins. Sapphyrin first invented by Woodard and co-workers in 1966 laid the foundation for expanded porphyrin chemistry.⁷ Later effort by E. Vogel's group and Sessler's group were successful in synthesizing range of expanded porphyrins such as 22π sapphyrin, 26π rubyirin, 24π rosarian, 28π heptaphyrin, 30π octaphyrin, 40π turcasarin by developing simple and efficient methodology.⁸ Later on the research groups of Latos-Grażyński in Poland and Osuka in Japan reported not only synthesis of various expanded porphyrin containing different number of π electrons but also exploited their properties in terms of Hückel-Möbius aromaticity,⁹ structural diversity¹⁰ and optical properties. Efforts from our laboratory mainly concentrated on core-modified expanded porphyrins and we were successful in synthesizing a 34π planar octaphyrin which exhibit large aromaticity.¹¹

Chapter 2: General experimental methods:

This chapter mainly describe the syntheses procedure of desire precursors and their spectral characterizations (NMR spectroscopy). We introduce DTT as fused and electron rich precursor to synthesize fused and bridged expanded porphyrin. We also introduce non-fused derivative such as bithiophene and terthiophene to compare the stability between fused and non-fused derivatives. We also introduce 1,2-dithienyl ethene to make the macrocycle more flexible.

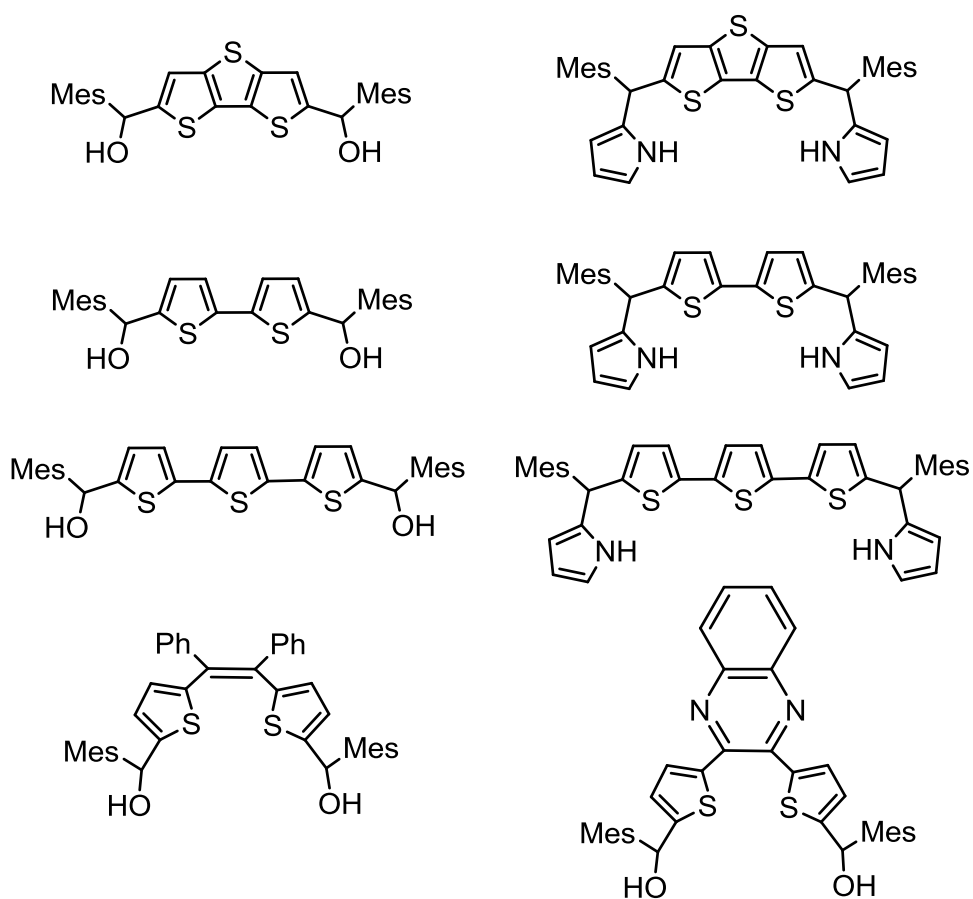
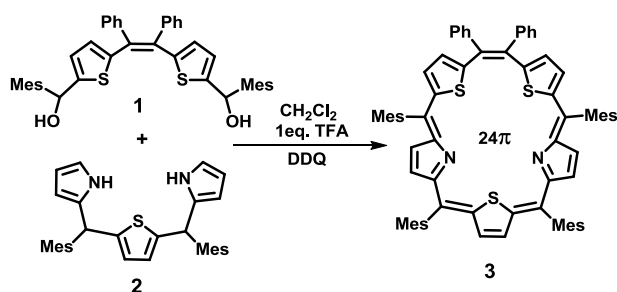


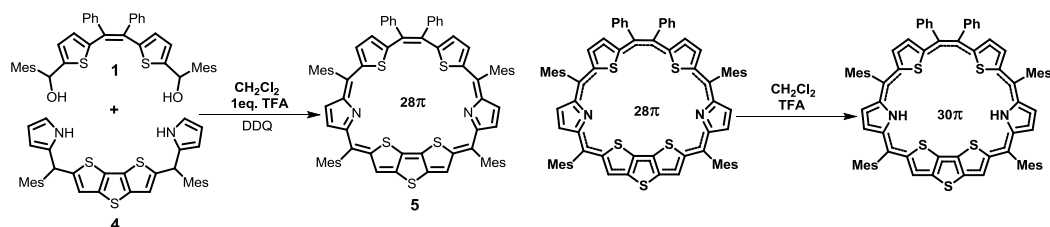
Chart-2: List of precursors

Chapter 3: Core-modified Porphyrin and Hexaphyrin: Syntheses and structural diversity.

In this chapter we report syntheses of expanded porphyrins containing five and six heterocyclic rings (pentaphyrin and Hexaphyrin respectively). A normal pentaphyrin macrocycle is reported to be an unstable and not amenable for evaluation of properties and structure. Osuka and co-workers used fusion approach to synthesize stable pentaphyrins.¹² In this chapter we were successful in synthesizing a pentaphyrin with [2,1,1,1,1] *meso* link and Hexaphyrin with [2,1,1,0,1,1] *meso* link. We followed simple acid catalysed condensation of tripyrrane (**2**) and diol (**1**) to get desired pentaphyrin (**3**) in 7% yield. [Scheme-1]. On the otherhand Hexaphyrin (**5**) was synthesized by using condensation reaction of fused tetrapyrane (**4**) with diol (**1**) followed by DDQ oxidation in 7% yield. [Scheme-2]. Both **3** and **5** have been well characterized by ESI mass spectrometry, UV-VIS absorption and ¹H and 2D NMR spectroscopy.



Scheme 1: Synthesis of Pentaphyrin



Scheme 2: Synthesis of Hexaphyrin.

Scheme 3: Changing in conjugation after protonation is shown

UV-VIS spectrum of **3** in its freebase form exhibits a Soret band at 490 nm and Q band 698 nm. However upon protonation at nitrogen centre there is a large red shift of 100 nm in Soret band suggesting a change in the conformation upon protonation. This is supported by ^1H NMR spectroscopy where β -thiophene protons of central thiophene ring (**a** proton) is shielded by about 4ppm and imine hydrogen proton appears around 3ppm. [Figure-1]. These changes probably support the induction of Möbius aromatic character to the molecule upon protonation.

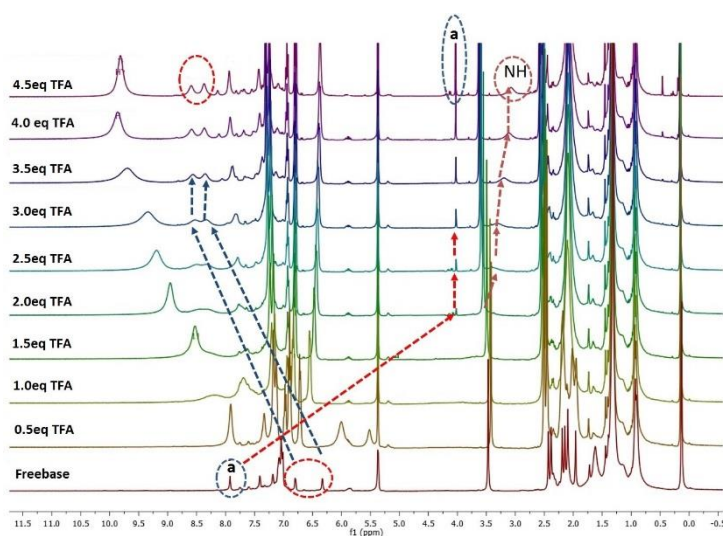
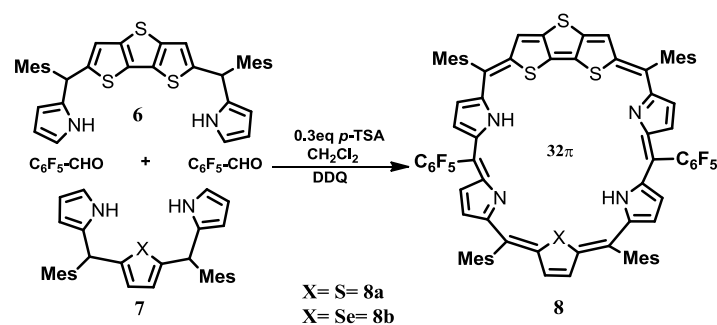


Figure-1: TFA titration ^1H NMR spectra of **3**.

On the other hand the Hexaphyrin (**5**) derivative which is 28π conjugated system in its freebase form changes the π -conjugation to a 30π system upon protonation and the protonated derivative exhibits Hückel aromatic character. [Scheme-3].

Chapter 4: Core-modified $4n\pi$ Heptaphyrins: Möbius aromaticity in freebase and protonated state.

In this chapter two different types of fused heptaphyrin (**8**) have been synthesized and characterized. [Scheme-4]. The fusion of the ring has been deliberately introduced only on one side of the macrocycle, while the opposite end remains flexible, thus allowing the twist to happen to attain Möbius aromaticity.



Scheme 4: Synthesis of fused Heptaphyrin.

Spectroscopic investigation (^1H NMR, UV-VIS spectroscopy) clearly indicates presence of Möbius aromatic character in both freebase and protonated state. For example, the methyl protons in *meso* mesityl unit resonate at -0.26ppm and -1.50ppm respectively for **8a** suggesting the methyl group is experiencing the ring current of the macrocycle. The X-ray structure of the freebase derivative clearly revealed the twisting expected for the molecule and the methyl group of the *meso* mesityl group is experiencing the ring current as revealed from ^1H NMR spectroscopy. [Figure-2]. The Nucleus Independent Chemical Shift (NICS) calculated for **8a** in freebase and protonated state are -8.1 and -9.9 ppm respectively clearly support the Möbius aromatic character.

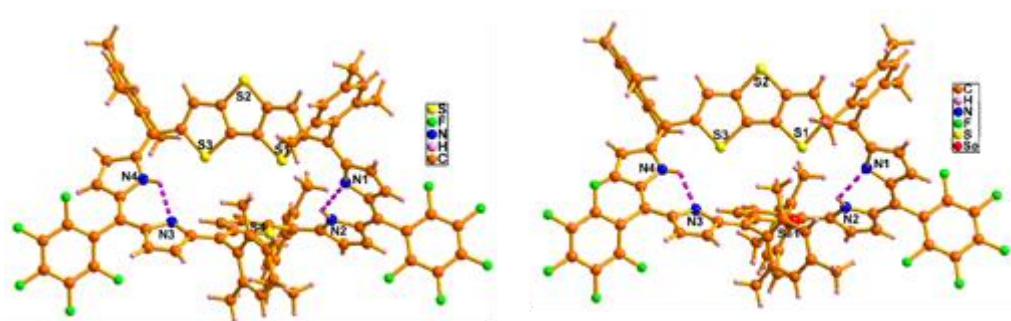


Figure 2: Structural characterization of both **8a** and **8b**.

Chapter 5: Core-modified $[4n+2]\pi$ octaphyrins: Structural diversity and 3-dimensional aromaticity.

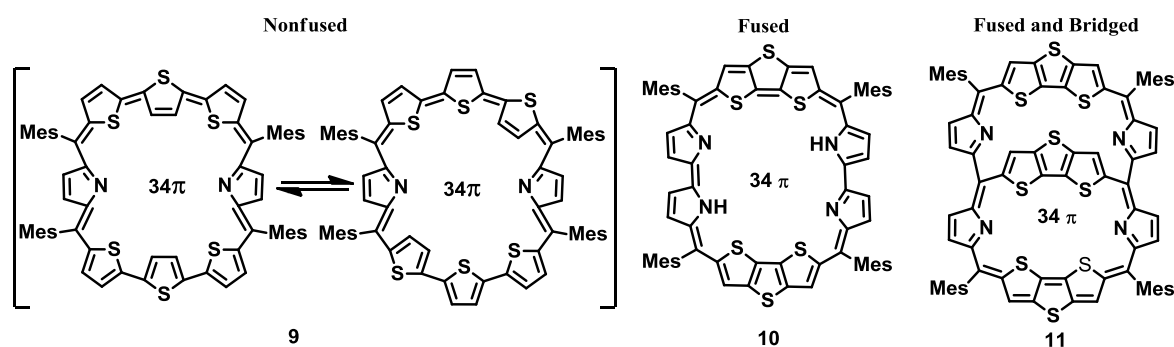


Chart-2: Three different 34π aromatic Octaphyrins synthesized.

In this chapter we have synthesized three different types of octaphyrins. In order to avoid figure-eight conformation, we have adopted; (i) reduction in the number of *meso* carbons with bulky meso substituents, (ii) fused approach and (iii) fused & bridging approach. In all the three cases, the expanded porphyrin skeleton adopt almost planar conformation, exhibiting aromaticity. The octaphyrin (**9**) exhibits two conformations, both in solution and solid state and the conformers differ with respect to ring inversion in the freebase form. To the best of our knowledge this is the first example of expanded porphyrin exhibiting two conformations in a single unit cell. **[Figure-3]**. However upon protonation only one conformation is stabilized.

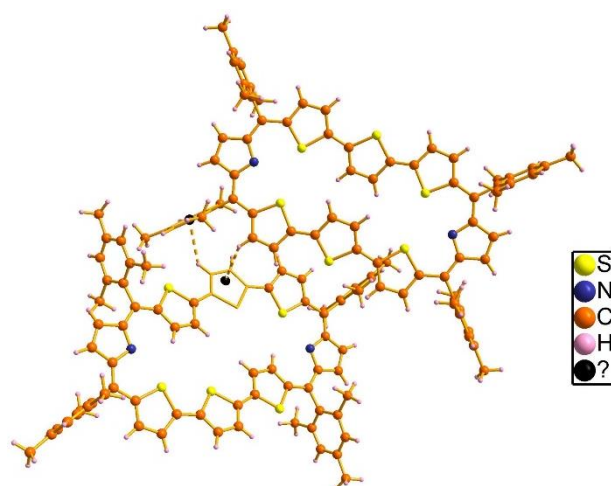


Figure 3: Single crystal X-ray structure of **9** showing two conformers.

The dithienothiophene (DTT) fused expanded octaphyrin (**10**) shows a very high degree of planarity and hence are aromatic. [Figure-4]. The existence of an imino and amino nitrogen in the skeleton allowed us to synthesize Rh(I) complex of the macrocycle.

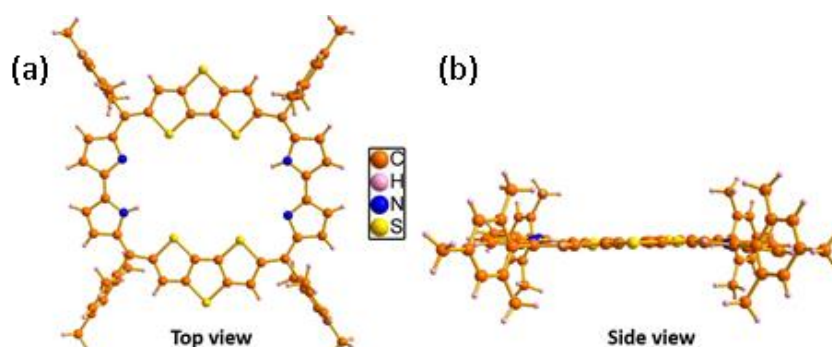


Figure 4: Structure of fused DTT octaphyrin **10**: (a) Top view, (b) Side view.

The fused and bridged octaphyrin (**11**) exhibit dual aromaticity (26π and 34π). The presence of dual aromaticity is confirmed by UV-VIS spectroscopy (two Soret bands) and ^1H NMR spectroscopy. The X-ray structure reveals almost planar porphyrin skeleton and inner bridged DTT unit is 22.73° tilted away from mean macrocyclic plane. [Figure-5]. This molecule contains 42π electron in conjugation and hence exhibits $[4n+2]\pi$ Hückel aromaticity.

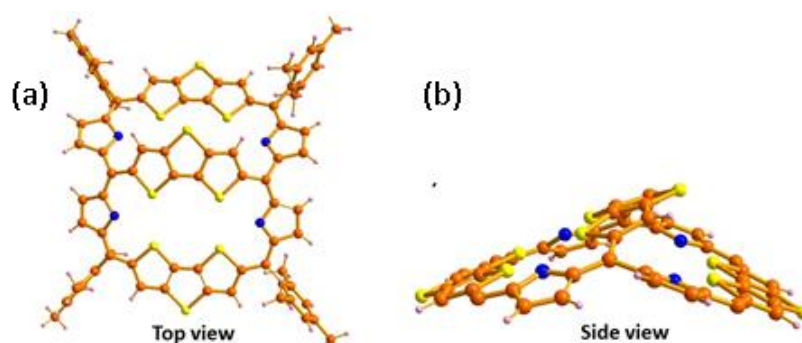


Figure 5: X-ray structure of **11**: (a) Top view & (b) Side view.

Excited state aromaticity:

According to **Baird's** prediction;

Aromatic molecules which have $[4n+2]\pi$ configuration in ground state are **anti-aromatic** in the lowest triplet excited state and **anti-aromatic** molecules which have $[4n]\pi$ configuration in ground state are **aromatic** in the lowest triplet excited state. This reversal of aromaticity upon going from ground state to excited triplet state was predicted by Baird in 1971.¹³

In order to test Baird's prediction, we used octaphyrin [**11**], which contains 42π electrons which exhibit Hückel aromaticity in ground state. Oxidation of this molecule by $2e^-$ will generate a 40π electronic system $[4n\pi]$, which according to Baird's rule should exhibit aromaticity in the lowest excited triplet state. We verified this by recording triplet state ESR spectra of the oxidised species of (**11**⁺⁺) [**Figure-6**] and evaluated the zero field splitting parameters D and E. The D and E values are 256G and 33G. Further support for the presence of aromaticity in the ground and excited state comes from; (a) NICS value calculation. (b) Anisotropy Induced Current Density (AICD) plot & (c) Harmonic Oscillator Model of Aromaticity (HOMA) value calculation. This is the second example in literature which verifies the Baird's prediction.

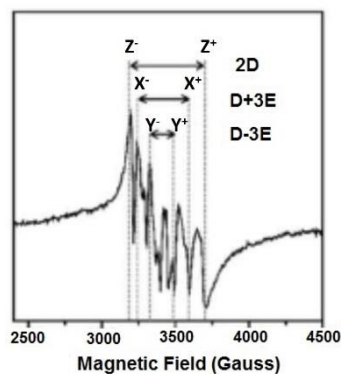
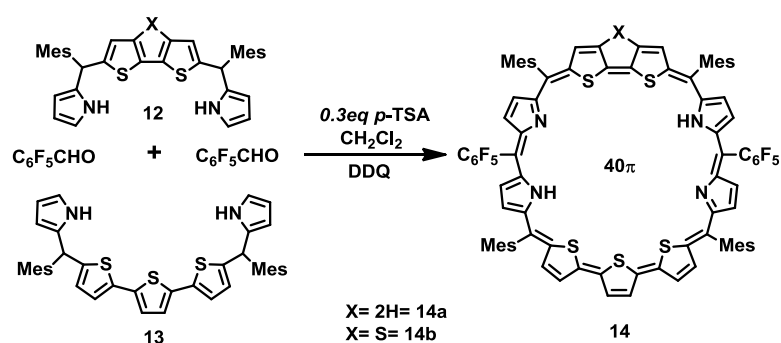


Figure-6: Triplet state EPR spectrum of **11**⁺⁺

Chapter 6: Core-modified [4n] π Nonaphyrins: Transformation from figure-eight to open conformation.

In this chapter we are discussing syntheses and structural diversity of next higher analogue, 40 π nonaphyrin (**14**). The synthetic strategy involve a [5+4] condensation reaction of appropriate precursors. Here also, we have adopted the fusion strategy at the one end of the molecule keeping other end flexible. [**Scheme-5**].



Scheme 5: Synthesis of non-fused and fused nonaphyrins **14**

14b have been characterized by both spectroscopic and single crystal X-ray structural analysis. Nonaphyrin exhibit a figure-eight conformation with non-aromatic character in its freebase form. However, upon protonation a major structural change happens, in which figure-eight structure is transformed into an open conformation triggered by formation of hydrogen bonds with TFA molecules. Such a structural change also induces ring inversions and the protonated state 1H NMR spectra reveals paratropic ring current. The inner and outer NH protons of the normal and inverted ring suggest the anti-aromatic nature of the macrocycle in the protonated state. [**Figure-7**].



Figure 7: Structure of **14b** in freebase and protonated state.

In summary, we have synthesized a range of core-modified expanded porphyrins and studied their properties in terms of their structural diversity, conformation and aromaticity both in ground and triplet excited states.

References:

1. Sessler, J. L.; Weghorn, S. J. *Expanded and Contracted and Isomeric Porphyrins*; Tetrahedron Organic Chemistry Series, Pergamon, New York, Vol. 15, **1997**.
2. Chandrashekar, T. K.; Venkataraman, V. *Acc. Chem. Res.* **2003**, *36*, 676-691.
3. Furuta, H.; Asano, T.; Ogawa, T. *J. Am. Chem. Soc.* **1994**, *116*, 767-768.
4. Karthik, G.; Lim, J. L.; Srinivasan, A.; Suresh, C. H.; Kim, D.; Chandrashekar, T. K. *Chem. Eur. J.* **2013**, *19*, 17011-17020.
5. Ghosh, A.; Srinivasan, A.; Suresh, C. H.; Chandrashekar, T. K. *Chem. Eur. J.* **2016**, *22*, 11152-11155.
6. Yoon, Z. S.; Osuka, A.; Kim, D. *Nat. Chem.* **2009**, *1*, 113-122.
7. Bauer, V. J.; Clive, D. R.; Dolphin, D.; Paine, J. B., III; Harris, F. L.; King, M. M.; Loder, J.; Wang, S.-W. C.; Woodward, R. B. *J. Am. Chem. Soc.* **1983**, *105*, 6429-6436

-
8. Kadish, K. M.; Smith, K.M.; Guillard, R. *The Porphyrin Handbook*; Academic Press, San Diego, CA, 2000.
 9. Stępień, M.; Latos-Grażyński, L.; Sprutta, N.; Chwalisz, P.; Szterenber, L. *Angew. Chem. Int. Ed.* **2007**, *46*, 7869-7873
 10. Saito, S.; Osuka, A. *Angew. Chem. Int. Ed.* **2011**, *50*, 4342-4373.
 11. Anand, V. G.; Pushpan, S. K.; Venkatraman, S.; Dey, A.; Chandrashekar, T. K.; Joshi, B. S.; Roy, R.; Teng, W.; Senge, K. R. *J. Am. Chem. Soc.* **2001**, *123*, 8620-8621.
 12. Shin, J.-Y.; Furuta, H.; Osuka, A. *Angew. Chem. Int. Ed.* **2001**, *40*, 619-621.
 13. Baird, N. C.; *J. Am. Chem. Soc.* **1972**, *94*, 4941-4948.

List of Tables

1	Table 3.1	Crystal data for 38.2H⁺	80
2	Table 4.1	Selected bond lengths (Å) and torsion angles (°) of 28 and 29 .	117
3	Table 4.2	Crystal data for 28 and 29	118
4	Table 5.1	Crystal data for 26a and 26.2H⁺	151
5	Table 5.2	Crystal data for 27	159
6	Table 5.3	Crystal data for 30a and 30b	169
7	Table 6.1	Crystallographic data for 17b	204

List of Schemes

1	Scheme 1.1	Au(III) complex of [26] π hexaphyrin	23
2	Scheme 1.2	Rh(I) complex of [26] π rubyrin	24
3	Scheme 1.3	Pd(II) complex of [36] π octaphyrin	25
4	Scheme 1.4	Trinuclear complex of [40] π nonaphyrin	26
5	Scheme 3.1	Synthesis of pentaphyrin 3	62
6	Scheme 3.2	Synthesis of pentaphyrin 6	63
7	Scheme 3.3	Synthesis of fused pentaphyrin 7	63
8	Scheme 3.4	Synthesis of 7c , 10 , 11	64
9	Scheme 3.5	Synthesis of 14 and 15	64
10	Scheme 3.6	Synthesis of 18 , 19 and 20	65
11	Scheme 3.7	Synthesis of 23	65
12	Scheme 3.8	Synthesis of hexaphyrin 26	67
13	Scheme 3.9	Synthesis of hexaphyrin 27	68
14	Scheme 3.10	Synthesis of 28 , 29 and 30	68
15	Scheme 3.11	Synthesis of 32	69
16	Scheme 3.12a	Synthesis of pentaphyrin 38 in Method-I	72
17	Scheme 3.12b	Synthesis of pentaphyrin 38 in Method-II	73
18	Scheme 3.13	Synthesis of Hexaphyrin 42	81
19	Scheme 4.1	Synthesis of heptaphyrin 4	96
20	Scheme 4.2	Synthesis of heptaphyrin 6	96
21	Scheme 4.3	Synthesis of heptaphyrin 8	97
22	Scheme 4.4	Synthesis of 10 and 11	97
23	Scheme 4.5	Synthesis of 12	98
24	Scheme 4.6	Synthesis of 13 , 14 and 15	99
25	Scheme 4.7	Synthesis of 18	99
26	Scheme 4.8	Synthesis of 22 and 23	100
27	Scheme 4.9	Synthesis of 24	101
28	Scheme 4.10	Synthesis of heptaphyrin 26	101
29	Scheme 4.11	Syntheses of singly fused heptaphyrin 28 and 29	103

30	Scheme 5.1a	Synthesis of figure-eight octaphyrin 4	134
31	Scheme 5.1b	Synthesis of figure-eight octaphyrin 6	134
32	Scheme 5.2	Synthesis of octaphyrin 10	135
33	Scheme 5.3	Synthesis of octaphyrin 11	135
34	Scheme 5.4	Synthesis of cyclo[8]pyrrole 12	136
35	Scheme 5.5	Synthesis of octaphyrin 14	137
36	Scheme 5.6	Synthesis of planar octaphyrin 16	137
37	Scheme 5.7	Synthesis of octaphyrin 18	138
38	Scheme 5.8	Synthesis of doubly fused octaphyrin 20	139
39	Scheme 5.9	Synthesis of bridged octaphyrin 23	140
40	Scheme 5.10	Synthesis of planar octaphyrin 26	142
41	Scheme 5.11	The possible isomeric unit of 26a	145
42	Scheme 5.12	Synthesis of octaphyrin 27 and metalated 28	154
43	Scheme 5.13	Synthesis of bridged octaphyrin 30	160
44	Scheme 6.1	Synthesis of nonaphyrin 2	184
45	Scheme 6.2	Synthesis of nonaphyrin 2 by [3+1] methodology	185
46	Scheme 6.3	Synthesis of figure-eight nonaphyrin 7	185
47	Scheme 6.4	Synthesis of cyclo[6]pyrrole[3]thiophene 9	186
48	Scheme 6.5	Synthesis of 12 and 13	187
49	Scheme 6.6	Synthesis of singly fused nonaphyrin 17	189
50	Scheme 6.7	Synthesis of non-fused nonaphyrin 18	190
51	Scheme 6.8	open conformation of 17.2H⁺ and 18.2H⁺	207

List of Figures

1	Figure 1.1	Example of antiaromatic expanded porphyrins	9
2	Figure 1.2	Examples of Möbius aromatic expanded porphyrins	12
3	Figure 1.3	Expanded porphyrin with Baird aromaticity	14
4	Figure 1.4	Expanded porphyrins with various structural diversity	19
5	Figure 1.5	Expanded porphyrin with various anionic interactions	22
6	Figure 2.3.1	^1H NMR spectrum of 5 in CDCl_3	42
7	Figure 2.3.2	^1H NMR spectrum of 6 in CDCl_3	43
8	Figure 2.3.3	^1H NMR spectrum of 7 in CDCl_3	44
9	Figure 2.3.4	^1H NMR spectrum of 8 in CDCl_3	45
10	Figure 2.3.5	^1H NMR spectrum of 9 in CDCl_3	46
11	Figure 2.3.6	^1H NMR spectrum of 11 in CDCl_3	48
12	Figure 2.3.7	^1H NMR spectrum of 12 in CDCl_3	49
13	Figure 2.3.8	^1H NMR spectrum of 13 in CDCl_3	50
14	Figure 2.3.9	^1H NMR spectrum of 14 in CDCl_3	51
15	Figure 2.3.10	^1H NMR spectrum of 17 in CDCl_3	53
16	Figure 2.3.11	^1H NMR spectrum of 19 in CDCl_3	55
17	Figure 2.3.12	^1H NMR spectrum of 20 in CDCl_3	56
18	Figure 2.3.13	^1H NMR spectrum of 21 in CDCl_3	57
19	Figure 3.1	Molecular structure of 33-35	70

20	Figure 3.2	ESI-MS spectrum of 38	74
21	Figure 3.3	ESI-MS spectrum of 39	74
22	Figure 3.4	^1H NMR spectrum of 38 in CD_2Cl_2	75
23	Figure 3.5	^1H - ^1H COSY correlation spectrum of 38 in CD_2Cl_2	75
24	Figure 3.6	^1H NMR spectrum of 38 with 4.5 equiv. of TFA in CD_2Cl_2	76
25	Figure 3.7	^1H NMR titration experiment of 38 with dilute solution of TFA in CD_2Cl_2	77
26	Figure 3.8	The electronic absorption spectra of 38 and 38.2H⁺ in CH_2Cl_2	78
27	Figure 3.9	Single crystal X-ray structure of 38 with HSO_4^- anions a) Top view and b) Side view	79
28	Figure 3.10	ESI-MS spectrum of 42	82
29	Figure 3.11	^1H NMR spectrum of 42 in CD_2Cl_2	83
30	Figure 3.12	Variable temperature ^1H NMR of 42 in CD_2Cl_2	83
31	Figure 3.13	^1H - ^1H COSY spectrum of 42 in CD_2Cl_2	84
32	Figure 3.14	^1H NMR spectrum of 42 with 5 equiv. TFA in CD_2Cl_2 at 298K	85
33	Figure 3.15	The electronic absorption spectra of 42 and 42.2H⁺ in CH_2Cl_2	86
34	Figure 4.1	Crystal structure of 28 and 29	102
35	Figure 4.2	ESI-MS spectrum of 28	104
36	Figure 4.3	ESI-MS spectrum of 29	104
37	Figure 4.4	^1H NMR spectrum of 28 at 298K in CDCl_3 (a) and ^1H - ^1H COSY correlation spectrum of 28 with pyrrolic β -CH proton correlation (b)	106

38	Figure 4.5	^1H NMR spectrum of 29 at 298K in CDCl_3 (a) and ^1H - ^1H COSY correlation spectrum of 28 with pyrrolic β -CH proton correlation (b)	107
39	Figure 4.6	Variable temperature ^1H NMR spectrum of 28 in CD_2Cl_2	108
40	Figure 4.7	^1H NMR spectrum of 28 at 183K in CD_2Cl_2 (a) and ^1H - ^1H COSY spectrum of 28 with thiophene and pyrrolic β -CH protons in correlation.	109
41	Figure 4.8	^1H NMR spectrum of 29 at 183K in CD_2Cl_2 (a) and ^1H - ^1H COSY spectrum of 29 with thiophene and pyrrolic β -CH protons in correlation.	110- 111
42	Figure 4.9	^1H -NMR spectrum of 28.2H⁺ at 298K in CD_2Cl_2	112
43	Figure 4.10	^1H -NMR spectrum of 29.2H⁺ at 298K in CD_2Cl_2	113
44	Figure 4.11	Single crystal X-ray structure of 28 a) Top view and b) Side view	115
45	Figure 4.12	Single crystal X-ray structure of 29 a) Top view and b) Side view	115
46	Figure 4.13	Self-assembled dimer of 28	116
47	Figure 4.14	One dimensional array of 28	116
48	Figure 4.15	Two dimensional array of 28	117
49	Figure 4.16	Electronic absorption spectra of 28 and 28.2H⁺ in CH_2Cl_2	119
50	Figure 4.17	Electronic absorption spectrum of 28 in various solvents at 298K	120
51	Figure 4.18	Electronic absorption spectra of 29 and 29.2H⁺ in CH_2Cl_2	121
52	Figure 4.19	NICS(0) value of 28 and 28.2H⁺	122

53	Figure 4.20	NICS(0) value of 29 and 29.2H⁺	122
54	Figure 4.21	AICD plot of 28 and 28.2H⁺	123
55	Figure 4.22	AICD plot of 29 and 29.2H⁺	124
56	Figure 5.1	Molecular structure 26 , 27 and 30	141
57	Figure 5.2	ESI-MS spectrum of 26a	142
58	Figure 5.3	ESI-MS spectrum of 26b	143
59	Figure 5.4	ESI-MS spectrum of 26c	143
60	Figure 5.5	Electronic absorption spectra of 26a and 26a.2H⁺ in CH ₂ Cl ₂	145
61	Figure 5.6	¹ H NMR spectra of 26a at 298K in Toluene-d ₈	145
62	Figure 5.7	Low temperature ¹ H NMR spectrum of 26a	146
63	Figure 5.8	¹ H- ¹ H COSY spectrum of 26a with correlation in normal heterocyclic rings (a) and inverted units (b)	147
64	Figure 5.9	¹ H NMR spectrum of 26.2H⁺ at 298K in Toluene-d ₈	148
65	Figure 5.10	¹ H- ¹ H COSY spectrum of 26a.2H⁺ with correlation in normal heterocyclic rings (a) and inverted units (b)	148
66	Figure 5.11a	Single crystal X-ray structure of 26a with intermolecular hydrogen bonding interaction.	150
67	Figure 5.11b	Side view X-ray structure of 26a	150
68	Figure 5.12	Single crystal X-ray structure of 26a.2H⁺ with intermolecular hydrogen bonding interaction with perchlorate anion (a) Top view, (b) Side view and (c) One dimensional array.	152-153
69	Figure 5.13	ESI-MS spectrum of 27	155
70	Figure 5.14	ESI-MS spectrum of 28	155

71	Figure 5.15	^1H NMR spectrum of 27	156
72	Figure 5.16	The electronic absorption spectra of 27 , 27.2H⁺ and 28 in CH_2Cl_2	157
73	Figure 5.17	Single crystal X-ray structure of 27 (a) Top view and (b) Side view	158
74	Figure 5.18	ESI-MS spectrum of 30a	161
75	Figure 5.19	ESI-MS spectrum of 30b	161
76	Figure 5.20	^1H NMR and ^1H - ^1H COSY spectrum of 30a with heterocyclic ring correlations	162
77	Figure 5.21	^1H NMR spectral comparison between 30a and monofused rubyrin	163
78	Figure 5.22	^1H NMR spectrum of 30a and 30a.4H⁺	164
79	Figure 5.23	Electronic absorption spectrum of 30a and 30a.4H⁺	165
80	Figure 5.24	NICS(0) value of 30a (a) and imaginary $[34]\pi$ octaphyrin (b). NICS values of hydrogen atom in 30a and the constituent $[26]\pi$ hexaphyrin. Hydrogen atoms in the DTT-bridge are shown in red(c)	166
81	Figure 5.25	NICS(0) value of 30a (a) and imaginary $[34]\pi$ octaphyrin (b)	167
82	Figure 5.26	AICD plots of 30a (a) and 30b (b)	167
83	Figure 5.27	Single crystal X-ray structure of 30a . (a) Top view and (b) Side view.	168
84	Figure 5.28	Single crystal X-ray structure of 30b . (a) Top view and (b) Side view.	168
85	Figure 5.29	EPR spectroscopy of $2e^-$ oxidized form of 30a and 30b	170

86	Figure 5.30	NICS(0) value of $2e^-$ oxidised form of 30a (a) and 30b (b)	171
87	Figure 5.31	AICD plots of $2e^-$ oxidised form of 30a (a) and 30b (b)	171
88	Figure 6.1	Crystal structure of 17b	188
89	Figure 6.2	ESI-MS spectrum of 17a	190
90	Figure 6.3	ESI-MS spectrum of 17b	191
91	Figure 6.4	ESI-MS spectrum of 18	191
92	Figure 6.5	The electronic absorption spectrum of 17a and 17a.2H⁺ in CH_2Cl_2	192
93	Figure 6.6	The electronic absorption spectrum of 17b and 17b.2H⁺ in CH_2Cl_2	192
94	Figure 6.7	The electronic absorption spectrum of 18 and 18.2H⁺ in CH_2Cl_2	193
95	Figure 6.8	1H NMR spectrum of 17a in $CDCl_3$ (a). The expansion in aromatic ring protons (b)	194
96	Figure 6.9	1H - 1H COSY spectrum of 17a with heterocyclic ring protons in $CDCl_3$.	195
97	Figure 6.10	1H NMR spectrum of 17a.2H⁺ in CD_2Cl_2 .	196
98	Figure 6.11	1H - 1H COSY spectrum of 17a.2H⁺ heterocyclic rings in CD_2Cl_2 .	196
99	Figure 6.12	1H NMR spectrum of 17b in CD_2Cl_2 (a). The expansion in aromatic ring protons (b)	197
100	Figure 6.13	1H - 1H COSY spectrum of 17b aromatic ring protons in CD_2Cl_2 .	198
101	Figure 6.14	1H NMR spectrum of 17b.2H⁺ in CD_2Cl_2 .	199
102	Figure 6.15	1H - 1H COSY spectrum of 17b.2H⁺ aromatic ring protons in CD_2Cl_2 .	199
103	Figure 6.16	1H NMR spectrum of 18 in $CDCl_3$	200

104	Figure 6.17	^1H NMR spectrum of 18.2H⁺ in CD_2Cl_2 . The inset shows the expansion between 11.00 & 13 ppm and 4.8 & 5.6 ppm	201
105	Figure 6.18	^1H - ^1H COSY spectrum of 18.2H⁺ aromatic ring protons in CD_2Cl_2	201
106	Figure 6.19	Single crystal X-ray structure of 17b . a) Top view and b) side view. The <i>meso</i> -aryl groups are omitted for clarity in the side view	203
107	Figure 6.20	Self-assembled dimer in 17b with intermolecular hydrogen bonding interactions	203
108	Figure 6.21	NICS (0) value of 17b . a) Freebase form and b) Diprotonated state	206
109	Figure 6.22	NICS (0) value of 18 . a) Freebase form and b) Diprotonated state.	206

List of Abbreviations

Ar	Aryl
AICD	Anisotropy Induced Current Density
BLA	Bond Length Alternation
BT	2, 2' Bithiophene
BF ₃ .Et ₂ O	Boron trifluoride diethyl etherate
Calcd.	calculated
COSY	Correlation Spectroscopy
CCDC	Cambridge Crystallographic Data Centre
CH ₂ Cl ₂	Dichloromethane
CD ₂ Cl ₂	Dideuteromethylenechloride
CHCl ₃	Chloroform
CDCl ₃	Deuterated chloroform
CH ₃ CN	Acetonitrile
CH ₃ OH	Methanol
C ₆ H ₅ COCl	Benzoyl chloride
C ₆ F ₅ CHO	Pentafluorobenzaldehyde
DMF	N, N' Dimethylformamide
DMSO	Dimethyl Sulphoxide
DDQ	2, 3-Dichloro-5, 6-dicyano-1, 4-benzoquinone
DTT	Dithieno[3,2-b:2',3'-d]thiophene
ESI	Electron Spray Ionization
equiv.	equivalent
EtOAc	Ethyl acetate
FB	Free-Base
FeCl ₃	Iron(III) chloride
HOMA	Harmonic oscillator measure of aromaticity
IR	Infrared
Mes	mesityl
MSA	methanesulfonic acid
NICS	nucleus independent chemical shift
NIR	Near infrared

NLO	Non Linear Optics
NMR	Nuclear Magnetic Resonance
Na ₂ SO ₄	Sodium sulphate
Py	pyrrole
ppm	parts per million
<i>p</i> -TSA	<i>para</i> -toluenesulphonic acid
[Rh(CO) ₂ Cl] ₂	Di- μ -chloro-tetracarbonyldirhodium(I)
Tol	tolyl
TFA	Trifluoroacetic acid
THF	Tetrahydrofuran
TLC	Thin Layer Chromatography
TMEDA	N, N, N, N, Tetramethylethylenediamine
Toluene-d ₈	Deuterated toluene
TPA	Two Photon Absorption
TEA	Triethylamine
TMS	Tetramethylsilane
UV-Vis	Ultraviolet–Visible

CHAPTER 1

General Introduction

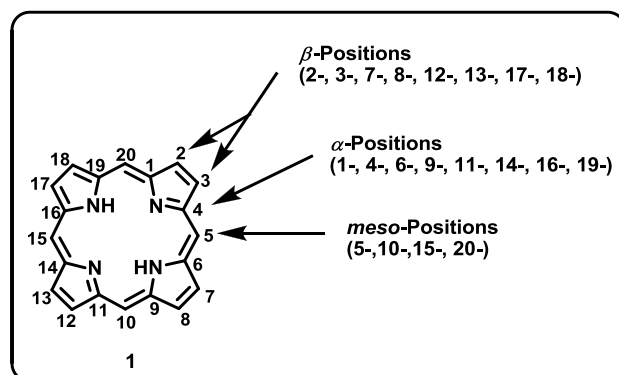
1.1	Introduction	3-7
1.2	Aromaticity	7-14
	1.2.1 Anti-aromaticity	7-9
	1.2.2 Möbius aromaticity	9-13
	1.2.3 Baird Aromaticity	13-14
1.3	Structural Diversity	14-19
	1.3.1 Figure-eight	15
	1.3.2 N-confusion	16
	1.3.3 Ring inversion	16-17
	1.3.4 Fusion	17-18
	1.3.5 Bridging	18-19
1.4	Anion Binding	19-22
1.5	Coordination Chemistry	22-26
1.6	Conclusion and Objective of the present thesis	26-27
1.7	References	27-34

1.1 Introduction

Porphyrins are naturally occurring macrocycles and are termed as “Pigments of Life.”^[1] It plays important role in numerous biological functions such as oxygen transport and storage in the form of Hemoglobin and Myoglobin,^[2,3] electron transport in cytochromes,^[4,5] harvesting the light energy in the form of chlorophyll^[6,7] and peroxide breakdown by catalase and peroxidase enzymes.^[8,9] Indeed, the life relies on biological processes which are performed or catalyzed by heme-containing proteins. In additions, it has also been proven to be efficient sensitizers for photodynamic therapeutic (PDT) applications,^[10,11] non-linear optical properties^[12,13] and catalysis.^[14-16]

The parent form of these macrocycles are called as Porphine. The name is derived from the Greek word “porphura” meaning “purple” color and the porphyrins and its derivatives are intensely colored. The four pyrrolic units are linked by four sp^2 hybridized *meso* carbon bridges with the molecular formula of $C_{20}H_{14}N_4$. The inner core contains 16 (C/N) atoms in the macrocyclic framework with 22 π electrons in the overall conjugation pathway and the main conjugation pathway contains 18 π electrons. Thus the macrocycle obeys $[4n+2]\pi$ Hückel rule and is aromatic. The typical aromatic nature is reflected from the electronic absorption and NMR spectral analyses. The electronic spectral analysis exhibits an intense absorption band at 400 nm and called as “Soret band” and four weak Q-like bands between 450 to 700 nm region. On the other hand, the diamagnetic ring current is reflected from the deshielding of the pyrrolic β -CH protons and *meso* protons, while the inner NH protons are appeared in the shielded region.

For nomenclature, according to the common convention, the 2- and 5- position of the heterocyclic units, such as pyrrole, furan and thiophene are referred as alpha (α) and 3- and 4- positions are referred as beta (β) positions. The same nomenclature was used when the heterocycles were incorporated in the macrocyclic framework. Thus, the positions such as, 1-, 4-, 6-, 9-, 11-, 14-, 16- and 19- are considered as α -positions, while the 2-, 3-, 7-, 8-, 12-, 13-, 17- and 18- are termed as β -positions. Similarly, the bridging methene units, such as 5-, 10-, 15- and 20- are considered as *meso*-positions.



Due to the complexity in the IUPAC nomenclature, the porphyrin and its derivatives were assigned trivial names by their discoverers. The trivial names are constructed either based on the color or other feature of the macrocycle, followed by the suffix “phyrin” or “rin” taken from porphyrin. For example, Woodward and co-workers have assigned a pentapyrrolic macrocycle as “sapphyrin” where the molecule crystallizes in dark blue color.^[17] In order to avoid trivial names, thenomenclature was put forward by Franck and Nonn. The nomenclature contains three parts: (1) the number of π electrons in the shortest conjugation pathway, which is kept in square brackets; (2) a core name indicating the number of pyrroles or other heterocycles in the overall systems (e.g., pentaphyrin, hexaphyrin, etc.)

and (3) numbers in round brackets separated by dots following the main name specify the number of bridging carbon atoms between each pyrrole subunit starting with the largest bridge. For instance, according to this nomenclature, porphyrin **1** would be named as [18]tetraphyrin(1.1.1.1).

There are many reports about modification of the porphyrin periphery and its core, most of them are listed here. (a) Peripheral modification: by changing the substituent at the periphery of the macrocyclic framework;^[18-20] (b) Contracted porphyrinoids: by reducing the number of pyrrole and / or *meso*-carbon units in the porphyrin skeleton, which leads to contraction in the porphyrin skeleton;^[21-23] (c) N-confused porphyrinoids: the α and β' position of one or more pyrrole units are connected to the *meso*-carbon bridges, where the pyrrole nitrogen is pointing outside the macrocyclic framework;^[24-29] (d) Core-modified porphyrinoids: one or more pyrrole nitrogen atoms in the porphyrin core are replaced by chalcogen atoms;^[30,31] (e) Expanded porphyrinoids: by increasing one or more pyrrolic units or number of *meso* carbon units in the porphyrin framework leads to increase in the π electron conjugation.^[32-34] These porphyrinoids are found suitable for various applications such as (i) sensitizers for PDT,^[10,11] (ii) MRI contrasting agents;^[35] (iii) multi-metallic chelates for catalysis;^[36-38] (iv) binds with various anions and neutral substrates^[87-93] and (v) as models for aromaticity,^[60-69] thus led to flurry of research activities, in particular for its synthesis, spectral and structural characterizations. The pioneering work was initiated by Woodward and co-workers in sixties, however, it is only in the late eighties and early nineties, the chemistry of expanded porphyrins has been exploited because of the readily available

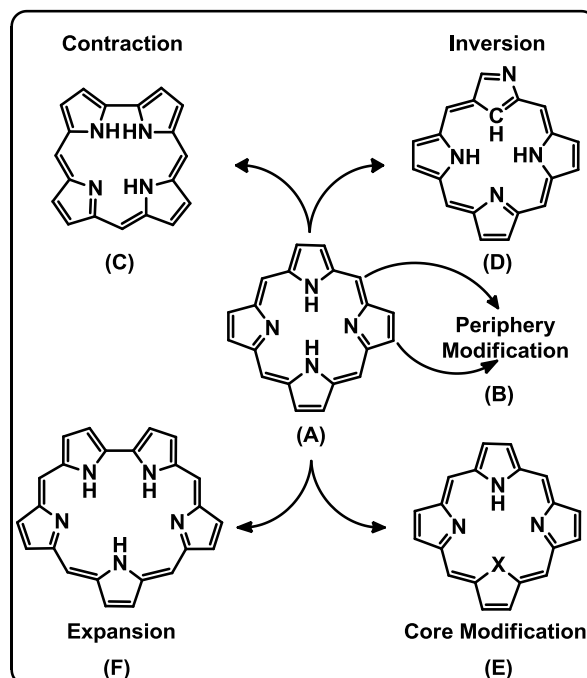


Chart 1. Molecular Structures of Porphyrinoids

precursors such as dipyrane and tripyrane. So far, a variety of expanded porphyrins with varying ring sizes are known which includes; sapphyrins,^[39] smaragdyrins,^[40,41] pentaphyrins,^[42,43] hexaphyrins,^[44,45] rosarian,^[46,47] rubyrin,^[48] amethyrin,^[41] heptaphyrin,^[49,50] octaphyrin,^[51,52] nonaphyrins,^[53] turcasarin,^[54] dodecaphyrins^[55] and the largest expanded porphyrin with 96π electrons in the macrocycles have been reported and their properties have been exploited for various applications. This thesis is mainly focused on the synthesis, spectral, structural characterization, Möbius aromaticity and structural diversity of core-modified pentaphyrin, hexaphyrin, heptaphyrin, octaphyrin and nonaphyrin. The synthesis of respective expanded porphyrinoid were highlighted in the introduction part of each chapters. Hence, in this chapter, we have mainly focused on the

aromaticity, structural diversity and receptor properties such as anion binding and coordination chemistry of the macrocycles.

1.2 Aromaticity

The concept of “Aromaticity” is well known in the porphyrinoid chemistry. The Hückel $[4n+2]\pi$ aromatic character in porphyrin changes into different form in expanded porphyrin chemistry. In addition to aromatic character, they exhibit Hückel $4n\pi$ non-aromatic, anti-aromatic, Möbius $4n\pi$ aromatic, Möbius $[4n+2]\pi$ anti-aromatic and Baird aromatic character. The aromatic and non-aromatic character is well-known in the literature, here we mainly focused on anti-aromatic, Möbius $4n\pi$ aromatic and Baird aromaticity, which are relevant to this thesis.

1.2.1 Anti-aromaticity

There are series of notable strategies for the synthesis of Hückel $4n\pi$ anti-aromatic expanded porphyrins. Some of the macrocycles are shown in Figure 1.1. The [28]hexaphyrins (**1**) was reported by Osuka and co-workers.^[56] The strong paratropic ring current was reflected from the ^1H NMR spectral analyses of **1**. The peripheral β -CH protons of **1** were resonated in the upfield region at 5.83 ppm to 4.23 ppm, the inner core imidazolyl protons were observed between 9.64 ppm and 8.95 ppm, whereas the pyrrolic NH protons were at 21.81 and 20.41 ppm, suggests the Hückel anti-aromatic character. The planar conformation of anti-aromatic **1** was reflected from the single crystal X-ray analyses and further supported by theoretical calculations, where nucleus-independent chemical shift (NICS) values of **1** was found to be +16.00 ppm.

The [32] π expanded isophlorin (**2**) was reported by Anand and co-workers.^[57] The ¹H NMR spectral analyses of **2** revealed the typical anti-aromatic character, where the ethylene protons resonated as a broad singlet which was further split into two doublets upon lowering the temperature to 175 K. Both the inner and outer CH protons were observed at 12.83 ppm (inner CH) and 5.37 ppm (outer CH). The chemical shift difference ($\Delta\delta$) of 7.5 ppm between the inner and outer CH, thus confirms the strong paratropic ring current. The planarity of the macrocycle was further reflected from the crystal analyses with strong intermolecular F...S; F...Se and F... π interactions. The calculated NICS(0) was observed at 11.8 ppm, thus proves the Hückel $4n\pi$ anti-aromatic character.

Our group have also demonstrated the synthesis of [36] π doubly fused octaphyrin (**3**) which exhibits non-aromatic figure-eight conformation in the freebase form into anti-aromatic open-extended conformation in the protonated state.^[58] Upon protonation, two of the pyrrole units in the dipyrin moiety were inverted and experienced the paratropic ring current, where the inverted pyrrole β -CH and NH protons were resonated at 15.91 ppm and -0.1 ppm and the respective protons in the normal pyrrole units were observed at 4.36 ppm and -18.7 ppm. In addition to crystal analyses, the anti-aromatic character was further supported by theoretical calculations, where the NICS(0) value at 9.94 ppm and the paratropic ring current from the anisotropy-induced current density (AICD) plots in the diprotonated form.

The synthesis and anti-aromatic character of core-modified [32] π mono fused heptaphyrin (**4**) was reported by our group.^[59] The deshielded signals of inverted dithienothiophene (DTT) and the pyrrolic ring which is opposite to the DTT unit, at 16.7 ppm and 15.2 ppm suggests the strong paratropic ring current in the conjugated pathway. The crystal analysis

reveals that the DTT unit is 28.8° deviated from the mean plane, however the other heterocyclic rings in the framework maintains the planarity. The large positive NICS(0) value at +24.6 ppm is in complete agreement with Hückel $4n\pi$ anti-aromatic electronic circuit.

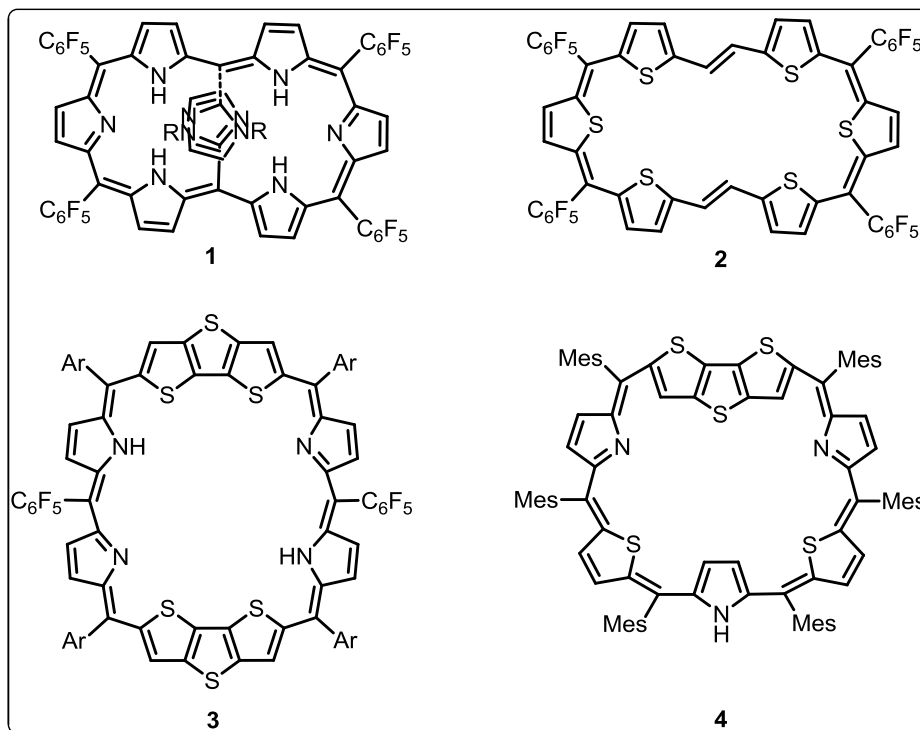


Figure 1.1: Examples of anti-aromatic expanded porphyrins

1.2.2 Möbius aromaticity

The concept of “Möbius aromaticity” in a closed shell configuration with $[4n]\pi$ -electron conjugation in molecular systems was proposed as early as 1964 by Heilbronner.^[60] However, the first real example of a Möbius aromatic hydrocarbon was realized only in 2003 by Herges and coworkers.^[61] Since then, several reports have appeared in literature on molecules which exhibit $[4n]\pi$ Möbius aromaticity especially in cyclic annulenes and its derivatives. More recently Mauksch and coworkers have demonstrated the presence of

Möbius aromaticity in planar metallocycles.^[62] The mechanisms involved in understanding of Möbius aromaticity in annulenes was reported by Karney and coworkers.^[63]

The first example of expanded porphyrin analogue which exhibit Möbius aromaticity was reported in 2007. Specifically, Latos-Grażyński and coworkers in an elegant study demonstrated that di-*p*-benzi-[28]Hexaphyrin (**5**) shuttles between Hückel and Möbius topologies depending on temperature and the solvent polarity.^[64] The results were summarized below: (i) at room temperature, **5** exhibited Hückel $4n\pi$ non-aromatic character, however, upon lowering temperature, the pyrrolic NH and phenylene CH protons at 16.51 ppm and 8.16 ppm were shifted upfield and resonated at 10.31 ppm and 6.60 ppm and (ii) the broad absorption band observed in the presence of non-polar solvent at room temperature was appeared as Soret and weak Q-like band by using polar solvents and the low temperature analyses reveals the sharp increase in intensity of the Soret and Q-like bands, along with color change from green to blue.

Since then, several reports have demonstrated presence of Möbius aromaticity in various expanded porphyrins such as conformationally flexible 28π hexaphyrins,^[66] 32π heptaphyrins,^[67] 36π octaphyrins,^[68] N-Fused pentaphyrins,^[65] N-fused 28π hexaphyrins^[70] under various conditions such as protonation,^[67] metal coordination,^[65] fusion of the ring,^[66] oxidation-reduction^[71] and variation in temperature and solvents.^[64] Some of the examples are shown in Figure 1.2.

The Rh(I) inserted N-fused $[24]\pi$ pentaphyrin (**6**) was reported by Osuka and co-workers.^[65] The **6** was synthesized from its free ligand with Rh(I) salt in the presence of sodium acetate. The complex was confirmed by crystal analysis, where the N-fused tripentacyclic ring

maintained the planarity. The Rh(I) ion coordinated with dipyrin unit was tilted from the mean plane to register the Möbius topology with reasonable conjugation in the framework. The results were further reflected from the ^1H NMR spectral analyses, where the inner β -CH and NH protons were resonated at 0.10 and 0.68 ppm. In addition, the NICS(0) value of -16.1 ppm and bond length alternation (BLA) value of 0.100 Å further supports the Möbius aromatic character.

The benzopyrane-fused [28]hexaphyrin(1.1.1.1.1.1) (**7**) was synthesized by same group by refluxing [26]hexaphyrin in acetic acid.^[66] At room temperature, the inverted pyrrolic β -CH were observed in the shielded region at 2.22 and 1.03 ppm, whereas the peripheral β -CH were at 7.44-7.03 ppm with the $\Delta\delta$ value of 6.41 ppm suggests the distinct diatropic ring current. The fused tricyclic ring imparts large strain in the rest of the framework and promotes twisted Möbius topology at room temperature. The NICS(0) value of -11.8 ppm and the harmonic oscillator model of aromaticity (HOMA) value of 0.73 were further supported the Möbius aromatic character.

The Möbius aromaticity was also reflected from the simple protonation experiment by using [32]heptaphyrins (**8**).^[67] The moderate paratropic ring current was displayed from the ^1H NMR spectral analyses, where the pyrrolic β -CH protons at the inner core of the framework were resonated at 11.27 and 8.50 ppm and the rest of the pyrrolic β -CH protons were observed from 6.42 to 5.11 ppm, subsequently, the NICS(0) value was calculated and found to be +10.1 ppm, suggested the typical Hückel $4n\pi$ anti-aromatic character. However upon protonation, the strong diatropic ring current was revealed from the spectral analyses, where the inner pyrrolic β -CH protons were observed at -0.69 and -0.18 ppm and the rest of the

protons were between 7.86 and 6.93 ppm. The large $\Delta\delta$ (chemical shift difference between the inner and outer β -protons) value of 10.75 suggested the typical Möbius aromaticity. The NICS(0) value at -9.5 ppm further supported the aromatic character in **8**.

As observed in **8**, similar trend was reflected from $[36]\pi$ octaphyrin (**9**).^[68] The structural analyses revealed that the molecule was in twisted figure-eight conformation where intramolecular hydrogen bonding interaction between imine and amine nitrogens promotes such conformation. Upon protonation, the doubly twisted figure-eight conformation was changed into half twisted open-type conformation, where all the intramolecular hydrogen bonding in freebase were replaced by intermolecular hydrogen bonding network created by TFA molecules, thus led to Möbius aromatic character in the molecular framework. The results were supported by spectral, structural and theoretical calculations.

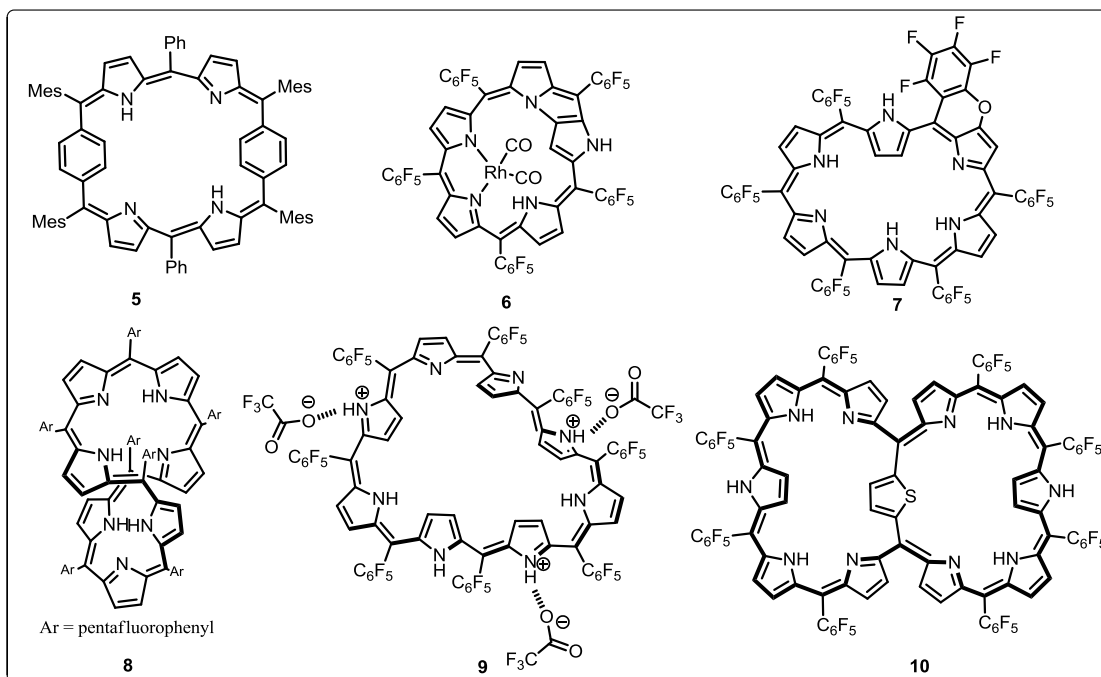


Figure 1.2: Examples of Möbius aromatic expanded porphyrins

The bridged expanded porphyrin was synthesized by Osuka and co-workers where the bridging unit in the macrocycle promotes Möbius aromatic character.^[69] The 2,5-thienyl bridged [46]decaphyrin (**10**) displayed larger aromatic character supported by two twisted thia[28]hexaphyrin with dual Möbius aromatic circuit and significant contribution from the bridging thiophene unit. The dual Möbius aromaticity was reflected from the electronic spectral analyses with two Soret like band at 603 and 776 nm and further supported by NMR spectral analyses. However, the twisted conformation as observed in the freebase state was transformed into planar structure in protonated state, where two individual Möbius aromatic circuit were turned into attain overall Hückel [46] π aromatic character.

1.2.3 Baird aromaticity

According to Baird's rule, "The $[4n+2]\pi$ system is Hückel aromatic in ground state will show anti-aromatic behavior in the lowest excited triplet state.^[72] On the other hand, the $4n\pi$ system is Hückel anti-aromatic character in the ground state will show aromaticity in the lowest triplet excited state. Only theoretical predictions like NICS, HOMA and AICD will give support behind the aromaticity of the molecule."

Such new type of aromaticity was first introduced in expanded porphyrins by Osuka and Kim et al (Figure 1.3).^[73] They observed such interesting results from the bis-Rh(I) ion inserted [26] and [28] π hexaphyrin(1.1.1.1.1.1) (**11**). At singlet ground state (S_0), [26] π (**11a**) and [28] π (**11b**) hexaphyrins were aromatic and anti-aromatic and its reversal aromaticity was reflected from the transient absorption spectra at triplet excited state (T_1), where the Soret band in **11a** was turned into broad absorption bands, whereas, in **11b**, the broad bands were changed into sharp Soret like band. The result was further supported by

theoretical calculations. The NICS(0) value of **11a** and **11b** in S_0 state was at -14.58 and 18.41 ppm, suggested the typical aromatic and anti-aromatic character, however, in T_1 state, the respective value of **11a** and **11b** 15.73 ppm and -14.00 ppm, proved the reversal of aromaticity. Similar trend was observed in AICD plots, where the clockwise (aromatic) and counter clockwise (anti-aromatic) ring current in S_1 state was altered into reversed aromatic character. Similar trend was also reflected from HOMA calculations, where the value of **11a** at S_0 state was reduced from 0.62 to 0.58 and in T_1 state, the respective values of **11b** was increased from 0.53 to 0.64, further confirms the Baird aromaticity.

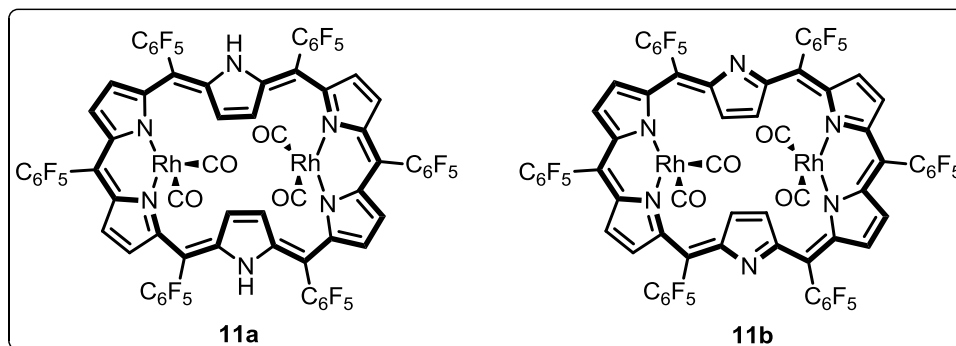


Figure 1.3: Expanded porphyrin with Baird aromaticity

1.3 Structural diversity

The structural diversity in expanded porphyrin exhibits in various forms which includes; planar, figure-eight, inverted, confused, fused, bridged and Möbius band. These forms mainly rely on the number and type of *meso*-carbon bridges and heterocyclic units present in the macrocyclic framework. The role of structural diversity is highly important in expanded porphyrin chemistry because which provides significant impact on electronic configuration, physical and chemical properties, aromaticity and electronic conjugation

pathway. Thus, in this section, we wish to highlight all such structural diversity in expanded porphyrinoids (Figure 1.4).

1.3.1 Figure Eight

The concept of “figure-eight conformation” is mainly observed in expanded porphyrins. The rigidity of the macrocycle gradually decreases upon increasing the number of *meso*-carbon units as well as the heterocyclic rings in the molecular framework. In order to attain the stable conformation, the higher expanded porphyrin tends to adopt figure-eight conformation. The simplest figure-eight conformation begins from hexaphyrin unit where six pyrrole units are linked by six *meso* carbon bridges,^[74] however, the respective macrocycle mostly prefers planar conformation depends on the nature of *meso*-aryl or β -alkyl substituted heterocyclic rings present in the framework. The similar trend was observed in the heptaphyrin units.^[75] The figure-eight conformation is mostly observed in octaphyrin (**12**) and higher expanded porphyrin analogues.^[76] The first such conformation was reported by Vogel and co-workers, where the reported octaphyrin contains eight pyrrole rings linked by four *meso*-carbon bridges with higher flexibility in the macrocycle, thus leads to attain the figure-eight conformation. As there is a twist in conformation, the macrocycle tend to loose its planarity and decrease in symmetry, thus, shows non-aromatic character which is reflected from the spectral studies and confirmed by structural analysis. The octaphyrin^[47] and nonaphyrin^[48] derivatives with Hückel $[4n+2]\pi$ or $4n\pi$ electrons in the conjugated pathway, due to figure-eight conformation, their spectral pattern mostly resembles non-aromatic character.

1.3.2 N-confusion

The N-confused porphyrin was serendipitously reported independently by Furuta et al and Latos-Grażyński et al.^[24,25] The α and β' positions of one of the pyrrole units in the porphyrin unit is linked with rest of the macrocycle, where the pyrrole N is pointing outward and provide additional coordination site to bind with metal ions and anions. The confused pyrrolic β -CH unit is inside the macrocyclic ring and able to stabilize variety of organometallic complexes. The N-confused expanded porphyrin was introduced by Chandrashekar and Furuta et al, where the confused pyrrole unit was included in the precursors itself (**13**).^[24] The spectral analyses suggested the strong diatropic ring current, where the inner CH proton was resonated at 2.73 ppm, whereas the outer CH observed at 9.79 ppm. The structure was confirmed by crystal analysis, where the N-confused pyrrole unit which is opposite to the bithiophene unit is inverted and 25.17° deviated from the mean macrocyclic plane. Since then, series of N-confused expanded porphyrins were mainly reported by Furuta and coworkers.^[26, 28] Till date, three confused pyrrole rings incorporated in the macrocyclic framework.^[29]

1.3.3 Ring Inversion

The first inverted expanded porphyrinoid was reported by Latos-Grażyński and co-workers.^[77] The *meso*-aryl sapphyrin (**14**) was synthesized from acid-catalyzed condensation of pyrrole and benzaldehyde followed by DDQ oxidation. The pyrrole unit ring which is opposite the bipyrrrole unit is inverted, where the inverted pyrrolic β -CH proton is resonated at -1.50 ppm, while the NH is observed at 12.24 ppm, suggests the aromatic character. Upon protonation, the inverted pyrrole ring undergoes 180° ring flipping, where

the β -CH and NH proton are observed at 8.87 ppm and -2.74 ppm and adopts normal conformation, where all the pyrrolic nitrogens are inside the framework. The core size and size of the heteroatoms decides the nature of structural diversity. In the presence of smaller heteroatoms (N or O) adjacent to the bipyrrrole unit lead to ring normal structure, while the presence of bigger heteroatoms (S/Se/Te) lead to inverted structure.^[12] Our group have also demonstrated the planar aromatic [34] π octaphyrin,^[78] where spectral and crystal analysis reveals that two of the heterocyclic units are inverted and experiencing aromatic ring current. So far, four heterocyclic rings inverted in macrocyclic framework is reported in the literature.^[79]

1.3.4. Fusion

In order to restrict the figure-eight conformation and achieve the planarity in the expanded porphyrin analogues, the fusion strategy was introduced. The first fused expanded porphyrin was reported by Furuta and Osuka et al.^[80] The fused pentaphyrin (**15**) was synthesized by acid-catalyzed condensation of pyrrole and benzaldehyde followed by oxidation, where the newly formed N-fused tripentacyclic ring in the core provides planarity as well as aromaticity. Later, stepwise synthetic strategies were adopted for the synthesis of fused expanded porphyrins, where the fusion was introduced in the starting material itself. The benzopyrrole and benzofuran incorporated expanded porphyrinoids was reported by C. H. Lee and co-workers.^[81] Our group have also utilized dithienothiophene (DTT) moiety as one of the potential precursor for the synthesis of fused expanded porphyrins.^[82] Overall, introduction in the fusion led to the following observations: (i) to restrict the inversion; (ii) sharp increase in the molar absorption coefficient; (iii) fluorescence emission in the near IR

region; (iv) increase in the planarity as well as aromaticity and (v) moderate increase in the two photon absorption (TPA) value. Till date, upto quadruply fused expanded porphyrinoids are known in the literature.^[83]

1.3.5. Bridging

An increase in number of pyrrole rings and *meso* carbon bridges result in conformational flexibility, leading to non-planar twisted structures. Various synthetic approaches have been followed to avoid twisting of the structures, in order to achieve planar aromatic expanded porphyrins. One such approach, we mentioned above. Another approach is to introduce an internal bridging group linking the *meso* carbon atoms. Such strategy was initially reported by Osuka and co-workers by introducing the *p*-phenylene bridge between two pentapyrrolic units to achieve the near planar decaphyrin (**16**).^[84] Later, same group have also synthesized planar hexaphyrin using an internal vinylene bridge which exist in two different resonating form such as; (a) 26π or 28π hexaphyrin unit and (b) 16π diazaannuleno[16]diazannulene.^[85] We have also demonstrated the synthesis of thienyl bridged hexaphyrin^[86] which exist in two different conjugative pathway such as; (a) 18π aromatic circuit and (b) 26π aromatic circuit and further used for non-linear optical applications and found that the two photon absorption values are higher as compared to the parent core-modified dithiahexaphyrin. Recently, series of bridged expanded porphyrins with dual aromatic character were introduced and combined together to generate overall larger aromatic electronic circuit were reported.^[69]

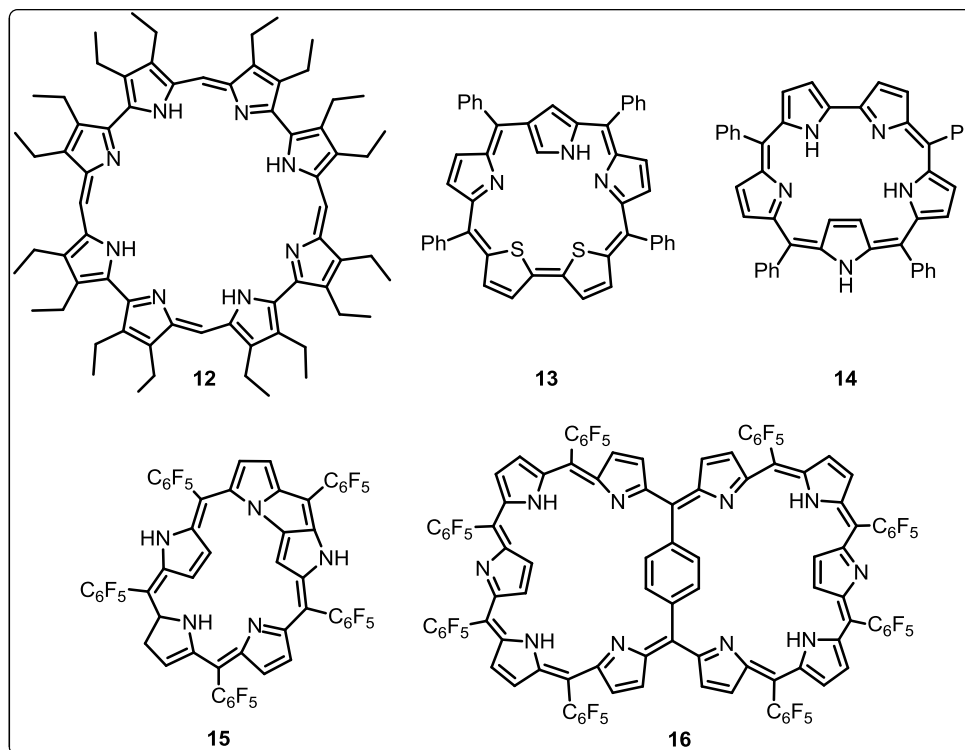


Figure 1.4: Expanded porphyrins with various structural diversity

1.4 Anion Binding

Expanded porphyrins with more than four pyrrole rings can selectively bind with neutral, cationic and anionic substrates under a variety of conditions. Earlier few examples were known in the literature, however not much progress was made due to no availability of easy and efficient synthetic methodologies to have multigram quantities of required macrocycles. The simple and straightforward synthetic methodologies were introduced for the synthesis of various expanded porphyrinoids by Sessler and co-workers and also exploited them for the selective recognition of anions especially and to lesser extent with the anion and neutral substrates.^[87-93] A wealth of data was accumulated about the molecular recognition of

expanded porphyrins by them, however, in this section, we wish to highlight the binding properties of some of the expanded porphyrins which are relevant to this thesis and shown in Figure 1.5.

The two imine pyrrolic nitrogens present in the planar sapphyrin is easily protonated to form a full pentameric NH-containing core.^[87] This core is quite unique with positive potential hydrogen bonding donors and relatively large and near circular planar array. The first diprotonated N-5 sapphyrin (**17**) with fluoride ion was obtained in quite an unusual fashion. The simple counter ion exchange reaction (PF_6^- for Cl^-) led to the stabilization of fluoride ion within the core size of 5.5 Å diameter, during the crystallization technique. The fluoride ion was bound exactly at the center of the macrocyclic ring with five N-H...F hydrogen bonding interactions with the bond distance of 2.7 Å (**17a**). The binding experiment was further performed between the diprotonated sapphyrin and tetrabutylammonium fluoride salt and the binding constant is found to be $2.8 \times 10^5 \text{ M}^{-1}$ in CH_3OH solution. The binding experiment was further performed with other halide salts.^[87] In the presence of chloride ion, binding interactions are different as observed as in the case of fluoride ion, where two chloride ion are bound with the sapphyrin unit (**17b**). The first chloride ion is bound by three N-H hydrogen bond interaction and is 1.77 Å above the plane of the macrocycle, whereas the second chloride ion is bound by two N-H hydrogen bond interaction and is 1.88 Å below the plane of the macrocycle.^[87] Same group have also demonstrated the binding interactions of various anions like carboxylic acids and phosphate anions by using diprotonated sapphyrin.^[88,89]

Sessler and co-workers have also reported the synthesis and binding interaction of [26] π ruyrin.^[90] In similar fashion as observed in **17b**, the diprotonated ruyrin was bound with two chloride ions above and below the macrocyclic plane with the distance of 1.60 Å, where three pyrrole units are in intermolecular hydrogen bonding interaction with each chloride ions with the distance of 1.84 Å (**18**).

The [28] π heptaphyrin(1.0.0.1.0.0.0) with two *meso*-carbon bridges was reported by Sessler and co-workers.^[91] The macrocycle was further treated with sulfuric acid to produce the sulfate anion complex (**19**). The crystal structure of anionic complex reveals that the heptaphyrin forms 1:1 complex with sulfate anion where the anion is slightly above the mean plane and generates seven N-H...O intermolecular hydrogen bonding interaction with the ranges from 1.76 Å to 2.17 Å and the N...O contacts range from 2.67 Å to 2.96 Å.

The [30] π octaphyrin without *meso* carbon bridges was synthesized by same group.^[92] The reaction was performed by oxidative coupling of bipyrrrole with FeCl₃ and 1M H₂SO₄ and obtained the sulfate anion incorporated octaphyrin complex (**20**). The crystal analyses proved that the sulfate anion was bound exactly at the center of the cavity. The four oxygen atoms of the sulfate anion interact with all the pyrrolic NH's through intermolecular hydrogen bonding with the N-H...O distance of 1.91 Å to 2.49 Å.

Our group have also demonstrated the synthesis of [34] π planar aromatic octaphyrin and exploited the anion binding interaction with TFA anion.^[93] The octaphyrin binds with TFA in 1:2 ratio, where the TFA anions are located above and below the mean macrocyclic plane (**21**). Each TFA anions interact with macrocyclic ring to form four intermolecular hydrogen interactions with two N-H...O; C-H...O and C-H...F with the bond distances are ranges

from 2.14 Å to 2.44 Å. The first two N-H...O interaction are electrostatic, whereas the rest are interaction between the anion and the host molecule.

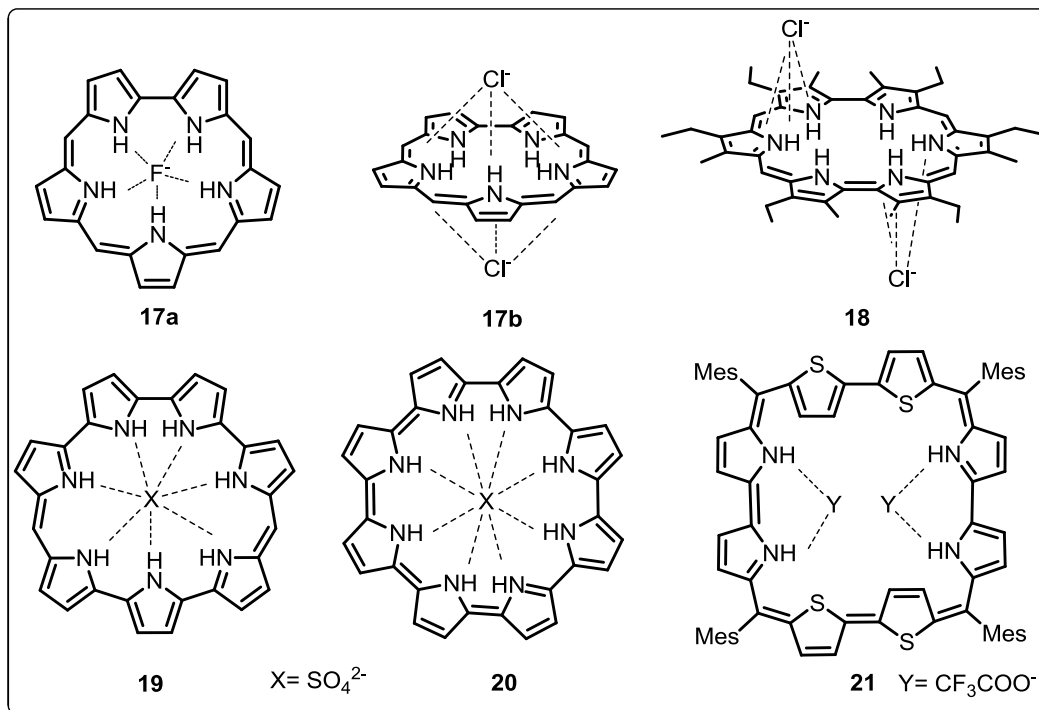


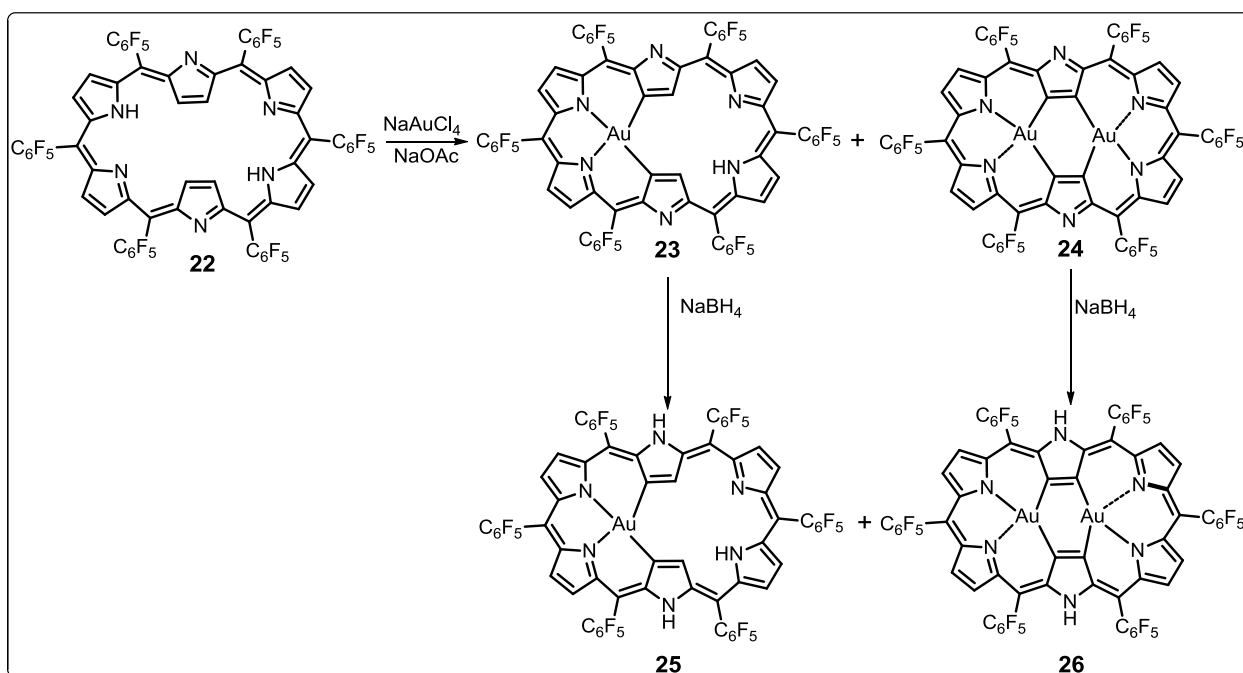
Figure 1.5: Expanded porphyrins with various anionic interactions

1.5 Coordination Chemistry

The size of the core as well as number of pyrrolic NHs in the expanded porphyrins suggest that these could be a potential candidate to display rich complexation chemistry. However, the coordination chemistry of expanded porphyrins are still in its infancy stage as compared to their anionic interactions, where only a handful of metal complexes were successfully characterized. Some of the complexes are highlighted in this section.

The Au(III) incorporated aromatic and anti-aromatic [26] π hexaphyrin with multiple Au-C bonds are reported by Osuka and co-workers.^[94] The complex was accomplished by refluxing the mixture of [26] π hexaphyrin (**22**) with NaAuCl₄ in the presence of NaOAc,

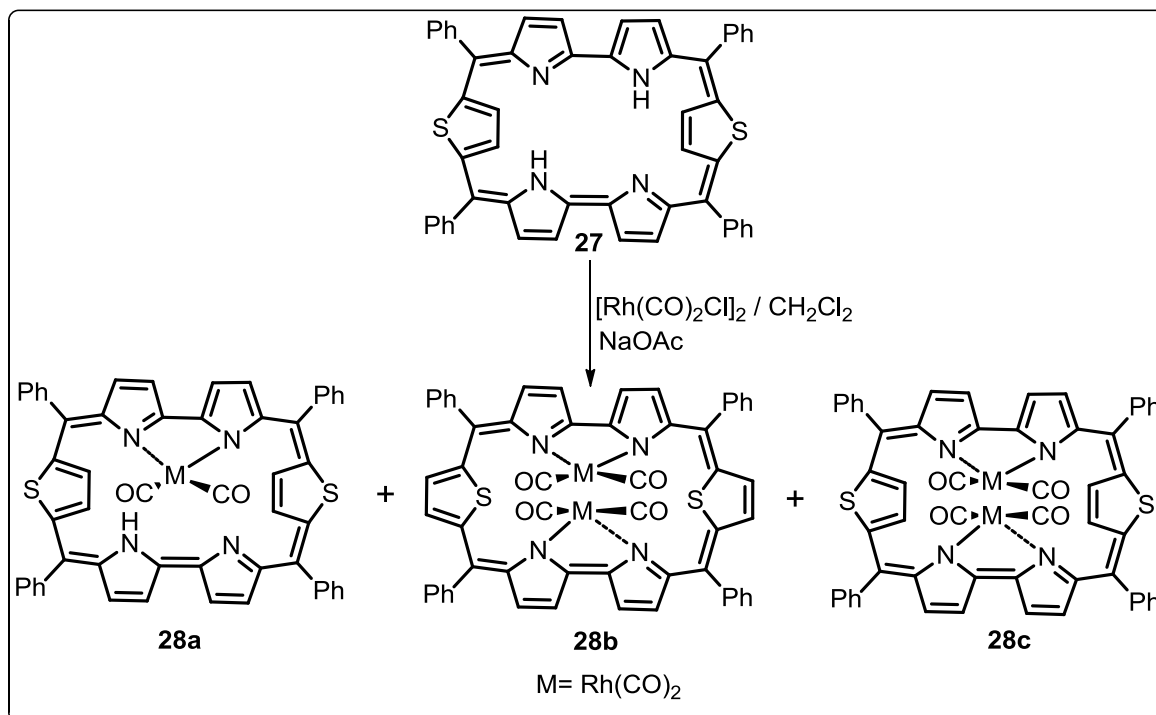
where the mono-Au(III) (**23**) and bis-Au(III) (**24**) complexes were obtained in 16 and 14% yields. Both the complexes were further reduced with NaBH₄ to afford [28]π mono-Au(III) (**25**) and bis-Au(III) (**26**) complex in quantitative yield (Scheme 1.1). The complex **23** is 0.520 Å deviated from the mean plane, however less tilted as compared to freebase **22**. On the hand, the complex **24** adopts the planar conformation. The geometry around the metal center is square planar. The β-CH and NH signals in **23** and **25** were resonated at -2.93 ppm & -2.03 ppm in **23** and 19.39 ppm & 24.57 ppm in **25**, thus confirms that both **23** and **25** retains its individual aromatic and anti-aromatic character.



Scheme 1.1: Au(III) complexes of [26]π hexaphyrin

The Rh(I) coordinated [26]π rubyrin was reported by our group.^[95] The [26]π rubyrin (**27**) was treated with 2 equiv. of [Rh(CO)₂Cl]₂ in the presence of NaOAc. Three different products, (a) mono- (**28a**) and (b) two-bimetallic Rh(I) complexes (**28b** and **28c**) were isolated in 25%, 6% and 1% yield (Scheme 1.2). One of the Rh(I) bimetallic complex (**28b**)

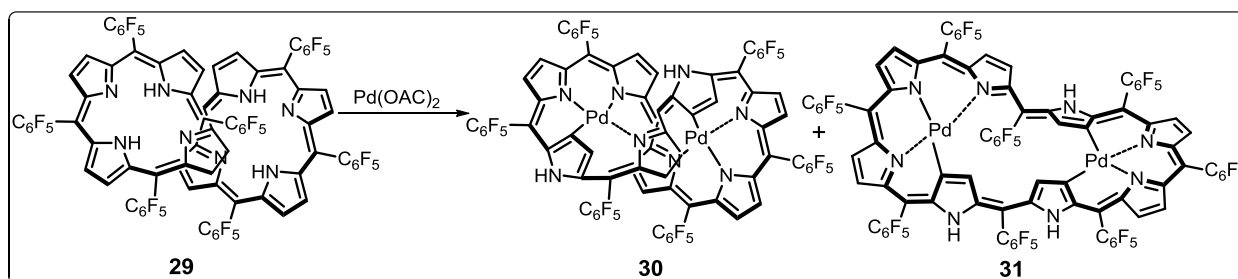
was confirmed by crystal analysis, where the geometry around the metal center is square planar. Both the Rh(I) ions are coordinated with each bipyrrrole units containing amine and imine nitrogen atoms, where both the thiophene units have undergone 180° ring inversion. Overall, the complex is in bowl shape structure and the Rh(I) ions are above the mean plane with the distance of 0.781 Å. In complex **28c**, without rearranging the freebase **27**, both the Rh(I) ions are coordinated above and below the macrocyclic framework.



Scheme 1.2: Rh(I) complexes of [26]π rbyrin

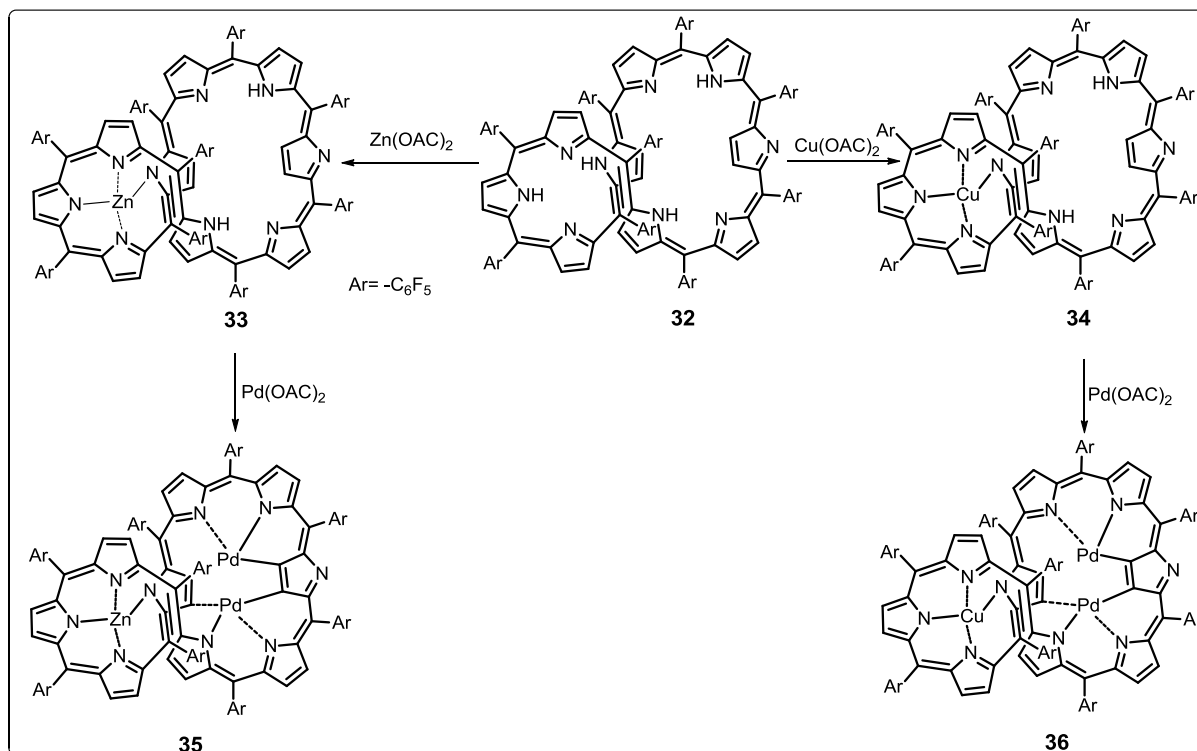
By refluxing CH₃OH solution of [36]π ocataphylin (**29**) with Pd(OAc)₂, two types of bis-Pd(II) (**30** and **31**) complexes were obtained in 51% and 20% yield (Scheme 1.3).^[96] The ligand (**29**) is in figure-eight conformation with non-aromatic character. Upon metal ion insertion, both the Pd(II) ion in **30** was coordinated with two NNNC core and maintained the figure-eight conformation. The theoretically calculated NICS(0) value of +38.4 ppm at

the center of the complex suggested typical anti-aromatic character. On the other hand, the complex **31** was adopted in slightly twisted structure, where the Pd(II) ions were coordinated with NNNC and NNCC core as reflected from crystal analyses. The spectral analyses and NICS(0) value of -14.6 ppm proved that the complex (**31**) was in Möbius aromatic character.



Scheme 1.3: Pd(II) complexes of [36] π octaphyrin

The [40] π nonaphyrin (**32**) with a porphyrin like segment and hexaphyrin like core in the framework is found suitable to stabilize different metal ions in the core.^[97] The macrocycle **32** was treated with $\text{Zn}(\text{OAc})_2 \cdot 2\text{H}_2\text{O}$ to obtain Zn(II) complex (**33**) in 75%, with $\text{Cu}(\text{OAc})_2$ to form Cu(II) complex (**34**) in 35% yield. Both **33** and **34** were coordinated at the porphyrin like segment. The vacant hexaphyrin core was further utilized to stabilize the heavier metal ions, where **33** and **34** were treated with $\text{Pd}(\text{OAc})_2$ to form quantitative yield of trinuclear complexes Zn(II)-Pd(II)-Pd(II) (**35**) and Cu(II)-Pd(II)-Pd(II) (**36**) (Scheme 1.4). The distorted nonplanar structure was reflected from the crystal analysis of **36**.



Scheme 1.4: Trinuclear complexes of [40] π nonaphyrin

1.6 Conclusion and objectives of the present thesis

In summary, the expanded porphyrins such as pentaphyrin, hexaphyrin, heptaphyrin, octaphyrin and nonaphyrin with structural diversity, aromaticity, receptor property with anions and coordination chemistry were highlighted in this chapter. The main objective of the present thesis is to develop novel methodologies for the synthesis of core-modified expanded porphyrins and its fused and bridged analogues. Mainly focus on the aromaticity and also highlights the receptor property and coordination chemistry of these macrocycles.

The second chapter describes the experimental procedure for various starting materials utilized in this thesis. The reported pentaphyrins with a tripentacyclic ring in the framework, and hexaphyrin with six *meso*-carbon bridges are known in the literature. Hence, the third

chapter describes the synthesis of pentaphyrin with six *meso*-carbon bridges and core-modified bridge hexaphyrin units.. The pentaphyrin unit with open framework is achieved and the aromatic characteristics of both the macrocycles are described.

The Möbius aromatic character is probed by various conditions such as protonation, metal coordination, fusion, oxidation and reduction, variation in temperature and solvents, however, the role of core-modified expanded porphyrins in general and heptaphyrin in particular are not explored. Hence, in the fourth chapter, we have demonstrated the synthesis of core-modified monofused $[32]\pi$ heptaphyrin and highlights its Möbius aromatic characteristics.

Most of the octaphyrins reported in the literature were in figure-eight conformation and \bar{u} -aromatic in nature. In the fifth chapter, we have adopted various strategies such as; (i) reducing the number of *meso*-carbon bridges and introducing the sterically hindered *meso*-aryl rings; (ii) fused and (iii) bridged techniques to achieve the planar aromatic octaphyrin and also discussed the Baird aromatic characteristic.

In the last chapter, we have demonstrated the synthesis of two new core-modified $[40]\pi$ nonaphyrins with fused and non-fused heterocyclic rings in the core. The macrocycles are non-aromatic and adopts figure-eight conformation in the freebase form. The protonation leads to open conformation and exhibits Hückel $4n\pi$ anti-aromatic character.

1.7 References

1. Battersby, A. R.; McDonald, E. *Acc. Chem. Res.* **1979**, *12*, 14-22.
2. Vanderkooi, J. M.; Erecinska, M. *Eur. J. Biochem.* **1975**, *60*, 199-207.

-
3. Anderson, J. L. R.; Armstrong, C. T.; Kodali, G.; Lichtenstein, B. R.; Watkins, D. W.; Mancini, J. A.; Boyle, A. L.; Farid, T. A.; Crump, M. P.; Moser, C. C.; Dutton, P. L. *Chem. Sci.* **2014**, *5*, 507-514.
 4. Lewis, L. A.; Sung, M.-H.; Gipson, M.; Hartman, K.; Dyer, D. W. *J. Bacterio.* **1998**, *22*, 6043-6047.
 5. Basolo, F.; Hoffman, B. M.; Ibers, J. A. *Syn. Oxy. Carr.* **1975**, *8*, 384-392.
 6. Osuka, A.; Kazuhiro, M. *Chem. Lett.* **1987**, *16*, 825-828.
 7. Kaplan, A.; Korin, E.; Bettelheim, A. *Eur. J. Inorg. Chem.* **2014**, 2288-2295.
 8. Heidari-Golafzani, M.; Rabbani, M.; Rahimi, R.; Azad, A. *RSC Adv.* **2015**, *5*, 99640-99645.
 9. Adam, S. M.; Garcia-Bosch, I.; Schaefer, A. W.; Sharma, S. K.; Siegler, M. A.; Solomon, E. I.; Karlin, K. D. *J. Am. Chem. Soc.* **2017**, *139*, 472-481.
 10. Tian, J.; Ding, L.; Xu, H.-J.; Shen, Z.; Ju, H.; Jia, L.; Bao, L.; Yu, J.-S. *J. Am. Chem. Soc.* **2013**, *135*, 18850-18858.
 11. Wang, T.; Zhu, D.; Liu, G.; Tao, W.; Cao, W.; Zhang, L.; Wang, L.; Chen, H.; Mei, L.; Huang, L.; Zeng, X. *RSC Adv.* **2015**, *5*, 50617-50627.
 12. Chandrashekar, T. K.; Venkatraman, S. *Acc. Chem. Res.* **2003**, *36*, 676-691.
 13. Shin, J.-Y.; Kim, K. S.; Yoon, M.-C.; Lim, J. M.; Yoon, Z. S.; Osuka, A.; Kim, D. *Chem. Soc. Rev.* **2010**, *39*, 2751-2767.
 14. Jiang, X.; Gou, F.; Chen, F.; Jing, H. *Green. Chem.* **2016**, *18*, 3567-3576.
 15. Liu, X.; Wang, Z.; Zhao, X.; Fu, X. *Inorg. Chem. Front.* **2016**, *3*, 861-865.
 16. Tam, C. M.; To, C. T.; Chan, K. S. *Organometallics* **2016**, *35*, 2174-2177.
-

-
17. Bauer, V. J.; Clive, D. L. J.; Dolphin, D.; Paine, J. B.; Harris, F. L.; King, M. M.; Loder, J.; Wang, S. W. C.; Woodward, R. B. *J. Am. Chem. Soc.* **1983**, *105*, 6429-6436.
 18. Xu, X.-D.; Zhang, J.; Chen, L.-J.; Guo, R.; Wang, D.-X.; Yang, H.-B. *Chem. Commun.* **2012**, *48*, 11223-11225.
 19. Yorimitsu, H.; Osuka, A. *Asian J. Org. Chem.* **2013**, *2*, 356-373.
 20. de Freitas Castro, K. A. D.; Wypych, F.; Antonangelo, A.; Mantovani, K. M.; Bail, A.; Ucoski, G. M.; Ciuffi, K. J.; Cintra, T. E.; Nakagaki, S. *J. Colloid. Interf. Sci.* **2016**, *478*, 374-383.
 21. Johnson, A.; Todd, A. *Vitamins & Hormones* **1957**, *15*, 1-30.
 22. Johnson, A.; Price, R. *J. Chem. Soc.* **1960**, 1649-1653.
 23. Gross, Z.; Galili, N.; Saltsman, I. *Angew. Chem. Int. Ed.* **1999**, *38*, 1427-1429.
 24. Furuta, H.; Asano, T.; Ogawa, T. *J. Am. Chem. Soc.* **1994**, *116*, 767-768.
 25. Chmielewski, P. J.; Latos-Grażyński, L.; Rachlewicz, K.; Glowiak, T. *Angew. Chem., Int. Ed. Engl.* **1994**, *33*, 779-781.
 26. Pushpan, S. K.; Srinivasan, A.; Anand, V. G.; Venkatraman, S.; Chandrashekar, T. K.; Joshi, B. S.; Roy, R.; Furuta, H. *J. Am. Chem. Soc.* **2001**, *123*, 5138-5139.
 27. Srinivasan, A.; Ishizuka, T.; Osuka, A.; Furuta, H. *J. Am. Chem. Soc.* **2003**, *125*, 878-879.
 28. Yamamoto, T.; Toganoh, M.; Mori, S.; Uno, H.; Furuta, H. *Chem. Sci.* **2012**, *3*, 3241-3248.
 29. Xie, Y.-S.; Yamaguchi, K.; Toganoh, M.; Uno, H.; Suzuki, M.; Mori, S.; Saito, S.; Osuka, A.; Furuta, H. *Angew. Chem. Int. Ed.* **2009**, *48*, 5496-5499.
-

-
30. Kumar, R.; Misra, R.; Chandrashekar, T. K. *Org. Lett.* **2006**, *8*, 4847-4850.
31. Pacholska-Dudziak, E.; Szczepaniak, M.; Książek, A.; Latos-Grażyński, L. *Angew. Chem. Int. Ed.* **2013**, *52*, 8898-8903.
32. Sessler, J. L.; Seidel, D. *Angew. Chem. Int. Ed.* **2003**, *42*, 5134-5175.
33. Saito, S.; Osuka, A. *Angew. Chem. Int. Ed.* **2011**, *50*, 4342-4373.
34. Stępień, M.; Sprutta, N.; Latos-Grażyński, L. *Angew. Chem. Int. Ed.* **2011**, *50*, 4288-4340.
35. Yoon, H.-J.; Lim, T. G.; Kim, J.-H.; Cho, Y. M.; Kim, Y. S.; Chung, U. S.; Kim, J. H.; Choi, B. W.; Koh, W.-G.; Jang, W.-D. *Biomacromol.* **2014**, *15*, 1382-1389.
36. Kido, H.; Shin, J.-Y.; Shinokubo, H. *Angew. Chem. Int. Ed.* **2013**, *52*, 13727-13730.
37. Tanaka, Y.; Yoneda, T.; Furukawa, K.; Koide, T.; Mori, H.; Tanaka, T.; Shinokubo, H.; Osuka, A. *Angew. Chem. Int. Ed.* **2015**, *54*, 10908-10911.
38. Yoneda, T.; Sung, Y. M.; Lim, J. M.; Kim, D.; Osuka, A. *Angew. Chem. Int. Ed.* **2014**, *53*, 13169-13173.
39. Karthik, G.; Srinivasan, A.; Chandrashekar, T. K. *Org. Lett.* **2014**, *16*, 3472-3475.
40. Broadhurst, M. J.; Grigg, R.; Johnson, A. W. *J. Chem. Soc., Perkin Trans. 1* **1972**, 2111-2116.
41. Narayanan, S. J.; Sridevi, B.; Chandrashekar, T. K.; Englich, U.; Ruhlandt-Senge, K. *Org. Lett.* **1999**, *1*, 587-590.
42. Rexhausen, H.; Gossauer, A. *J. Chem. Soc., Chem. Commun.* **1983**, 275.
43. Gokulnath, S.; Chandrashekar, T. K. *Org. Lett.* **2008**, *10*, 637-640.
44. Neves, M. G. P. M. S.; Martins, R. M.; Tome, A. C.; Silvestre, A. J. D.; Silva, A. M. S.; Felix, V.; Cavaleiro, J. A. S.; Drew, M. G. B. *Chem. Commun.* **1999**, 385-386.
-

-
45. Sessler, J. L.; Seidel, D.; Vivian, A. E.; Lynch, V.; Scott, B. L.; Keogh, D. W. *Angew. Chem. Int. Ed.* **2001**, *40*, 591-594.
46. Setsune, J.-i.; Toda, M.; Yoshida, T.; Imamura, K.; Watanabe, K. *Chem. Eur. J.* **2015**, *21*, 12715-12727.
47. Fukuzumi, S.; Ohkubo, K.; Ishida, M.; Preihs, C.; Chen, B.; Borden, W. T.; Kim, D.; Sessler, J. L. *J. Am. Chem. Soc.* **2015**, *137*, 9780-9783.
48. Zhou, Z.; Chang, Y.; Shimizu, S.; Mack, J.; Schütt, C.; Herges, R.; Shen, Z.; Kobayashi, N. *Angew. Chem. Int. Ed.* **2014**, *53*, 6563-6567.
49. Saito, S.; Osuka, A. *Chem. Eur. J.* **2006**, *12*, 9095-9102.
50. Anand, V. G.; Pushpan, S. K.; Venkatraman, S.; Narayanan, S. J.; Dey, A.; Chandrashekar, T. K.; Roy, R.; Joshi, B. S.; Deepa, S.; Sastry, G. N. *J. Org. Chem.* **2002**, *67*, 6309-6319.
51. Bröring, M.; Jendry, J.; Zander, L.; Schmickler, H.; Lex, J.; Wu, Y.-D.; Nendel, M.; Chen, J.; Plattner, D. A.; Houk, K. N.; Vogel, E. *Angew. Chem., Int. Ed. Engl.* **1995**, *34*, 2515-2517.
52. Sprutta, N.; Latos-Grażyński, L. *Chem. Eur. J.* **2001**, *7*, 5099-5112.
53. Shimizu, S.; Taniguchi, R.; Osuka, A. *Angew. Chem. Int. Ed.* **2005**, *44*, 2225-2229.
54. Sessler, J. L.; Weghorn, S. J.; Lynch, V.; Johnson, M. R. *Angew. Chem., Int. Ed. Engl.* **1994**, *33*, 1509-1512.
55. Soya, T.; Kim, W.; Kim, D.; Osuka, A. *Chem. Eur. J.* **2015**, *21*, 8341-8346.
56. Mori, H.; Sung, Y. M.; Lee, B. S.; Kim, D.; Osuka, A. *Angew. Chem. Int. Ed.* **2012**, *51*, 12459-12463.
-

-
57. Gopalakrishna, T. Y.; Reddy, J. S.; Anand, V. G. *Angew. Chem. Int. Ed.* **2013**, *52*, 1763-1767.
58. Karthik, G.; Lim, J. M.; Srinivasan, A.; Suresh, C. H.; Kim, D.; Chandrashekar, T. K. *Chem. Eur. J.* **2013**, *19*, 17011-17020.
59. Karthik, G.; Srinivasan, A.; Suresh, C. H.; Chandrashekar, T. K. *Chem. Commun.* **2014**, *50*, 12127-12130.
60. Heilbronner, E. *Tetrahedron Lett.* **1964**, *29*, 1923-1928.
61. Ajami, D.; Oeckler, O.; Simon, A.; Herges, R. *Nature*, **2003**, *426*, 819-821.
62. Mauksch, M.; Tsogoeva, S. B. *Chem. Eur. J.* **2010**, *16*, 7843-7851.
63. Castro, C.; Karney, W. L. *J. Phys. Org. Chem.* **2012**, *25*, 612-619.
64. Stępień, M.; Latos-Grażyński, L.; Sprutta, N.; Chwalisz, P.; Szterenber, L. *Angew. Chem. Int. Ed.* **2007**, *46*, 7869-7873.
65. Park, J. K.; Yoon, Z. S.; Yoon, M.-C.; Kim, K. S.; Mori, S.; Shin, J.-Y.; Osuka, A.; Kim, D. *J. Am. Chem. Soc.* **2008**, *130*, 1824-1825.
66. Tokuji, S.; Shin, J.-Y.; Kim, K. S.; Lim, J. M.; Youfu, K.; Saito, S.; Kim, D.; Osuka, A. *J. Am. Chem. Soc.* **2009**, *131*, 7240-7241.
67. Saito, S.; Shin, J.-Y.; Lim, J. M.; Kim, K. S.; Kim, D.; Osuka, A. *Angew. Chem. Int. Ed.* **2008**, *47*, 9657-9660.
68. Lim, J. M.; Shin, J.-Y.; Tanaka, Y.; Saito, S.; Osuka, A.; Kim, D. *J. Am. Chem. Soc.* **2010**, *132*, 3105-3114.
69. Soya, T.; Mori, H.; Hong, Y.; Koo, Y. H.; Kim, D.; Osuka, A. *Angew. Chem. Int. Ed.* **2017**, *56*, 3232-3236.
70. Higashino, T.; Inoue, M.; Osuka, A. *J. Org. Chem.* **2010**, *75*, 7958-7961.
-

-
71. Inoue, M.; Osuka, A. *Angew. Chem. Int. Ed.* **2010**, *49*, 9488-9491.
72. Baird, N. C. *J. Am. Chem. Soc.* **1972**, *94*, 4941-4948.
73. Sung, Y. M.; Yoon, M.-C.; Lim, J. M.; Rath, H.; Naoda, K.; Osuka, A.; Kim, D. *Nat. Chem.* **2015**, *7*, 418-422.
74. Rath, H.; Anand, V. G.; Sankar, J.; Venkatraman, S.; Chandrashekar, T. K.; Joshi, B. S.; Khetrupal, C. L.; Schilde, U.; Senge, M. O. *Org. Lett.* **2003**, *5*, 3531-3533.
75. Rath, H.; Sankar, J.; Prabhuraja, V.; Chandrashekar, T. K.; Joshi, B. S. *Org. Lett.* **2005**, *7*, 5445-5448.
76. Shin, J.-Y.; Furuta, H.; Yoza, K.; Igarashi, S.; Osuka, A. *J. Am. Chem. Soc.* **2001**, *123*, 7190-7191.
77. Chmielewski, P. J.; Latos-Grażyński, L.; Rachlewicz, K. *Chem. Eur. J.* **1995**, *1*, 68-73.
78. Anand, V. G.; Pushpan, S. K.; Venkatraman, S.; Dey, A.; Chandrashekar, T. K.; Joshi, B. S.; Roy, R.; Teng, W.; Senge, K. R. *J. Am. Chem. Soc.* **2001**, *123*, 8620-8621.
79. Jeong, S.-D.; Park, K. J.; Kim, H.-J.; Lee, C.-H. *Chem. Commun.* **2009**, 5877-5879.
80. Shin, J.-Y.; Furuta, H.; Osuka, A. *Angew. Chem. Int. Ed.* **2001**, *40*, 619-621.
81. Panda, P. K.; Kang, Y.-J.; Lee, C.-H. *Angew. Chem. Int. Ed.* **2005**, *44*, 4053-4055.
82. Chandrashekar, T. K.; Prabhuraja, V.; Gokulnath, S.; Sabarinathan, R.; Srinivasan, A. *Chem. Commun.* **2010**, *46*, 5915-5917.
83. Jeong, S.-D.; Park, K. J.; Kim, H.-J.; Lee, C.-H. *Chem. Commun.* **2009**, 5877-5879.
84. Anand, V. G.; Saito, S.; Shimizu, S.; Osuka, A. *Angew. Chem. Int. Ed.* **2005**, *44*, 7244-7248.
-

-
85. Suzuki, M.; Osuka, A. *J. Am. Chem. Soc.* **2007**, *129*, 464-465.
86. Karthik, G.; Sneha, M.; Prabhuraja, V.; Lim, J. M.; Kim, D.; Srinivasan, A.; Chandrashekar, T. K. *Chem. Eur. J.* **2013**, *19*, 1886-1890.
87. Shionoya, M.; Furuta, H.; Lynch, V.; Harriman, A.; Sessler, J. L. *J. Am. Chem. Soc.* **1992**, *114*, 5714-5722.
88. Král, V.; Furuta, H.; Shreder, K.; Lynch, V.; Sessler, J. L. *J. Am. Chem. Soc.* **1996**, *118*, 1595-1607.
89. Sessler, J. L.; Camiolo, S.; Gale, P. A. *Coordin. Chem. Rev.* **2003**, *240*, 17-55.
90. Sessler, J. L.; Morishima, T.; Lynch, V. *Angew. Chem., Int. Ed. Engl.* **1991**, *30*, 977-980.
91. Sessler, J. L.; Seidel, D.; Lynch, V. *J. Am. Chem. Soc.* **1999**, *121*, 11257-11258.
92. Seidel, D.; Lynch, V.; Sessler, J. L. *Angew. Chem. Int. Ed.* **2002**, *41*, 1422-1425.
93. Anand, V. G.; Venkatraman, S.; Rath, H.; Chandrashekar, T. K.; Teng, W.; Ruhlandt-Senge, K. *Chem. Eur. J.* **2003**, *9*, 2282-2290.
94. Mori, S.; Osuka, A. *J. Am. Chem. Soc.* **2005**, *127*, 8030-8031.
95. Narayanan, S. J.; Sridevi, B.; Chandrashekar, T. K.; English, U.; Ruhlandt-Senge, K. *Inorg. Chem.* **2001**, *40*, 1637-1645.
96. Tanaka, Y.; Saito, S.; Mori, S.; Aratani, N.; Shinokubo, H.; Shibata, N.; Higuchi, Y.; Yoon, Z. S.; Kim, K. S.; Noh, S. B.; Park, J. K.; Kim, D.; Osuka, A. *Angew. Chem. Int. Ed.* **2008**, *47*, 681-684.
97. Kamimura, Y.; Shimizu, S.; Osuka, A. *Chem. Eur. J.* **2007**, *13*, 1620-1628.
-

CHAPTER 2

General Experimental methods and Techniques

2.1	Chemicals for Syntheses	37
2.2	Physico-chemical techniques	38-39
2.2.1	ESI-Mass analysis	38
2.2.2	Spectrophotometer analysis	38
2.2.3	NMR measurement	38
2.2.4	X-ray structure determination	38
2.2.5	Quantum mechanical calculation	38-39
2.3	Experimental Procedures	39-57
2.4	References	57-58

The experimental procedure for synthesis of desired precursors and the important physico-chemical techniques used for analysis in the course of investigation are described in this chapter. This chapter also highlights the materials and instruments used for the syntheses and characterization of precursor compounds.

2.1 Chemicals for Syntheses:

All the solvents required for syntheses and analyses were purified and dried according to known procedures.^[1, 2] Pyrrole and thiophene were purchased from Sigma-Aldrich and distilled before use. Selenophene, mesitaldehyde, *p*-tolualdehyde, pentafluorobenzaldehyde, benzoyl chloride, thiophene-2-boronic acid, 2-bromothiophene, *p*-chloroanil, 2,3-dichloro-5,6-dicyano-1,4-benzoquinone (DDQ), *n*-butyllithium, Trifluoroacetic acid, *p*-toluenesulphonic (*p*-TSA) acid and all the deuterated solvents for NMR measurements used as received from Sigma-Aldrich. Oxalyl chloride and titanium tetrachloride from Spectrochem chemicals, aluminium chloride from Alfa-acer chemicals. Aluminium oxide (basic and neutral) and silica gel (100-200 mesh) for column chromatography were purchased from Merck and used as received. Solvents needed for column chromatography (*n*-hexane, dichloromethane, ethyl acetate and methanol) were purchased from Rankem, Merck and used as received. N,N,N',N'-Tetramethylethylenediamine was procured from Sigma-Aldrich and distilled over KOH before use.^[1] Tetrabutylammonium hexafluorophosphate was received from Sigma-Aldrich and vacuum dried in desiccator for more than two hours before use.

2.2 Physico-chemical techniques:

2.2.1 ESI-Mass analysis: Mass spectrometry of the required compounds were recorded by electron spray ionization-mass spectra-Time of flight (ESI-MS-TOF) instrument of Brüker, microOTOF-QII mass spectrometer.

2.2.2 Spectrophotometer analysis: Electronic absorption spectra were recorded with Perkin Elmer-Lambda 750 UV-Visible spectrophotometer and data analyses were done using Origin pro 8 software package. For all measurement dichloromethane was used as the reference.

2.2.3 NMR measurement: ^1H , ^{13}C and ^1H - ^1H COSY correlation spectra were recorded on either 400MHz or 500MHz Brücker NMR spectrometer. The NMR protonation titration experiments were carried out with TFA solution quantitatively dissolved in required deuterated solvent. Chemical shifts are expressed in parts per million (ppm) relative to residual CDCl_3 and CD_2Cl_2 .

2.2.4 X-ray structure determinations: X-ray quality single crystals were grown using appropriate solvent mixture through diffusion methods. X-ray data were recorded at 100K on BRUKER-APEX X-ray diffractometer equipped with a large area CCD detector. The structure were solved by Patterson synthesis and refined with the SHELX-97 programme.^[3] The crystal analysis were done by Diamond (3.2 version)^[4] and Mercury (3.8 version)^[5] software.

2.2.5 Quantum mechanical Calculation: All the calculations were carried out using Gaussian 09 programme. All the structures were optimized without any symmetry restriction. The calculations were performed by the density functional theory (DFT) method with restricted B3LYP (Becke's three-parameter hybrid exchange functional and the Lee-Yang-Parr correlation functional) level, employing a basis set 6-311G (d,p). The

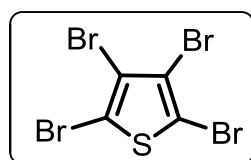
Nucleus Independent Chemical Shift (NICS) values were obtained with the GIAO method at the B3LYP/6-311G (d,p) level. The global ring centres for the NICS values were designed at the non-weighted means of the carbon and sulfur coordinates on the peripheral position of the macrocycles. In addition, NICS values were also calculated on centre of other local cyclic structures. Anisotropy Induced Current Density (AICD plot) and Harmonic Oscillator Model of Aromaticity (HOMA) value calculation were done at M06L/6-31G** level of DFT.^[6-9]

2.3: Experimental procedure:

The essential precursors required for the synthesis of desired macrocycles described in the thesis such as fused, non-fused and bridged expanded porphyrins are described below.

Tetrabromothiophene (1):

22 ml (0.431 mol) bromine was slowly added into the mixture of 8 ml (8.4 g, 0.1 mol) thiophene and 3 ml CHCl₃ for 2h on ice bath. The mixture was refluxed for 5h, then, cooled to ambient temperature. To the reaction mixture, 5 ml of 2N NaOH was added and vigorously stirred for 30 min. The solid product was separated and washed with water and crystallised over hot CHCl₃. Yield: 16 g, 75%.

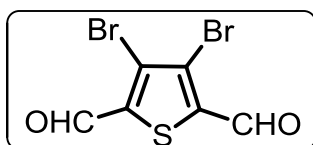


¹³C NMR (100 MHz, CDCl₃, 298K): δ (ppm): 117.10; 110.44.

3,4-dibromo-2,5-difomylthiophene (2):

The 500 ml two-necked round-bottom flask was equipped with a magnetic bar and rubber septum. Under a gentle flow of nitrogen, the tetrabromothiophene (1) (8 g, 20 mmol) and

freshly distilled tetrahydrofuran (100 ml) was added into the flask. The solution was cooled in methanol/2-propanol bath with an internal temperature of less than -65°C and a solution of *n*-butyllithium (25 ml, 1.6 M in hexane, 40 mmol) was added via syringe. The addition proceeds at a rate that kept the internal temperature below -60°C . When addition was complete, the brown solution was stirred at about -65°C for 30 mins. The anhydrous *N*-formylpiperidine (5 ml, 45 mmol) was added quickly by syringe to the reaction mixture, which was then allowed to warm gently to the ambient temperature overnight. The reaction mixture was cooled to 0°C in an ice water bath, hydrochloric acid (100 ml, 6M) was added slowly to the mixture, where the yellow precipitate was formed. The mixture was stirred at 0°C for 45 mins then filtered immediately under vacuum through a sintered-glass funnel. The solid was washed with water (150 ml) and dried in vacuum desiccator overnight. Yield: 5 g, 70%.

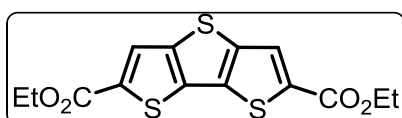


$^1\text{H NMR}$ (400 MHz, CDCl_3 , 298K): δ (ppm): 10.12 (s, 2H).

Dithieno[3,2-*b*:2'3'*d*]thiophene-2,6-dicarboxylic acid diethyl ester (**3**):

To the 500-ml two necked round-bottom flask equipped with a magnetic stir bar, nitrogen inlet rubber septum, **2** (8.0 g, 26.9 mmol) was suspended in anhydrous *N,N'*-dimethylformamide (250 ml), potassium carbonate (9.65 g, 69.8 mmol) and ethyl-2-mercaptoacetate (6 ml, 55 mmol) were added to the slurry, causing a slight exotherm. The reaction mixture was stirred under nitrogen atmosphere at ambient temperature for three days. After three days, the dark solution was poured into a beaker containing 500 ml of water stirred with a magnetic stir bar, where the yellow precipitate was formed.

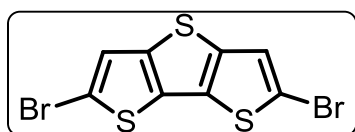
The suspension was extracted with CH₂Cl₂ (3 x 250 ml). The red organic layer was washed with brine solution (4 x 500 ml) and dried over anhydrous Na₂SO₄. The solvent was reduced to 100 ml by rotary evaporator, where the yellow color solid was begun to form. The solid was further filtered under vacuum by Buchner funnel, washed with water (100 ml) and dried in vacuum desiccator for overnight (7-8 mm Hg, silica gel desiccant with moisture indicator) to give crude diester. Yield: 6.5 g, 74%.



¹H NMR (400 MHz, CDCl₃, 298K): δ (ppm): 8.03 (s, 2H); 4.44 (q, 4H); 1.42 (t, 6H).

2,6-dibromo dithieno[3,2-b;2',3'-d]thiophene (4):

To the suspension of **3** (2.5 g 7.3 mmol), 40 ml of 1M aqueous solution of LiOH was added. The reaction mixture was refluxed for 3h and water was added to give a clear brownish solution. Excess N-bromosuccinimide (6.28 g, 35.3 mmol) was added and the reaction mixture was stirred overnight in ambient temperature. The crude mixture was extracted with CH₂Cl₂. The organic layer was washed with saturated NaHCO₃ and brine solution and dried over anhydrous Na₂SO₄. After the solvent was removed under reduced pressure, the residue was precipitated in ethanol and filtered to give white solid. Yield: 1.7 g, 85%.

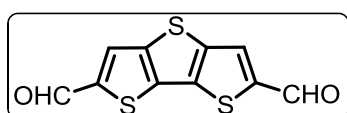


¹H NMR (400 MHz, CDCl₃, 298K): δ (ppm): 7.28 (s, 2H).

Dithieno[3,2-b;2',3'-d]thiophene-2,5-dicarboxaldehyde (5):

To the solution of **4** (0.5 g, 1.41 mmol) in 50 ml dry THF at -78 °C *n*-butyllithium (4.4 ml, 1.6 M in hexane, 5.64 mmol) was added drop wise. The temperature was maintained as such for 3h under the same condition. Then, *N,N'*-dimethylformamide (DMF) (3 ml,

4.23 mmol) was added. The reaction mixture was warmed up to room temperature and stirred over night to ambient temperature. The reaction mixture was quenched with HCl solution in ice cool condition. Yellowish color precipitate appeared, which was kept in same temperature for another 30 mins. The precipitate was filtered through Buckner funnel and washed with water and dried in vacuum desiccator for overnight to give dialdehyde (**5**). Yield: 0.3 g, 40%.



$^1\text{H NMR}$ (400 MHz, CDCl_3 , 298K): δ (ppm): 10.02(s, 2H);
8.01 (s, 2H).

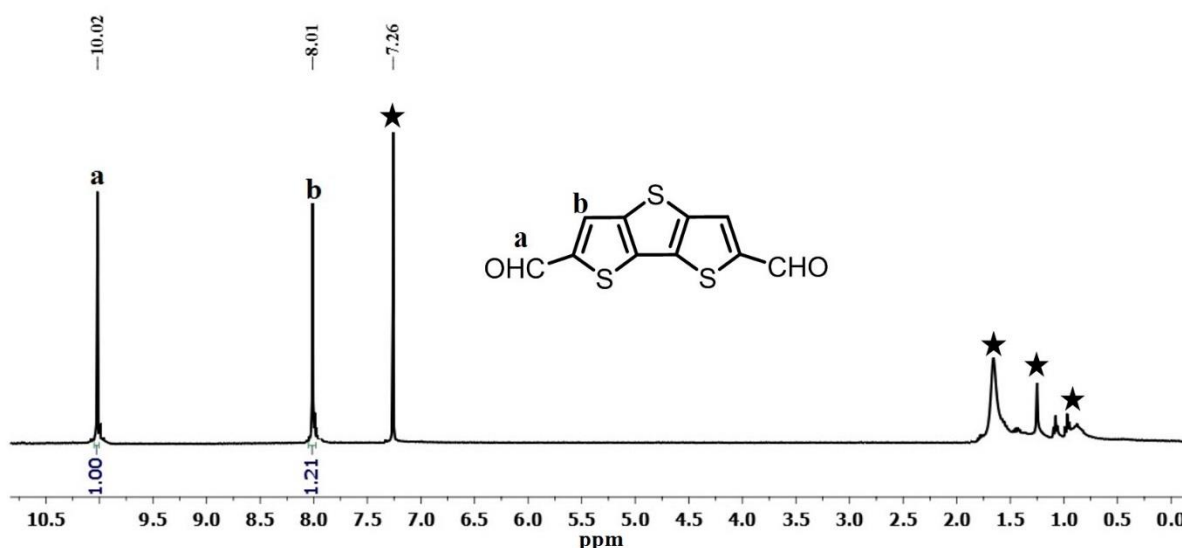
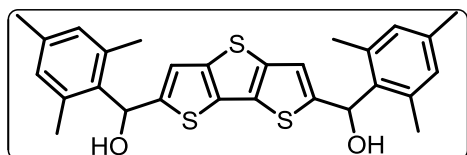


Figure 2.3.1: $^1\text{H NMR}$ spectrum of **5** in CDCl_3 . “Asterisk symbols are for impurities”

5,5'-Bis-(mesitylhydroxymethyl)-dithienothiophene (**6**):

To the solution of **4** (0.7 g, 3.5 mmol) in 50 ml dry THF, *n*-butyllithium (5ml, 1.6 M in hexane, 7.8 mmol) was added slowly at -78°C under inert atmosphere. The reaction mixture was allowed to stir for 1h. Mesityldehyde (1.154 g, 7.8 mmol) in 30 ml dry THF was added dropwise at 273K. The mixture was allowed to warm to room temperature and stirred for overnight. To the reaction mixture, 75 ml of saturated NH_4Cl solution was

added and extracted with diethyl ether. The organic layer was washed with brine solution and dried over Na_2SO_4 . After evaporation the crude mixture was subjected to silica gel column chromatography (100-200 mesh). A pink color band eluted with ethyl acetate/hexane (15:85, V/V) was identified as **6**. Yield: 0.65 g, 65%.



^1H NMR (400 MHz, CDCl_3 , 298K): δ (ppm): 6.83 (s, 4H); 6.74 (s, 2H); 6.45 (s, 2H); 2.47 (s, 1H); 2.32(s, 12H); 2.26(s, 6H).

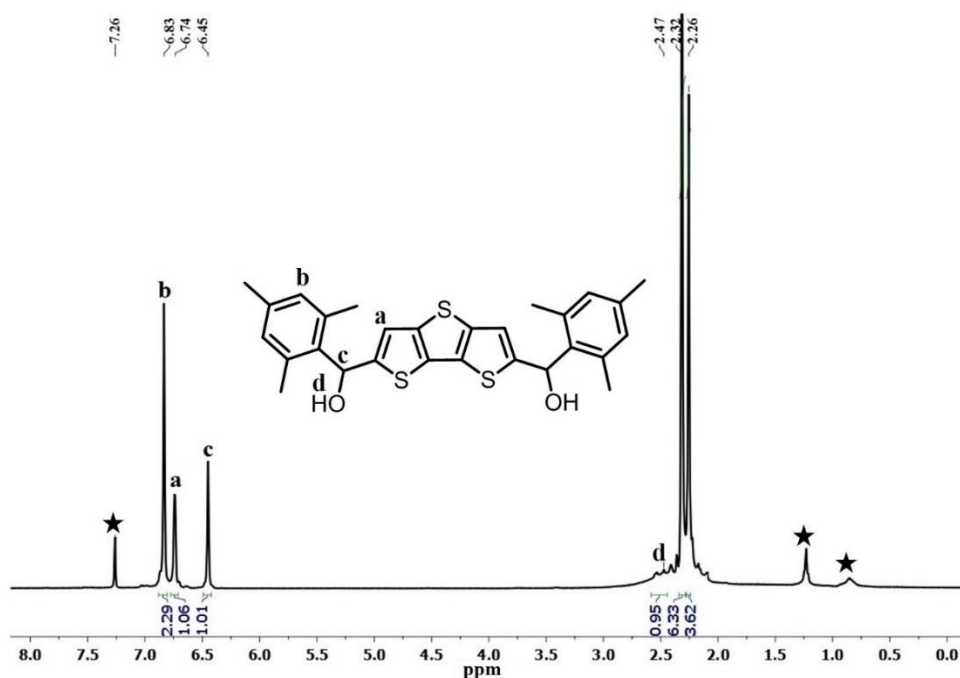
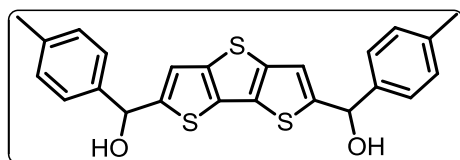


Figure 2.3.2: ^1H NMR spectrum of **6** in CDCl_3 . “Asterisk symbols are for impurities”

5,5'-Bis-(tolylhydroxymethyl)-dithienothiophene (**7**):

Dibromo dithienothiophene (**4**), (0.5 g, 2.6 mmol) in dry THF (40 ml), *n*-butyllithium (10 ml, 1.6 M in hexane, 7.8 mmol) and *p*-tolualdehyde (1.20 ml, 7.8 mmol) were mixed in 10 ml dry THF under similar condition as maintained above. The crude diol (**7**) was subjected to silica gel column chromatography (100-200 mesh). A pink color band eluted with ethyl acetate/hexane (17:83, V/V) was identified as diol (**7**). Yield: 0.47 g, 65%.



^1H NMR (400 MHz, CDCl_3 , 298K): δ (ppm):
 7.36 (d, $J=5.1$ Hz, 4H); 7.19 (d, $J=5.1$ Hz, 4H);
 7.02 (s, 2H); 6.05 (s, 2H); 2.52 (s, 2H); 2.36 (s,

6H).

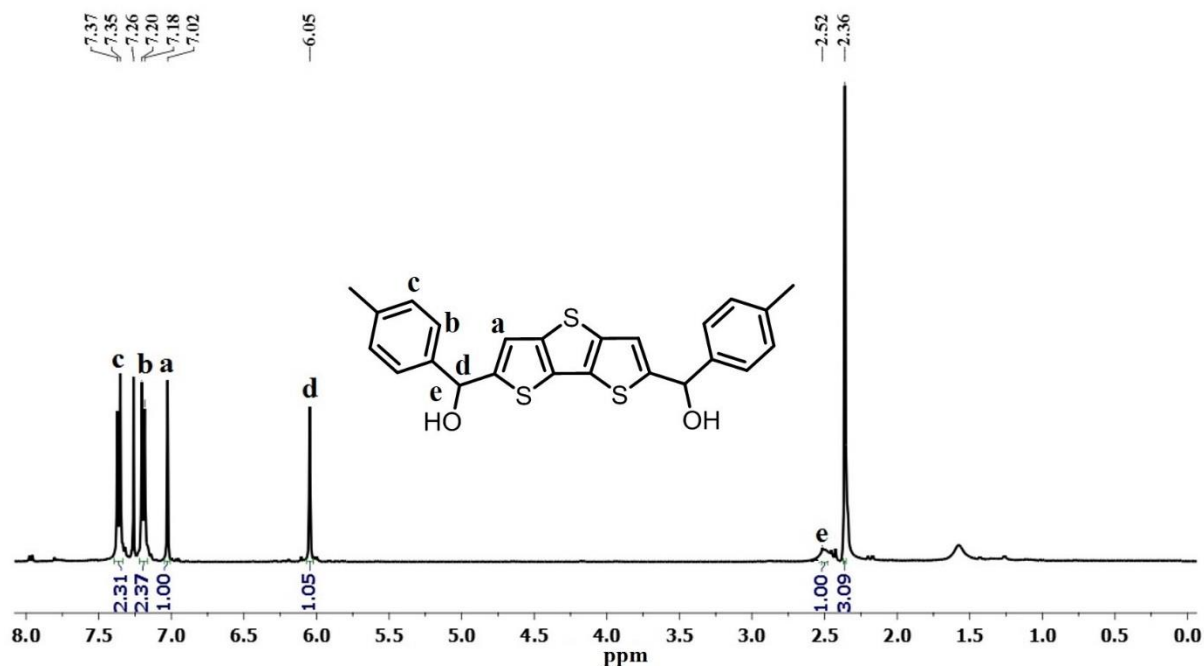
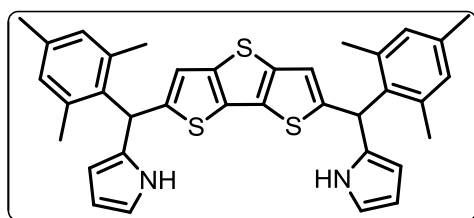


Figure 2.3.3: ^1H NMR spectrum of **7** in CDCl_3

5,5'-Bismesityl-2,2'-dithienothiophenetetrapyrane (**8**):

To the diol (**7**) (0.5 g, 1.01 mmol), pyrrole (3.66 ml, 56.5 mmol) was added. The mixture was degassed by bubbling with nitrogen gas. To this mixture, TFA (0.03 ml 0.38 mmol) was added and the resulting mixture was stirred in dark condition for 30 min in room temperature. After completion of reaction, 100 ml of CH_2Cl_2 was added in open air condition and the mixture was neutralized with 100 ml of 0.1 M NaOH solution. Organic layer was separated, twice washed with water and dried over anhydrous Na_2SO_4 . The solvent and excess pyrrole were removed by vacuum. The crude product was purified by

silica gel column chromatography (100-200 mesh) with ethyl acetate/hexane (8:92, V/V) and identified as **8**. Yield: 0.43 g, 90%.



^1H (400 MHz, CDCl_3 , 298K): δ (ppm): 7.85 (brs, 2H); 6.85 (s, 4H); 6.65 (d, $J=3.7$ Hz, 2H); 6.62 (s, 2H); 6.16 (d, $J=3.7$ Hz, 2H); 6.03 (d, $J=3.7$ Hz, 2H); 5.99 (s, 2H); 2.27 (s, 12H); 2.12 (s, 6H).

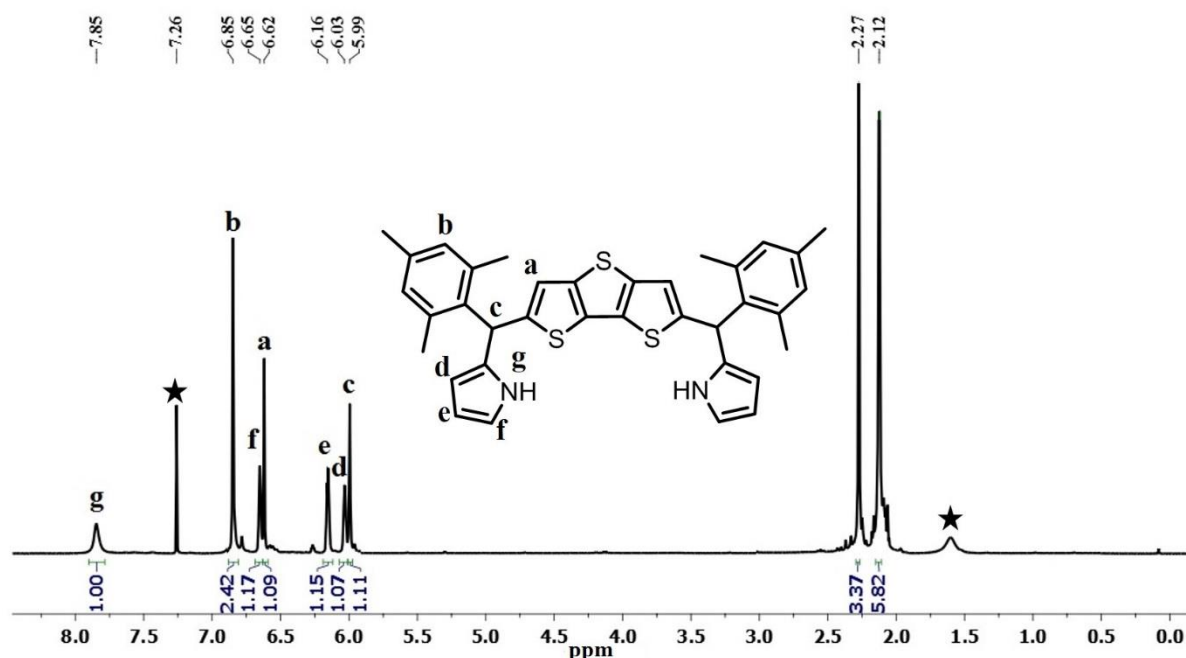
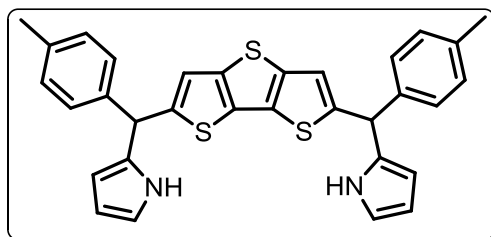


Figure 2.3.4: ^1H NMR spectrum of **8** in CDCl_3 . “Asterisk symbols are for impurities”

5,5'-Bistolyl-2,2'-dithienothiophenetetrapyrane (**9**):

Diol (**7**) (0.5 g 1.15 mmol) and pyrrole (3 ml) with TFA (0.007 ml, 0.1 mmol) were mixed under similar reaction condition as mentioned above. The crude product was purified by using silica gel column chromatography (100-200 mesh) with ethyl acetate/hexane (9:91, V/V) and identified as **9**. Yield: 0.45g, 92%.



^1H NMR (400 MHz, CDCl_3 , 298K): δ (ppm): 7.99 (brs, 2H); 7.27 (m, 8H); 7.03 (s, 2H); 6.77 (d, 2H); 6.28 (d, 2H); 6.11 (d, 2H); 5.73 (s, 2H); 2.46 (s, 6H).

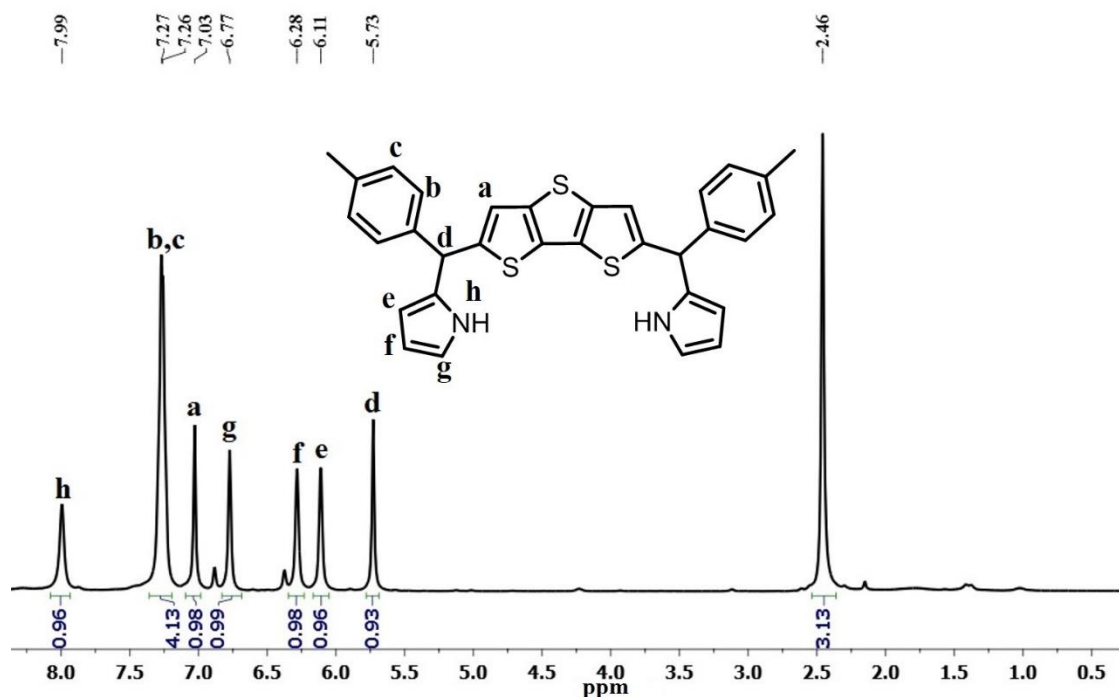
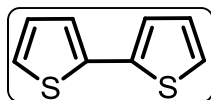


Figure 2.3.5: ^1H NMR spectrum of **9** in CDCl_3

Synthesis of 2,2'-bithiophene (**10**):

To a solution of thiophene (1 g, 12 mmol) in 1:1 mixture of dry ether (20 ml) and dry THF (20 ml), *n*-butyllithium (8.4 ml, 1.6 M in hexane, 13 mmol) was added at -70°C and the resulting mixture was allowed to stir for 2h at same temperature. After 2h, anhydrous CuCl_2 (2.88 g, 21 mmol) was added to the above mixture and quenched with saturated NH_4Cl solution (25 ml) at 0°C . The reaction mixture was extracted with ethyl acetate. Organic layer was washed with brine solution and the crude product was purified

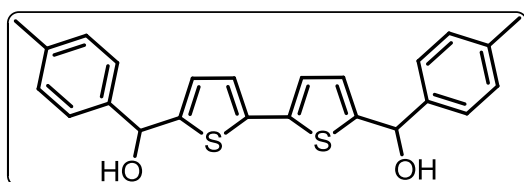
by silica gel column (100-200 mesh) chromatography. A colorless solution eluted with *n*-hexane identified as **10**. After evaporation it gave light blue solid. Yield: 0.32 g 30%.



^1H NMR (400 MHz, CDCl_3 , 298K): δ (ppm): 7.73 (d, 2H);
7.68 (m, 2H); 7.17 (d, 2H),

5,5'-bis-(mesitylhydroxymethyl)-2,2'-bithiophene (11):

To a solution of *N,N,N',N'*-tetramethylethylenediamine (TMEDA) (2.7 ml, 18 mmol) in dry THF (40 ml), *n*-butyllithium (11 ml, 1.6 M in hexane, 1 mmol) was added followed by 2,2'-bithiophene (1 g, 6 mmol) under nitrogen atmosphere. The reaction mixture was stirred at room temperature for 45 min and heated under reflux for another 1h. The reaction mixture was then allowed to attain room temperature slowly. Mesitylaldehyde (2.2 ml, 15 mmol) in dry THF was added dropwise to the reaction mixture at 0 °C. The resulting mixture was allowed to stirred at room temperature for overnight. The reaction was quenched by using saturated NH_4Cl (100 ml) solution and extracted with diethyl ether. The crude product was purified by silica gel column chromatography (100-200 mesh). A yellow band was eluted with ethyl acetate/hexane (20:80, V/V) afforded desired diol (**11**) as pale yellow color solid. Yield: 0.74 g, 54%.



^1H NMR (400 MHz, CDCl_3 , 298K): δ
(ppm): 6.92 (d, $J=3.7$ Hz, 2H); 6.87 (s, 4H),
6.52 (d, 2H); 6.46 (d, $J=3.7$ Hz, 2H); 2.34
(s, 12H); 2.29 (s, 6H).

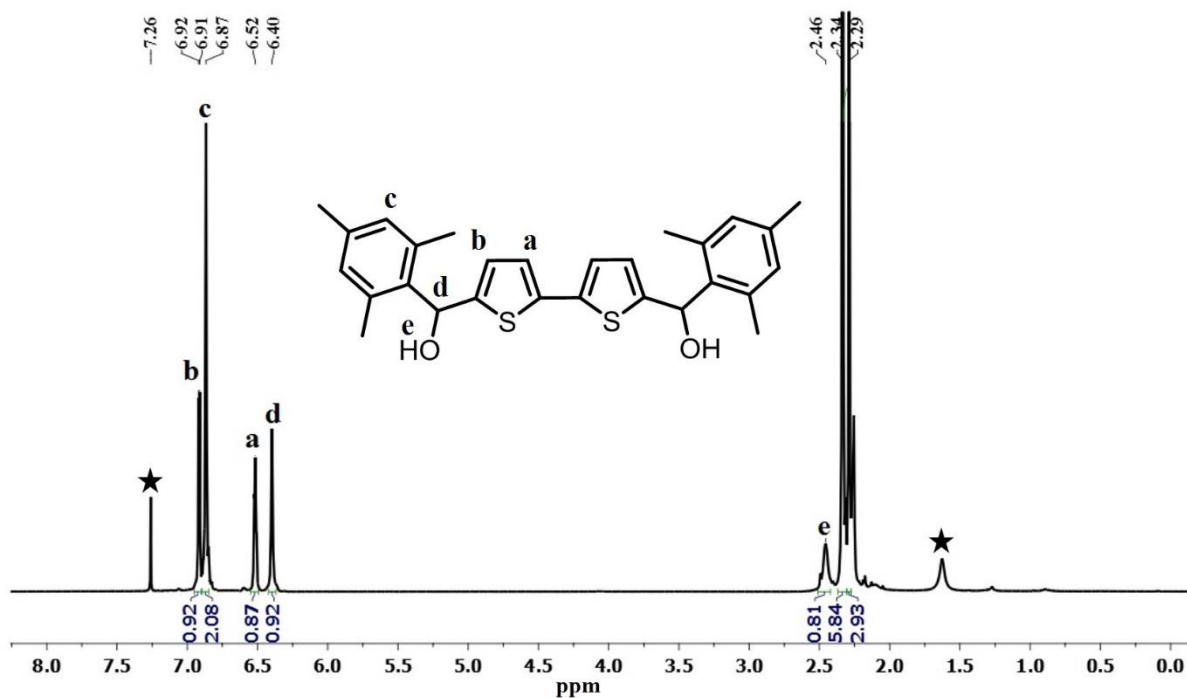
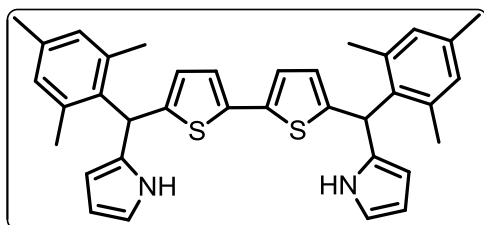


Figure 2.3.6: ^1H NMR spectrum of **11** in CDCl_3 . “Asterisk symbols are for impurities”

5,5'-Bismesityl-2,2'-bithiophenetetrapyrane (**12**):

Bithiophene diol **11** (0.5 g, 1mmol), pyrrole (3 ml, 43 mmol) and TFA (0.008 ml, 0.1 mmol) under same reaction condition as mentioned for the synthesis of **8**. The crude product was purified by using silica gel column chromatography (100-200 mesh) with ethyl acetate/ hexane (8:92, V/V) and identified as **12**. Yield: 0.46 g, 94% yield.



^1H NMR (400 MHz, CDCl_3 , 298K): δ (ppm): 7.88 (brs, 2H); 6.93 (d, 2H); 6.88 (s, 4H); 6.74 (d, 2H); 6.67 (d, 2H); 6.18 (d, 2H); 6.11 (d, 2H); 6.03 (s, 2H); 2.20 (s, 6H); 2.08 (s, 12H).

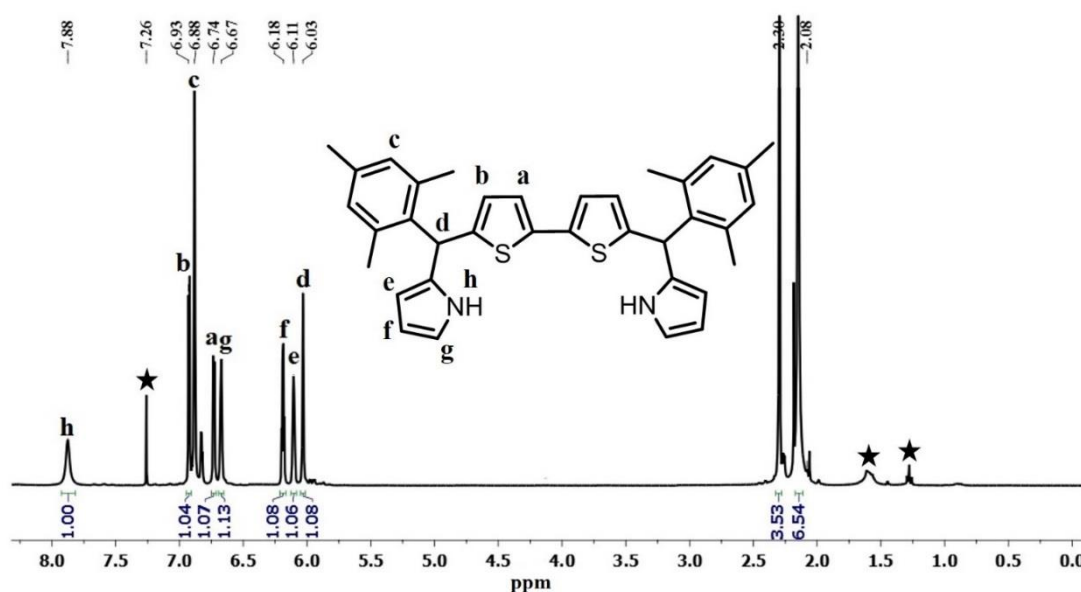
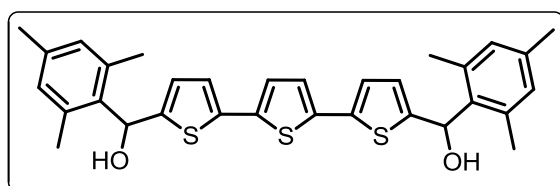


Figure 2.3.7: ^1H NMR spectrum of **12** in CDCl_3 . “Asterisk symbols are for impurities”

5,5'-bis(mesitylhydroxymethyl)-2,2':5,2''-terthiophene (**13**):

2,2':5,2'' terthiophene (1 g, 4 mmol), N,N,N',N' -tetramethylethylene diamine (1.8 ml, 12 mmol), *n*-butyllithium (7.8 ml, 1.6 M in hexane, 12 mmol) and mesitaldehyde (1.07 ml, 12 mmol) in 15 ml dry THF were mixed under similar condition as mentioned for the synthesis of **11**. The crude product was purified by silica gel (100-200 mesh) column chromatography. Pale yellow color band eluted with ethyl acetate/hexane (25:75, V/V) considered as desire diol (**13**). Yield: 0.65g, 51%.



^1H NMR (400 MHz, CDCl_3 , 298K): δ (ppm): 6.98 (s, 2H); 6.95 (d, 2H); 6.88 (s, 4H); 6.54 (d, 2H); 6.41 (s, 2H); 2.35 (s, 12H); 2.30 (s, 6H).

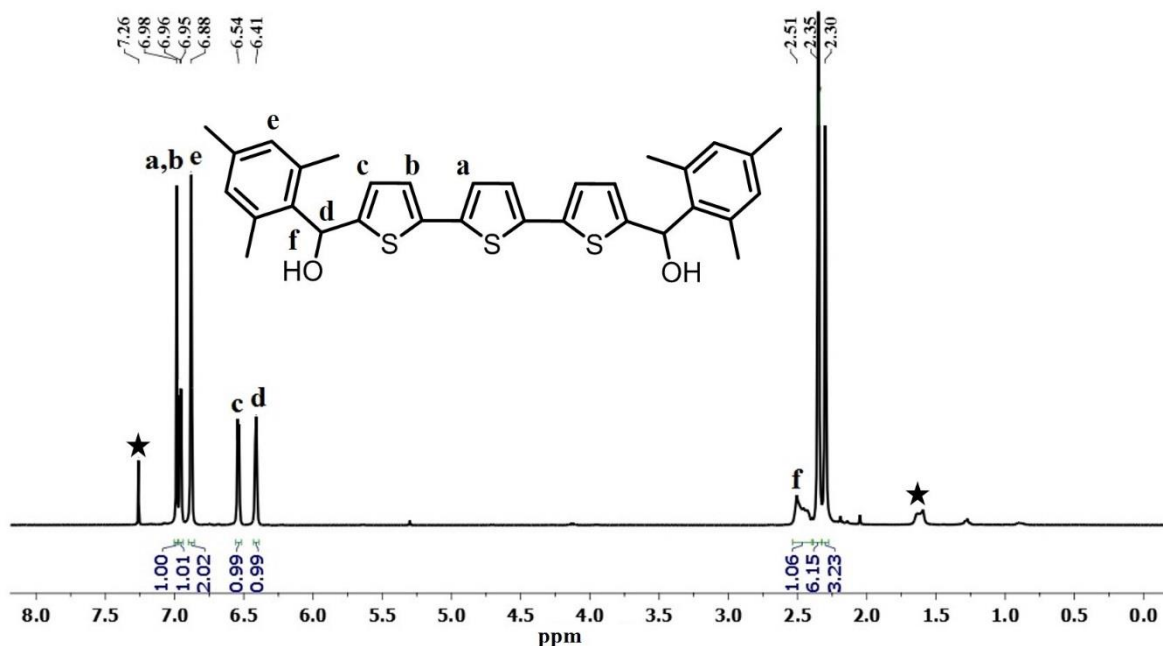
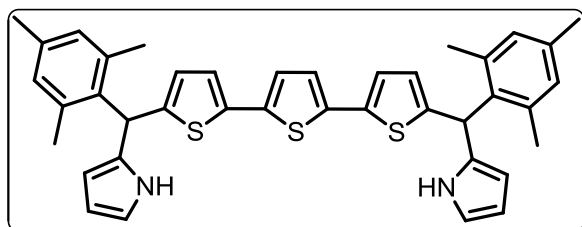


Figure 2.3.8: ^1H NMR spectrum of **13** in CDCl_3 . “Asterisk symbols are for impurities”

5,18-dimesityl-24,25,26-trithiapentapyrrane (**14**):

Diol **13** (0.5 g, 0.92 mmol), and pyrrole (2.6 ml, 36 mmol) and TFA (0.007 ml, 0.09 mmol) were mixed under similar reaction condition as mentioned for the synthesis of **12**. The crude product was purified by silica gel (100-200 mesh) column chromatography. The light yellow color compound was eluted with ethyl acetate/hexane (8:92) identified as desired pentapyrrane (**14**). Yield: 0.35 g, 85%.



^1H NMR (400 MHz, CDCl_3 , 298K):

δ (ppm): 7.80 (brs 2H); 6.98 (d, $J=4.3$ Hz, 2H); 6.94 (s, 2H); 6.88 (s, 4H); 6.76 (m, $J=4.3$ Hz, 2H); 6.68 (d, $J=3.2$ Hz, 2H); 6.19 (m, $J=3.2$ Hz, 2H); 6.11 (d, $J=3.2$ Hz, 2H); 6.04 (s, 2H); 2.29 (s, 2H); 2.15 (s, 12H).

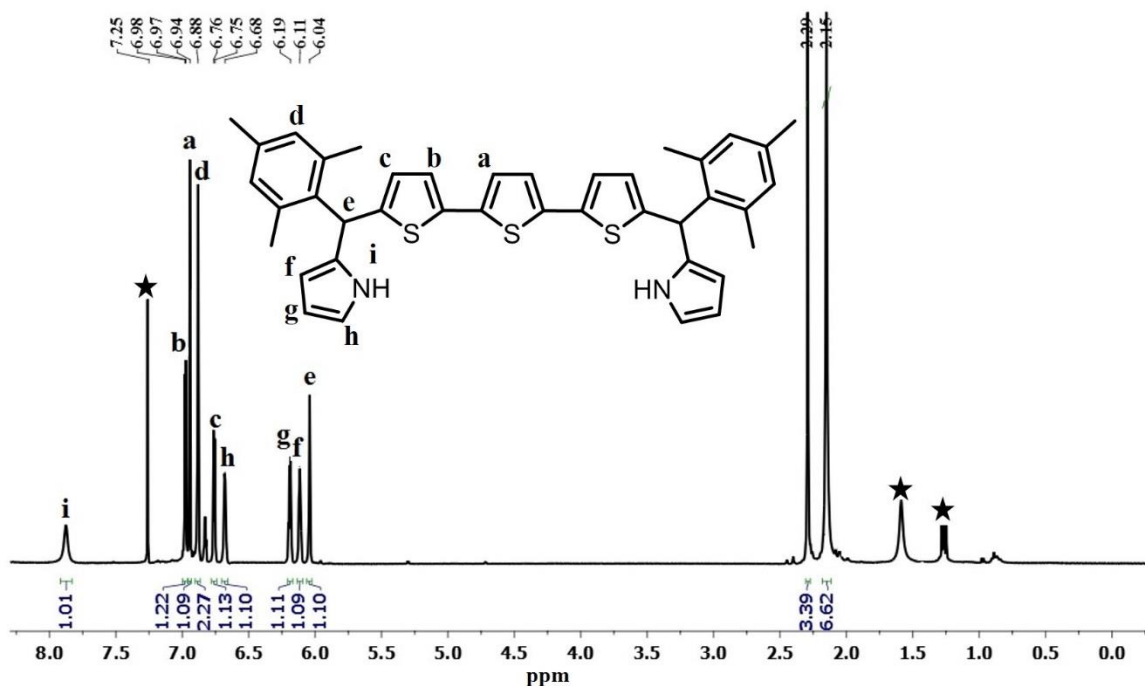
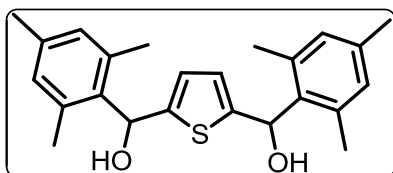


Figure 2.3.9: ¹H NMR spectrum of **14** in CDCl₃. “Asterisk symbols are for impurities”

2,5-Bis(mesitylhydroxymethyl)thiophene (**15**):

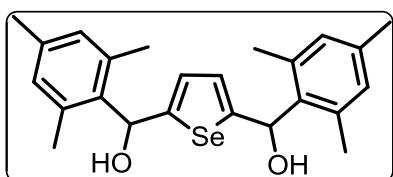
To a solution of N,N,N',N'-tetramethylethylene diamine (8.05 ml, 53.5 mmol) in dry hexane (160 ml), *n*-butyllithium (35.67 ml, 1.6 M in hexane, 53.5 mmol) was added followed by thiophene (1.43 ml, 17.8 mmol) under nitrogen atmosphere. The reaction mixture was stirred for 1h and later refluxed for another 1h. The reaction mixture was then allowed to attain room temperature. Mesitaldehyde (6.56 ml, 44.57 mmol) in dry THF (25 ml) was added dropwise to the ice cooled condition. The resultant solution was stirred at ambient temperature overnight. The reaction was quenched with 100 ml saturated NH₄Cl solution and extracted with diethyl ether. Organic layer was washed with brine solution and dried over anhydrous Na₂SO₄. After evaporation of the solvent, the crude product was purified by silica gel (100-200 mesh) column chromatography. The diol (**15**) was eluted with ethyl acetate/hexane (20:80, V/V) and obtained as pale yellow color solid. Yield: 4.1 g, 56%.



^1H NMR (400 MHz, CDCl_3 , 298K): δ (ppm): 6.82 (s, 4H); 6.39 (s, 2H); 6.36 (s, 2H); 2.29 (s, 12H); 2.25 (s, 6H); 1.65 (brs, 2H).

2,5-bis(mesitylhydroxymethyl) selenophene (**16**):

Selenophene (2.5 g, 19 mmol), N,N,N'N' -tetramethylethylene diamine (8.6 ml, 57 mmol) in dry *n*-hexane, *n*-butyllithium (38 ml, 1.6 M in hexane, 57 mmol) and mesitaldehyde (8.5 ml 57 mmol) in 35 ml of dry THF were mixed under similar reaction condition as mentioned above. The crude product was purified by silica gel (100-200 mesh) column chromatography. A light pink color band was eluted with ethyl acetate/hexane (22:78, V/V) identified as diol (**16**). Yield: 1.7 g, 48%.



^1H NMR (400 MHz, CDCl_3 , 298K): δ (ppm): 6.82 (s, 4H); 6.52 (s, 1H); 6.50 (s, 1H); 6.35(s, 1H); 6.34(s, 1H); 2.31(s, 12H); 2.25 (s, 6H); 1.62(brs 2H).

5,10-dimesityl-16-thiatripyrrane (**17**):

Diol (**15**) (1 g, 2.63 mmol), pyrrole (7.3 ml, 105.28 mmol) and TFA (0.06 ml, 0.79 mmol) were mixed under similar conditions as mentioned for the synthesis of **12**. The crude product was purified by silica gel (100-200 mesh) column chromatography. The light yellow color compound was eluted with ethyl acetate/hexane (3:97, V/V) and identified as tripyrrane (**17**). Yield: 0.78 g, 90%

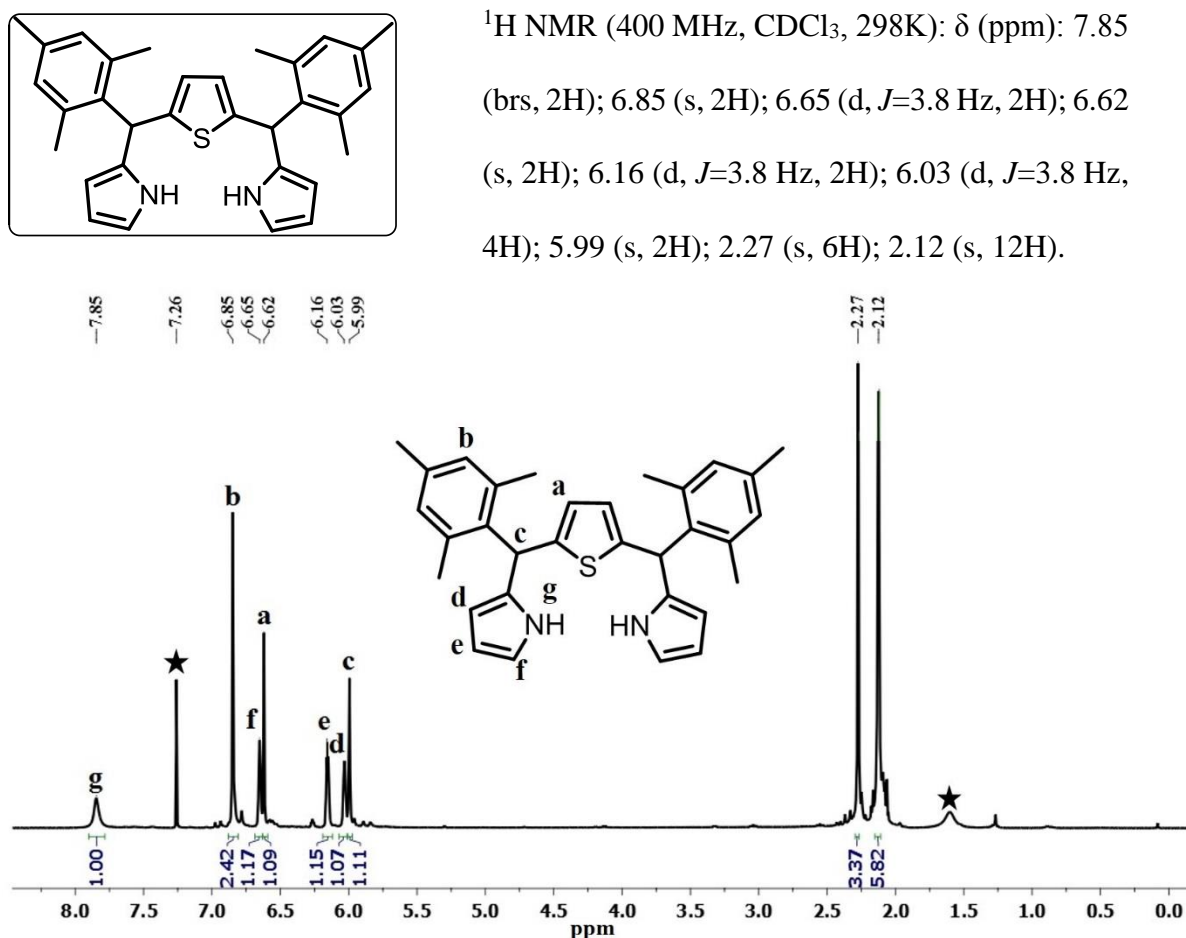
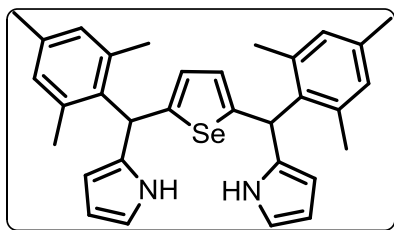


Figure 2.3.10: ¹H NMR spectrum of **17** in CDCl₃. “Asterisk symbols are for impurities”

5,10-dimesityl-16-selenatripyrrane (**18**):

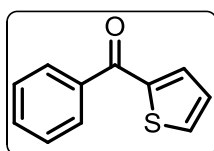
Diol (**16**) (1 g, 2.34 mmol), pyrrole (5 ml, 93.6 mmol) and TFA (0.018 ml, 0.23 mmol) were mixed under similar conditions as mentioned for the synthesis of **12**. The crude product was purified by silica gel (100-200 mesh) column chromatography. The light yellow color compound was eluted with ethyl acetate/hexane (5:95, V/V) and identified as tripyrrane (**18**). Yield: 0.78 g, 90%.



^1H NMR (400 MHz, CDCl_3 , 298K): δ (ppm): 7.84 (brs, 2H); 6.83 (s, 4H); 6.79 (s, 2H); 6.61 (s, 2H); 6.12-6.16 (m, 2H); 6.05 (s, 2H); 6.0 (s, 2H); 2.24 (s, 6H); 2.12 (s, 12H).

2-Benzoyl thiophene (19):

In a 250 ml two-necked round bottom flask equipped with a magnetic stirrer and reflux condenser, the anhydrous AlCl_3 (10 g, 75 mmol) was mixed with 30 ml of dry CH_2Cl_2 and the resultant suspension was stirred for 15 min. A solution of thiophene (6 g, 71 mmol) and benzoyl chloride (10 g, 75 mmol) with 25 ml dry CH_2Cl_2 was added slowly with syringe, over a period of 3.5 h. The resultant solution was stirred for overnight at ambient temperature. The mixture was refluxed for 2 h, cooled, poured on ice water and extracted with diethyl ether. The organic layer was washed with Na_2CO_3 water and dried over anhydrous Na_2SO_4 . After evaporation of the solvent, the product was recrystallized over petroleum ether and afforded the desired product **19**. Yield: 6.3 g, 80%.



^1H NMR (400 MHz, CDCl_3 , 298K): δ (ppm): 7.85-7.83 (m, 2H). 7.69-7.43 (m, 5H); 7.09 (d, 1H).

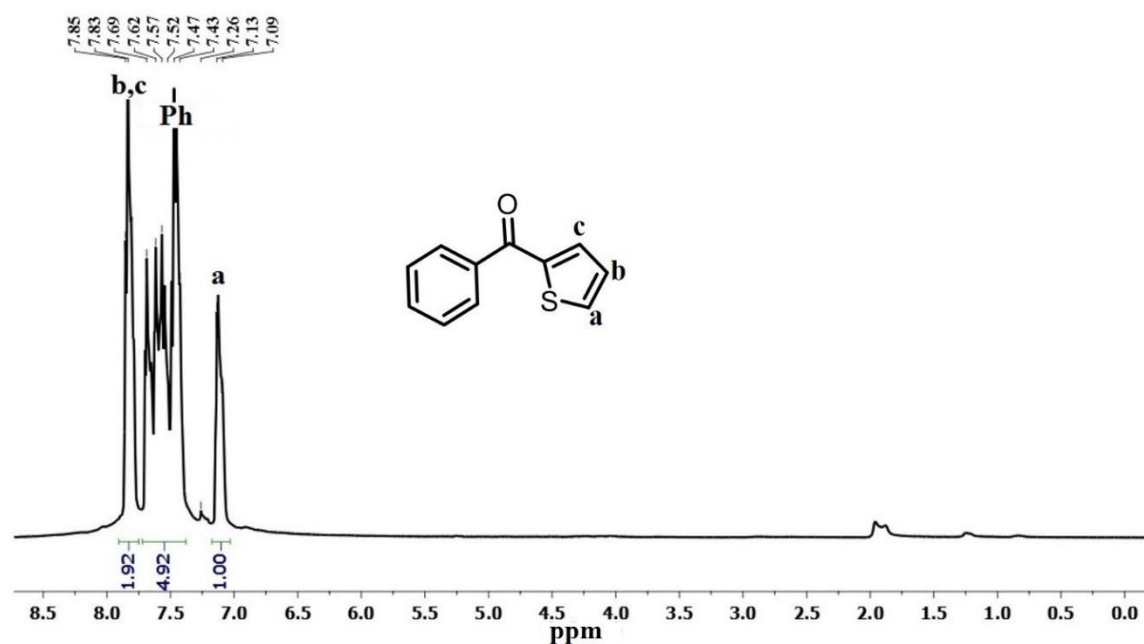
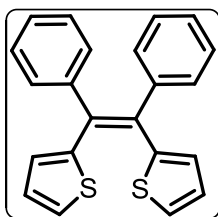


Figure 2.3.11: ¹H NMR spectrum of **19** in CDCl₃.

1,2-diphenyl-1,2-dithienylethene (**20**):

In a 250 ml two-necked round-bottom flask equipped with a magnetic stirrer and reflux condenser under nitrogen atmosphere, activated Zn powder (3.0 g, 46 mmol) was mixed with dry THF (80 ml) and resultant mixture was stirred for 20 min. TiCl₄ (2.52 ml, 23 mmol) was added slowly in ice cool condition. The resultant solution was stirred at room temperature for 30 mins and refluxed for another 3h. The mixture was cooled to 0 °C and 2-benzoyl thiophene (**19**) (1 ml, 5.3 mmol) in dry THF (25 ml) was added slowly and the resultant solution was refluxed for another 12h. The progress of the reaction was monitored by TLC analysis. The reaction mixture was quenched with 10% aqueous NaHCO₃ solution and extracted with diethyl ether. The crude product was purified by silica gel (100-200 mesh) column chromatography. A pale yellow color band was eluted with hexane and identified as **20**. Yield: 2.6 g, 56%.



^1H NMR (400 MHz, CDCl_3 , 298K): δ (ppm): 7.40-7.41 (m, 10H); 7.06 (d, $J=5.8$ Hz, 2H); 6.71(t, $J=5.8$ Hz, 2H); 6.37 (d, $J=5.8$ Hz, 2H);

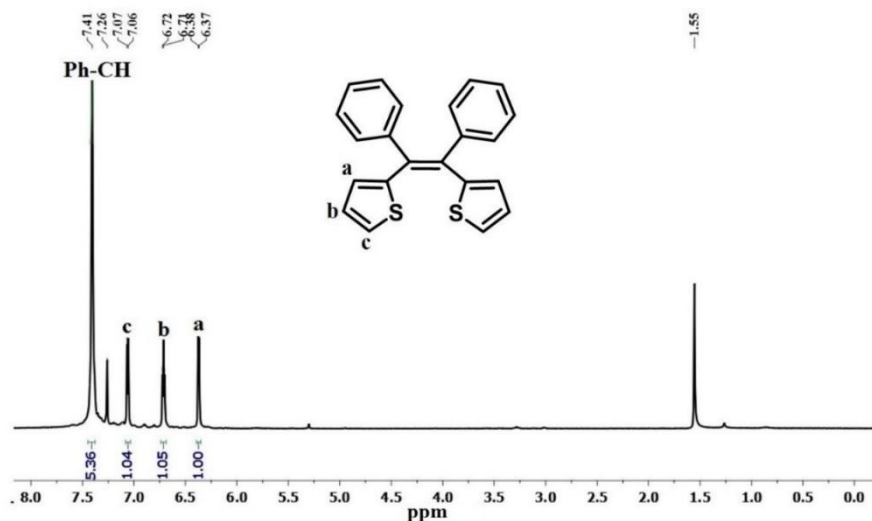
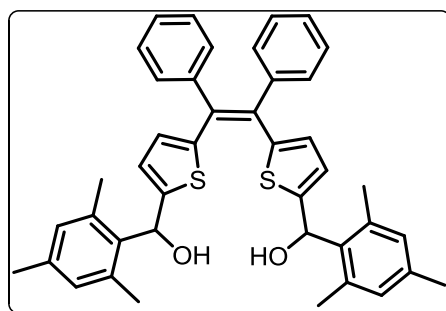


Figure 2.3.12: ^1H NMR spectrum of **20** in CDCl_3 .

2,11-bis(mesitylhydroxymethyl) 1,2-diphenyl-1,2-dithienylethene (**21**):

In a 100 ml two necked round bottom flask equipped with reflux condenser, **20** (1 g, 2.9 mmol) was placed into it under nitrogen atmosphere. Dry hexane (30 ml) was added and the resulting solution was stirred for 15 min under nitrogen atmosphere. N,N,N',N' -tetramethylethylene diamine (1.3 ml, 7.8 mmol) solution was added and resultant mixture was stirred for another 5 min. *n*-Butyllithium (10 ml, 1.6 M in hexane, 29 mmol) solution was added and the resultant solution was stirred at room temperature for 1h. The mixture was refluxed for 1h. The mesitaldehyde (1.32 ml, 7.8 mmol) with dry THF (10 ml) was added slowly to the reaction mixture at room temperature. Resultant mixture was stirred for overnight at room temperature. After workup with diethyl ether and water, the crude product was purified through silica gel column chromatography (100-200 mesh). A pale yellow color solution was eluted with ethyl acetate/hexane (20:80, V/V) and identified as **21**. Yield: 0.54 g, 60%



$^1\text{H NMR}$ (400 MHz, CDCl_3 , 298K): δ (ppm):
 7.35-7.30 (m, 6H); 7.07 (s, 2H); 6.88-6.78 (m,
 12H); 2.51 (s, 1H); 2.28 (s, 6H); 2.25 (s, 6H);
 2.21 (s, 6H).

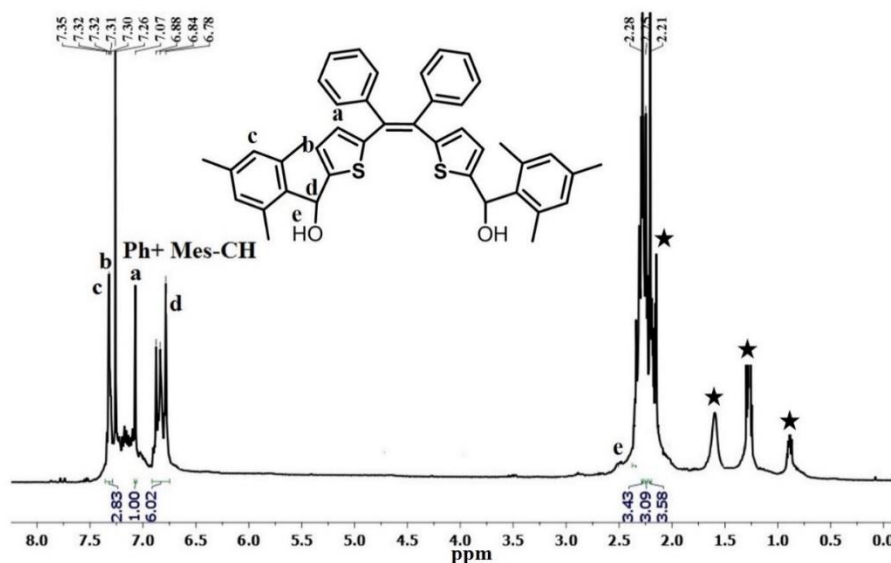


Figure 2.3.13: $^1\text{H NMR}$ spectrum of **21** in CDCl_3 . “Asterisk symbols are for impurities”

2.4 References:

1. Furniss, B. S. Vogel's text book of practical organic chemistry, Ed: ELBS and Longmann, 4th edition, **1978**.
2. Riddick, J. A.; Bunger, W. B. Organic solvents in technique of organic chemistry, 3rd edition, Wiley. New York, **1970**.
3. Sheldrick, G. M. SHELXS-93f, Universitat Gottingen, **1993**.

4. Brandenburg, K. [or Brandenburg, K. & Putz, H., or Brandenburg, K. & Berndt, M.] (1999). *DIAMOND*. Crystal Impact GbR, Bonn, Germany.
[avoid using the reference 'W. T. Pennington (1999). *J. Appl. Cryst.* 32, 1028-1029' as this is just a software review].
5. Macrae, C. F., Edgington, P. R., McCabe, P., Pidcock, E., Shields, G. P., Taylor, R., Towler, M. & van de Streek, J. (2006). *J. Appl. Cryst.* 39, 453-457.
6. Becke, A. D. *J. Chem. Phys.* **1993**, 98, 1372-1376.
7. Lee, C.; Yang, W.; Parr, R. G. *Phys. Rev. B.* **1988**, 37, 785-789.
8. Krygowski, T. M.; Cyranski, M. K. *Chem. Rev.* **2001**, 101, 1385-1390.
9. Schleyer, P. V. R.; Maerker, C.; Dransfeld, A.; Jiao, H.; Hommes, N. J. R. *J. Am. Chem. Soc.* **1996**, 118, 6317-6320.

CHAPTER 3

Core-modified Porphyrin and Hexaphyrins: Syntheses and Structural Diversity

3.1	Introduction	61-71
3.1.1	Porphyrin with five and six <i>meso</i> carbon bridges	62-66
3.1.2	Hexaphyrin with five and six <i>meso</i> carbon bridges and fused derivatives	67-71
3.2	Objective of the work	71
3.3	Results and Discussion	72-80
3.3.1	Syntheses	72-73
3.3.2	Spectral characterization	73-80
3.3.2.1	Mass spectrometric analysis	73-74
3.3.2.2	NMR analysis	74-77
3.3.2.3	Electronic spectral analysis	77-78
3.3.2.4	Single crystal X-ray analysis	78-80
3.4	Core-modified fused Hexaphyrin	81-86
3.4.1	Synthesis	81
3.4.2	Spectral characterizations	81-86
3.4.2.1	Mass spectrometric analysis	81-82
3.4.2.2	NMR analysis	82-85
3.4.2.3	Electronic spectral analysis	85-86
3.5	Conclusion	86
3.6	Experimental Procedures	87-89
3.6.1	Synthesis of 38	87-88
3.6.2	Synthesis of 42	88-89
3.7	References	89-92

3.1 Introduction

Porphyrins are 18π aromatic units, where four pyrrolic units are linked by four *meso*-carbon bridges. These are widely studied as functional pigments and found potential application in materials,^[1,2] medicine^[2] and catalysis.^[4-6] The next higher analogues in the series is the expanded porphyrins which contains more than 18π electrons in its conjugated pathway. As compared to porphyrins, this can be achieved by (i) maintaining the four heterocyclic rings and increasing the *meso*-carbon bridges (**A**);^[7] (ii) maintaining the *meso* carbon bridges and increasing the heterocyclic rings (**B**);^[8] (iii) Increasing the heterocyclic rings and reducing the *meso* carbon bridges (**C**)^[9] and (iv) increasing both the heterocyclic rings and *meso*-carbon bridges (**D**).^[10] The details are shown in the Chart-3.1. In this chapter, we mainly focus on the last part and wish to highlight the synthesis, spectral and structural characterization of core-modified pentaphyrin and core-modified fused hexaphyrin derivatives.

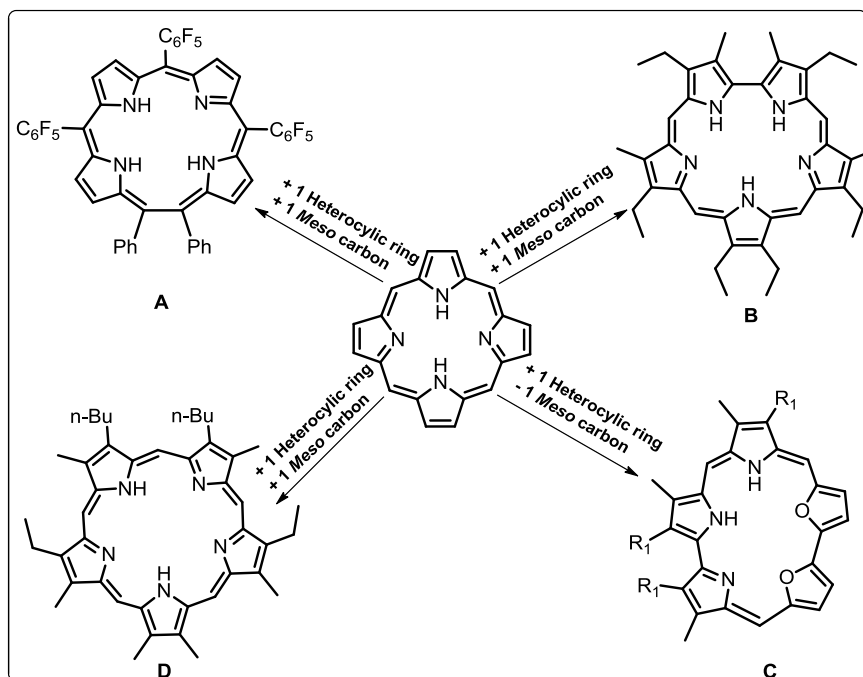
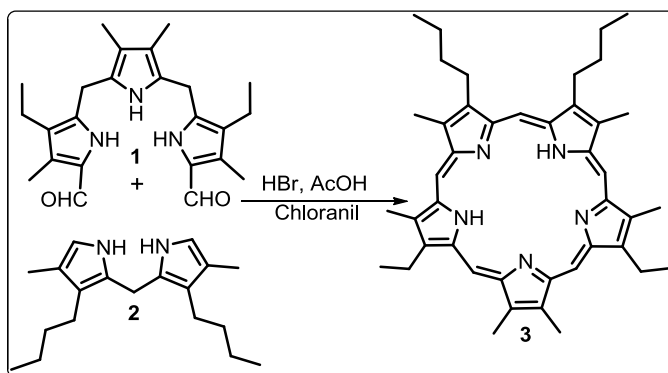


Chart 3.1

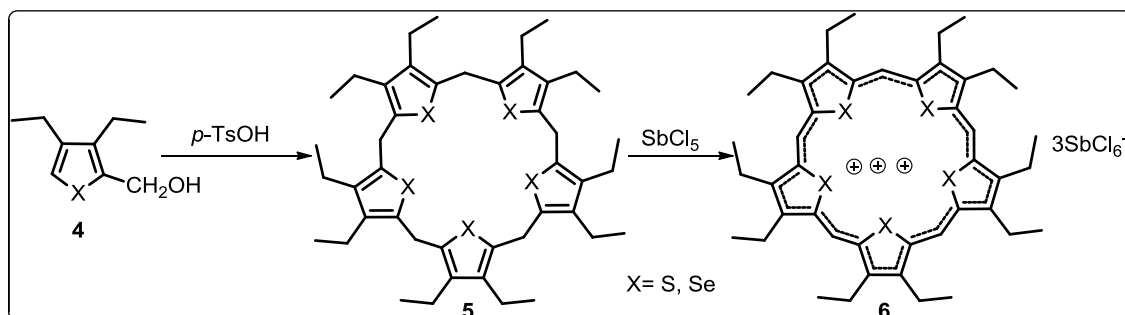
3.1.1 Pentaphyrin with Five and Six *meso*-carbon Bridges

Pentaphyrins are macrocyclic system where five heterocyclic units are linked by five *meso*-carbon bridges. The first pentaphyrin was reported by Rexhausen and Gossauer in 1983.^[10] They mainly adopted acid-catalyzed condensation reaction by using 33% HBr in Acetic acid. The tripyrrane dialdehyde (**1**) and dipyrromethane (**2**) were mixed in the presence of acid-catalyst followed by oxidation with chloranil to afford the *meso*-free [22] π pentaphyrin(1.1.1.1.1) (**3**) in 31% yield (Scheme 3.1). Later, Dolphin and co-workers have also demonstrated the synthesis of **3** by using trifluoroacetic acid (TFA) as acid-catalyst and partially introduced *meso*-aryl units in the macrocyclic framework.



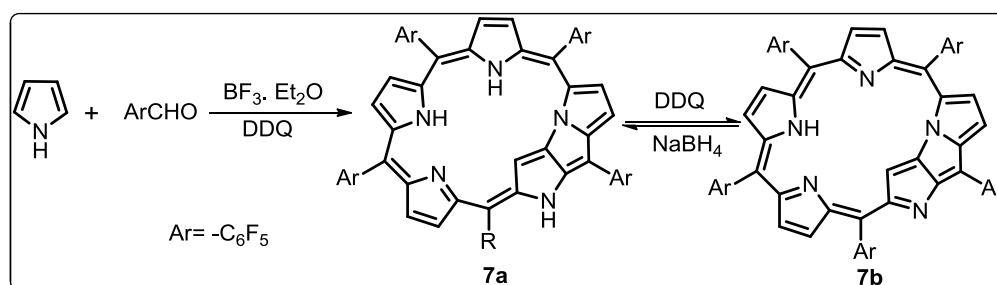
Scheme 3.1: Synthesis of **3**.

The pentathia- (**6a**) and pentaselenapentaphyrin (**6b**) were reported by Vogel and co-workers in 2001 (Scheme 3.2).^[11,12] The 3,4-diethyl-2-hydroxymethyl-thiophene (**4a**) / selenophene (**4b**) was subjected to self-condensation reaction in the presence of *p*-toluenesulphonic acid (*p*-TSA) to form the respect porphyrinogen **5a** / **5b** in 16% (**5a**) / 3% (**5b**) yield. The porphyrinogen (**5a** / **5b**) was further oxidized by SbCl₅, where the aromatic tricationic form of **6a** / **6b** was isolated as its antimony salt.



Scheme 3.2: Synthesis of **6**.

The first *meso*-aryl pentaphyrin (**7**) was synthesized by Osuka and co-workers.^[13,14] They adopted modified Lindsey type condition, where the pyrrole and pentafluorobenzaldehyde in the presence of $\text{BF}_3 \cdot \text{Et}_2\text{O}$ as acid-catalyst followed by oxidation with DDQ to afford two pentaphyrins (**7a** / **7b**) in approximately 15% yield (Scheme 3.3). The spectral and structural analyses of **7a** revealed $[24]\pi$ anti-aromatic circuit, whereas **7b** exhibited $[22]\pi$ aromatic character. Both **7a** and **7b** were interconvertible by simple oxidation and reduction reaction by using DDQ and NaBH_4 . The **7a** and **7b** were further treated with Rh(I) salts and stabilized the respective metal ion.

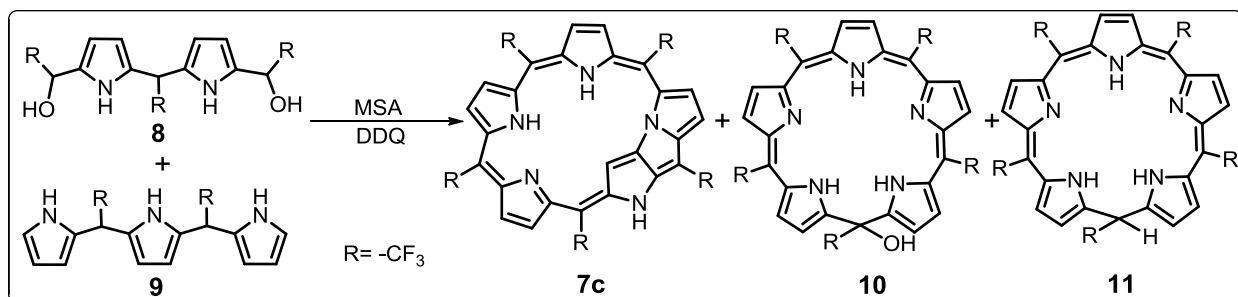


Scheme 3.3: Synthesis of **7**.

The same group have also highlighted the synthesis of *meso*-trifluoromethyl substituted pentaphyrins.^[15] The methanesulfonic (MSA) acid-catalyzed condensation of dipyrrene dicarbinol (**8**) with tripyrrane (**9**) followed by oxidation obtained $[24]\pi$ pentaphyrin (**7c**),

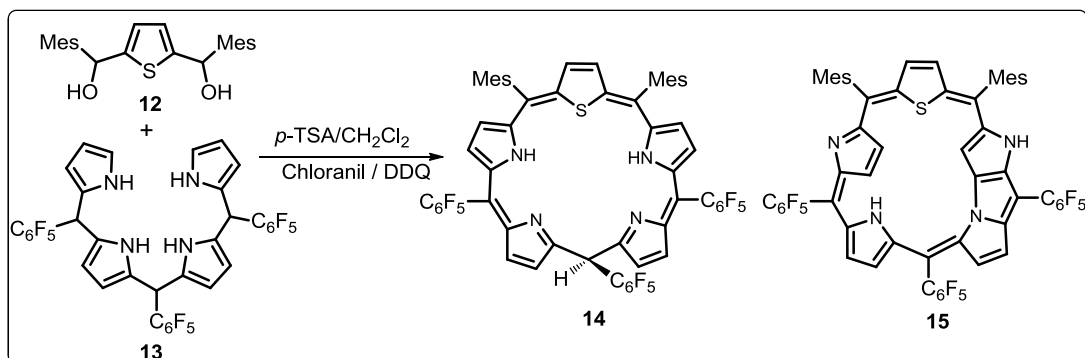
meso-hydroxy substituted calix[5]phyrin (**10**) and calix(5)phyrin (**11**) in 1.5% to 5% yield

(Scheme 3.4).



Scheme 3.4: Synthesis of **7c** and **10 - 11**.

The core-modified fused pentaphyrin was reported by our group in 2008.^[16] The 2,5-bis(mesitylhydroxymethyl)thiophene (**12**) and tetrapyrane (**13**) were treated in the presence of *p*-TSA followed by oxidation with chloranil afforded calixthia[5]phyrin (**14**) in 20% yield, however, in the presence of stronger oxidizing agent such as DDQ obtained non-aromatic N-fused [24] π thiapentaphyrin (**15**) in 15% yield (Scheme 3.5).

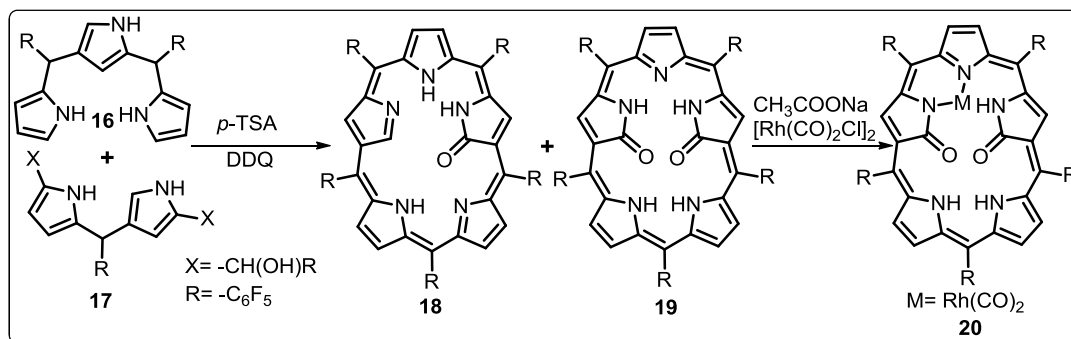


Scheme 3.5: Synthesis of **14 - 15**.

The confused pyrrole rings were introduced in pentaphyrins by Furuta and co-workers.^[17a]

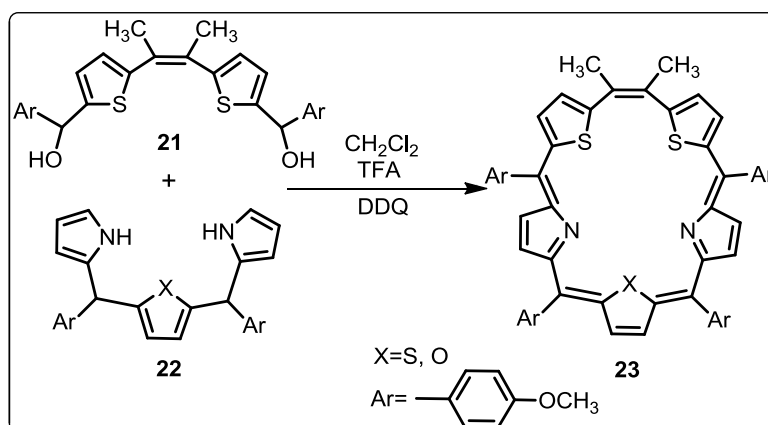
The *p*-TSA acid-catalyzed condensation of N-confused tripyrrane (**16**) and N-confused dipyrane dicarbonyl (**17**) followed by oxidation with DDQ afforded doubly N-confused mono oxo-pentaphyrin (**18**) and dioxo pentaphyrin (**19**) in 32% and 42% yield. The spectral

analyses of **18** and **19** were proved as $[22]\pi$ aromatic and the core of **19** was effectively utilized to stabilize Rh(I) ion (**20**) (Scheme 3.6). They have also described the synthesis of mono- and doubly-fused non-aromatic pentaphyrins.^[17b, 17c]



Scheme 3.6: Synthesis of **18-20**.

The pentaphyrins with six *meso*-carbons were introduced by Ravikanth and coworkers in 2015.^[18] The $[3+2]$ TFA acid-catalyzed condensation of butane-2,3-diyl-bisthiophene-2,5-diyl-bis(*p*-methoxyphenylmethanol) (**21**) with core-modified tripyrrane (**22**) followed by oxidation formed non-aromatic core-modified $[24]\pi$ pentaphyrin(2.1.1.1.1) (**23**) in 10% yield (Scheme 3.7). The protonated thiapentaphyrin (**23a**) derivative was further utilized to sense specifically the acetate ion.



Scheme 3.7: Synthesis of **23**.

So far, we have mainly focused on the synthesis of pentaphyrin macrocycles with five and above *meso*-carbon bridges. The pentaphyrin analogues with less than five *meso* carbon bridges are well-known in the literature which includes; (i) sapphyrin,^[8] N-confused sapphyrin,^[19] carba-sapphyrin,^[20] fused sapphyrin,^[21] Ozaphyrin^[22,23] and dehydropentaphyrin^[24] with four *meso* carbon bridges, (ii) isosmaragdyrin^[25] and smaragdyrin^[26] with three *meso* carbon bridges and (iii) orangarin^[27] with two *meso* carbon bridges (Chart 3.2). In this chapter, we wish to highlight the synthesis of pentaphyrin macrocycles with six *meso* carbon bridges, hence, the synthetic methodologies of these pentaphyrin analogues are not included in this section.

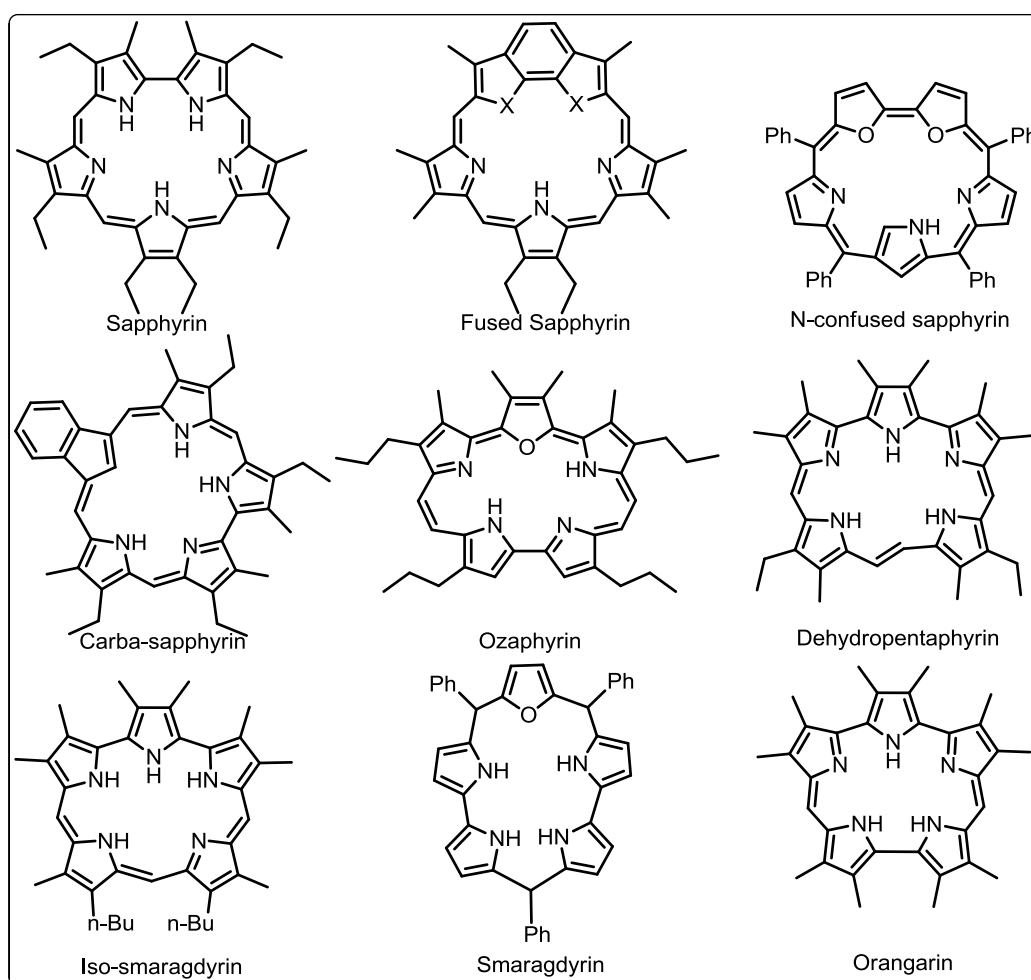
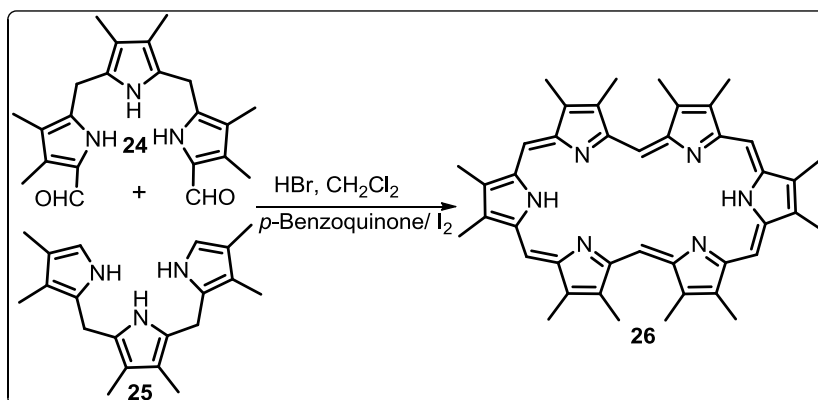


Chart 3.2: Pentaphyrin analogues with less than five *meso* carbon bridges.

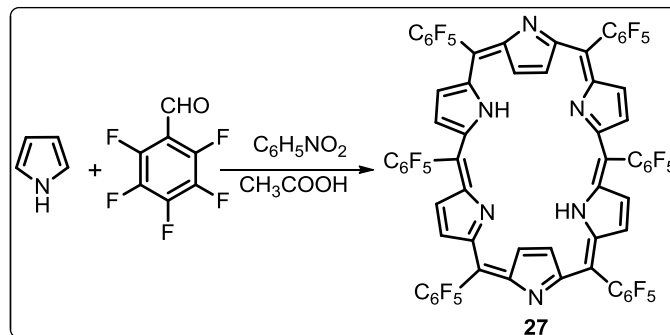
3.1.2 Hexaphyrin with Six *meso*-carbon Bridges and Fused derivatives

The first hexaphyrin with β -substituted derivative was reported by Gossauer and coworkers in 1983.^[28] They adopted [3+3] acid-catalyzed condensation reaction, where tripyrrane (**24**) and tripyrrane dialdehyde (**25**) were mixed in the presence of HBr as an acid-catalyst followed by oxidation with *p*-benzoquinone / I₂ and afforded [26] π hexaphyrin(1.1.1.1.1.1) (**26**) in 20% yield (Scheme 3.8). The presence β -substitution prevents the pyrrolic ring inversion and also exhibits cis-trans isomerization.



Scheme 3.8: Synthesis of **26**.

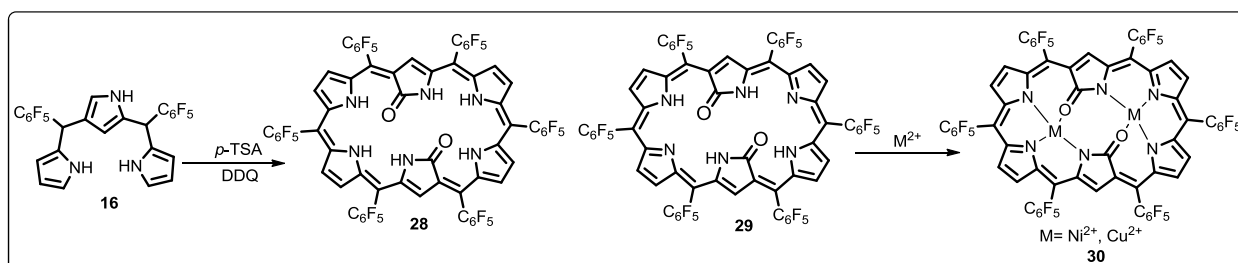
Later, Dolphin and coworkers described the synthesis of *meso*-aryl hexaphyrin by using *meso*-phenyl tripyrrane with benzaldehyde in the presence of TFA followed by oxidation with chloranil.^[29] The synthesized macrocycle was turned out to be unstable due to presence less sterically hindered *meso*-phenyl substituents. The stable *meso*-aryl hexaphyrin was reported by Cavaleiro and coworkers through Rothmund type synthetic strategy.^[30a] The pyrrole was added dropwise to the refluxing mixture of pentafluorobenzaldehyde in acetic acid and nitrobenzene and obtained the aromatic [26] π hexaphyrin(1.1.1.1.1.1) (**27**) in 1% yield (Scheme 3.9). The spectral and structural analyses revealed that two of the pyrrolic rings in **27** were inverted in the macrocyclic framework.



Scheme 3.9: Synthesis of **27**.

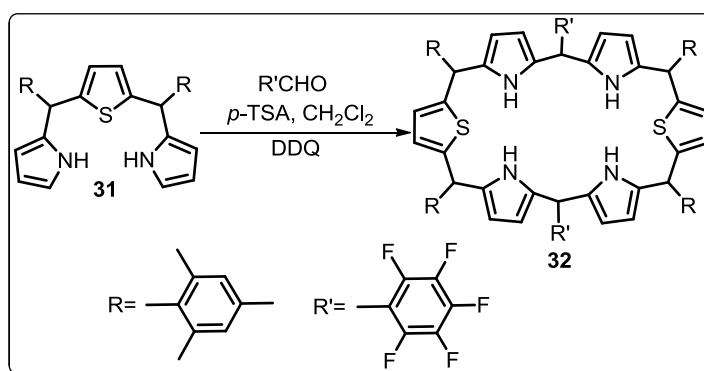
By using similar starting materials as mentioned above, Osuka and co-workers were synthesized the hexaphyrin **27** in 16 – 20% along with porphyrin and other expanded porphyrin derivatives in the presence $\text{BF}_3 \cdot \text{Et}_2\text{O}$ as the acid-catalyst followed by oxidation with DDQ.^[30b] Same group have also demonstrated the synthesis of various *meso*-aryl substituted hexaphyrin (**27**) derivatives by MSA along with DDQ oxidation by using 5-pentafluorophenyl dipyrane with aryl aldehydes / 5-aryl dipyrane with electron withdrawing aryl aldehydes as precursors.^[31]

The doubly N-confused hexaphyrin was reported by Furuta and coworkers. The N-confused tripyrrane (**16**) was treated with pentafluorobenzaldehyde in the presence of *p*-TSA followed by oxidation with DDQ afforded non-aromatic $[28]\pi$ (**28**) and aromatic $[26]\pi$ dioxo hexaphyrin (**29**) in 7 and 10% yield (Scheme 3.10). The core of **30** was further utilized to stabilize Ni^{II} (**30a**) and Cu^{II} (**30b**) metal ions.^[32]



Scheme 3.10: Synthesis of **28** - **30**.

The core-modified *meso*-aryl hexaphyrin was reported by our group.^[33] The macrocycle **32** was obtained from *p*-TSA acid-catalyzed condensation of thiatripyrrane **31** with pentafluorobenzaldehyde followed by oxidation in 10% yield (Scheme 3.11). In the freebase form, **32** was in figure-eight conformation. At partial protonated stage, two pyrrole rings were inverted and upon completely protonated state, four heterocyclic rings were inverted and maintained [26] π aromatic character in the solid state.



Scheme 3.11: Synthesis of **32**.

The syntheses of fused derivatives by using *meso*-aryl hexaphyrin were exclusively demonstrated by Osuka and co-workers. The mono- (**33**),^[34] doubly-fused [28] π hexaphyrin (**34**)^[35] and benzopyrane-fused [28] π hexaphyrin (**35**)^[36] were shown in Figure 3.1. The mono fused [28] π hexaphyrin (**33**) was obtained from refluxing toluene and pyridine mixture of [26] π hexaphyrin (1.1.1.1.1.1) (**27**) in 17% yield. The core is effectively used to stabilize Pd^{II} ions and the respective metal ion promotes Möbius aromatic character in the macrocyclic framework. The doubly fused [28] π hexaphyrin (**34**) was synthesized from **27** by refluxing toluene with excess amount of sodium acetate in 30% yield. By heating **27** in acetic acid afforded the formation of benzopyrane-fused [28] π hexaphyrin (**35**) in 27% yield and the spectral analysis revealed the Möbius aromatic character under wide range of

temperature. In addition, hexaphyrin fused with two anthracenes was also reported by Osuka and co-workers with flat and elongated π -conjugated network.^[37]

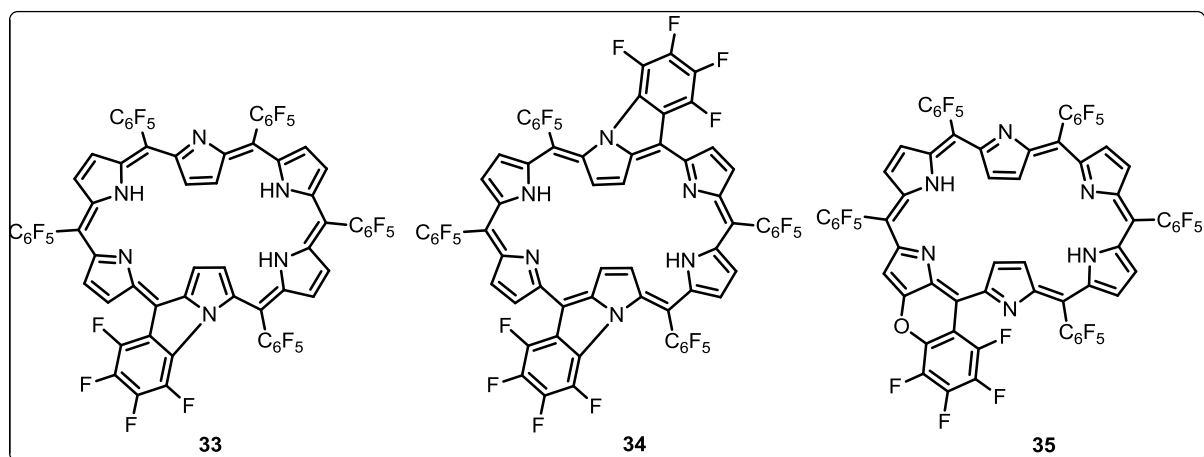


Figure 3.1: Molecular structures of **33** - **35**.

So far, we have highlighted the syntheses of hexaphyrin(1.1.1.1.1.1) macrocycle with six *meso*-carbon bridges and its fused analogues. The hexaphyrin analogues with less than six *meso* carbon bridges are also well-known in the literature which includes; (i) rubyrin^[38] and bronzaphyrin^[39] with four *meso* carbon bridges, (ii) rosarian^[40] with three *meso* carbon bridges, (iii) amethyrin^[26] and iso-amethyrin^[41] with two *meso* carbon bridges and (iv) cyclo[6]pyrrole^[42] without *meso* carbon bridge (Chart 3.3). This chapter is mainly focused on the synthesis of core-modified fused hexaphyrin with seven *meso* carbon bridges, hence, the synthetic methodologies of these hexaphyrin analogues are not included in this section.

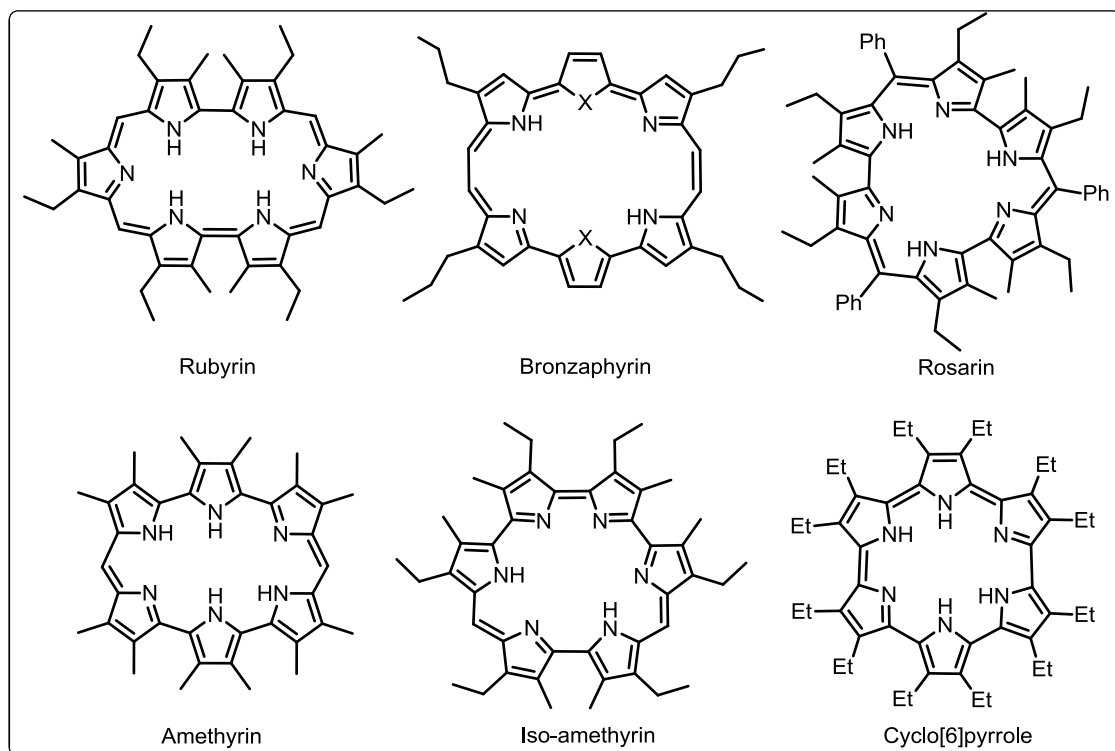


Chart 3.3: Hexaphyrin analogues with less than six *meso* carbon bridges.

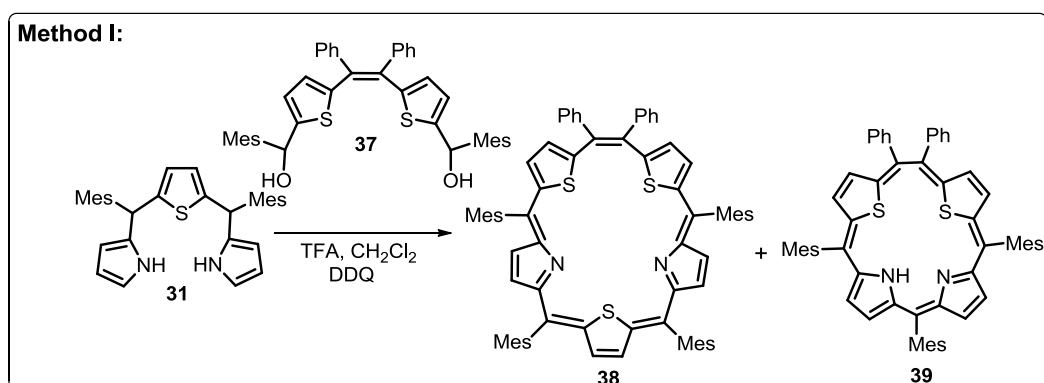
3.2 Objective of the work

Various pentaphyrin and its analogues with five and less number of *meso*-carbon bridges were well-established in the literature. In particular, the *meso*-aryl pentaphyrin derivatives were reported with fused tripentacyclic ring in the macrocyclic framework which restricts the coordination as well as binding properties of this ligand. On the other hand, the hexaphyrin macrocycles with six and less number of *meso*-carbon bridges were highlighted, however, the respective fused analogues are scarcely known in the literature. Thus, the main objective of this chapter is to introduce pentaphyrin with six *meso* carbon bridges and fused hexaphyrin with six *meso* carbon bridges. The protonated form of pentaphyrin analogue exhibits Möbius $[24]\pi$ aromatic character, whereas the hexaphyrin displays Hückel $[30]\pi$ aromaticity.

3.3 Results and Discussion

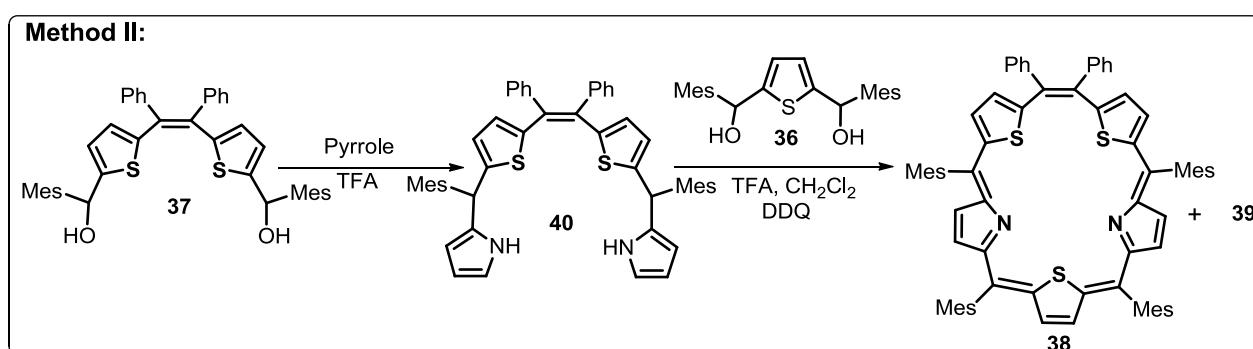
3.3.1 Syntheses

Basically, we adopted acid-catalyzed condensation methodology for the synthesis of desired pentaphyrin (**38**). In Scheme 3.12a, the required starting materials such as 5,10-dimesityl-16-thiatripyrrane (**31**) was synthesized by trifluoroacetic (TFA) acid-catalyzed condensation of 2,5-bis(mesitylhydroxymethyl)thiophene (**36**) with pyrrole.^[33] Whereas 5,5'-bis(mesitylhydroxymethyl)-1,2-diphenyl-1,2-di(thiophene-2-yl)ethene (**37**) was synthesized from respective 1,2-diphenyl-1,2-di(thiophene-2-yl)ethane with *n*-BuLi and mesitaldehyde.^[18] In the final step, the **31** and **37** were mixed in 1:1 ratio in the presence of TFA acid-catalyzed condensation followed by DDQ oxidation to obtain the crude product. The crude mixture was subjected through basic alumina followed by silica gel (100-200 mesh) column chromatographic purification. The first yellowish green band was eluted with 20% CH₂Cl₂/*n*-Hexane and identified as core-modified [24] π pentaphyrin(2.1.1.1.1) (**38**) in 10% yield. The second greenish band was eluted with 25% CH₂Cl₂/*n*-Hexane and identified as core-modified [20] π homoporphyrin(2.1.1.1.1) (**39**) in 9% yield.



Scheme 3.12a: Synthesis of **38**.

In Scheme 3.12b, the required starting material 1,2-diphenyl-1,2-di(thiophene-2-yl)ethene tetrapyrane (**40**) was achieved from **37** by TFA acid-catalyzed reaction with pyrrole in 60% yield. In the final step, the TFA acid-catalyzed condensation reaction of 1:1 mixture of **40** with **36** followed by DDQ oxidation to obtain the crude product. After column chromatographic purification, the compound **38** and **39** were obtained in 8% and 3% yield respectively (Scheme 3.12b).



Scheme 3.12b: Synthesis of **38**.

3.3.2 Spectral Characterization

3.3.2.1 Mass Spectrometric Analysis

The electron spray ionization (ESI) mass spectrometric analyses of **38** and **39** were shown in Figure 3.2 and 3.3. The molecular ion signals at m/z 1077.8893 [$M+1$] for **38** (Figure 3.2) and 865.2124 [$M+1$] for **39** (Figure 3.3) were consistent with exact composition of the macrocycles.

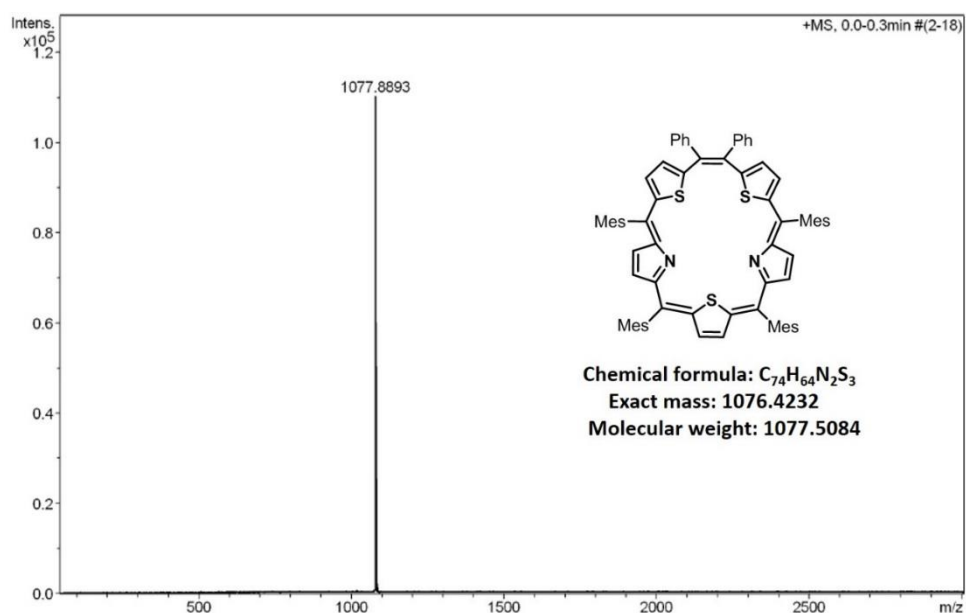


Figure 3.2: ESI-MS spectrum of **38**

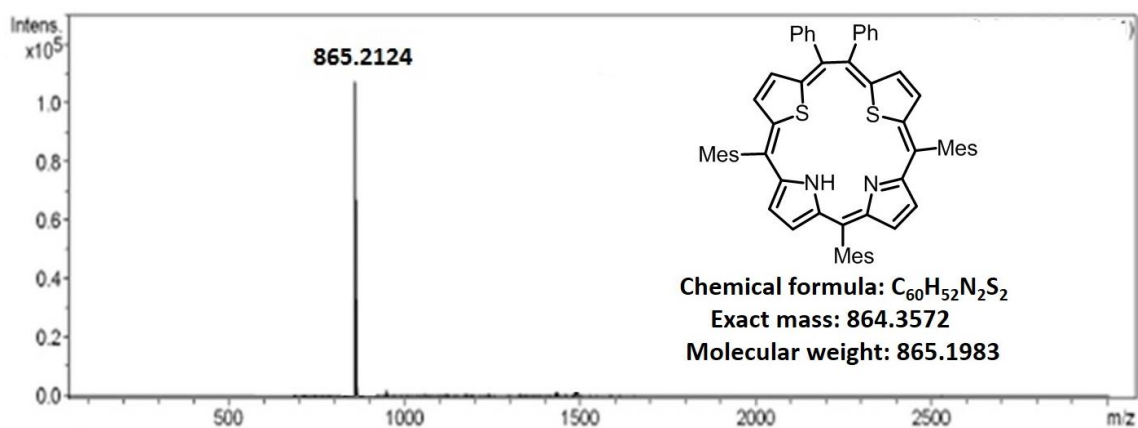


Figure 3.3: ESI-MS spectrum of **39**

3.3.2.2 NMR Analysis

The 1H NMR spectrum of **38** was recorded in CD_2Cl_2 and shown in Figure 3.4. The β -CH protons of pyrrole rings and thiophene units which are part of the ethene bridge are resonated as four doublets between 7.41 ppm and 6.35 ppm (b-e). These proton signals were further confirmed by 1H - 1H COSY correlation spectroscopy (Figure 3.5). The thiophene ring which

is opposite to the ethene bridge, is appeared as singlet at 7.86 ppm. The *meso*-phenyl and mesityl ring protons are observed as a multiplet between 7.12 and 6.95 ppm, whereas the *meso*-mesityl methyl protons are resonated as six singlet from 2.46 ppm to 1.97 ppm. Overall, the spectral pattern resembles typical Hückel [24] π non-aromatic character.

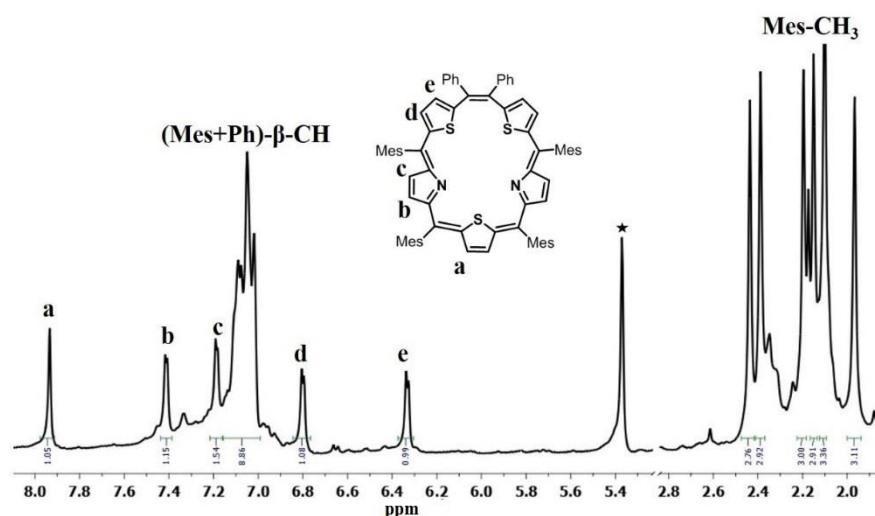


Figure 3.4: ^1H NMR spectrum of **38** in CD_2Cl_2

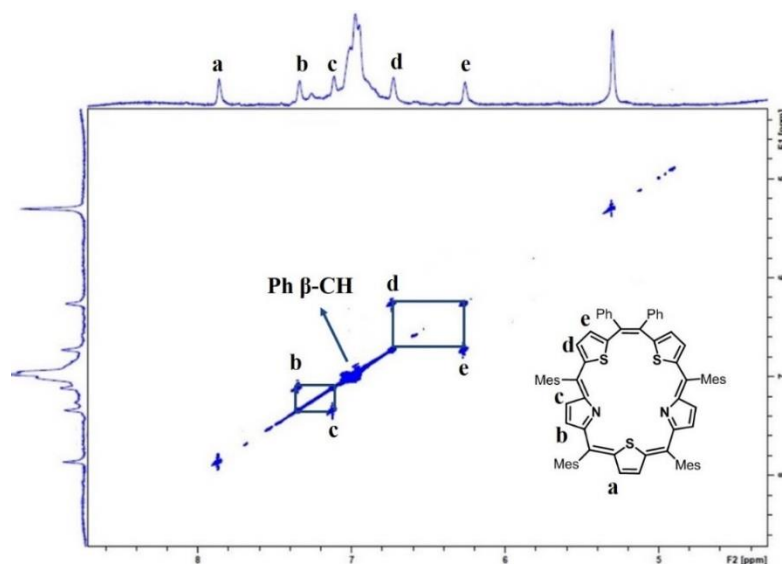


Figure 3.5: ^1H - ^1H COSY spectrum of **38** with correlation in pyrrole and thiophene rings as part of the ethene bridge

A drastic change was occurred during the protonation experiment of **38** with 4.5 equiv. of TFA in CD₂Cl₂ and shown in Figure 3.6. The titration experiment of was performed with dilute solution of TFA in CD₂Cl₂. Up to 3.0 equiv., the spectral pattern were broad and at 4.5 equiv., it became sharper (Figure 3.7). The β-CH protons of pyrrolic unit and ethene bridge thiophene rings are shifted down field and resonated between 8.53 ppm and 7.36 ppm. The thiophene ring which is opposite to the ethene is 3.90 ppm upfield shifted and resonated at 3.96 ppm, suggests that the ring is inverted and the respective β-CH protons are experiencing the diatropic ring current. The newly formed protonated imine NH protons are observed as a broad signal at 3.01 ppm. The NH signal was further confirmed by D₂O exchange experiment. The *meso*-mesityl protons are appeared at 7.25-7.18 ppm, whereas the *meso*-phenyl protons are from 6.87 ppm to 6.31 ppm. The *meso*-mesityl methyl protons are displayed between 3.56 ppm to 2.46 ppm, respectively. Overall, the downfield shift of the pyrrole, thiophene rings which are part of the ethene bridge and drastic upfield of the thiophene β-CHs and protonated NH signals confirm that the Hückel [24]π non-aromatic character in the free-base state is transformed into Möbius aromatic character upon protonation.

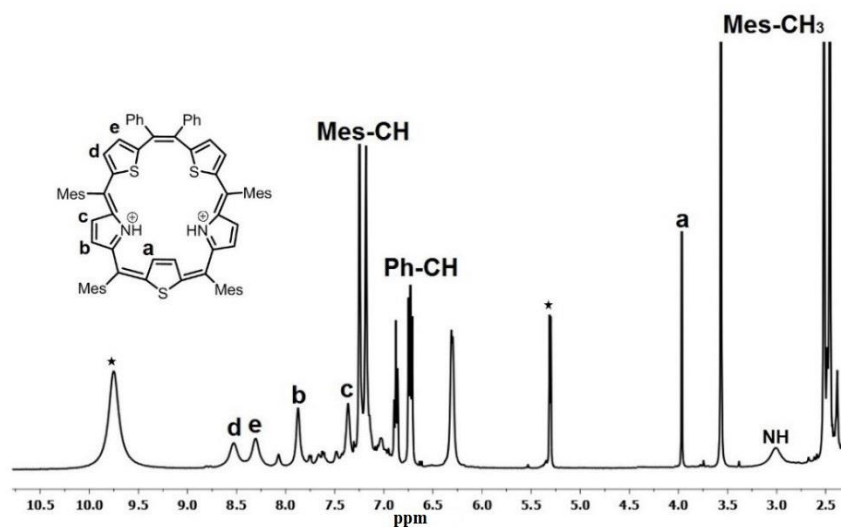


Figure 3.6: ¹H NMR spectrum of **38** with 4.5 equiv. of TFA in CD₂Cl₂.

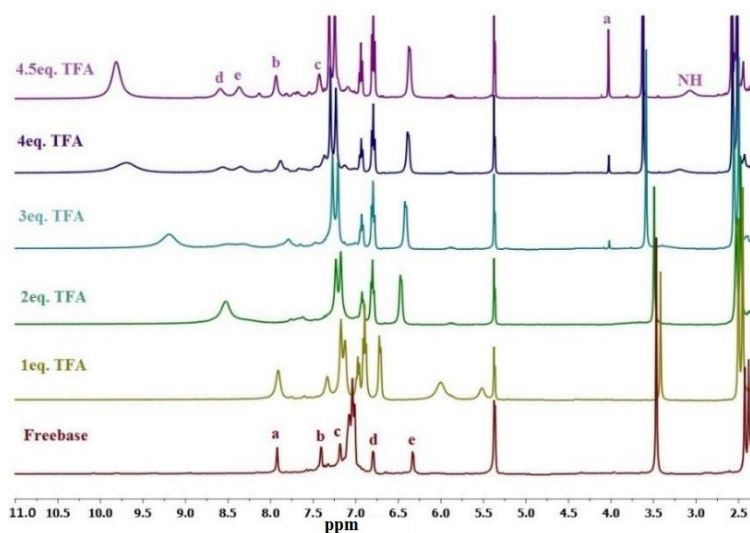


Figure 3.7: ^1H NMR titration experiment of **38** with dilute solution of TFA in CD_2Cl_2

3.3.2.3 Electronic Spectral Analysis

The electronic absorption spectrum of **38** in freebase and its protonated form is shown in Figure 3.8. The broad spectral pattern was observed from 375 to 700 nm region in the freebase form. The intense band is appeared at 490 nm with molar absorption coefficient of 10^4 . The lower energy band is observed at 698 nm. The spectral pattern suggests the typical $4n\pi$ non-aromatic character. Upon protonation of **38** with dilute solution of TFA in CH_2Cl_2 , the intense band and lower energy bands are red shifted by 110 nm & 166 nm and displayed as Soret-like band at 590 and weak Q-like band at 864 nm, respectively. The molar extinction coefficient of Soret band is 1.7 times higher as compared to the freebase state. Overall, as reflected from the ^1H NMR spectral analyses, the spectral pattern in the electronic spectral analysis maintains the Möbius aromatic character as such in the protonated state.

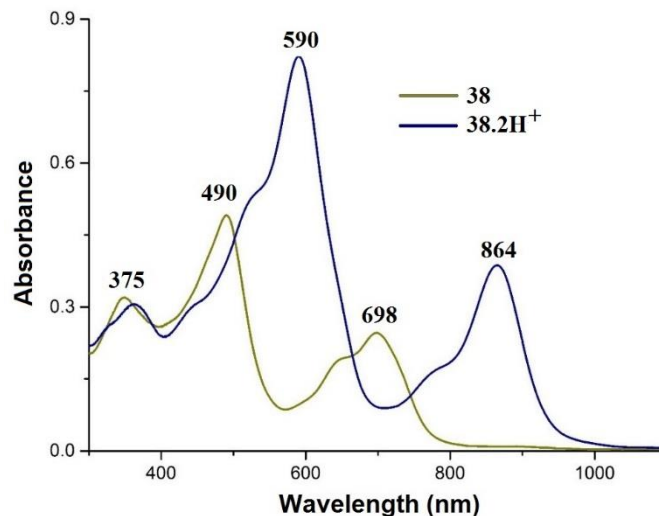


Figure 3.8: The electronic absorption spectrum of **38** and **38.2H⁺** in CH₂Cl₂.

3.3.2.4 Single Crystal X-ray Analysis

The structure of **38** with HSO₄⁻ anions was unambiguously confirmed by single crystal X-ray analysis. The results were shown in Figure 3.9 and the crystal data were in Table 3.1. The crystal was grown by slow evaporation of CHCl₃ solution over acetonitrile. The compound was crystallized in tetragonal crystal lattice with *P-4* space group. The molecule contains a 1,2-diphenyl-1,2-di(thiophene-2-yl)ethene moiety and a thiatripyrrane moiety which are connected with two *meso* mesityl groups (Figure 3.9a) and overall, adopt nonplanar structure with [24] π -electronic circuit. As reflected from the NMR spectral analysis, the thiophene unit in the tripyrrane moiety is inverted and deviated by 12.05° from mean macrocyclic plane containing *meso* carbon atoms (C1, C6, C11, C11', C6', C1'). The pyrrolic and remaining thiophene moieties are maximum tilted by 44.13° and 32.69° from the mean plane. The crystal analysis reveals that two units of HSO₄⁻ anions are in intermolecular hydrogen bonding interaction with the protonated imine NH (N1-H1) with

bond distance and angle of N1- H1...O1 is 2.00Å and 140.74° (Figure 3.9b).

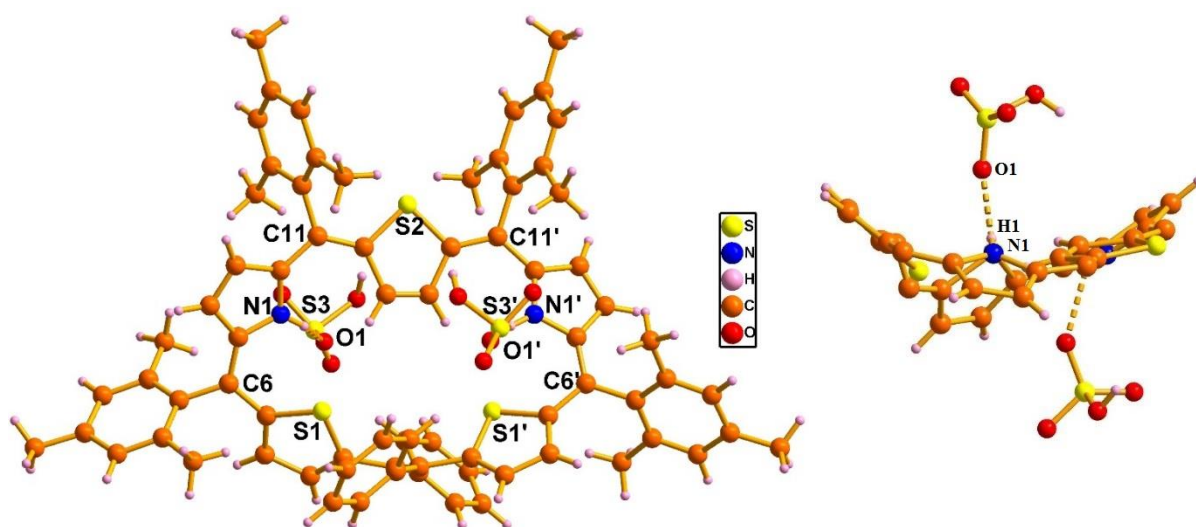


Figure 3.9: Crystal structure of **38** with HSO₄⁻ anions. (a) Top view and (b) side view.

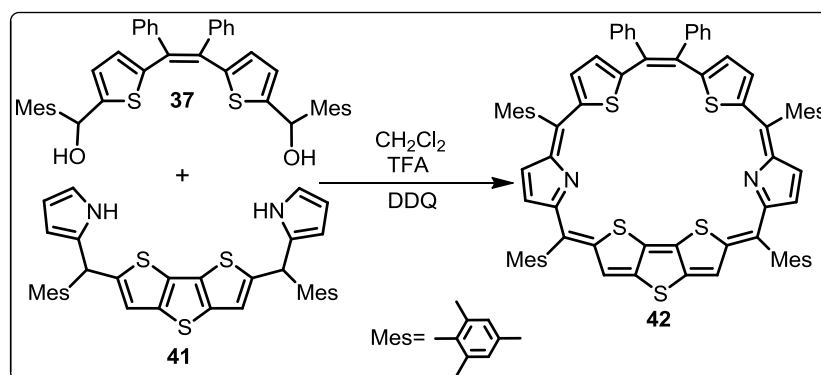
Table 3.1: Crystal data for **38**

	Pentaphyrin +2H⁺
<i>T</i> , K	100 K
Formula	C ₇₄ H ₆₈ N ₂ O ₈ S ₅
Formula weight	1273.60
Color and Habit	Dark green
Crystal system	tetragonal
Space group	<i>P</i> -4
<i>a</i> , Å	17.156(5)
<i>b</i> , Å	17.156(5)
<i>c</i> , Å	15.450(5)
α , deg	90
β , deg	90
γ , deg	90
<i>V</i> , Å ³	4547(3)
Radiation (λ , Å)	Mo K α (0.71073)
<i>Z</i>	2
d_{calcd} , g•cm ⁻³	0.930
μ , mm ⁻¹	0.169
<i>F</i> (000)	1340.0
No. of unique reflns	58104
No. of params. refined	392
GOF on <i>F</i> ²	1.046
<i>R</i> 1 ^a [<i>I</i> > 2 σ (<i>I</i>)]	0.0670
<i>R</i> 1 ^a (all data)	0.0898
<i>wR</i> 2 ^b (all data)	0.1911

3.4 Core-modified Fused Hexaphyrin

3.4.1 Synthesis

The synthesis of core-modified fused hexaphyrin (**42**) is shown in Scheme 3.13. The required precursors such as 5,5'-bis(phenylhydroxymethyl)-1,2-diphenyl-1,2-di(thiophene-2-yl)ethene (**37**) and DTT-tetrapyrane (**41**) were synthesized from our earlier reported methods.^[43] In the final step, TFA acid-catalyzed condensation of 1:1 mixture of **37** and **41** followed by DDQ oxidation afforded the crude product. After repeated column chromatographic purification by basic alumina followed by silica gel (100-200 mesh), the pink color band was eluted with 35% CH₂Cl₂/*n*-hexane solvent mixture and identified as core-modified fused hexaphyrin (**42**) in 10% yield.



Scheme 3.13: Synthesis of **42**.

3.4.2 Spectral Characterization

3.4.2.1 Mass Spectrometric Analysis

The electron spray ionization mass spectrometric analysis of **42** is shown in Figure 3.10. The molecular ion signal of **42** at *m/z* 1189.3868 [M+1] confirms the exact composition of macrocycle.

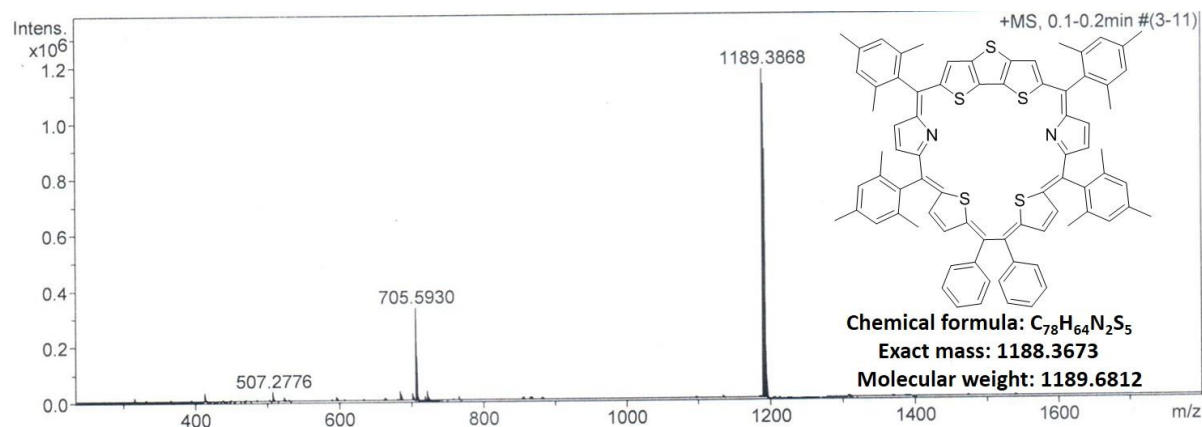


Figure 3.10: ESI-MS spectrum of **42**

3.4.2.2 NMR spectral Analysis

The 1H NMR spectrum of **42** was recorded in CD_2Cl_2 at 273 K and shown in Figure 3.11. The spectrum was broad at room temperature and became prominent upon lowering the temperature. The variable temperature 1H NMR spectrum was shown in Figure 3.12. The DTT β -CH proton (a) is resonated as sharp singlet at 7.38 ppm, whereas the β -CH protons of pyrrole (b, c) and thiophene (d, e) units are appeared between 7.50 and 6.66 ppm as four doublets. These assignments were further confirmed by 1H - 1H correlation spectroscopy (Figure 3.13). The *meso*-mesityl and methyl protons are observed at 7.04 ppm and 2.38-1.99 ppm, whereas the *meso*-phenyl protons are appeared between 6.80 and 6.59 ppm, respectively. Overall, the spectral pattern resembles Hückel [28] π non-aromatic character.

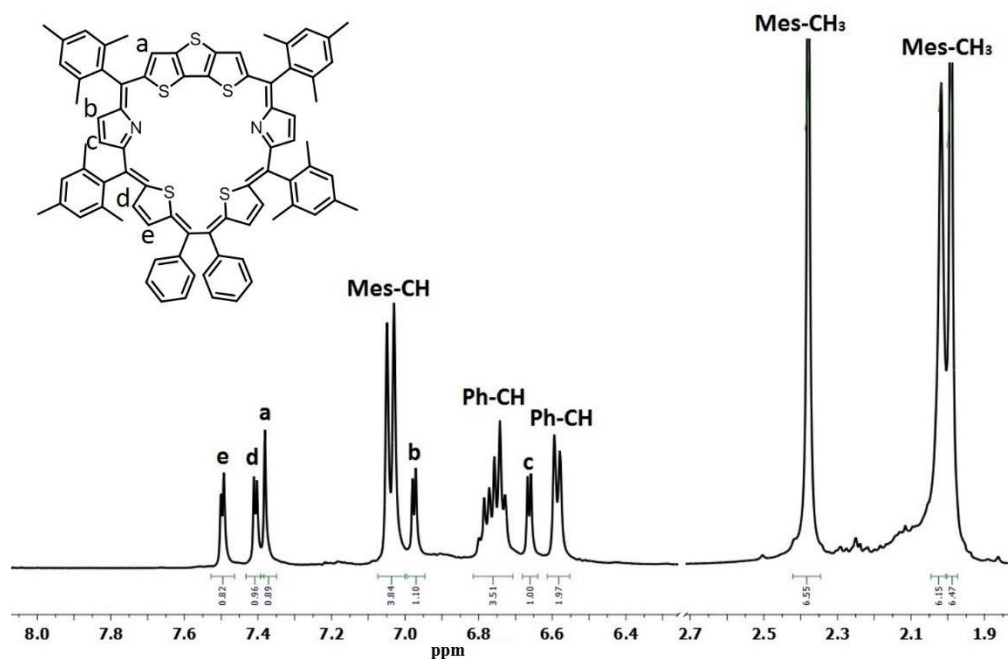


Figure 3.11: ^1H NMR spectrum of **42** in CD_2Cl_2 at 273K

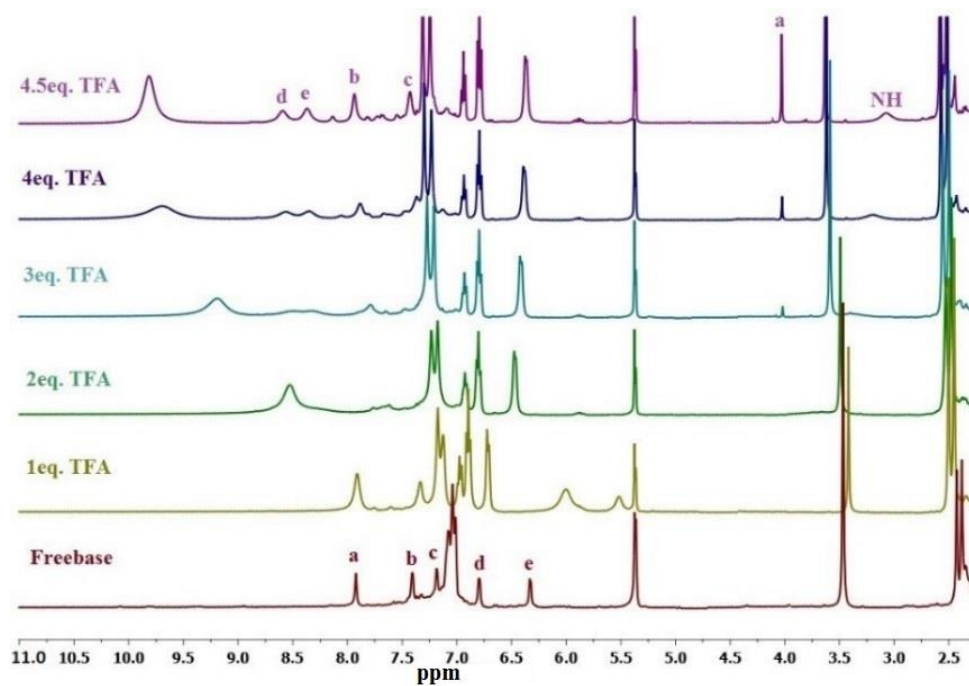


Figure 3.12: Variable temperature ^1H NMR spectrum of **42** in CD_2Cl_2

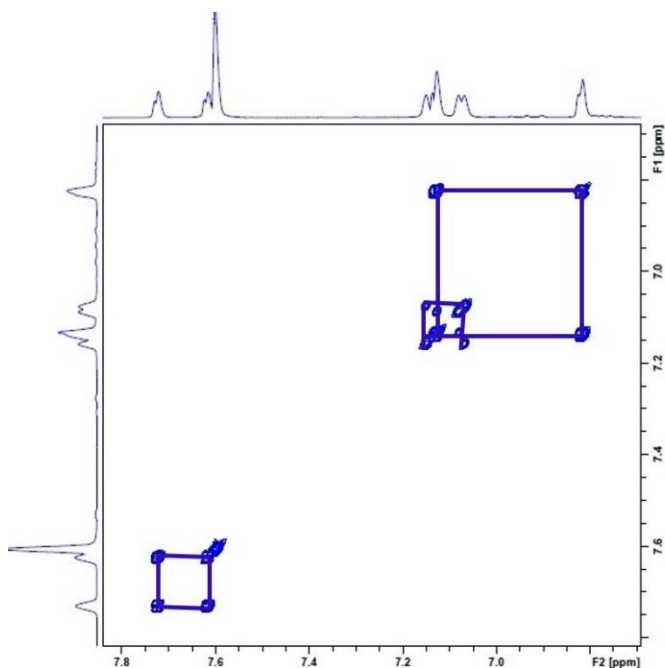


Figure 3.13: ^1H - ^1H COSY spectrum of **42** with correlation in pyrrole and thiophene rings.

The protonation experiment of **42** was further performed with dilute solution of TFA in CD_2Cl_2 at 298 K and shown in Figure 3.14. At 5 equiv. of TFA, the β -CH protons of DTT, thiophene and pyrrole units are shifted downfield and resonated between 9.94 ppm and 8.75 ppm. The *meso*-mesityl CHs are appeared from 7.36 ppm to 6.25 ppm, whereas the *meso*-mesityl methyl protons are at 2.67 ppm to 1.55 ppm, respectively. The *meso*-phenyl units, which are in the ethene bridge, are resonated between 8.37 and 6.46 ppm. The protonated imine NH protons are observed as a broad peak at -1.02 ppm and further confirmed by D_2O exchange experiment. Overall, the result suggests that the drastic spectral change was observed, where the Hückel [28] π non-aromatic conformation in the freebase state is changed into Hückel [30] π aromatic conformation upon protonation.

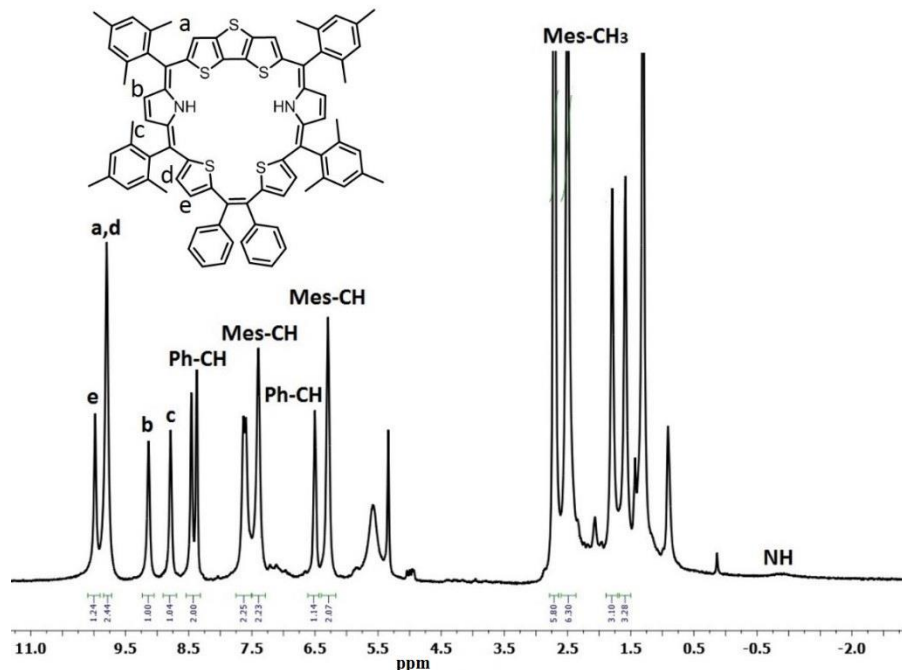


Figure 3.14: ^1H NMR spectrum of **42** with 5 equiv. of TFA in CD_2Cl_2 at 298 K.

3.4.2.3 Electronic Spectral Analysis

The electronic absorption spectrum of **42** and its protonated derivatives were recorded in CH_2Cl_2 and shown in Figure 3.15. At freebase form, **42** shows moderate intense band at 542 nm and prominent higher wavelength band at 796 nm. Upon protonation of **42** with dilute solution of TFA in CH_2Cl_2 , the bands at freebase form is further red-shifted by 53 nm and 195 nm and appeared as Soret like band at 595 nm and Q-like band at 991 nm. The molar extinction coefficient of Soret like band is 1.5 fold higher upon protonation as compared to freebase state. As reflected from the NMR spectral analyses, the aromatic character is maintained as such in the protonated state.

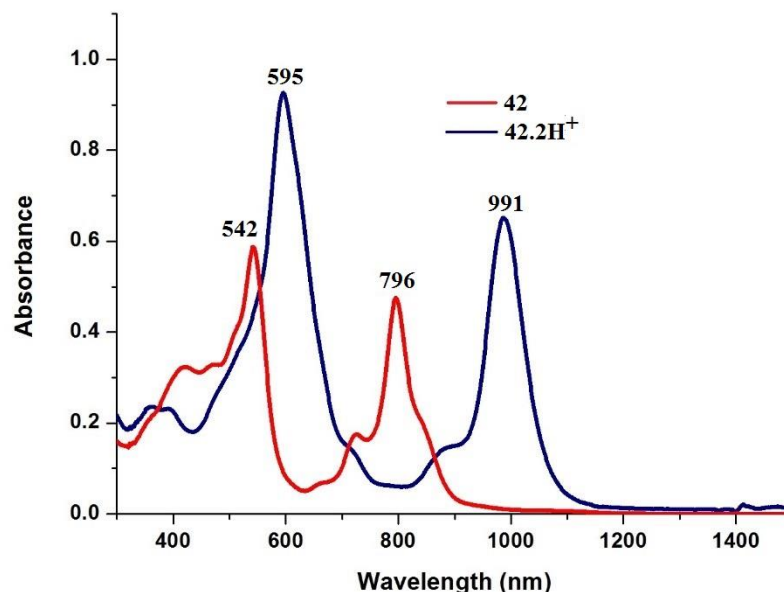


Figure 3.15: The electronic absorption spectrum of **42** and **42.2H⁺** in CH₂Cl₂.

3.5 Conclusion

In summary, we have successfully demonstrated the syntheses of core-modified [24] π pentaphyrin(2.1.1.1.1) with six *meso* links and fused hexaphyrin with seven *meso* links by introducing the *meso*-aryl ethene bridge for the first time. The synthetic methodology adopted here is simple and straightforward. The molecules were in non-aromatic conformation in the freebase form. However, upon protonation, the pentaphyrin was adopted Möbius [24] π aromatic character, whereas the hexaphyrin displayed Hückel [30] π aromatic character.

3.6 Experimental Procedure

3.6.1 Synthesis of **38**

Method I

A mixture of thiatripyrrane (**31**) (150 mg, 0.31 mmol) and diol (**37**) (200 mg, 0.31 mmol) were dissolved in dry CH₂Cl₂ under nitrogen atmosphere for 10 min. Trifluoroacetic acid (24 μ l, 0.31 mmol) was added and the resultant mixture was stirred for 1h under N₂ atmosphere. 2,3-dichloro-5,6-dicyano-*p*-benzoquinone (DDQ) (213 mg, 0.93 mmol) was added and resultant mixture was stirred in open air for another 1h. Progress of the reaction was monitored through TLC. Solvent was evaporated under vacuum. Residue was purified through basic alumina column chromatography followed by silica gel (100-200 mesh) column chromatography. The first moving green band was eluted with CH₂Cl₂/*n*-Hexane (20:80, V/V) and identified as pentaphyrin (**38**). The second greenish band was eluted with CH₂Cl₂/*n*-Hexane (25:75, V/V) and identified as homoporphyrin (**39**). After evaporation, pentaphyrin (**38**) gave greenish color solid in 9% yield.

Method II:

In this method, tetrapyrane (**40**) (300 mg, 0.40 mmol) and thiophene diol (**36**) (154 mg, 0.40 mmol), dry CH₂Cl₂ (200 ml), trifluoroacetic acid (31 μ l, 0.40 mmol) and DDQ (277 mg, 1.2 mmol) were mixed as mentioned above. The pentaphyrin (**38**) was separated in 8% yield as greenish solid and homoporphyrin (**39**) was isolated in 3% yield.

Compound **38**:

¹H NMR (400 MHz, CD₂Cl₂, 298K): δ (in ppm) = 7.86 (s, 2H), 7.41 (d, 2H, *J*=2.8), 7.19 (d, 2H, *J*=2.8), 7.12 (d, 4H, *J*=3.6), 6.97 (s, 5H), 6.95 (d, 4H, *J*=3.6), 6.81 (d, 2H, *J*= 4.2),

6.35 (d, 2H, $J=4.2$), 2.46 (s, 6H), 2.39 (s, 6H), 2.21 (s, 6H), 2.17 (s, 6H), 2.08 (s, 6H), 1.97 (s, 6H).

38·2H⁺: ¹H NMR (400 MHz, CDCl₃) δ (in ppm) = 8.53 (d, 2H), 8.30 (d, 2H), 7.87 (d, 2H), 7.36 (d, 2H), 7.25 (s, 4H), 7.18 (s, 4H), 6.87 (t, 2H), 6.73 (t, 4H), 6.31 (t, 4H), 3.96 (s, 2H), 3.56 (s, 6H), 3.01 (Br, 2H, NH), 2.52 (s, 6H), 2.46 (s, 6H).

38: UV/Vis (CH₂Cl₂): λ_{\max} in nm (ϵ in dm³mol⁻¹cm⁻¹) = 375 (5.49×10^4), 490 (8.32×10^4), 698 (3.96×10^4); **38·2H⁺** (TFA/CH₂Cl₂): λ_{\max} in nm (ϵ in dm³mol⁻¹cm⁻¹) = 590 (1.45×10^5), 684 (7.36×10^4);

3.6.2 Synthesis of 42

A mixture of DTT-tetrapyrane (**41**) (200 mg, 0.34 mmol) and diol (**37**) (217 mg, 0.34 mmol) were dissolved in 200 ml of dry CH₂Cl₂ and the resulting solution was allowed stir for 15 min under nitrogen atmosphere. Trifluoroacetic acid (26 μ l, 0.34 mmol) was added and the solution was stirred under nitrogen atmosphere for 1h. DDQ (230 mg, 1.02 mmol) was added and the mixture was stirred for another 1h in open air condition. After evaporation of solvent, the compound was purified by basic alumina followed by silica gel (100-200 mesh) column chromatography. A pink color band was eluted with CH₂Cl₂/*n*-Hexane (35:65, V/V) and identified as hexaphyrin (**42**) in 12% yield.

Compound 42:

¹H NMR (400 MHz, CD₂Cl₂, 273K): δ (in ppm) = 7.50 (d, 2H), 7.41(d, 2H), 7.38 (s, 2H), 7.05 (s, 4H), 7.03 (s, 4H), 6.97 (d, 2H), 6.80-6.73 (m, 6H), 6.66 (d, 2H), 6.59 (d, 4H), 2.38 (s, 12H), 2.02 (s, 2H), 1.99 (s, 12H).

42·2H⁺: ¹H NMR (400 MHz, CDCl₃) δ (in ppm) = 9.94 (s, 2H), 9.78 (m, 4H), 9.09 (d, 2H), 8.75 (d, 2H), 8.37 (d, 2H), 7.57 (d, 4H), 7.36 (s, 4H), 6.46 (d, 2H), 6.25 (s, 2H), 2.67 (s, 12H), 2.46 (s, 12H), 1.75 (s, 6H), 1.55 (s, 6H).

42: UV/Vis (CH₂Cl₂): λ_{max} in nm (ε in dm³mol⁻¹cm⁻¹) = 421 (5.04×10⁴), 466 (4.97×10⁴), 542 (9.43×10⁴), 796 (7.96×10⁴);

42.2H⁺: UV/Vis (CH₂Cl₂): λ_{max} in nm (ε in dm³mol⁻¹cm⁻¹) = 595 (1.41×10⁵), 991 (1.03×10⁵).

3.7 References

1. Zhang, C.; Chen, P.; Dong, H.; Zhen, Y.; Liu, M.; Hu, W. *Adv. Mater.* **2015**, *27*, 5379-5387.
2. Bobe, M. S. R.; Al Kobaisi, M.; Bhosale, S. V.; Bhosale, S. V. *Chem. Open.* **2015**, *4*, 516-522.
3. Ikeda, A.; Hino, S.; Mae, T.; Tsuchiya, Y.; Sugikawa, K.; Tsukamoto, M.; Yasuhara, K.; Shigeto, H.; Funabashi, H.; Kuroda, A.; Akiyama, M. *RSC Adv.* **2015**, *5*, 105279-105287.
4. Jiang, X.; Gou, F.; Chen, F.; Jing, H. *Green. Chem.* **2016**, *18*, 3567-3576.
5. Liu, X.; Wang, Z.; Zhao, X.; Fu, X. *Inorg. Chem. Front.* **2016**, *3*, 861-865.
6. Tam, C. M.; To, C. T.; Chan, K. S. *Organometallics* **2016**, *35*, 2174-2177.
7. Callot, H. J.; Tschamber, T. *Tetrahedron Lett.* **1974**, *15*, 3155-3158.
8. Woodward, R.B. *Aromaticity Conference*, Sheffield, U.K., **1966**.
9. Broadhurst, M. J.; Grigg, R.; Johnson, A. W. *J. Chem. Soc., Perkin Trans. 1* **1972**, 2111-2116.
10. Rexhausen, H.; Gossauer, A. *J. Chem. Soc., Chem. Commun.* **1983**, 275.

-
11. Vogel, E.; Pohl, M.; Herrmann, A.; Wiss, T.; König, C.; Lex, J.; Gross, M.; Gisselbrecht, J. P. *Angew. Chem., Int. Ed. Engl.* **1996**, *35*, 1520-1524.
 12. Vogel, E.; Fröde, C.; Breihan, A.; Schmickler, H.; Lex, J. *Angew. Chem., Int. Ed. Engl.* **1997**, *36*, 2609-2612.
 13. Shin, J.-Y.; Furuta, H.; Osuka, A. *Angew. Chem. Int. Ed.* **2001**, *40*, 619-621.
 14. Mori, S.; Shin, J.-Y.; Shimizu, S.; Ishikawa, F.; Furuta, H.; Osuka, A. *Chem. Eur. J.* **2005**, *11*, 2417-2425.
 15. Shimizu, S.; Aratani, N.; Osuka, A. *Chem. Eur. J.* **2006**, *12*, 4909-4918.
 16. Gokulnath, S.; Chandrashekar, T. K. *Org. Lett.* **2008**, *10*, 637-640.
 17. a) Srinivasan, A.; Ishizuka, T.; Maeda, H.; Furuta, H. *Angew. Chem. Int. Ed.* **2004**, *43*, 2951-2955. b) Mori, S.; Shin, J.-Y.; Shimizu, S.; Ishikawa, F.; Furuta, H.; Osuka, A. *Chem. Eur. J.* **2005**, *11*, 2417-2425. c) Srinivasan, A.; Ishizuka, T.; Furuta, H. *Angew. Chem. Int. Ed.* **2004**, *43*, 876-879.
 18. Ganapathi, E.; Chatterjee, T.; Lee, W.-Z.; Ravikanth, M. *Asian. J. Org. Chem.* **2015**, *4*, 638-645.
 19. Pushpan, S. K.; Srinivasan, A.; Anand, V. G.; Venkatraman, S.; Chandrashekar, T. K.; Joshi, B. S.; Roy, R.; Furuta, H. *J. Am. Chem. Soc.* **2001**, *123*, 5138-5139.
 20. Richter, D. T.; Lash, T. D. *J. Org. Chem.* **2004**, *69*, 8842-8850.
 21. Shetti, V. S.; Kee, S.-Y.; Lee, C.-H. *Chem. Asian J.* **2014**, *9*, 734-738.
 22. Miller, D. C.; Johnson, M. R.; Becker, J. J.; Ibers, J. A. *J. Heterocycl. Chem.*, **1993**, *30*, 1485-1490.
 23. Miller, D. C.; Johnson, M. R.; Becker, J. J.; Ibers, J. A. *J. Org. Chem.* **1994**, *59*, 2877-2879.
-

-
24. Weghorn, S. J.; Lynch, V.; Sessler, J. L. *Tetrahedron Lett.* **1995**, *36*, 4713-4716.
 25. Sessler, J. L.; Davis, J. M.; Lynch, V. *J. Org. chem.* **1998**, *63*, 7062-7065.
 26. Narayanan, S. J.; Sridevi, B.; Chandrashekar, T. K.; English, U.; Ruhlandt-Senge, K. *Org. Lett.* **1999**, *1*, 587-590.
 27. Sessler, J. L.; Weghorn, S. J.; Hiseada, Y.; Lynch, V. *Chem. Eur. J.* **1995**, *1*, 56-67.
 28. Charriere, R.; Jenny, T. A.; Rexhausen, H.; Gossauer, A. *Heterocycles* **1993**, *36*, 1561-1575.
 29. Brückner, C.; D. Sternberg, E.; Boyle, R. W.; Dolphin, D. *Chem. Commun.* **1997**, 1689-1690.
 30. a) Neves, M. G. P. M. S.; Martins, R. M.; Tome, A. C.; Silvestre, A. J. D.; Silva, A. M. S.; Felix, V.; Cavaleiro, J. A. S.; Drew, M. G. B. *Chem. Commun.* **1999**, 385-386.
b) Shin, J.-Y.; Furuta, H.; Yoza, K.; Igarashi, S.; Osuka, A. *J. Am. Chem. Soc.* **2001**, *123*, 7190-7191.
 31. Suzuki, M.; Osuka, A. *Org. Lett.* **2003**, *5*, 3943-3946.
 32. Wei, P.; Zhang, K.; Li, X.; Meng, D.; Ågren, H.; Ou, Z.; Ng, S.; Furuta, H.; Xie, Y. *Angew. Chem. Int. Ed.* **2014**, *53*, 14069-14073.
 33. Rath, H.; Anand, V. G.; Sankar, J.; Venkatraman, S.; Chandrashekar, T. K.; Joshi, B. S.; Khetrupal, C. L.; Schilde, U.; Senge, M. O. *Org. Lett.* **2003**, *5*, 3531-3533.
 34. Higashino, T.; Inoue, M.; Osuka, A. *J. Org. Chem.* **2010**, *75*, 7958-7961.
 35. Suzuki, M.; Taniguchi, R.; Osuka, A. *Chem. Commun.* **2004**, 2682-2683.
 36. Tokuji, S.; Shin, J.-Y.; Kim, K. S.; Lim, J. M.; Youfu, K.; Saito, S.; Kim, D.; Osuka, A. *J. Am. Chem. Soc.* **2009**, *131*, 7240-7241.
-

-
37. Naoda, K.; Mori, H.; Aratani, N.; Lee, B. S.; Kim, D.; Osuka, A. *Angew. Chem. Int. Ed.* **2012**, *51*, 9856-9859.
38. Sessler, J. L.; Morishima, T.; Lynch, V. *Angew. Chem., Int. Ed. Engl.*, **1991**, *30*, 977-980.
39. Johnson, M.R.; Miller, D.C.; Bush, K.; Becker, J.J. *J. Org. Chem.* **1992**, *57*, 4414-4417.
40. Sessler, J.L.; Weghorn, S. J.; Morishima, T.; Rosingana, M.; Lynch, V. *J. Am. Chem. Soc.* **1992**, *114*, 8306-8307.
41. Sessler, J. L.; Seidel, D.; Vivian, A. E.; Lynch, V.; Scott, B. L.; Keogh, D. W. *Angew. Chem. Int. Ed.* **2001**, *40*, 591-594.
42. Köhler, T.; Seidel, D.; Lynch, V.; Arp, F. O.; Ou, Z.; Kadish, K. M.; Sessler, J. L. *J. Am. Chem. Soc.* **2003**, *125*, 6872-6873.
43. Chandrashekar, T. K.; Prabhuraja, V.; Gokulnath, S.; Sabarinathan, R.; Srinivasan, A. *Chem. Commun.* **2010**, *46*, 5915-5917.

CHAPTER 4

Core-modified Heptaphyrins with Möbius Aromaticity

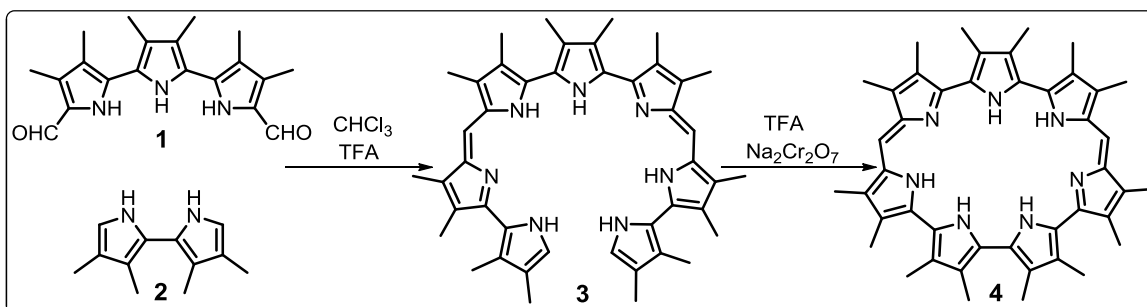
4.1	Introduction	95-101
4.2	Object of the work	102
4.3	Result and discussion	103-124
4.3.1	Syntheses	103
4.3.2	Spectral Characterization	104-124
4.3.2.1	Mass Spectrometric Analysis	104
4.3.2.2	NMR Analysis	105-113
4.3.2.3	Single crystal X-ray analysis	113-118
4.3.2.4	Electronic spectral analysis	119-121
4.3.2.5	Nucleus Independent Chemical Shift (NICS)	121-122
4.3.2.6	Anisotropy Induced Current Density (AICD)	123-124
4.4	Conclusions	124
4.5	Experimental Procedures	125-126
4.5.1	Synthesis of 28	125-126
4.5.2	Synthesis of 29	126
4.6	References	127-129

4.1 Introduction

The basic concept, ‘aromaticity’^[1-5] has received much attention in expanded porphyrin chemistry^[6-14] which provide an ideal platform for studying the various concepts of aromaticity. Depending upon the oxidation state and conformation, they show different aromatic properties such as Hückel aromatic,^[1-5] non-aromatic,^[15-19] anti-aromatic^[20-22] and Möbius aromatic electronic structure.^[23-29] The initial three concepts are well known in the literature, however the last one is less explored. The first example of expanded porphyrin analogue with Möbius aromaticity was reported by Latos-Grażyński and coworkers by using di-*p*-benzi-[28]Hexaphyrin.^[24] Since then, several reports have demonstrated the presence of Möbius aromaticity in various expanded porphyrins under various conditions. Such details were described in the first chapter. This chapter mainly highlights the synthesis of [32] π fused core-modified heptaphyrin and explores the Möbius aromatic character.

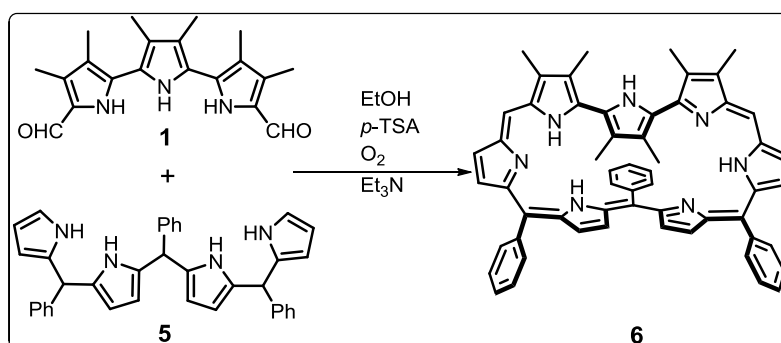
Heptaphyrins are expanded porphyrins in which seven heterocyclic units are linked through multiple *meso*-carbon bridges. The first [28] π heptaphyrin(1.0.0.1.0.0.0) (**4**) with two *meso*-links was reported by Sessler and co-workers.^[30] The trifluoroacetic (TFA) acid-catalyzed condensation of terpyrrole precursor (**1**) with bipyrrrole (**2**) obtained the linear oligopyrrole (**3**). The oxidative coupling reaction of **3** with Na₂Cr₂O₇ in TFA afforded heptaphyrin (**4**) in 43% yield (Scheme 4.1). The compound **4** was further reacted with sulfuric acid to produce the respective sulfate salt (**4.2H⁺.SO₄²⁻**), which showed typical Hückel anti-aromatic behavior from the NMR spectral analysis. The single crystal X-ray analyses revealed that

the sulfate anion was tightly bound inside cavity through intermolecular hydrogen bonding interaction with N...O bond distances range from 2.669 Å to 2.961 Å.

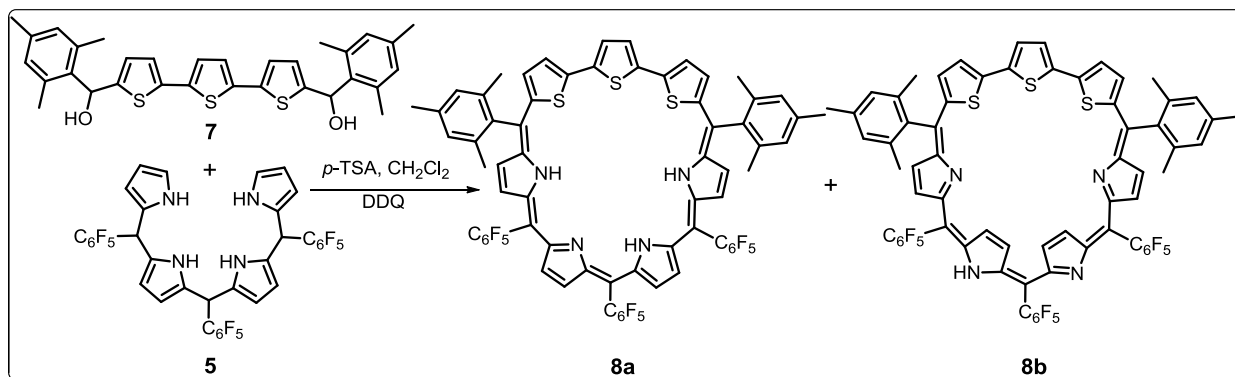


Scheme 4.1: Synthesis of **4**

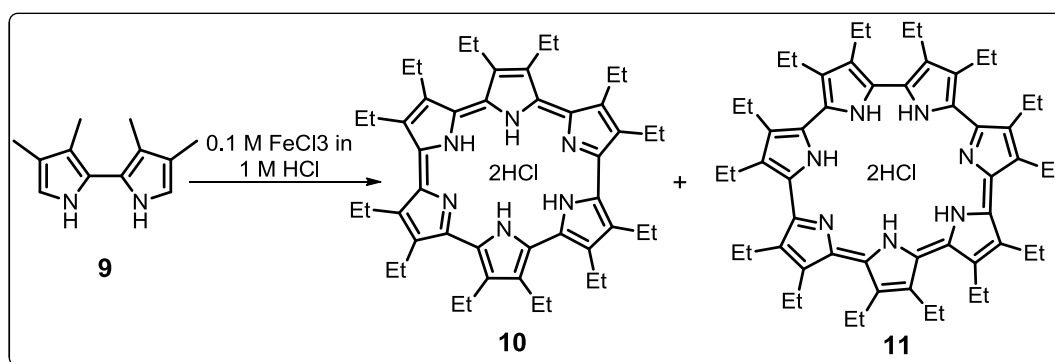
The Hückel aromatic heptaphyrin (**6**) was reported by same group.^[31] The *p*-toluenesulfonic (*p*-TSA) acid-catalyzed condensation of 1:1 mixture of diformylterpyrrole (**1**) with tetrapyrane (**5**) under aerial oxidation, the $[30]\pi$ heptaphyrin(1.1.1.1.1.0.0) with five *meso*-links was obtained in 16% yield (Scheme 4.2). The molecule (**6**) was in figure-eight conformation in the solid state, however maintained the aromatic character in solution. By adopting similar synthetic strategy, the non-aromatic (**8a**) and aromatic (**8b**) core-modified $[30]\pi$ heptaphyrin with five *meso*-links was obtained from one-pot synthesis of terthiophene diol (**7**) with tetrapyrane (**5**) in 7% and 16% yield, respectively (Scheme 4.3).^[32] The **8a** and **8b** were interconvertible by simple oxidation and reduction reactions using DDQ as well as NaBH_4 .



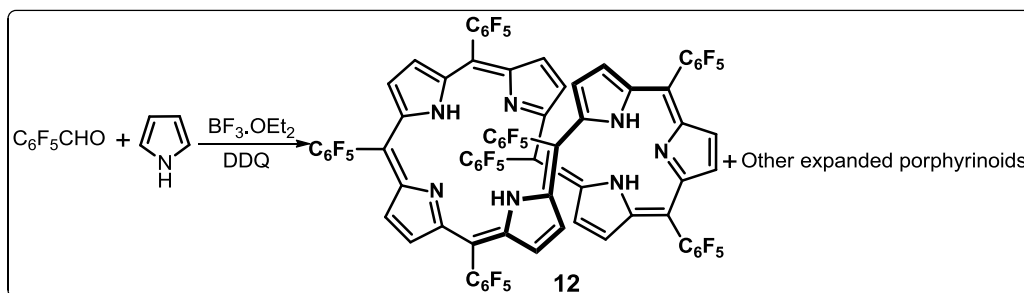
Scheme 4.2: Synthesis of **6**

Scheme 4.3: Synthesis of **8**

In 2003, Sessler and co-workers have also demonstrated the synthesis of cyclo[7]pyrrole (**11**) without any *meso*-carbon bridges.^[33] Oxidative coupling of bipyrrole precursor (**9**) with FeCl_3 in HCl afforded HCl salt of [22] π hexaphyrin(0.0.0.0.0.0) (**10**) and [26] π heptaphyrin(0.0.0.0.0.0.0) (**11**) in 15% and 5% yield (Scheme 4.4). The aromatic nature of **11** was reflected from the electronic and NMR spectral analysis, where the inner NH signal was upfield shifted and observed at -2.12 ppm. Two chloride anions were bound above and below the macrocyclic plane with six intermolecular hydrogen bonding interaction with the $\text{NH}\cdots\text{Cl}$ distances from 2.31 Å to 2.66 Å.

Scheme 4.4: Synthesis of **10** and **11**

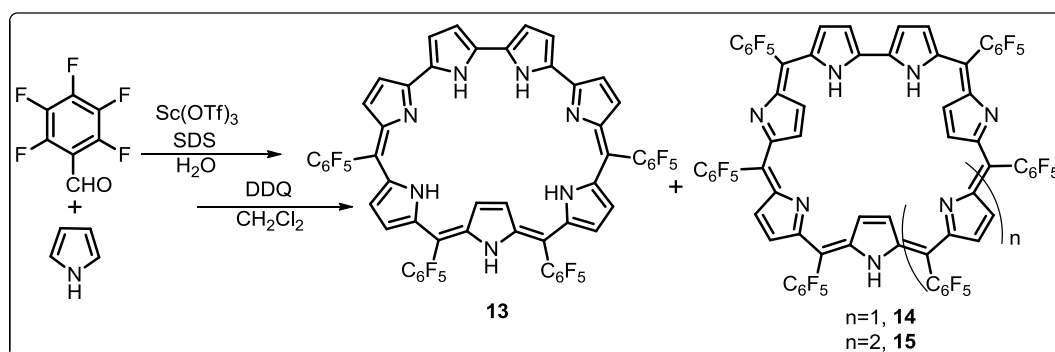
The heptaphyrin (**12**) with seven *meso*-carbon bridges was reported by Osuka and co-workers^[34] by modified Lindsey condition by using pyrrole and pentafluorobenzaldehyde in the presence of $\text{BF}_3 \cdot \text{Et}_2\text{O}$ as acid-catalyst followed by oxidation with DDQ to afford the $[28]\pi$ heptaphyrin(1.1.1.1.1.1.1) (**12**) in 4-5% yield along with porphyrin and other expanded porphyrinoids (Scheme 4.5).



Scheme 4.5: Synthesis of **12**

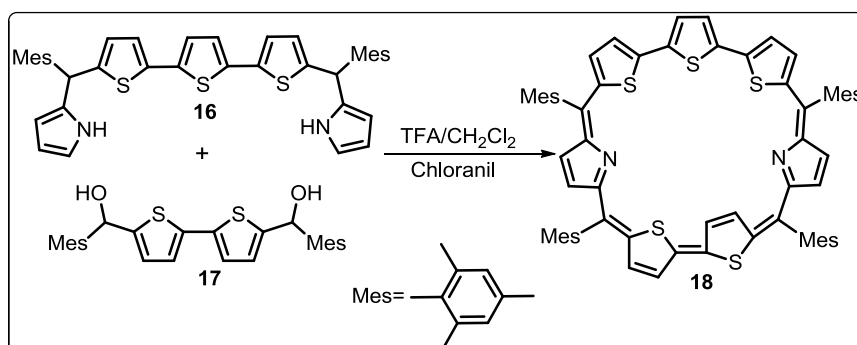
The $\text{Sc}(\text{OTf})_3$ -catalyzed reaction of pentafluorobenzaldehyde and pyrrole in the presence of sodium dodecyl sulfate (SDS) in aqueous afforded two different fractions from the silica gel column chromatographic separation.^[26] The first fraction was in green color whereas the second fraction was in red-purple porphyrinoid in color. The aromatic nature of the second fraction was reflected from the NMR spectral analysis, where one of the pyrrolic unit was inverted and observed at 0.33 ppm and suggested the formation of $[30]\pi$ heptaphyrin(1.1.1.1.0.0.0) (**13**) (Scheme 4.6). Upon protonation by using TFA, the red solution was turned into blue and maintained the aromatic nature as such. The spectral analyses revealed that two pyrrolic units were inverted and further confirmed by single crystal X-ray analyses. On the other hand, the first fraction was further purified and separated as two green color compounds, where the major fraction was identified as $[30]\pi$ heptaphyrin(1.1.1.1.1.1.0) (**14**) in 5% yield, while the minor fraction was identified as $[34]\pi$ octaphyrin(1.1.1.1.1.1.1.0) (**15**) (Scheme 4.6). The NMR spectral analyses and single crystal

X-ray structure revealed that the free base **14** was in figure-eight conformation with non-aromatic character, whereas the protonated **14** was in planar conformation with aromatic nature.



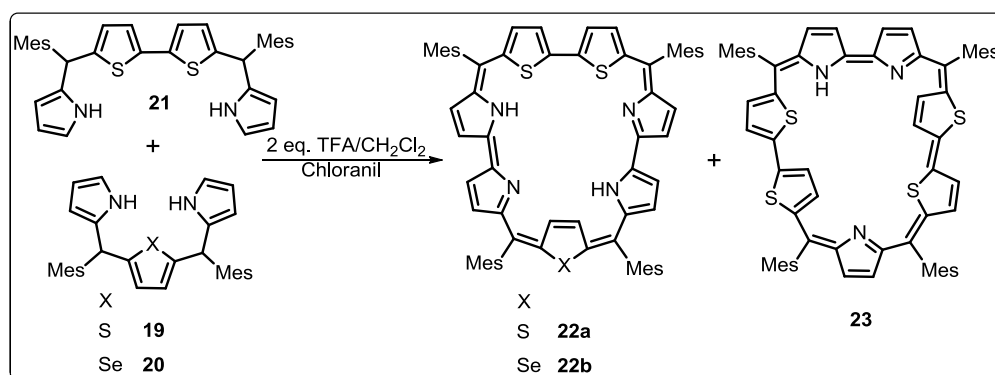
Scheme 4.6: Synthesis of **13 - 15**

The first core-modified heptaphyrins **18**, **22** and **23** were introduced by our group.^[35] The [30] π heptaphyrins (**18**) was synthesized either through an acid-catalyzed condensation or oxidative coupling reaction. The [5 + 2] synthetic strategy was adopted for acid-catalyzed condensation reaction. The condensation of terthiapentapyrrane (**16**) with bithiophene diol (**17**) in presence of TFA followed by oxidation with chloranil afforded [30] π heptaphyrin(1.1.0.0.1.1.0) (**18**) in 20% yield (Scheme 4.7). The spectral analyses suggested that one of the thiophene rings in the bithiophene unit was inverted and retained as such during protonation experiment.



Scheme 4.7: Synthesis of **18**

On the other hand, [4 + 3] synthetic strategy was followed for acid-catalyzed oxidative coupling reaction.^[36] The core-modified [30] π heptaphyrin(1.0.1.1.0.1.0) (**22**) was synthesized from thia-(**19**) / selenatripyrrane (**20**) and tetrapyrane (**21**) by using TFA acid-catalyst followed by chloranil oxidation in 20% yield. By changing the *meso*-aryl substituent from phenyl to mesityl derivative, in addition to **22**, our group has also obtained a new core-modified [30] π heptaphyrin(1.0.1.1.0.1.0) (**23**) in 9% yield (Scheme 4.8). In **22**, the thiophene unit which was opposite to the bithiophene unit was inverted, whereas in **23**, two of the thiophene rings from the bithiophene units were inverted. In **18**, **22** and **23**, the [30] π aromatic character was reflected from the spectral studies and protonation experiments.



Scheme 4.8: Synthesis of **22** and **23**

In 2005, our group has also demonstrated the synthesis of twisted core-modified heptaphyrins (**24**) with six *meso* links.^[37] The [4 + 3] acid catalyzed condensation strategy was involved for the synthesis of **24** by using thia-(**19**) / selenatripyrrane (**20**) and tetrapyrane (**21**) precursors and pentafluorobenzaldehyde. The *p*-toluenesulphonic acid-catalyst condensation followed by oxidation with chloranil afforded [30] π heptaphyrin(1.1.1.1.1.1.0) (**24**) in 10% yield (Scheme 4.9). Though the macrocycle **24** was in twisted conformation, the aromatic nature was reflected from the solution state spectral analyses.

4.2 Objective of the work:

A series of non-fused heptaphyrins and core-modified fused heptaphyrins with various *meso*-carbon links were highlighted in the previous section. All these macrocycles distinguish each other depending on; (i) the number of π -electrons; (ii) the number of *meso*-links; (iii) the conformational behavior and (iv) aromatic / anti-aromatic / non-aromatic character. However, the core-modified expanded porphyrins in general and fused heptaphyrins in particular, the Möbius aromatic character is hitherto unknown in the literature. Herein, we wish to report the synthesis of monofused core-modified 32π heptaphyrins (**28** and **29**) with six *meso*-positions (Figure 4.1), which exhibits Möbius aromatic character in solution as well as solid state and retains the Möbius aromaticity in the protonated state.

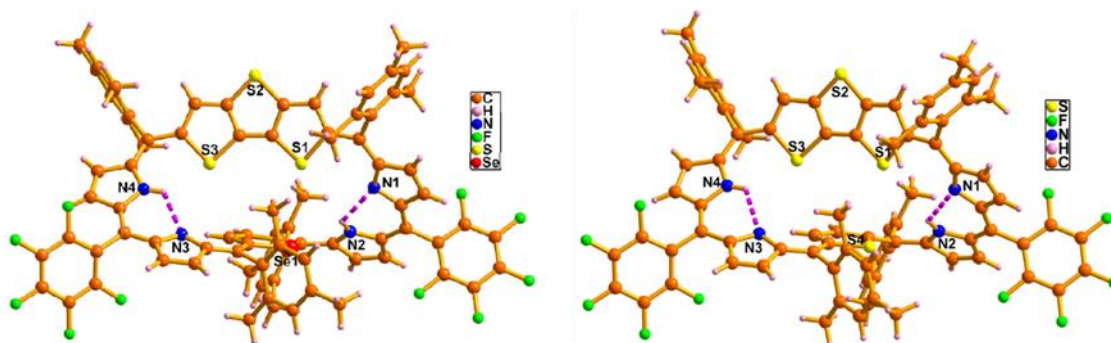
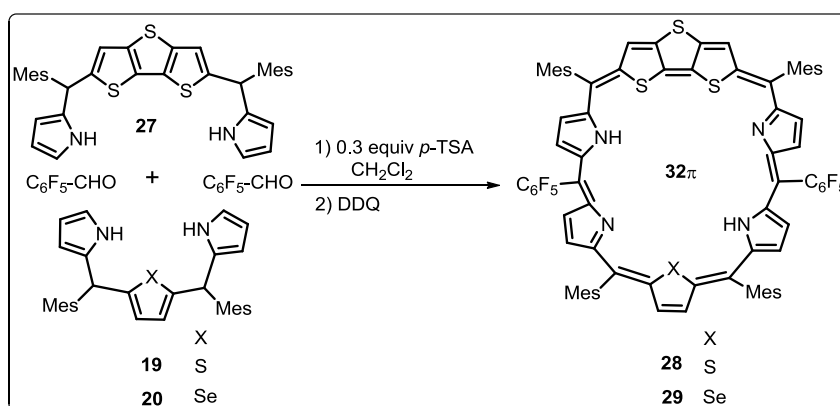


Figure 4.1: Crystal structures of **28** and **29**

4.3 Results and Discussion

4.3.1 Syntheses

The synthesis is outlined in Scheme 4.11. We have followed the acid-catalyzed condensation reaction of DTT-tetrapyrane **27**, a rigid precursor with electron rich center,^[39] and thia- or selenatripyrrane (**19** or **20**),^[36] for the synthesis of fused heptaphyrin **28** and **29**. The rigid precursor was synthesized from the TFA acid catalyzed condensation with excess pyrrole afforded **27** in 85% yield. The precursors **19** and **20** were synthesized from our earlier reported procedure. The final step involves the condensation of 1:1 equiv. of **27** and **19** or **20** with 2 equiv. of pentafluorobenzaldehyde in presence of 0.3 equiv. of *p*-toluenesulfonic acid (*p*-TSA) followed by oxidation with 2,3-dichloro-5,6-dicyano-1,4-benzoquinone (DDQ) gave the crude product. Repeated purification by column chromatography over basic alumina followed by silica gel (100-200 mesh) column with CH₂Cl₂/*n*-hexane (35:65) gave a blue fraction, which was identified as **28** and **29**. After evaporation of the solvent, further recrystallization from CH₂Cl₂/CH₃OH provides greenish-blue color solid in 6-7% yield.



Scheme 4.11: Synthesis of **28** and **29**.

4.3.2 Spectral Characterization

4.3.2.1 Mass Spectrometric Analysis

The electron spray ionisation (ESI) mass spectrometric analysis of **28** and **29** shows the molecular ion signal at m/z 1417.3250 [$M+H^+$] and 1464.2340 [M^+] and confirms the exact composition of the macrocycle (Figure 4.2 and 4.3).

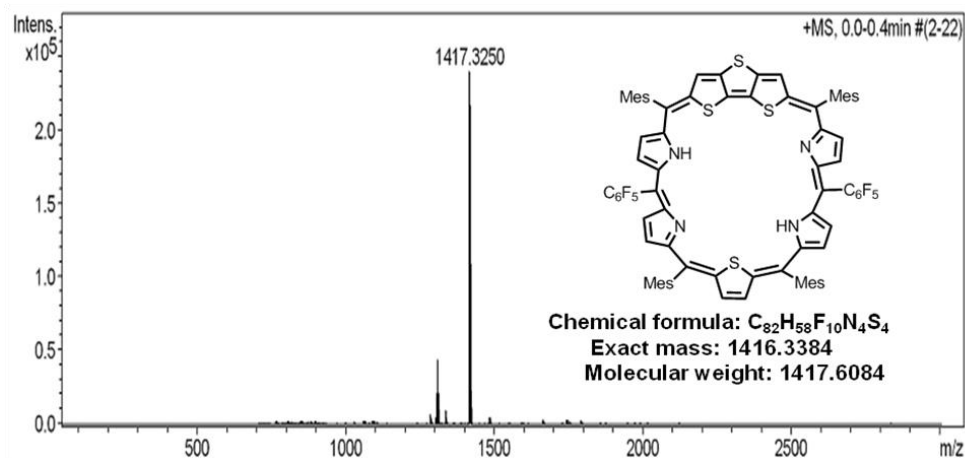


Figure 4.2: ESI-MS spectrum of **28**

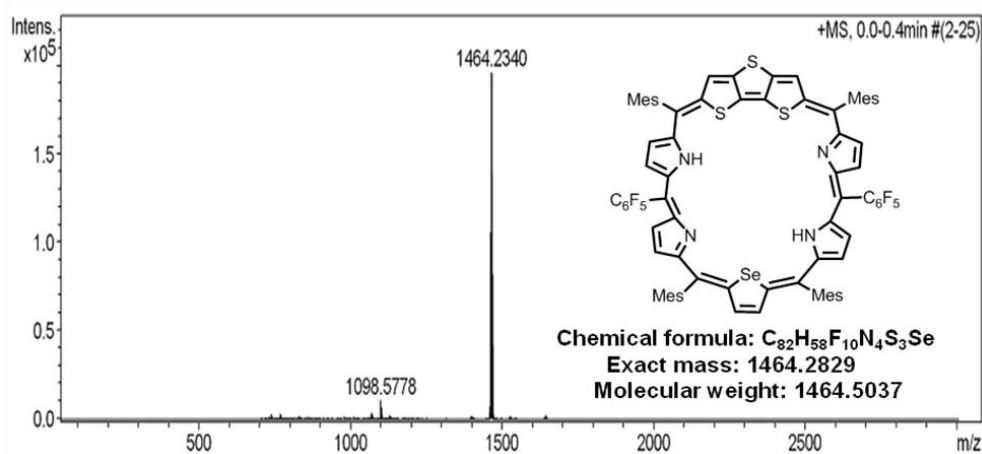
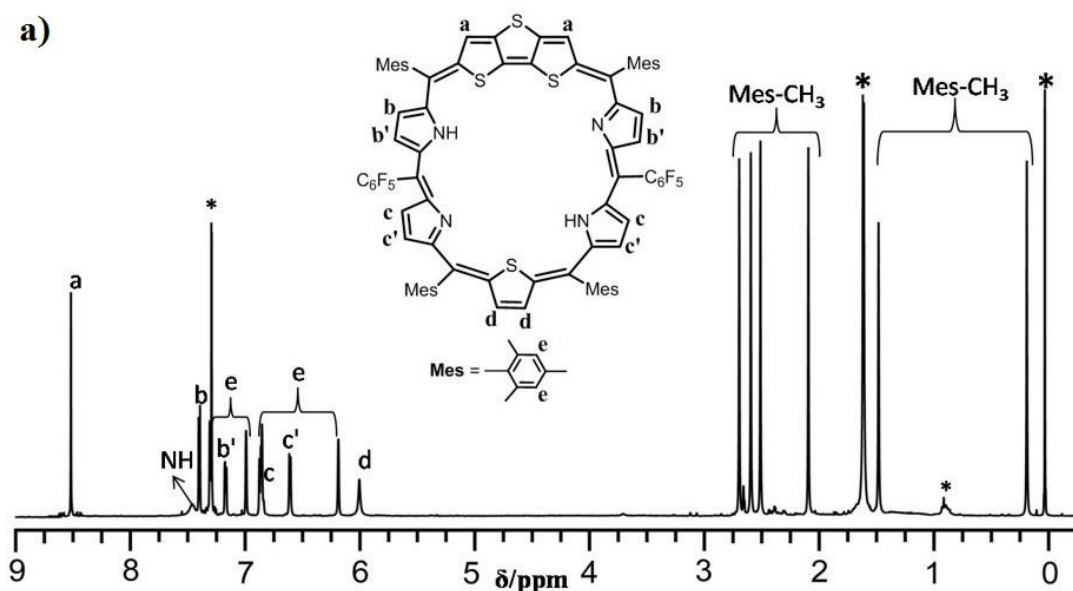


Figure 4.3: ESI-MS spectrum of **29**

4.3.2.2 NMR Analysis

The solution state analyses of **28** and **29** were confirmed by ^1H and 2D NMR spectroscopy in CDCl_3 . At 298K, the molecule **28** exists in C_2 -symmetry, where the two DTT protons are resonated as a sharp singlet at 8.48 ppm (a). The four doublet signals between 7.30 ppm and 6.51 ppm (bb' , cc') are assigned for pyrrolic β -CH protons (Figure 4.4a). These signals are confirmed by ^1H - ^1H correlation spectroscopy (COSY) experiment (Figure 4.4b). A sharp singlet at 6.03 ppm (d) corresponds to two β -CH of thiophene ring, which are opposite to DTT moiety. The *meso*-mesityl-CH protons are observed as singlet between 7.26 and 6.22 ppm (e), whereas six sharp singlets are resonated between 2.56 and 0.24 ppm in the upfield region corresponds to *meso*-mesityl methyl protons. A broad signal at 7.77 ppm attributed to NH protons of pyrrolic unit and this assignment was confirmed by D_2O -exchange experiment. Overall, the appearance of thiophene β -CH and the *meso*-mesityl methyl signals in the upfield region reflects the weak Möbius aromatic character in **28**.



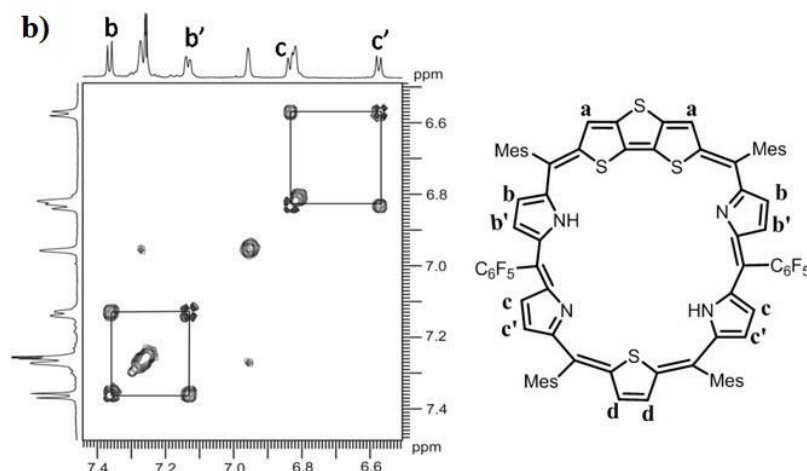


Figure 4.4: ¹H NMR spectrum of **28** at 298K in CDCl₃ (a) and ¹H-¹H COSY spectrum of **28** with pyrrolic β-CH proton correlations (b).

Similar pattern was observed in **29** and shown in Figure 4.5. The DTT-β-CH protons are resonated as sharp singlet at 8.51 ppm (a). The pyrrolic-β-CHs are between 7.22 and 6.46 ppm (bb' and cc') as four doublets (Figure 4.5a) and confirmed by ¹H-¹H COSY correlation spectroscopy (Figure 4.5b). The *meso*-mesityl-CH singlets are from 7.23 to 6.27 ppm (e) as four sharp singlets. The selenophene β-CH proton is appeared as singlet at 6.17 ppm (d). The *meso*-mesityl methyl protons are observed between 2.49 and 0.38 ppm as six singlets (Figure 4.5a). The spectral analysis reveals that the macrocycle **29** is less aromatic (0.38 ppm vs 0.24 ppm) as compared to **28**, however maintains the weak Möbius aromatic character at 298K.

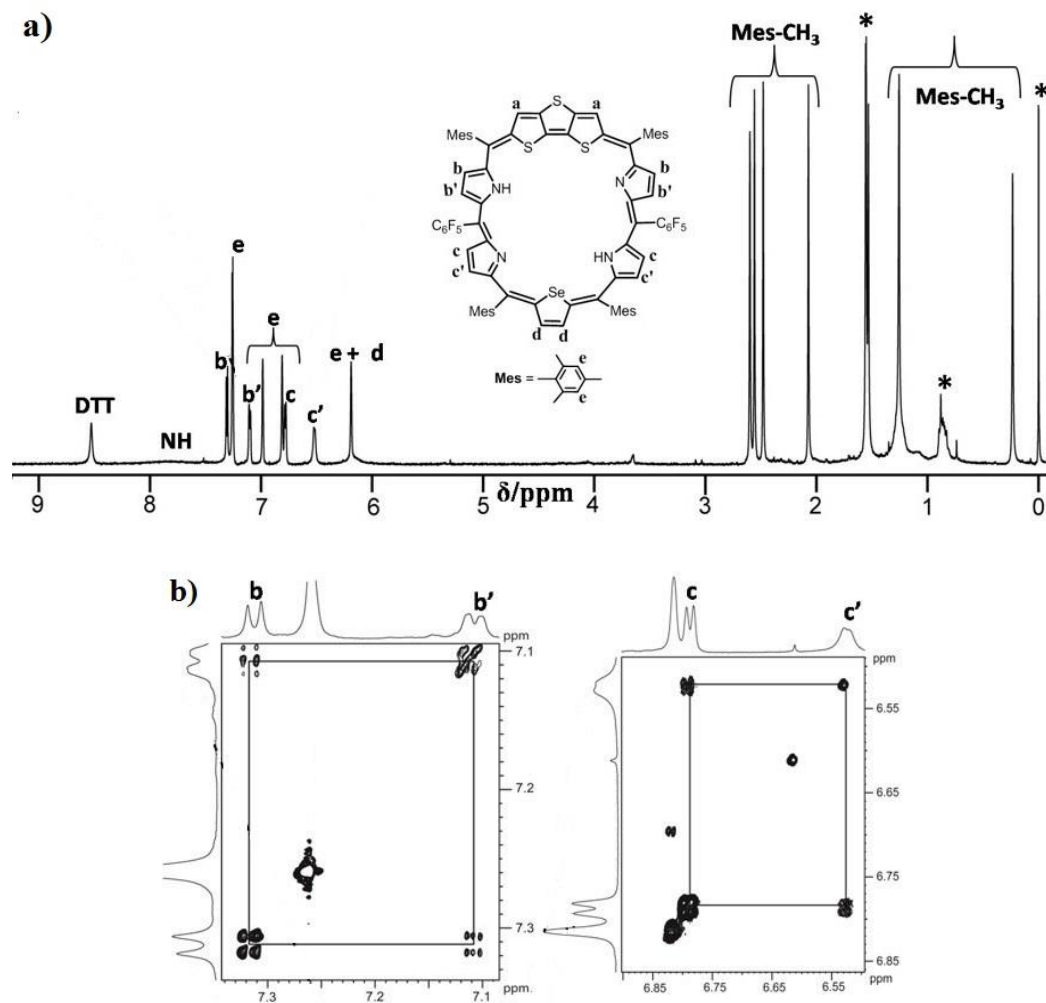


Figure 4.5: ^1H NMR spectrum of **29** at 298K in CDCl_3 (a) and ^1H - ^1H COSY spectrum of **29** with pyrrolic β -CH proton correlations (b).

The variable temperature ^1H NMR of **28** was recorded in CDCl_3 , which reveals that NH proton gradually downfield shifted upon increasing the temperature from 298 to 323 K. On the other hand, upon lowering the temperature from 298 to 223K, the DTT protons are slightly downfield shifted and rest of the β -CH of pyrrole, thiophene and *meso*-mesityl-CH protons are gradually broadened, however, the *meso*-mesityl methyl protons are slightly upfield shifted.

The significant Möbius topology was observed upon lowering the temperature where the broad signals observed in CDCl_3 at 223K is well resolved at 213-183K in CD_2Cl_2 (Figure 4.6). A set of sharp signals for DTT 8.73 & 8.64 ppm (aa'), β -CH thiophene 5.60 & 5.18 ppm (dd'), eight doublets for β -CH pyrrole between 7.49 and 6.04 ppm (bb', b₁b₁', cc' and c₁c₁') eight sharp signals for *meso*-mesityl-CH from 7.63 to 6.02 ppm (e) and twelve signals for *meso*-mesityl methyl protons between 2.71 and -0.32 ppm were observed, in addition, the pyrrolic-NH signal become sharp and upfield shifted to 5.08 and 3.55 ppm (Figure 4.7a). The thiophene and pyrrolic β -CH signals are further confirmed by ^1H - ^1H COSY studies (Figure 4.7b) and the NH signals are vanished by $\text{CD}_2\text{Cl}_2/\text{D}_2\text{O}$ experiment. These observations suggest that there is an anomalous change in structure upon lowering the temperature. Overall, the ^1H NMR at 213-183K proves that molecule lost C_2 -symmetry orientation and thus adopts Möbius conformation with stronger diatropic ring current.

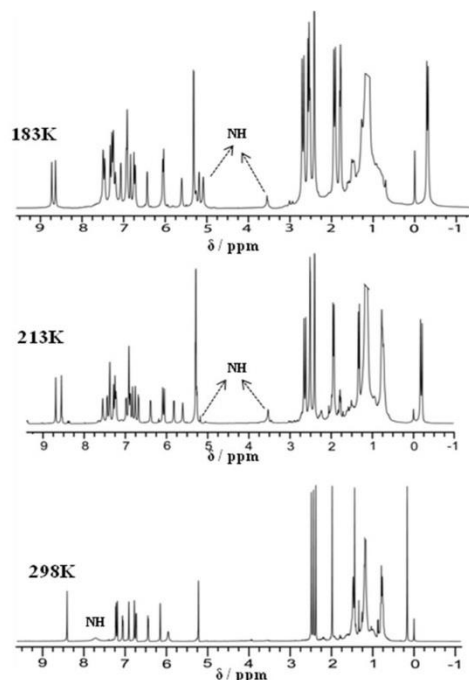


Figure 4.6: Variable temperature ^1H NMR spectrum of **28** in CD_2Cl_2

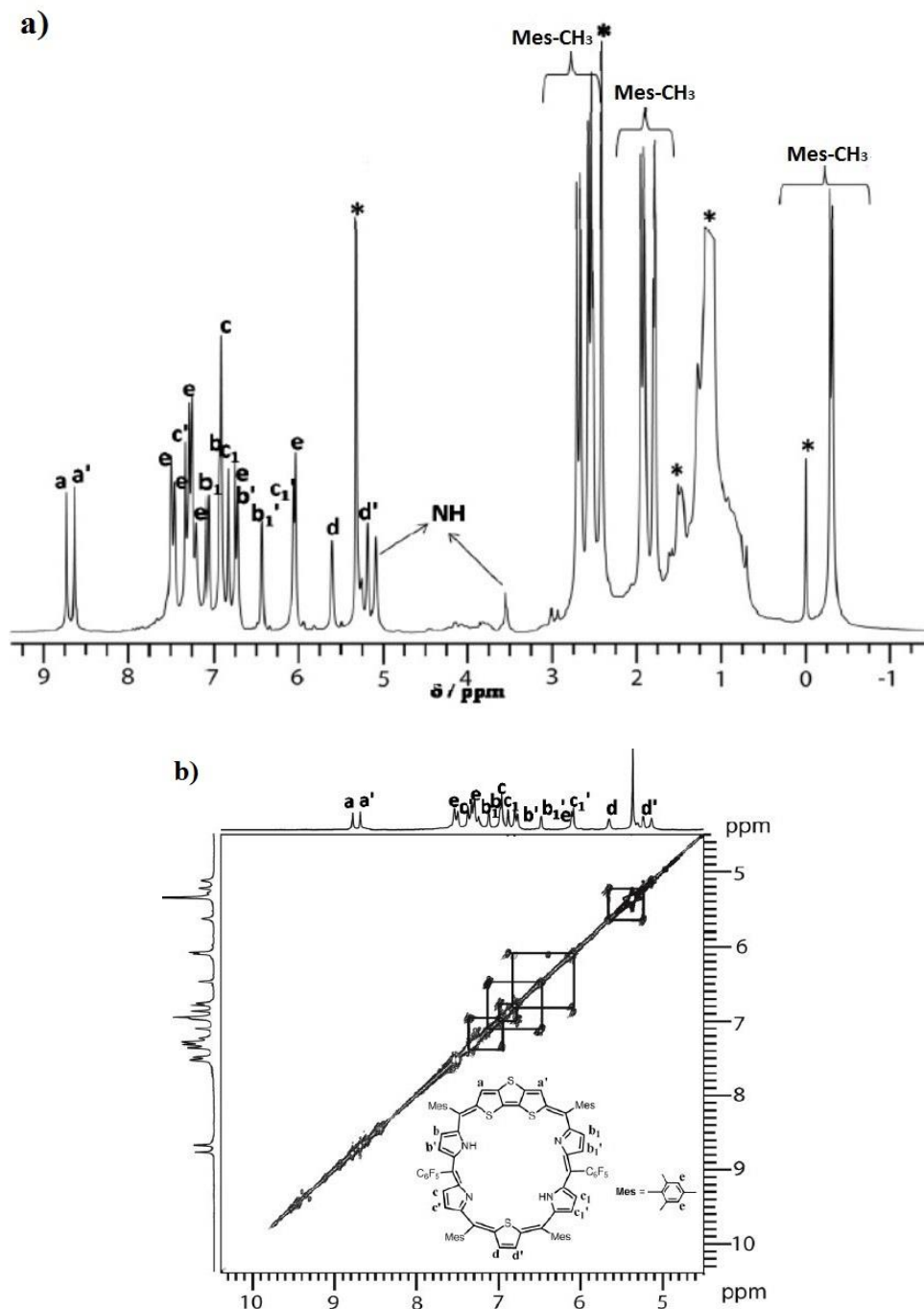
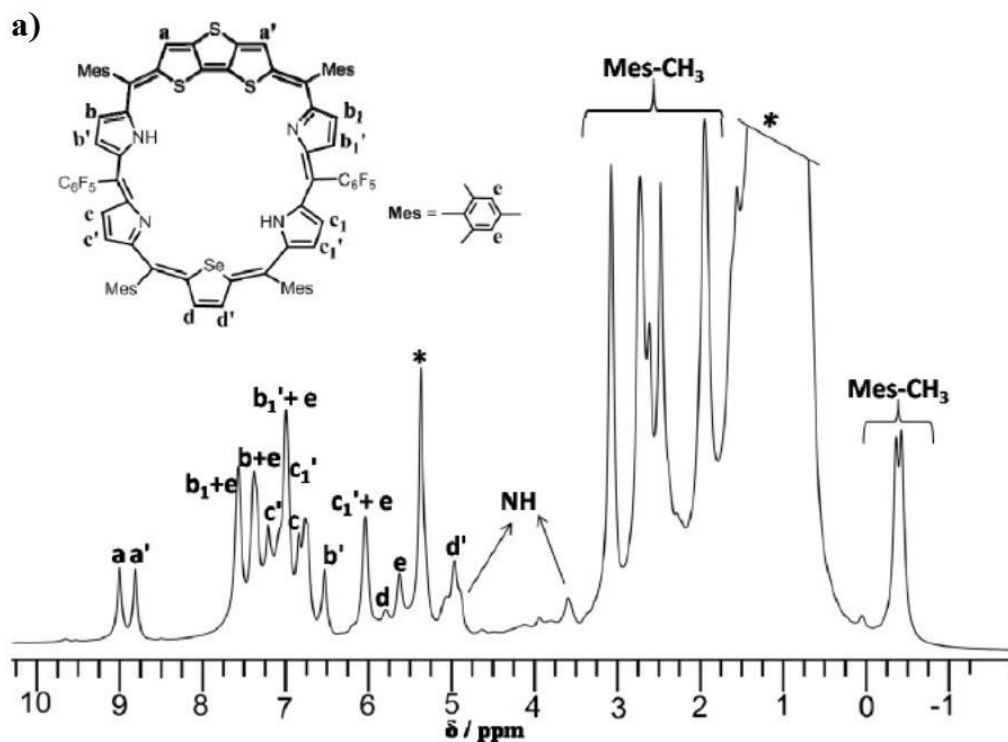


Figure 4.7: ^1H NMR spectrum of **28** at 183K in CD_2Cl_2 (a) and ^1H - ^1H COSY spectrum of **28** with thiophene and pyrrolic β -CH proton correlations (b).

Similar spectral pattern was observed in **29** upon lowering temperature from 298K to 183K. DTT β -CH are appeared at 8.93 ppm (a) and 8.74 ppm (a'). The four pyrrolic β -CH are at

7.67 ppm to 5.97 ppm (bb' , b_1b_1' , cc' and c_1c_1') as eight signals. Selenophene β -CH are appeared at 5.82 ppm and 4.99 ppm (d , d') (Figure 4.8a). These were further confirmed by ^1H - ^1H COSY spectral analysis (Figure 4.8b). The *meso*-mesityl CH protons are at 7.65 ppm to 6.66 ppm (e) as eight sharp signals. The inner NH signals are resonated as sharp singlet at 4.89 and 3.35 ppm. The *meso*-mesityl methyl signals are observed at 3.01-1.49 ppm and the respective protons which are in the diatropic ring current are resonated at -0.43 ppm and -0.49 ppm. Overall, the Möbius aromatic character was maintained as such upon introducing the bulkier heteroatom in the macrocyclic framework.



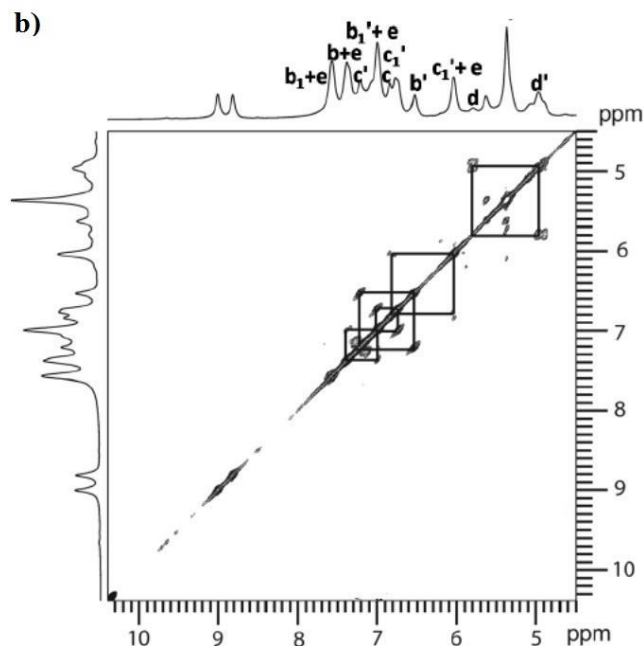


Figure 4.8: ^1H NMR spectrum of **29** at 183K in CD_2Cl_2 (a) and ^1H - ^1H COSY spectrum of **29** with thiophene and pyrrolic β -CH proton correlations (b).

The results are further compared with **12** and **26**; (i) the figure-eight conformation in **12a** adopts non-aromatic character; (ii) the non-symmetrical pattern was observed in **12b** at 183K^[26] and (iii) the DTT and pyrrole units in **26** are inverted and experiencing the paratropic ring current.^[40] Overall, the results observed in **28** and **29** are comparable with **12b**, further confirms the Möbius aromatic character.

Upon protonation of **28** and **29** with TFA in CD_2Cl_2 at 298K illustrates the following; (i) DTT proton, pyrrole- β -CH and *meso*-mesityl-CH protons are slightly downfield shifted; (ii) the NH protons are shifted upfield at 5.66 & 3.43 ppm (**28**) (Figure 4.9) and 5.37 & 3.81 ppm (**29**) (Figure 4.10) upon increasing the concentration of TFA; (iii) the β -CH proton of thiophene is slightly shielded by 0.17 ppm and resonated at 5.79 ppm (d) (**28**) and the selenophene β -CH proton is observed at 5.66 ppm (d) (**29**); (iv) similarly, the *meso*-mesityl

methyl protons, which are in the aromatic ring current in the freebase form, are further upfield shifted and observed at -1.16 ppm (**28**) and -1.46 ppm (**29**), respectively. Overall, it has been concluded that the retention of Möbius aromaticity with effective π -electron delocalization even after protonation. A comparison of these results with protonated derivatives of **12** and **26** reveals that **12** adopts figure-eight conformation with Möbius aromatic character,^[26] while **26** maintains the Hückel anti-aromatic character as such in solution.^[40]

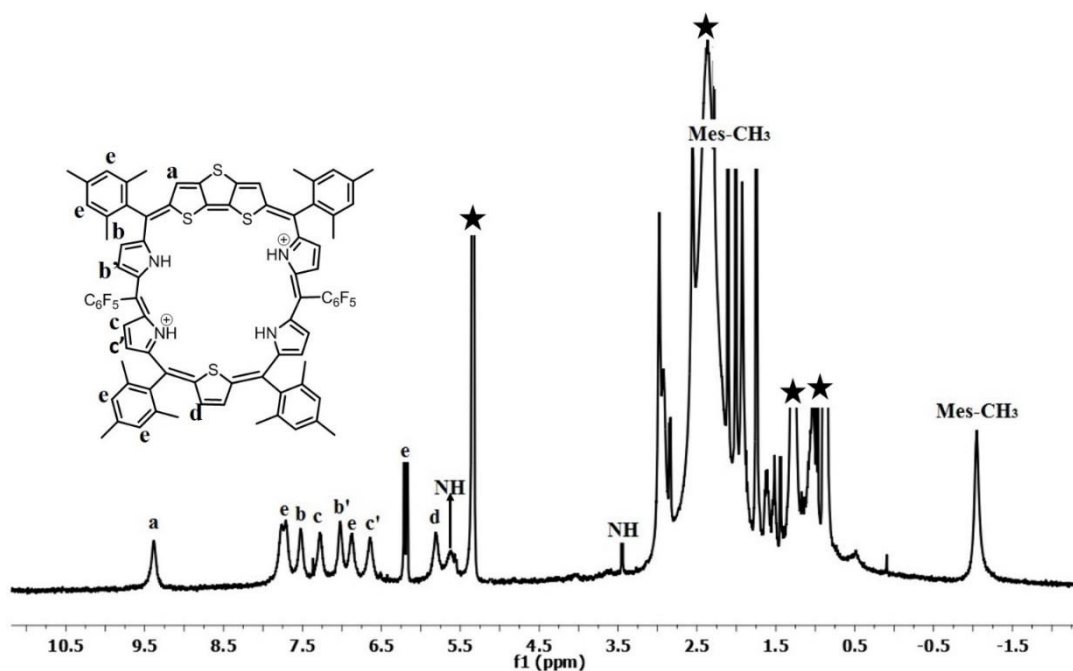


Figure 4.9: ¹H NMR spectrum of **28.2H⁺** at 298K in CD₂Cl₂.

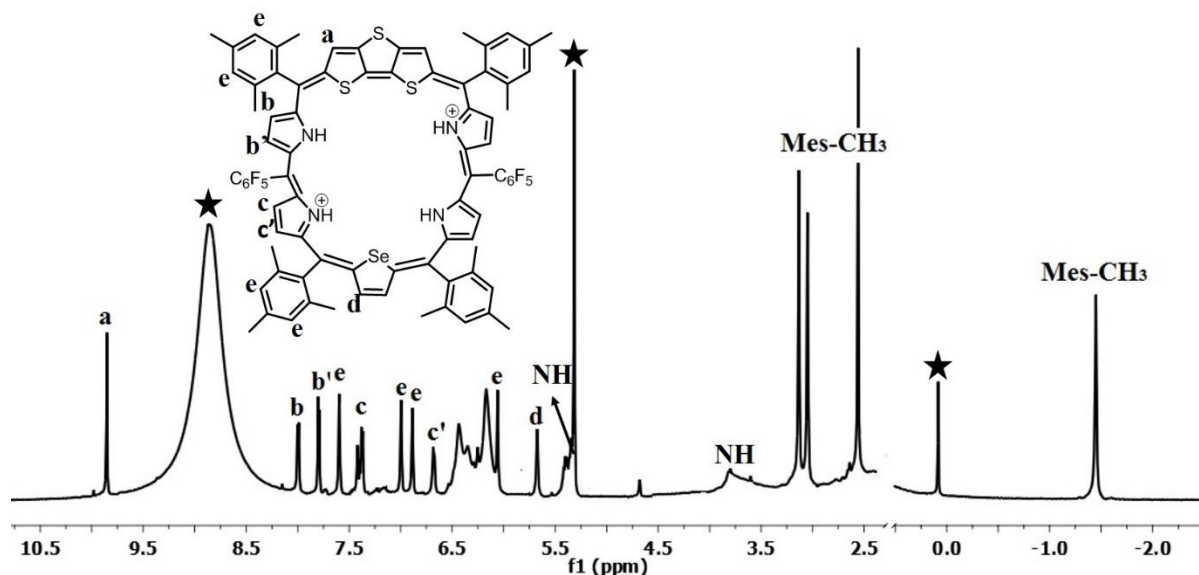


Figure 4.10: ^1H NMR spectrum of 29.2H^+ at 298K in CD_2Cl_2 .

4.3.2.3 Single Crystal X-ray Analysis

The structure of **28** and **29** was unambiguously confirmed by single-crystal X-ray diffraction analysis (Figure 4.11 – 4.12, Table 4.2). Both the compounds were crystallized in a triclinic crystal system with the *P*-1 space group. The crystal structure of **28** is shown in Figure 4.11. As reflected from the spectral analysis, the DTT-dipyrin moiety and thia-tripyrin units are connected by pentafluorophenyl groups and adopts a nonplanar structure with $[32]\pi$ -electron circuit, in addition, one of the *meso*-mesityl methyl protons are in the macrocyclic aromatic ring current. The observed torsion angles of 32.13° (C5-C6-C7-S1) and 30.27° (S3-C14-C15-C16) in **28** and respective values in **29** are 30.44° and 29.54° (Table 4.1) favor the overall π electron conjugation and facilitating the aromatic Möbius stabilization in the freebase form. Thus, the large strain associated with the figure eight conformation is nicely distributed across the macrocycle, which leads to effective π electron delocalization in the framework.

The amino and imino nitrogen atoms present in dipyrin moiety in **28** are in strong intramolecular hydrogen bonding interactions (N2-H2...N1 and N4-H4...N3) with distances of 2.23 and 2.16 Å and angles of 119° and 122°, (Figure 4.11a) respectively. Similar such interaction with bond distances and angles in **29** are 2.25 & 2.17 Å and 117.27° & 122.33° (Figure 4.12a). The DTT moiety in **28** is almost perpendicular to the thiophene unit with an angle of 84.61° (Figure 4.11b) and are appended one over the other with the nonbonding distance between the π -electron cloud of thiophene ring and S1 & S3 of DTT ring is 3.93 and 3.83 Å respectively. In the case of **29**, the respective angle is 83.30° (Figure 4.12b) and the nonbonding distance between selenophene ring and S2 & S3 of DTT ring is 3.90 and 3.88 Å. On the other hand, the crystal analysis of **12a** in protonated form and **12b** in freebase adopt Möbius conformation,^[26] while **26** retains the Hückel anti-aromatic character in the solid state. An intriguing fact also noticed from crystal structure of **28** that the molecule exists as self-assembled dimer and one dimensional arrays through intermolecular hydrogen bonding interactions. The self-assembled dimers are generated between (i) pyrrolic β -CH (C3-H63) with one of the fluorine atoms (F4) from pentafluorophenyl unit and (ii) one of the *meso*-mesityl methyl units (C54-H2A) with adjacent molecule *meso*-mesityl π -cloud (Mes- π). The bond distances and angles of C3-H63...F4 and C54-H2A...Mes(π) are 2.66 Å & 138.23° and 2.75 Å & 148.17°, respectively (Figure 4.13). Similarly, the one dimensional arrays are generated between (i) one of the *meso*-mesityl CH units (C67-H48) with neighboring unit F2 atom and (ii) one of the *meso*-mesityl methyl CH units (C78-H21) with adjacent molecule F9 atom. The bond distances and angles of C67-H48...F2 and C78-H21...F9 are 2.85 Å & 147.37° and 2.5 Å & 163.12° (Figure 4.14). Both the self-assembled dimers and one dimensional arrays were combined

together to generate two dimensional supramolecular assembly in the solid state (Figure 4.15).

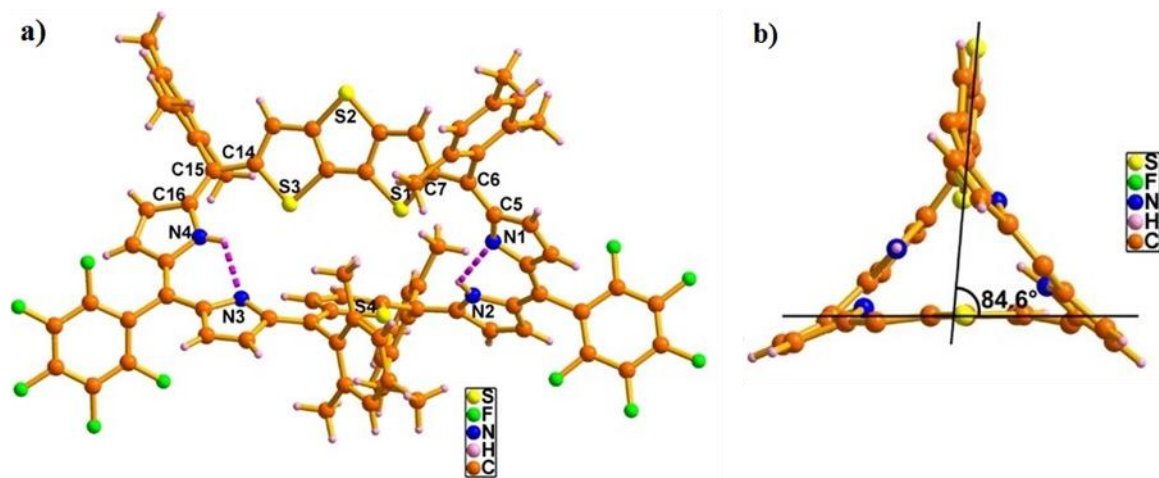


Figure 4.11: Single crystal X-ray structure of **28** (a) top view and (b) side view.

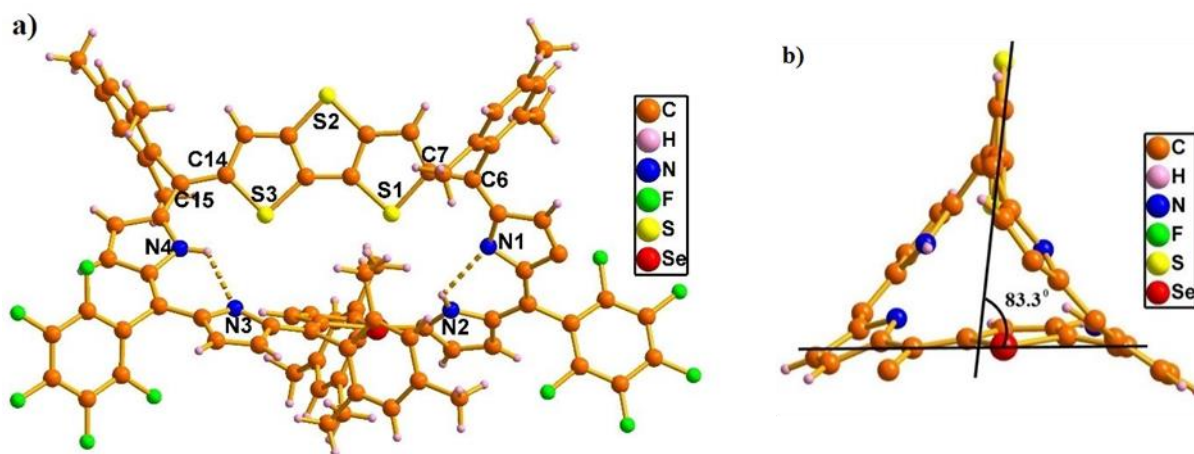


Figure 4.12: Single crystal X-ray structure of **29** (a) top view and (b) side view.

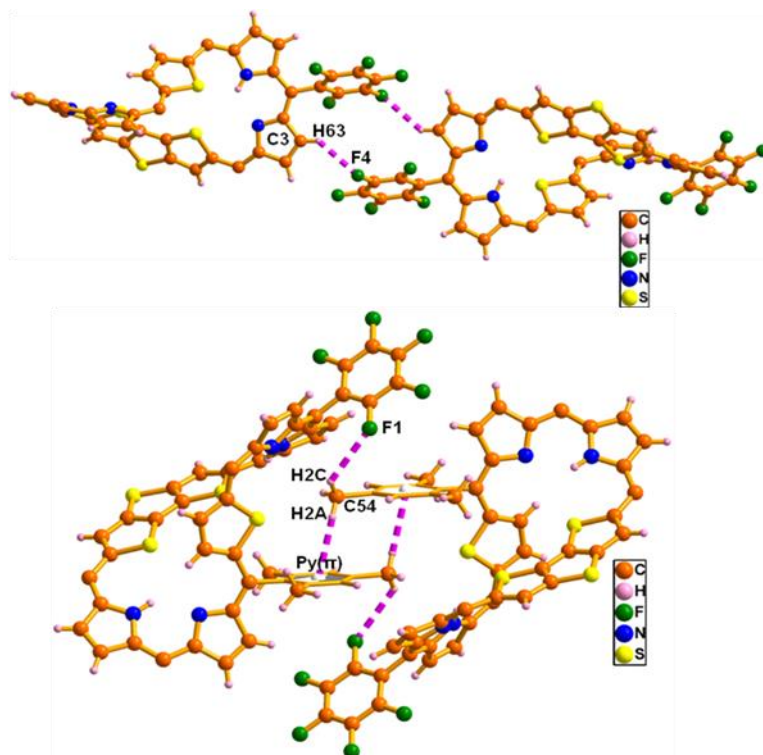


Figure 4.13: Self-assembled dimer of **28**.

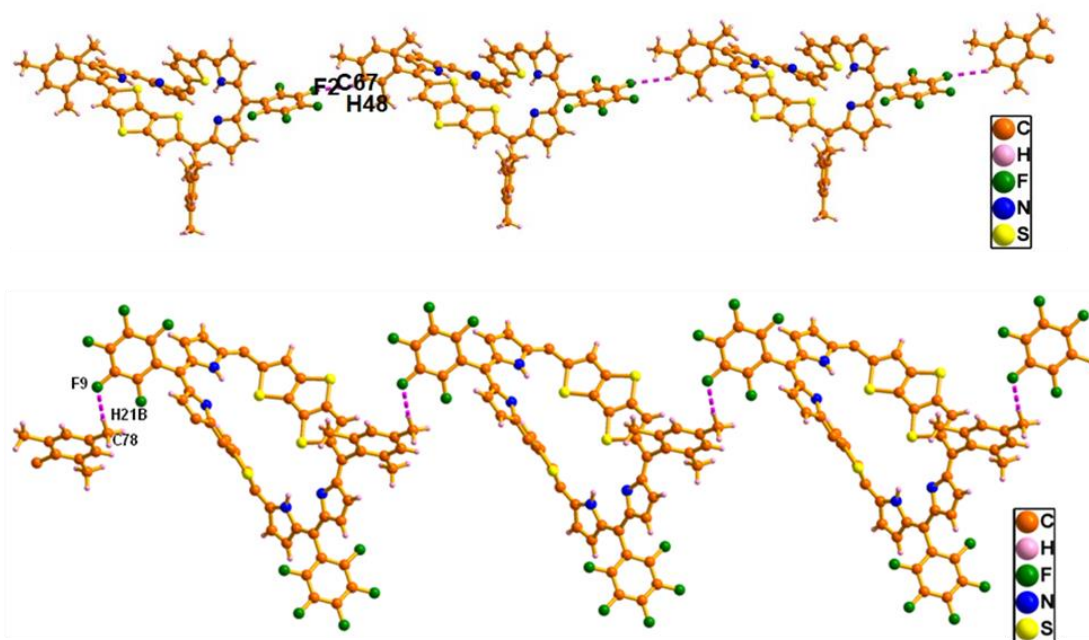


Figure 4.14: One dimensional array of **28**.

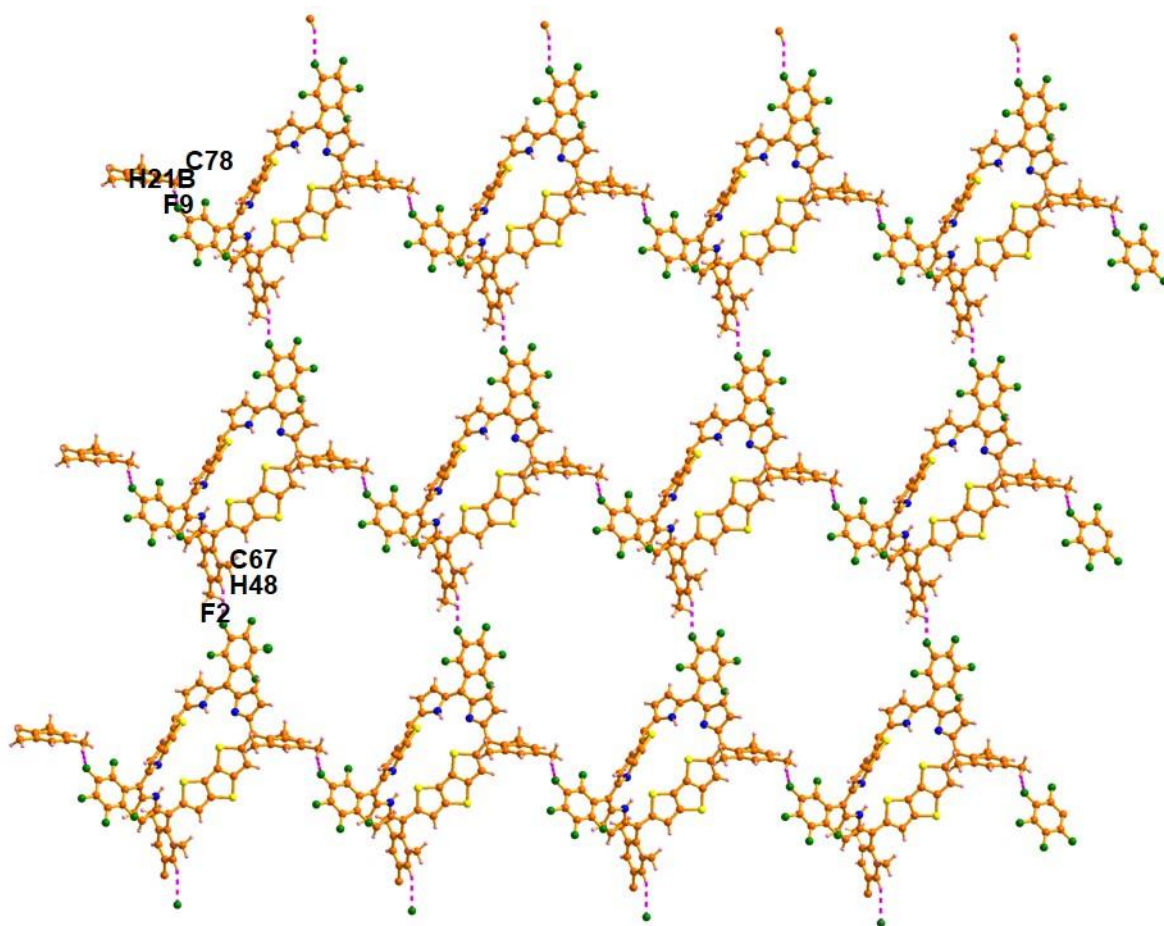


Figure 4.15: Two dimensional array of **28**.

28				29			
Bond Length (Å)		Tarsion angle (°)		Bond Length (Å)		Tarsion angle (°)	
C1-C2	1.419	C34-C1-C2-N1	9.05	C1-C2	1.402	C34-C1-C2-N1	7.48
C5-C6	1.37	N1-C5-C6-C7	7.24	C5-C6	1.36	N1-C5-C6-C7	8.47
C6-C7	1.443	C5-C6-C7-S1	32.13	C6-C7	1.432	C5-C6-C7-S1	30.44
C14-C15	1.445	S3-C14-C15-C16	30.27	C14-C15	1.452	S3-C14-C15-C16	29.54
C20-C21	1.427	C19-C20-C21-N3	19.4	C20-C21	1.432	C19-C20-C21-N3	19.88
C24-C25	1.389	N3-C24-C25-C26	9.38	C24-C25	1.392	N3-C24-C25-C26	8.52
C25-C26	1.440	C24-C25-C26-C27	9.97	C25-C26	1.413	C24-C25-C26-C27	10.24
C29-C30	1.426	S4-C29-C30-C31	22.2	C29-C30	1.423	Se1-C29-C30-C31	22.13
C30-C31	1.381	C29-C30-C31-N2	20.49	C12-C11	1.382	C22-C12-C11-N4	17.80
C34-C1	1.384	N2-C34-C1-C2	10.5	C8-C1	1.389	N2-C34-C1-C2	12.65

Table 4.1: Selected bond lengths (Å) and torsion angles (°) of **28** and **29**.

Table 4.2: Crystal data for **28** and **29**

	28	29
<i>T</i> , K	100(2)	100(2)
Formula	C ₈₂ H ₅₈ F ₁₀ N ₄ S ₄	C ₈₂ H ₅₈ F ₁₀ N ₄ S ₃ Se
Formula weight	1574.55	1583.84
Color and Habit	Dark blue	Dark blue
Crystal system	Triclinic	Triclinic
Space group	<i>P</i> -1	<i>P</i> -1
<i>a</i> , Å	12.7779(4)	12.836(5)
<i>b</i> , Å	15.9694(5)	15.847(5)
<i>c</i> , Å	21.8023(7)	21.762(5)
α , deg	107.888(2)	107.623(5)
β , deg	100.997(2)	100.230(5)
γ , deg	100.881(2)	100.971(5)
<i>V</i> , Å ³	4006.6(2)	4009(2)
Radiation (λ , Å)	Mo K α (0.71073)	Mo K α (0.71073)
<i>Z</i>	2	2
d_{calcd} , g•cm ⁻³	1.305	1.312
μ , mm ⁻¹	0.256	0.715
<i>F</i> (000)	1620	1616
No. of unique reflns	14916	14039
No. of params. refined	994	949
GOF on <i>F</i> ²	0.991	1.036
<i>R</i> 1 ^a [<i>I</i> > 2 σ (<i>I</i>)]	0.0734	0.0977
<i>R</i> 1 ^a (all data)	0.0787	0.0987
wR 2 ^b (all data)	0.2318	0.3170

4.3.2.4 Electronic spectral analysis

The electronic absorption spectrum of **28** in freebase as well as protonated form is shown in Figure 4.16. The compound **28** in its freebase form illustrates well-defined peaks, with intense Soret-like band at 604 nm and a distinct Q-band at 868 nm with molar absorption coefficient (ϵ) of the Soret band is 10^5 , suggests the aromatic character. The spectral pattern is similar to other Möbius aromatic expanded porphyrins. The results are further compared with **24** and **26**; (i) the red shift of both the Soret and Q-bands in **28**, as compared to **24**,^[39] reflects the extension in the π -electron conjugation and (ii) one fold higher in the molar absorption coefficient of intense band in **28**, as compared to **26**, indicates the aromatic character. The absorption spectra of **28** remain unaltered upon changing the polarity of the solvent (Figure 4.17), as observed in **12b**, proves the conformation remain intact, however, **12a** in polar solvent adopts Möbius aromaticity.

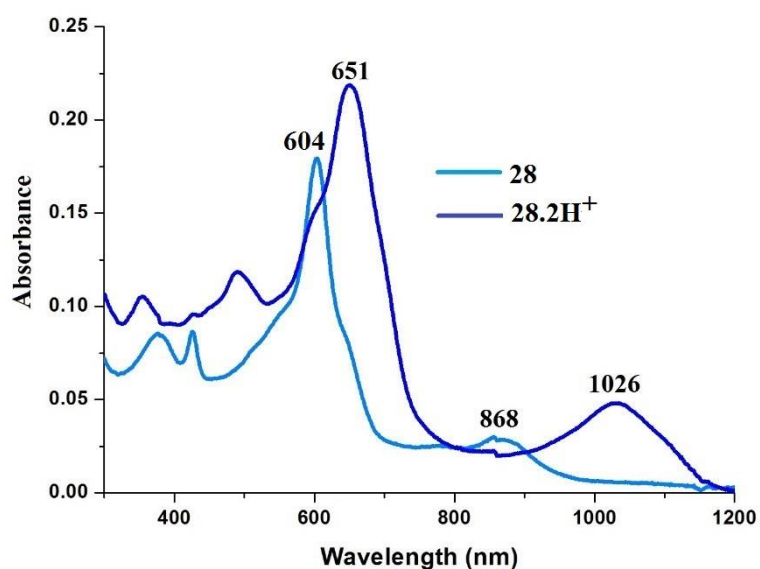


Figure 4.16: The electronic absorption spectrum of **28** and **28.2H⁺** in CH₂Cl₂.

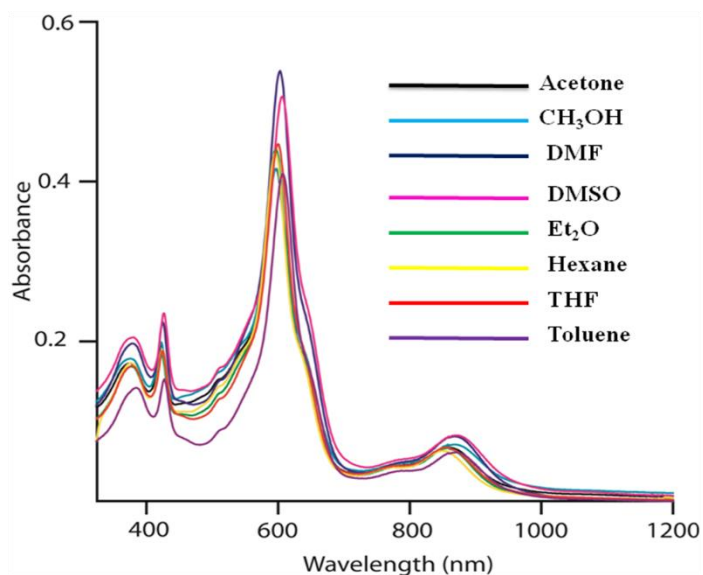


Figure 4.17: The electronic absorption spectrum of **28** in various solvents at 298K.

Protonation by using a dilute solution of TFA, the intense band in **28** is red-shifted to 651 nm with a shift value of 48 nm and a weak Q-band in the near IR region at 1026 nm (Figure 4.16). The ϵ value of the Soret band is 1.2 times higher as compared to free-base ligand, suggests the protonated derivative is more-aromatic. Similar trend was observed in **29** (Figure 4.18). The Soret band at 608 nm and weak Q-band at 895 nm in **29** are red-shifted by 47 nm and 127 nm upon protonation and appeared at 655 nm and 1022 nm, respectively. The electronic spectral analysis reveals that **29** maintains the Möbius aromaticity in the free-base state and enhanced aromaticity in the protonated state. Overall, the extension in the π -electron conjugation as well as reduction in the number of heteroatom reflects the Möbius aromaticity in **28** and **29** both in freebase as well as protonated state.

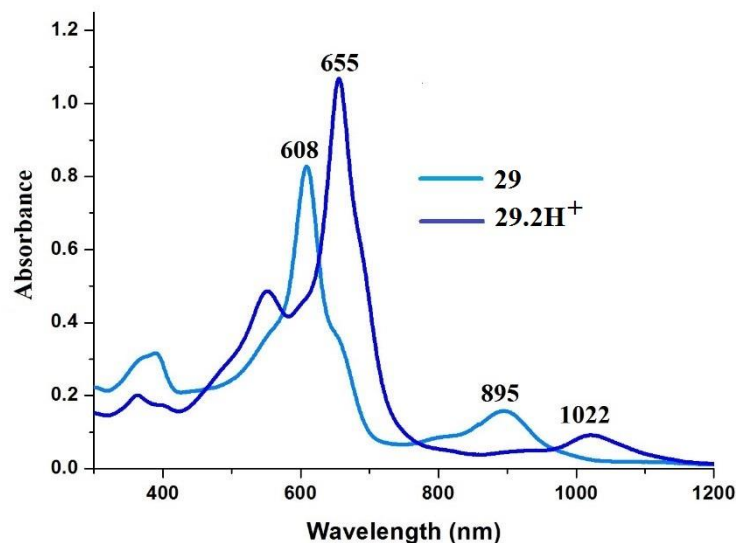


Figure 4.18: The electronic absorption spectrum of **29** and **29.2H⁺** in CH₂Cl₂.

4.3.2.5 Nucleus Independent Chemical Shift (NICS)

The computational studies of **28**, **29** and its protonated derivatives were performed with *Gaussian09*^[40] at the M06L/6-31G** level^[41] to visualize the geometry and electronic structure (Figure 4.19 and 4.20). The nucleus-independent chemical shift (NICS)(0) values calculated at various geometrical positions within **28** indicate that center position of pyrrolic rings containing amino nitrogen have large negative values (-7.2 to -8.4 ppm) compared to imino nitrogen (-1.5 to -2.7 ppm). Similarly higher negative values are observed for terminal thiophene rings of DTT (-16.3 to -18.3 ppm) as compared to core thiophene unit (-13.8 ppm). The NICS(0) value calculated at the center of the macrocycle is found to be -8.1 ppm clearly reflects the Möbius aromaticity (Figure 4.19a). Moreover, upon protonation, the NICS(0) value for (i) the imino and amino nitrogen values are more negative (-10.2 ppm to -11.4 ppm) and (ii) moderate decrease in core-thiophene unit and increase in terminal thiophene

rings of DTT unit, as compared to free-base ligand. Overall, the centroid NICS(0) value is found to be -9.9 ppm (Figure 4.19b).

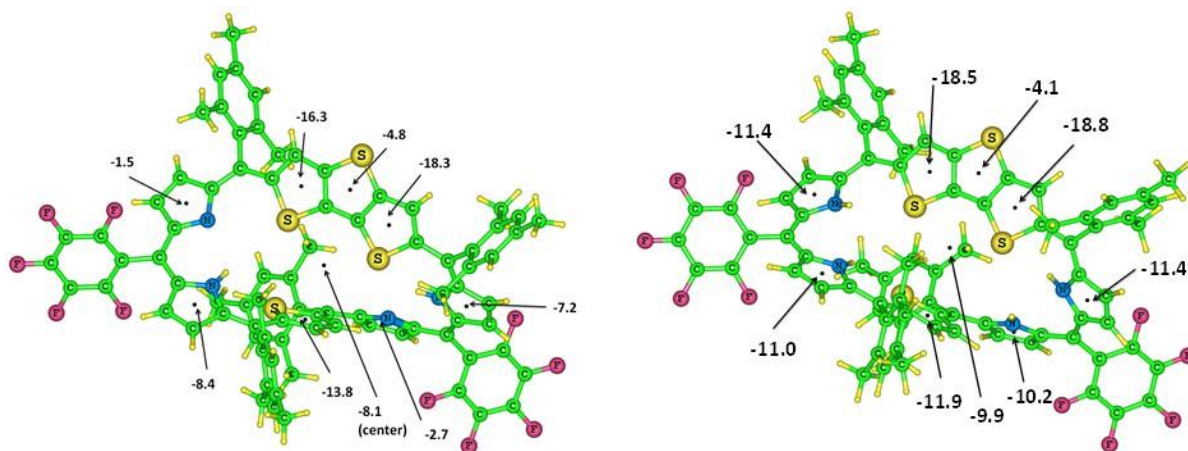


Figure 4.19: NICS(0) values of **28** and **28.2H⁺**.

The theoretical results are consistent with **29** and its protonated derivative, where the NICS(0) values are -7.2 and -10.9 ppm, respectively (Figure 4.20). Overall, as observed from the spectral and structural analyses, the Möbius character is reflected in the neutral stage and the extent of aromaticity is enhanced upon protonation.

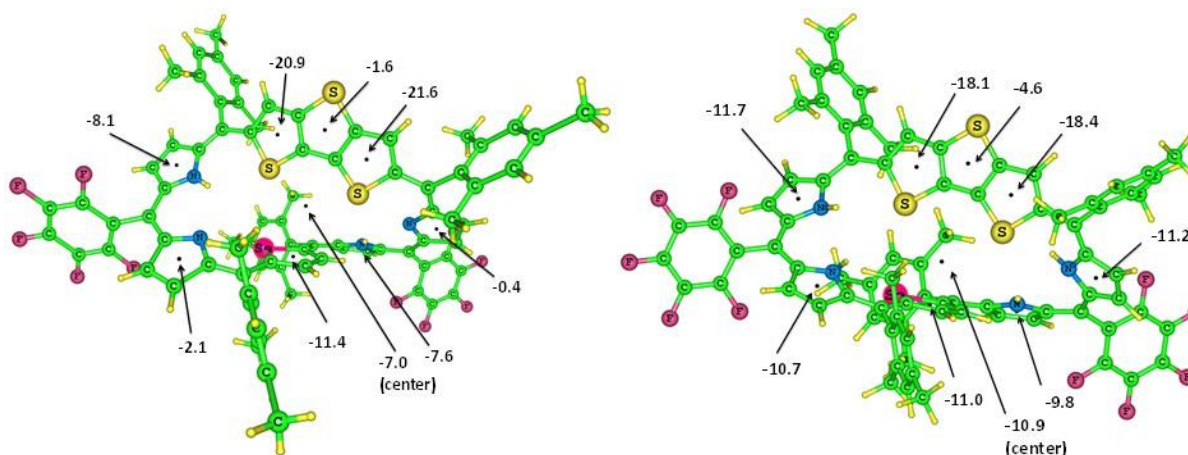


Figure 4.20: NICS(0) values of **29** and **29.2H⁺**.

4.3.2.6 Anisotropy Induced Current Density (AICD)

Like NICS(0), the AICD calculations are considered as the best index to evaluate the aromaticity of the macrocycle. We have also attempted to directly visualize the induced ring current by using AICD method which describes the 3D image of delocalized electron densities with scalar field. The AICD method illustrates the paramagnetic term of the induced current density, the aromatic molecule shows clockwise current density, whereas anti-aromatic molecule displays counter-clockwise current density. In the AICD plot of both freebase as well as protonated derivatives of **28** (Figure 4.21) and **29** (Figure 4.22) allows clockwise current delocalization, thus confirms the aromatic behaviour inside the macrocycles although not planar, as reflected from the spectral and structural analyses.

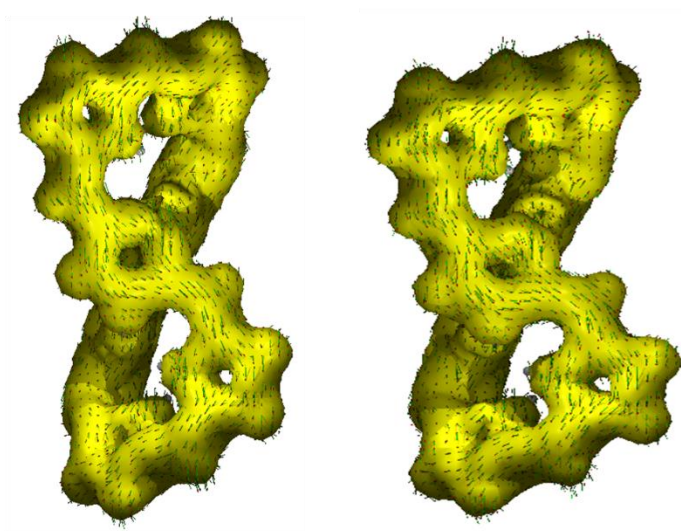


Figure 4.21: AICD plot for **28** and **28.2H⁺**.

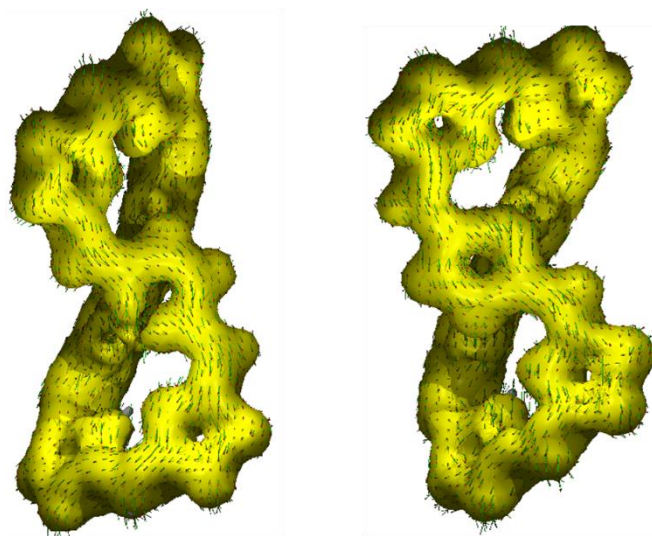


Figure 4.22: AICD plot for **29** and **29.2H⁺**.

4.4 Conclusions

In summary, we have successfully synthesized the $[32]\pi$ fused core-modified heptaphyrin and demonstrated its Möbius aromatic character without any external stimuli. It is known in the literature that the right combination of certain degree of planarity as well as distortion in the molecular framework, in order to achieve the Möbius topology. Here, (i) the introduction of rigid & planar DTT core and the core-modified & flexible tripyrrane unit in the macrocyclic framework; (ii) reduction of number of heteroatoms in the framework; (iii) the number and right mixing of *meso*-aryl units and (iv) protonation, which keeps control over the geometry and modulate the system from $[4n]\pi$ Hückel non-/anti-aromatic topology towards $[4n]\pi$ Möbius aromaticity with nonplanar conformation. In addition to the spectral and structural analyses, the Möbius aromaticity is unambiguously confirmed by theoretical calculations.

4.5 Experimental Procedure

4.5.1 Synthesis of **28**

DTT-dipyrrane (**27**) (0.300 g, 0.51 mmol) and thiatripyrrane (**19**) (0.244 g, 0.51 mmol) were dissolved in dry CH₂Cl₂ (200 ml) and reaction mixture was stirred under gentle flow of nitrogen gas. Pentafluorobenzaldehyde (0.063 ml, 0.51 mmol) was initially added to solution, after 10 min *paratoluenesulfonic acid* (0.032 g, 0.17 mmol) was added and the progress of the reaction was monitored by TLC. After 1.5h, DDQ (0.212 g, 0.76 mmol) was added to the reaction mixture and stirring was continued for further 2h. The resulting solution was completely dried under vacuum and crude residue was purified by column chromatography over basic alumina followed by silica gel (100–200 mesh). The blue fraction eluted with CH₂Cl₂/*n*-hexane (35:65, v/v) was identified as desired heptaphyrin (**28**). Further recrystallization from CH₂Cl₂/CH₃OH provides greenish-blue solid crystals in 6% yield.

Compound 28: ¹H NMR (400 MHz, CD₂Cl₂) δ (in ppm) = 8.48 (s, 1H), 7.43 (s, NH), 7.36 (d, $J = 5.0$ Hz, 1H), 7.27 (s, 1H), 7.13 (d, $J = 3.9$ Hz, 1H), 6.96 (s, 1H), 6.83 (d, $J = 5.0$ Hz, 1H), 6.82 (s, 1H), 6.57 (d, $J = 4.9$ Hz, 1H), 6.15 (s, 1H), 5.97 (s, 1H), 2.66 (s, 3H), 2.56 (s, 3H), 2.48 (s, 3H), 2.06 (s, 3H), 1.45 (s, 3H), 0.16 (s, 3H); **28**·**2H**⁺: ¹H NMR (400 MHz, CD₂Cl₂) δ (in ppm) = 9.32 (s, 1H), 7.39 (d, $J = 8.6$ Hz, 1H), 7.32 (s, 1H), 7.25 (d, $J = 5.5$ Hz, 1H), 7.08 (d, $J = 7.4$ Hz, 1H), 6.91 (d, $J = 5.8$ Hz, 1H), 6.12 (s, 1.5H), 6.08 (s, 1.5H), 5.73 (s, 1H), 5.57 (s, NH), 2.88 (s, 2H), 2.45 (s, 2H), 2.01 (s, 6H), 1.92 (s, 6H), -1.16 (s, 1H). **28**: UV/Vis (CH₂Cl₂): λ_{\max} in nm (ϵ in dm³mol⁻¹cm⁻¹) = 377 (5.01×10⁴), 604 (1.59×10⁵), 868 (2.52×10⁴); **28**·**2H**⁺ (TFA/CH₂Cl₂): λ_{\max} in nm (ϵ in dm³mol⁻¹cm⁻¹) = 355 (1.1×10⁴), 545

(1.33×10^5), 651 (2.1×10^5) 1025 (4.24×10^4); Elemental analysis calcd (%) for $C_{82}H_{58}F_{10}N_4S_4$: C 69.47, H 4.12, N 3.95; found: C 69.36, H 4.32, N 3.84.

4.5.2 Synthesis of **29**

DTT-dipyrrane (**27**) (0.300 g, 0.51 mmol), selenatripyrrane (**20**) (0.267 g, 0.51 mmol) in dry CH_2Cl_2 (200 ml), pentafluorobenzaldehyde (0.063 ml, 0.51 mmol) and *paratoluenesulfonic* acid (0.032 g, 0.17 mmol) were mixed under similar reaction condition as mentioned above. After 1.5h, DDQ (0.212 g, 0.76 mmol) was added to the reaction mixture and stirring was continued for further 2h. The resulting solution was completely dried under vacuum and crude residue was purified by column chromatography over basic alumina followed by silica gel (100–200 mesh). The blue fraction eluted with CH_2Cl_2/n -hexane (38:62, v/v) was identified as desired heptaphyrin (**29**). Further recrystallization from CH_2Cl_2/CH_3OH provides greenish-blue solid crystals in 7% yield.

Compound 29: 1H NMR (400 MHz, CD_2Cl_2) δ (in ppm) = 8.53 (s, 1H), 7.83 (s, NH), 7.31 (d, $J = 4.9$ Hz, 1H), 7.26 (s, 1H), 7.10 (d, $J = 4.0$ Hz, 1H), 6.98 (s, 1H), 6.81 (s, 1H), 6.78 (d, $J = 3.8$ Hz, 1H), 6.52 (d, $J = 3.8$ Hz, 1H), 6.19 (s, 1H), 6.17 (s, 1H), 2.60 (s, 3H), 2.56 (s, 3H), 2.48 (s, 3H), 2.07 (s, 3H), 1.53 (s, 3H), 0.23 (s, 3H); **29·2H⁺**: 1H NMR (400 MHz, CD_2Cl_2) δ (in ppm) = 9.76 (s, 1H), 7.91 (d, $J = 4.9$ Hz, 1H), 7.71 (d, $J = 5.0$ Hz, 1H), 7.50 (s, 1H), 7.29 (d, $J = 4.8$ Hz, 1H), 6.90 (s, 1H), 6.79 (s, 1H), 6.60 (d, $J = 4.1$ Hz, 1H), 5.98 (s, 1H), 5.40 (s, NH), 3.05 (s, 5H), 2.97 (s, 5H), 2.48 (s, 6H), -1.58 (s, 2H). **29**: UV/Vis (CH_2Cl_2): λ_{max} in nm (ϵ in $dm^3 mol^{-1} cm^{-1}$) = 390 (6.06×10^4), 608 (1.59×10^5), 895 (3.03×10^4); **29·2H⁺** (TFA/ CH_2Cl_2): λ_{max} in nm (ϵ in $dm^3 mol^{-1} cm^{-1}$) = 363 (3.85×10^4), 553 (9.3×10^4), 655 (2.24×10^5), 1022 (1.7×10^4); Elemental analysis calcd (%) for $C_{82}H_{58}F_{10}N_4S_3Se$: C 67.24, H 3.99, N 3.82; found: C 67.32, H 3.78, N 3.76.

4.6 References:

1. Ménand, M.; Sollogoub, M.; Boitrel, B.; Le Gac, S. *Angew. Chem. Int. Ed.* **2016**, *55*, 297-301.
2. Rana, A.; Lee, S.; Kim, D.; Panda, P. K. *Chem. Eur. J.* **2015**, *21*, 12129-12135.
3. Sung, Y. M.; Oh, J.; Cha, W.-Y.; Kim, W.; Lim, J. M.; Yoon, M.-C.; Kim, D. *Chem. Rev.* **2017**, *117*, 2257-2312.
4. Ho, I. T.; Zhang, Z.; Ishida, M.; Lynch, V. M.; Cha, W.-Y.; Sung, Y. M.; Kim, D.; Sessler, J. L. *J. Am. Chem. Soc.* **2014**, *136*, 4281-4286.
5. Gopee, H.; Kong, X.; He, Z.; Chambrier, I.; Hughes, D. L.; Tizzard, G. J.; Coles, S. J.; Cammidge, A. N. *J. Org. Chem.* **2013**, *78*, 9505-9511.
6. Saito, S.; Osuka, A. *Angew. Chem. Int. Ed.* **2011**, *50*, 4342-4373.
7. Sessler, J. L.; Seidel, D. *Angew. Chem. Int. Ed.* **2003**, *42*, 5134-5175.
8. Stępień, M.; Sprutta, N.; Latos-Grażyński, L. *Angew. Chem. Int. Ed.* **2011**, *50*, 4288-4340.
9. Umetani, M.; Tanaka, T.; Kim, T.; Kim, D.; Osuka, A. *Angew. Chem. Int. Ed.* **2016**, *55*, 8095-8099.
10. Osuka, A.; Saito, S. *Chem. Commun.* **2011**, *47*, 4330-4339.
11. Shimizu, S.; Aratani, N.; Osuka, A. *Chem. Eur. J.* **2006**, *12*, 4909-4918.
12. Tanaka, Y.; Shin, J.-Y.; Osuka, A. *Eur. J. Org. Chem.* **2008**, 1341-1349.
13. Chatterjee, T.; Theophall, G. G.; Silva, K. I.; Lakshmi, K. V.; Ravikanth, M. *Inorg. Chem.* **2016**, *55*, 6873-6881.
14. Zhang, Z.; Cha, W.-Y.; Williams, N. J.; Rush, E. L.; Ishida, M.; Lynch, V. M.; Kim, D.; Sessler, J. L. *J. Am. Chem. Soc.* **2014**, *136*, 7591-7594.

-
15. Shin, J.-Y.; Furuta, H.; Yoza, K.; Igarashi, S.; Osuka, A. *J. Am. Chem. Soc.* **2001**, *123*, 7190-7191.
 16. Saito, S.; Osuka, A. *Chem. Eur. J.* **2006**, *12*, 9095-9102.
 17. Kumar, R.; Misra, R.; Chandrashekar, T. K.; Nag, A.; Goswami, D.; Suresh, E.; Suresh, C. H. *Eur. J. Org. Chem.* **2007**, 4552-4562.
 18. Tanaka, Y.; Shin, J.-Y.; Osuka, A. *Eur. J. Org. Chem.* **2008**, 1341-1349.
 19. Soya, T.; Kim, W.; Kim, D.; Osuka, A. *Chem. Eur. J.* **2015**, *21*, 8341-8346.
 20. Gopalakrishna, T. Y.; Reddy, J. S.; Anand, V. G. *Angew. Chem. Int. Ed.* **2013**, *52*, 1763-1767.
 21. Reddy, B. K.; Gadekar, S. C.; Anand, V. G. *Chem. Commun.* **2016**, *52*, 3007-3009.
 22. Reddy, B. K.; Basavarajappa, A.; Ambhore, M. D.; Anand, V. G. *Chem. Rev.* **2017**, *117*, 3420-3443.
 23. Ajami, D.; Oeckler, O.; Simon, A.; Herges, R. *Nature* **2003**, *426*, 819-821.
 24. Stępień, M.; Latos-Grażyński, L.; Sprutta, N.; Chwalisz, P.; Szterenber, L. *Angew. Chem. Int. Ed.* **2007**, *46*, 7869-7873.
 25. Higashino, T.; Soya, T.; Kim, W.; Kim, D.; Osuka, A. *Angew. Chem. Int. Ed.* **2015**, *54*, 5456-5459.
 26. Saito, S.; Shin, J.-Y.; Lim, J. M.; Kim, K. S.; Kim, D.; Osuka, A. *Angew. Chem. Int. Ed.* **2008**, *47*, 9657-9660.
 27. Lim, J. M.; Shin, J.-Y.; Tanaka, Y.; Saito, S.; Osuka, A.; Kim, D. *J. Am. Chem. Soc.* **2010**, *132*, 3105-3114.
 28. Marcos, E.; Anglada, J. M.; Torrent-Sucarrat, M. *J. Org. Chem.* **2014**, *79*, 5036-5046.
-

-
29. Möbius, K.; Plato, M.; Klihm, G.; Laurich, C.; Savitsky, A.; Lubitz, W.; Szyszko, B.; Stepien, M.; Latos-Grazynski, L. *Phys. Chem. Chem. Phys.* **2015**, *17*, 6644-6652.
30. Sessler, J. L.; Seidel, D.; Lynch, V. *J. Am. Chem. Soc.* **1999**, *121*, 11257-11258.
31. Bucher, C.; Seidel, D.; Lynch, V.; Sessler, J. L. *Chem. Commun.* **2002**, 328-329.
32. Gokulnath, S.; Prabhuraja, V.; Chandrashekar, T. K. *Org. Lett.* **2007**, *9*, 3355-3357.
33. Köhler, T.; Seidel, D.; Lynch, V.; Arp, F. O.; Ou, Z.; Kadish, K. M.; Sessler, J. L. *J. Am. Chem. Soc.* **2003**, *125*, 6872-6873.
34. Hiroto, S.; Shinokubo, H.; Osuka, A. *J. Am. Chem. Soc.* **2006**, *128*, 6568-6569.
35. Anand, V. G.; Pushpan, S. K.; Srinivasan, A.; Narayanan, S. J.; Sridevi, B.; Chandrashekar, T. K.; Roy, R.; Joshi, B. S. *Org. Lett.* **2000**, *2*, 3829-3832.
36. Anand, V. G.; Pushpan, S. K.; Venkatraman, S.; Narayanan, S. J.; Dey, A.; Chandrashekar, T. K.; Roy, R.; Joshi, B. S.; Deepa, S.; Sastry, G. N. *J. Org. Chem.* **2002**, *67*, 6309-6319.
37. Rath, H.; Sankar, J.; Prabhuraja, V.; Chandrashekar, T. K.; Joshi, B. S. *Org. Lett.* **2005**, *7*, 5445-5448.
38. Karthik, G.; Srinivasan, A.; Suresh, C. H.; Chandrashekar, T. K. *Chem. Commun.* **2014**, *50*, 12127-12130.
39. Chandrashekar, T. K.; Prabhuraja, V.; Gokulnath, S.; Sabarinathan, R.; Srinivasan, A. *Chem. Commun.* **2010**, *46*, 5915-5917.
40. Frisch M. J. *et al. Gaussian09, Revision D.01*, Gaussian, Inc., Wallingford CT, **2010**
41. Zhao, Y.; Truhlar, D. G. *J. Chem. Phys.* **2006**, *125*, 194101-194116.

CHAPTER 5

Core-modified Octaphyrins with Structural diversity

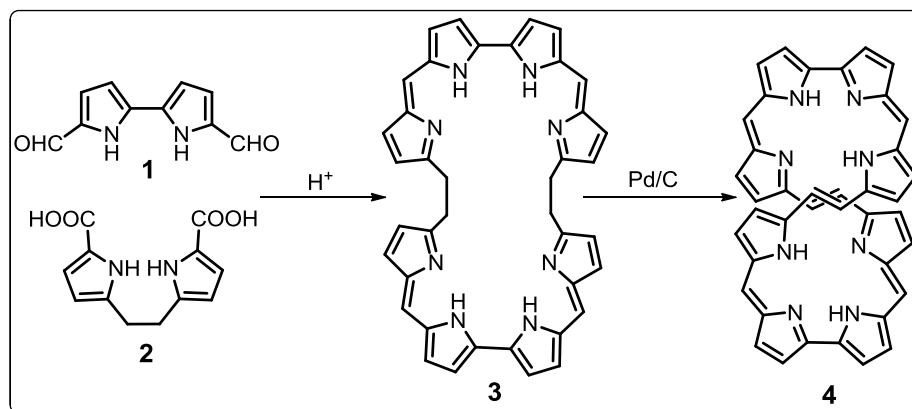
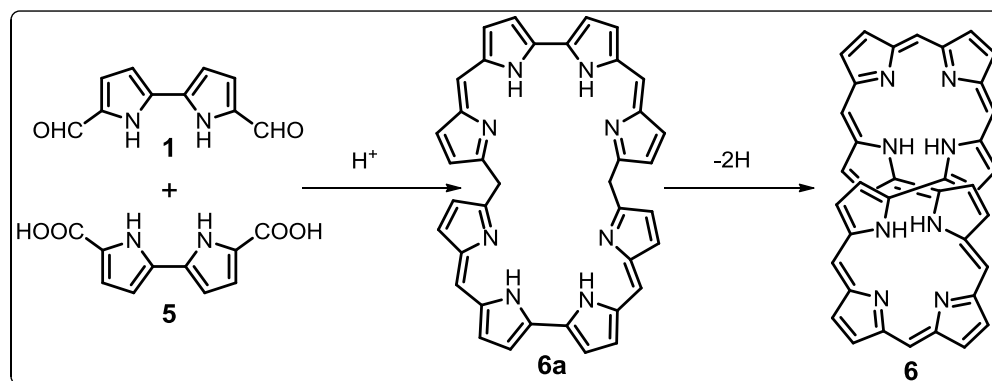
5.1	Introduction	133-140
5.2	Objective of the work	140-141
5.3	Results and Discussion	141-153
5.3.1	Syntheses	141-142
5.3.2	Spectral Characterization	142-153
5.3.2.1	Mass Spectrometric Analysis	142-143
5.3.2.1	Electronic spectral analysis	143-144
5.3.2.3	NMR analysis	144-148
5.3.2.4	Single crystal X-ray analysis	149-153
5.4	Core-modified fused Octaphyrin	154-159
5.4.1	Syntheses	154
5.4.2	Spectral Characterization	155-159
5.4.2.1	Mass spectrometric analysis	155
5.4.2.2	NMR spectral analysis	156
5.4.2.3	Electronic spectral analysis	157
5.4.2.4	Single crystal X-ray analysis	158-159
5.5	Core-modified Bridged Octaphyrin	160-171
5.5.1	Syntheses	160
5.5.2	Spectral Characterization	161-171
5.5.2.1	Mass spectrometric analysis	161
5.5.2.2	NMR spectral analysis	162-164
5.5.2.3	Electronic spectral analysis	164-165
5.5.2.4	NICS(0) calculations and AICD plots for [42] π electronic system	165-167
5.5.2.5	Single crystal X-ray analysis of 30	167-169
5.5.2.6	Excited state aromaticity	170-171
5.5.2.7	NICS(0) calculations and AICD plots for [40] π electronic system	171
5.6	Conclusion	172
5.7	Experimental Procedure	172-176
5.7.1	Synthesis of 26a	172-173

5.7.2	Synthesis of 26b	173-174
5.7.3	Synthesis of 27	174
5.7.4	Synthesis of 30a	175
5.7.5	Synthesis of 30b	176
5.8	References	177-180

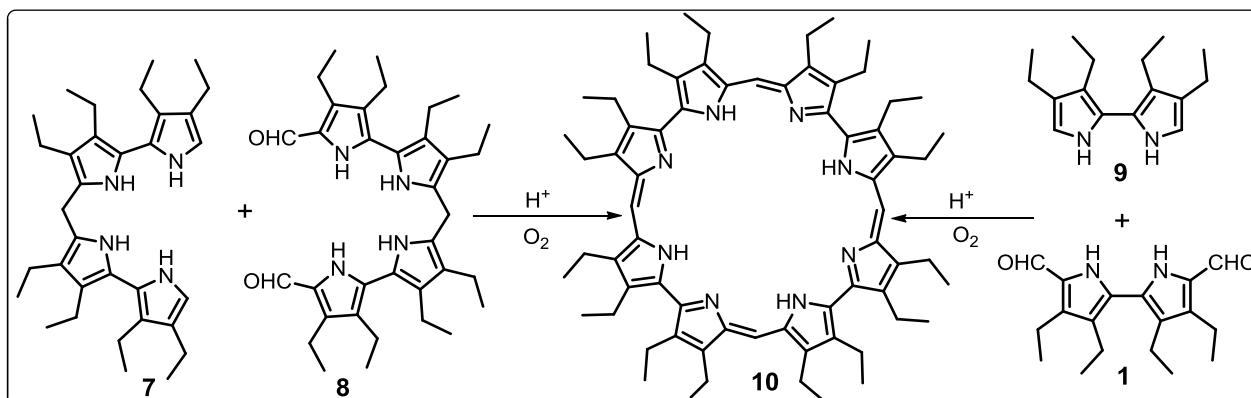
5.1 Introduction

Octaphyrins are class of expanded porphyrins^[1-9] in which eight pyrrole rings are connected through *meso*-carbon bridges or through direct pyrrole-pyrrole links. The structural diversity in octaphyrin exhibits in various forms which includes; planar, figure-eight,^[10-14] inverted,^[15-18] fused,^[19-22] bridged^[23-26] and Möbius band^[27-32]. These forms mainly rely on; (i) nature of the *meso* aryl substituents; (ii) the number and type of *meso*-carbon bridges and (iii) the heterocyclic units present in the macrocyclic framework. The octaphyrins with figure-eight conformation leads to loss in aromaticity. Thus, in order to maintain the aromaticity in octaphyrin framework, this chapter mainly highlights the syntheses, spectral and structural characterization of core-modified octaphyrins with different structural diversity such as; planar, fused and bridged system and three dimensional aromaticity.

The first octaphyrin **4** was synthesized by Vogel and co-workers^[33] in 1995 by perchloric acid-catalysed condensation of bipyrrrole dialdehyde **1** with dipyrroethane dicarboxylic acid **2** to afford the tetrahydrooctaphyrin(2.1.0.1.2.1.0.1) **3** in 30% yield. The DDQ oxidation of **3** did not lead to final conjugated product. The thermal dehydrogenation of **3** with 10% Pd / C under reflux condition resulted the formation of conjugated product **4** in 85% yield (Scheme 5.1a). Under similar reaction condition, dipyrromethane dicarboxylic acid **5** was mixed with **1** to form the octaphyrin(1.1.1.0.1.1.1.0) **6** in 10% yield (Scheme 5.1b).

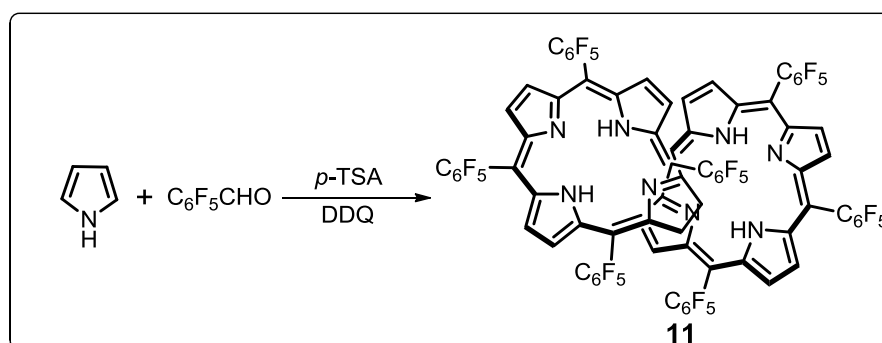
Scheme 5.1a: Synthesis of **4**Scheme 5.1b: Synthesis of **6**

The [32] π octaphyrin(1.0.1.0.1.0.1.0) **10** was also reported by the same group.^[34] The linear tetrapyrrole **7** and its α,ω -dialdehyde **8** were mixed in 1:1 ratio under acidic condition followed by open-air oxidation to form the octaphyrin **10** in 7% yield (Scheme 5.2). Alternatively, the reaction was also performed with 2 equiv. of bipyrrole **9** and its diformyl derivative **1** to obtain the octaphyrin **10** in 10% yield. As observed in **4** and **6**, the compound **10** was in figure-eight conformation and maintained the non-aromatic character.



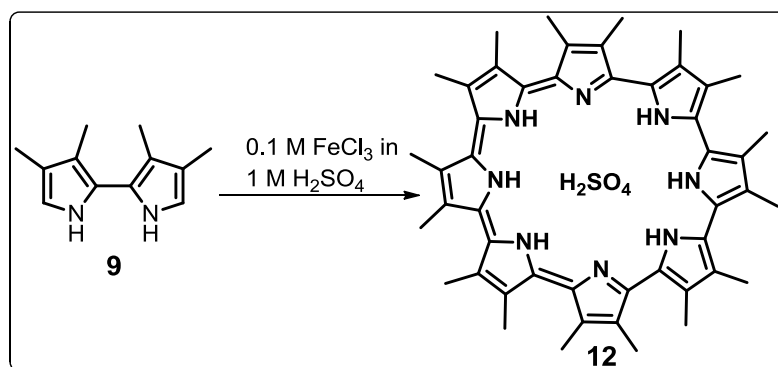
Scheme 5.2: Synthesis of **10**

The octaphyrin with eight *meso*-links **11** was reported by Osuka and co-workers.^[14] They adopted modified Lindsey condition for the synthesis of non-aromatic [36]octaphyrin(1.1.1.1.1.1.1.1) **11** by using pyrrole and pentafluorobenzaldehyde followed by DDQ oxidation in 6% yield (Scheme 5.3). The figure-eight conformation was reflected from crystal analyses. The core was effectively utilized to stabilize the Group 10 metal ions and displayed Möbius aromaticity.^[32b] The deprotonation experiment of **11** was further performed with tetrabutylammonium fluoride (TBAF) salt and afforded the monoanionic twisted Möbius aromatic and dianionic Hückel anti-aromatic [36]octaphyrin.^[32c]



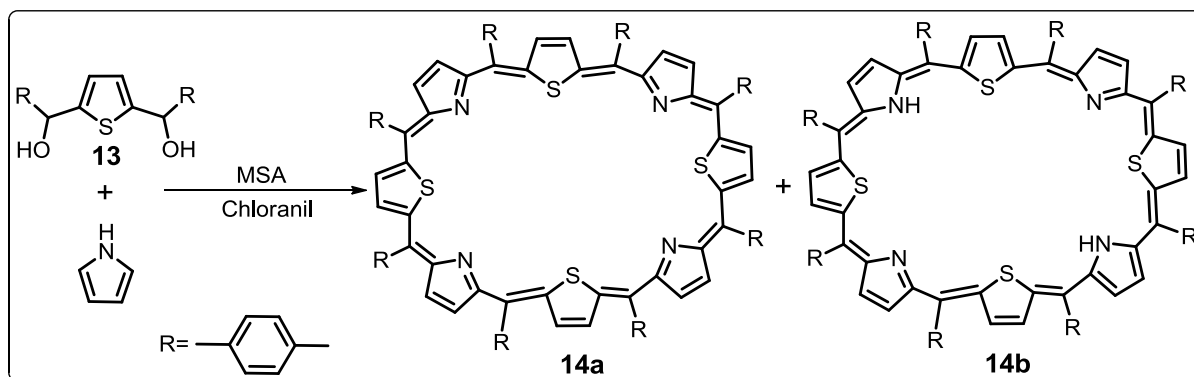
Scheme 5.3: Synthesis of **11**

The first planar octaphyrin **12** without *meso*-carbon bridges was synthesized by Sessler and co-workers.^[35] The 1M H₂SO₄ acid-catalyzed oxidative coupling of bipyrrrole **9** in the presence of FeCl₃ afforded the [30] π octaphyrin(0.0.0.0.0.0.0.0) **12** in 70% yield (Scheme 5.4). The crystal analyses revealed that the sulphate ion was trapped inside the macrocyclic framework and bound with eight intermolecular hydrogen bonding interaction with N-H...O bonding distance of 1.91 to 2.49 Å. The aromatic nature of **12** was reflected from ¹H NMR analysis, where the inner NH proton was resonated at 0.64 ppm at room temperature.



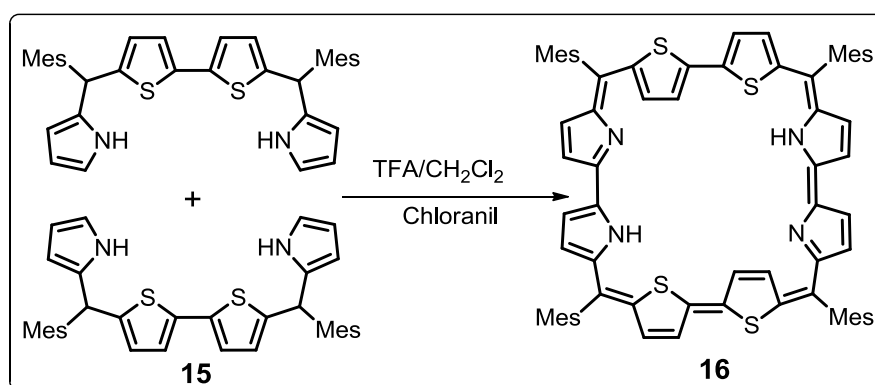
Scheme 5.4: Synthesis of **12**

The core-modified octaphyrin with eight *meso*-carbon bridges was reported by Latos-Grażyński and co-workers.^[36] The MSA acid catalyzed condensation of 2,5-bis(*p*-tolylhydroxymethyl)thiophene **13** with pyrrole followed by chloranil oxidation afforded the tetrathia[36]octaphyrin(1.1.1.1.1.1.1.1) **14a** in 2% yield along with trace amount of dihydrotetrathia[38]octaphyrin(1.1.1.1.1.1.1.1) **14b** (Scheme 5.5). Both **14a** and **14b** were interconvertible by simple oxidation and reduction reaction using DDQ and NaBH₄. The ¹H NMR spectral analyses suggested that the overall [38] π macrocyclic aromaticity for **14b** and overall [36] π macrocyclic anti-aromaticity for **14a**.



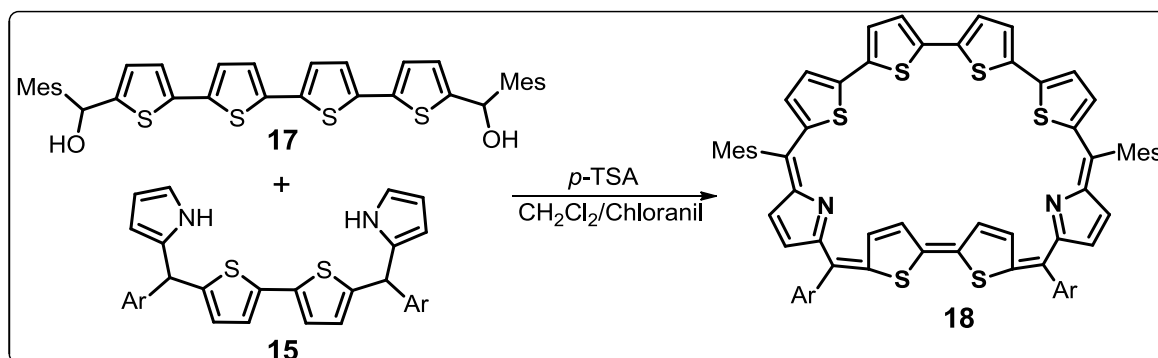
Scheme 5.5: Synthesis of **14**

The planar core-modified octaphyrin was reported by our group by (i) reducing the number of *meso*-carbon bridges and (ii) introducing bulkier *meso*-aryl substituents.^[37] The TFA acid-catalyzed [4 + 4] oxidative coupling reaction of bithiophene tetrapyrane (**15**) in the presence of chloranil gave a [34] π octaphyrin(1.0.1.0.1.0.1.0) (**16**) with four *meso*-carbon bridges in 5% yield (Scheme 5.6). One of the thiophene rings in the bithiophene unit was inverted and experiencing the aromatic ring current effect and overall maintained the planarity as well as aromatic character.



Scheme 5.6: Synthesis of **16**

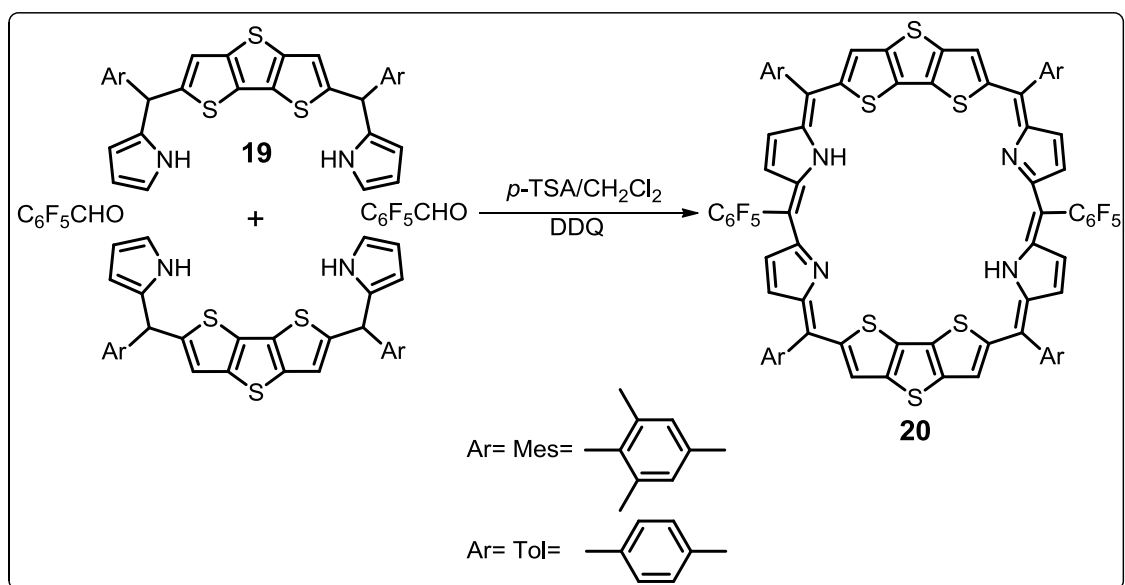
The near IR absorbing planar aromatic [34]octaphyrin(1.1.0.1.1.0.0.0) (**18**) with quaterthiophene unit in the framework was introduced by our group.^[38] The **18** was synthesized from 5,5'''-bis(mesitylhydroxymethyl)2,5':2',2'':5'',2'''-quaterthiophene **17** with bithiophene tetrapyrane **15** in the presence of *p*-TSA acid as acid-catalyst followed by chloranil oxidation in 20% yield (Scheme 5.7). Upon protonation by using TFA, the weak Q-like band was shifted from 842 nm and appeared in the near IR region at 1090 nm. The bithiophene unit which was opposite to the quaterthiophene unit was inverted and adopted planar conformation in solution and further confirmed by crystal analysis.



Scheme 5.7: Synthesis of **18**

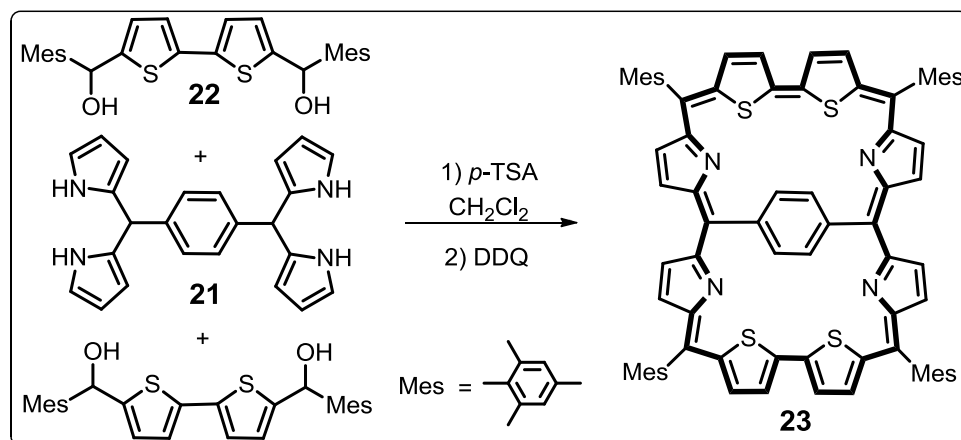
In order to maintain the planarity and aromaticity in the octaphyrin framework, the fused and bridged synthetic strategies were introduced. The core-modified fused octaphyrin was synthesized by our group.^[21a] The fusion was introduced in the starting material, where the electron rich dithienothiophene (DTT) dipyrane (**19**) was condensed with pentafluorobenzaldehyde by using 0.3 equiv. of *p*-TSA followed by DDQ oxidation afforded the doubly fused core-modified [36] π octaphyrin(1.1.1.0.1.1.1.0) (**20**) in 10% yield (Scheme 5.8). The figure-eight conformation of **20** was reflected from crystal analyses, where the DTT moieties were oriented in staggered conformation with a π cloud distance of 3.7Å. However, upon protonation, the figure-eight conformation was changed into extended open

structure and the aromaticity was shifted from non-aromatic to $[4n]\pi$ Hückel anti-aromatic character in the diprotonated state. Prior to this result, the fused octaphyrin was randomly reported in the literature; (i) the regio- and stereoselective mono and bis-pyrrolidine fused octaphyrins were synthesized from [36]octaphyrin **11** with azomethine ylide ^[21b] and (ii) N-thienyl fused aromatic [38]octaphyrin was obtained from [36]octaphyrin bearing 3-thienyl substituent. ^[21c]



Scheme 5.8: Synthesis of **20**

Our group have also demonstrated the synthesis of bridged core-modified octaphyrin by introducing a phenylene bridge in the macrocyclic framework. ^[26] The *p*-TSA acid-catalyzed condensation of 1,4-phenyl-bis(dipyrromethane) (**21**) with bithiophene diol (**22**) followed by oxidation with DDQ gave the bridged $[34]\pi$ octaphyrin (**23**) in 10% yield (Scheme 5.9). The spectral and theoretical analyses revealed that fight-eight conformation was restricted and adopted the planarity in the macrocyclic framework. In addition, the macrocycle was Hückel aromatic and followed a major $[34]\pi$ single conjugation pathway, where the *p*-phenylene bridge was not involved in the macrocyclic conjugation.



Scheme 5.9: Synthesis of **23**

5.2 Objective of the work:

The octaphyrins described in the previous section were in figure-eight conformation or planar conformation. In order to achieve a planar conformation exclusively, the following strategies were introduced; (i) reduce the number of *meso*-carbon bridges; (ii) right combination of heterocyclic rings and *meso*-aryl substituents; (iii) Fusion and (iv) bridged techniques. The main objective of this chapter is to achieve a planar aromatic octaphyrin, where we adopted all the strategies as mentioned above. In the first part of this chapter, we have introduced four *meso*-carbon bridges and *meso*-mesityl (**26**) and tolyl as substituents. In the second part, the fused octaphyrin (**27**) and its aromatic characteristics are highlighted and in the last chapter, we mainly focused on the bridged octaphyrin (**30**) where dithienothiophene (DTT) ring is utilized as bridge and also described its three dimensional aromaticity in the system.

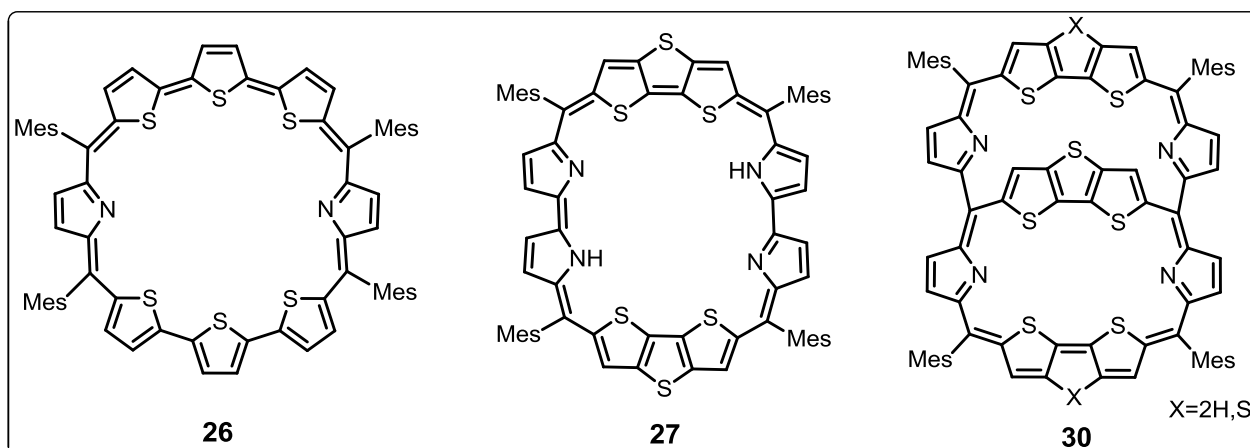
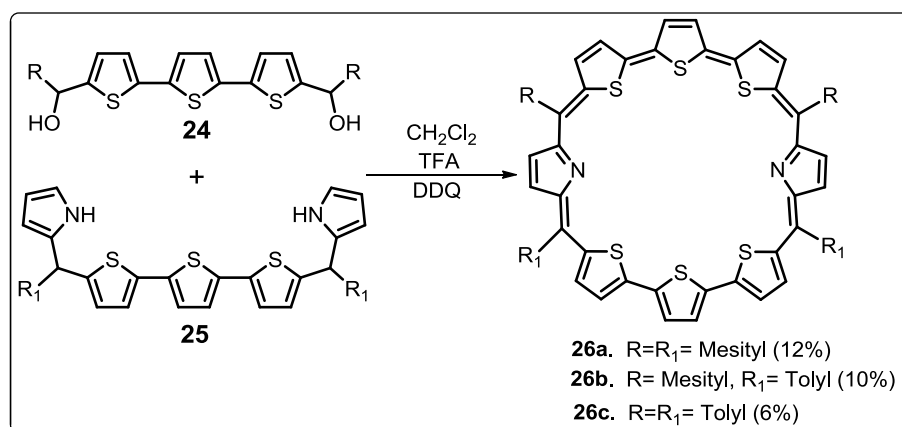


Figure 5.1: Molecular structures of **26**, **27** and **30**

5.3 Results and Discussion

5.3.1 Syntheses

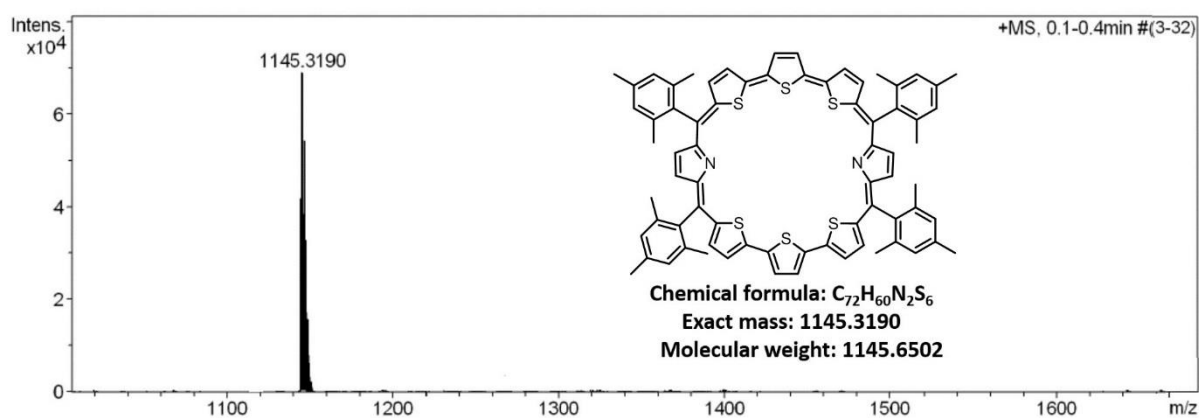
The synthesis is outlined in Scheme 5.10. We have adopted [5 + 3] acid-catalyzed Macdonald type condensation reaction. The required precursors terthiophene diol (**24**) and terthiophene pentapyrrane (**25**) were synthesized from our earlier reported procedures.^[39] The diol **24** was synthesised from terthiophene with *n*-BuLi (1.6M in *n*-hexane) and respective arylaldehyde, whereas the precursor **25** was obtained from TFA acid-catalyzed condensation of **24** with excess pyrrole. The final target molecule was achieved by TFA acid-catalyzed condensation of 1:1 mixture of **24** and **25** followed by oxidation with DDQ afforded the curde product. After repeated column chromatographic purification by basic alumina followed by silica gel (100 – 200), the bluish color fraction was eluted with CH₂Cl₂ and *n*-hexane and identified as octaphyrin **26** in 10 – 12% yield. The compound **26a** and **26b** are reasonable stable, however **26c** is found to be unstable. Hence the spectral analysis are done mainly **26a**.

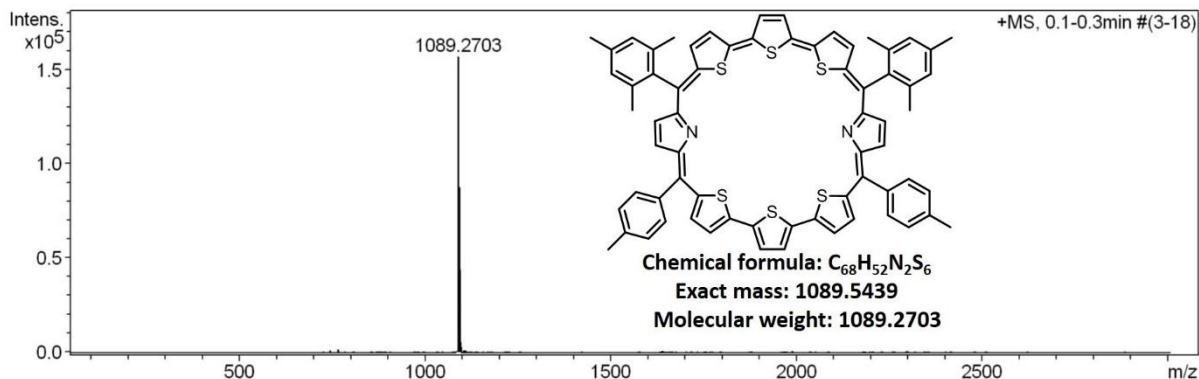
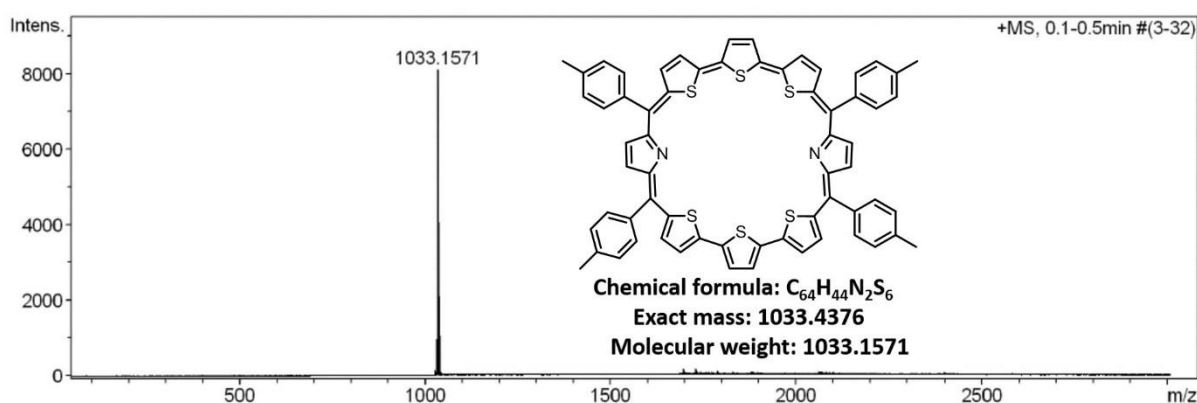
Scheme 5.10: Synthesis of **26**.

5.3.2 Spectral Characterization

5.3.2.1 Mass Spectrometric Analysis

The electron spray ionisation (ESI) mass spectrometric analysis of **26a-c** were shown in Figure 5.2 – 5.4. The molecular ion signals of **26a-c** at m/z 1145.3190 for **26a** (Figure 5.2), 1089.2703 for **26b** (Figure 5.3) and 1033.1571 for **26c** (Figure 5.4) confirm the composition that is consistent with the expected macrocycles.

Figure 5.2: ESI-MS spectrum of **26a**

Figure 5.3: ESI-MS spectrum of **26b**Figure 5.4: ESI-MS spectrum of **26c**

5.3.2.2 Electronic Spectral Analysis

The electronic absorption spectrum of **26a** was recorded in CH_2Cl_2 . To our surprise, **26a** shows two split Soret like bands at 600 nm and 647 nm with higher molar absorption coefficient of later band ($\sim 10^5$) and a Q band at 905 nm (Figure 5.5). These Soret like bands suggest the existence of the two different isomeric / tautomeric units. There is a moderate change in the band positions upon varying the solvent polarity from polar to nonpolar, however, both the species were present under different solvent conditions. The titration experiment was further performed by gradual increase of TFA in CH_2Cl_2 solution of **26a**. At monoprotinated stage, both the split Soret bands are merged together and shows a broad

band centered at 625 nm & shoulder at 757 nm along with Q bands at 1186 and 1393 nm. At 5 equiv. of TFA, the broad Soret band becomes sharp, red-shifted by 9 nm and observed at 634 nm with two fold increase in the molar absorption coefficient along with Q band at 1153 nm (Figure 5.5). Overall, the reduction in Soret band and red shift absorption in the Q-band reflects that one of the tautomers / isomers is stabilized at higher concentration of TFA. The band positions and the molar extinction coefficient in the freebase as well as protonated state of **26a** reflect the typical aromatic octaphyrin. Similar trend was observed in the electronic absorption spectral analyses of **26b** and **26c** both in the freebase as well as protonated form.

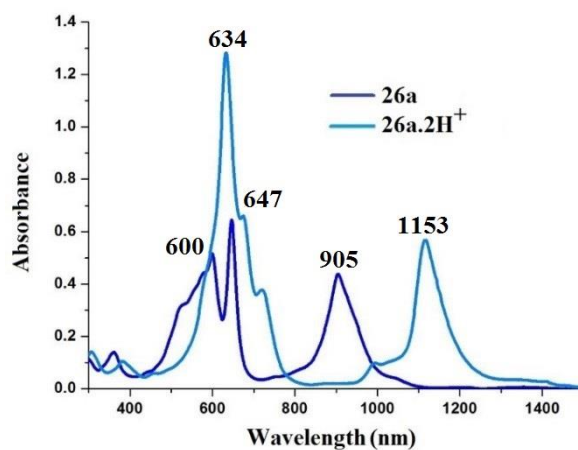


Figure 5.5: The electronic absorption spectrum of **26a** and **26a.2H⁺**

5.3.2.3 NMR Analysis

The ¹H NMR spectrum of **26a** was recorded in Toluene-d₈ at 298 K (Figure 5.6). The more number of proton signals in **26a** suggests the presence of two different tautomeric / isomeric units in its freebase form. These units are in C₄ and C₂ symmetry, thus, only one fourth of the signals for C₄ symmetry and half of the signals for C₂ symmetry were observed in the ¹H NMR spectral analyses. One of the three thiophene rings is inverted in each tautomer and

experiencing the diatropic ring current. In C₄ symmetry, the middle thiophene in the terthiophene unit is inverted and the respective thiophene β-CH protons are resonated at 0.37 ppm (a), whereas, in C₂ symmetry, one of the terminal thiophenes is resonated between 0.37 ppm (5) and -1.26 ppm (6). The normal thiophene (b, c, 1, 2, 3 and 4) and pyrrolic β-CH (d, 7 and 8) protons in both the units are observed from 9.85 to 8.49 ppm. Overall there is no major structural change in both units, thus ruled out the possibility of tautomerism between the units (Scheme 5.11). The *meso*-mesityl CH signals are appeared between 8.06 and 7.15 ppm as four sharp singlets, whereas the mesityl methyl CH signals are at 2.60 to 2.15 ppm as six singlets.

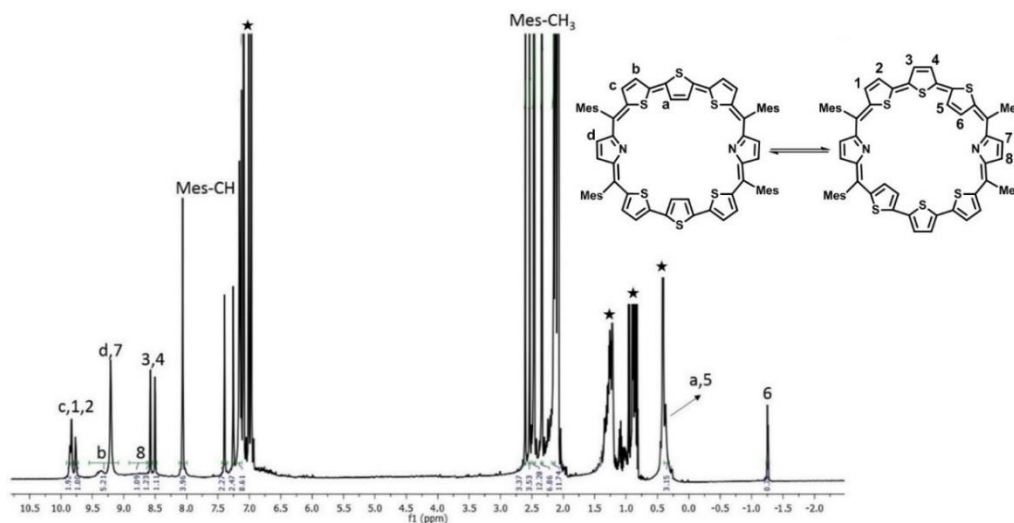
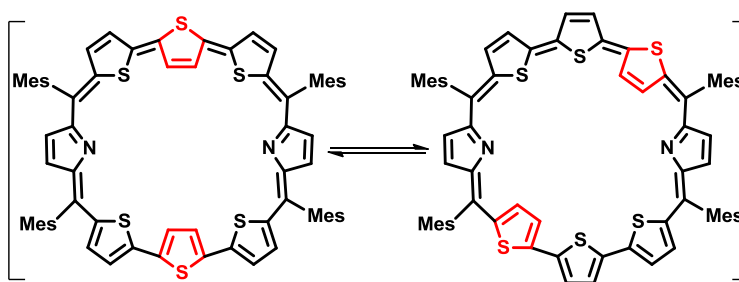


Figure 5.6: ¹H NMR spectrum of **26a** in Toluene-*d*₈



Scheme 5.11: The possible isomeric units in **26a**

Upon decreasing the temperature from 298 K to 193 K, the inverted thiophene β -CH protons are further upfield shifted, where the respective β -CH proton in C4 symmetry is resonated at -0.70 ppm (a), on the other hand, in C2 symmetry, the respective protons are observed between -0.62 (5) and -2.35 ppm (6). The normal thiophene and pyrrolic β -CH protons are further downfield shifted and observed from 10.02 to 8.86 ppm (Figure 5.7). These signals were further confirmed by ^1H - ^1H correlation spectroscopy (COSY) experiment (Figure 5.8). There is moderate downfield shift of the *meso*-mesityl CH signal and upfield shift of the *meso*-mesityl methyl CH signals. Overall, the aromaticity and planarity of each isomers in **26a** increases upon decreasing the temperature.

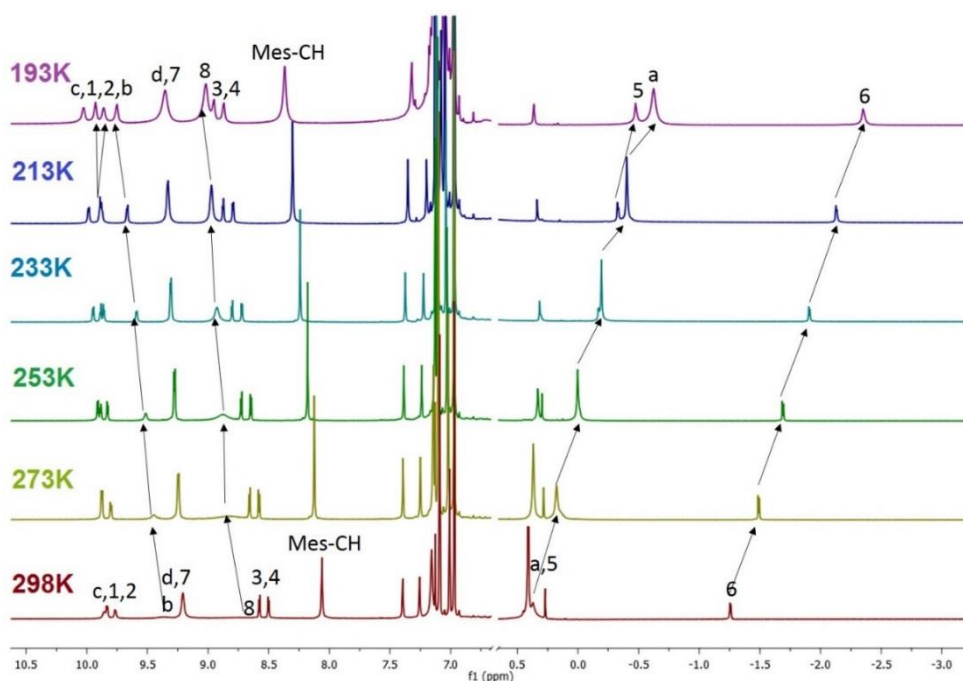


Figure 5.7: Low temperature ^1H NMR spectrum of **26a**

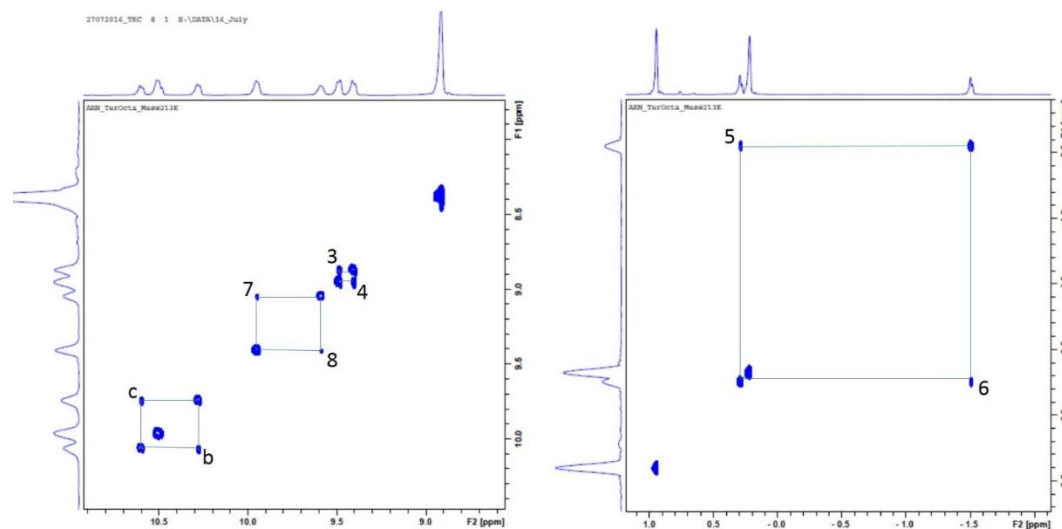


Figure 5.8: ^1H - ^1H COSY spectrum of **26a** with correlation in normal heterocyclic rings (a) and inverted units (b).

The protonation experiment was further performed with **26a** in the presence of TFA in Toluene- d_8 at room temperature and the results are shown in Figure 5.9. Upon protonation, one of the isomers with C2 symmetry is predominantly stabilized over the C4 symmetry. As observed in freebase with C2 symmetry, one of the terminal thiophenes in terthiophene unit is retained inversion. The respective β -CH protons are -4.19 ppm and -3.71 ppm upfield shifted and resonated at -4.56 ppm (5) and -4.97 ppm (6) as compared to freebase **26a**. The newly protonated inner imine NH protons are observed as a broad singlet at -3.03 ppm and further confirmed by D_2O exchange experiment. The normal thiophene protons are appeared between 11.01 ppm and 10.25 ppm (1, 2, 3 and 4), whereas the pyrrolic β -CH protons are at 9.04 ppm (7) to 9.02 ppm (8) as doublet. All these assignments were further confirmed by ^1H - ^1H COSY spectral analysis (Figure 5.10). The *meso*-mesityl protons are displayed from 7.34 ppm to 7.18 ppm and the mesityl methyl protons are from 2.48 ppm to 1.74 ppm, respectively. Overall, the upfield shift of the inverted thiophene unit and downfield shift of the normal heterocyclic rings as compared to free-base **26a**, thus confirms the increase in

aromaticity as well as planarity upon protonation. Similar trend was observed in the ^1H NMR analyses of **26b** in the free-base form and its protonated state.

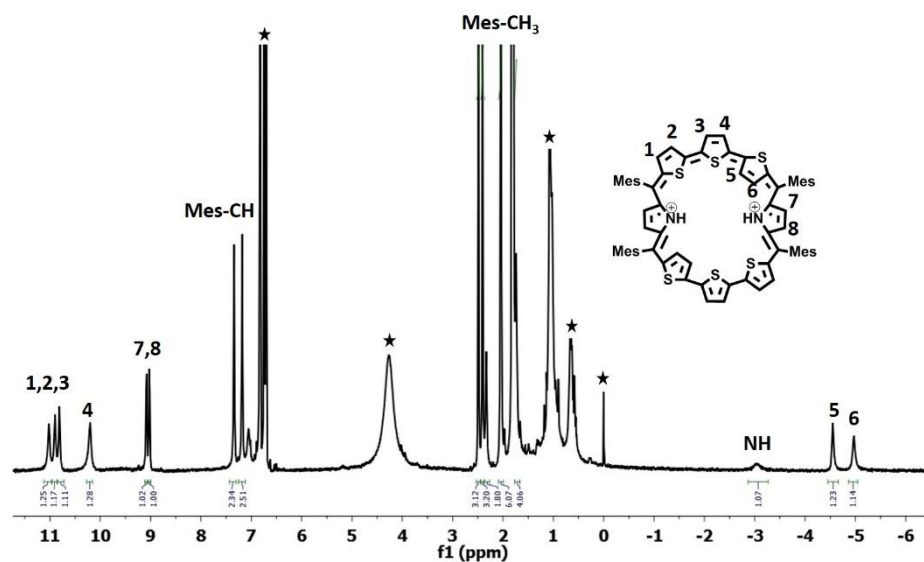


Figure 5.9: ^1H NMR spectrum of **26a.2H⁺** in Toluene- d_8

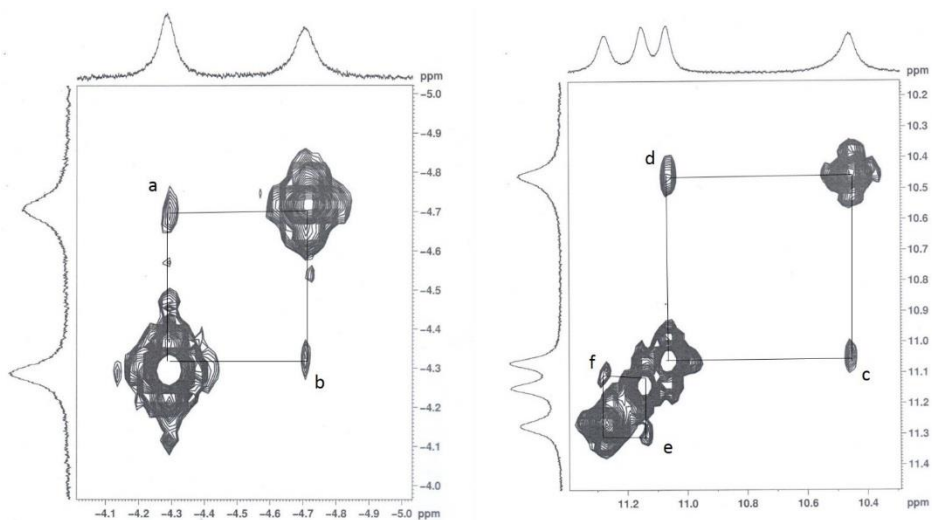


Figure 5.10: ^1H - ^1H COSY spectrum of **26a.2H⁺** with correlation in normal heterocyclic rings (a) and inverted units (b).

5.3.2.4 Single Crystal X-ray Analysis

The structural isomers of octaphyrin **26a** were finally confirmed through single crystal X-ray structural analysis and shown in Figure 5.11 (Table 5.1). The single crystal of **26a** was obtained by slow diffusion of CH₂Cl₂ solution in *n*-hexane. Compound was crystallised in monoclinic crystal lattice with *P21/n* space group. As reflected from the ¹H NMR spectral analyses, two different isomers with same empirical formula are exist in the crystal lattice. Both the molecule contains two terthiophene units connected with two pyrrole units via *meso* carbon bridges. The only difference is observed in the structural diversity of one of the thiophene rings in the terthiophene units. The middle thiophene is inverted in the molecule with C₄ symmetry, whereas in C₂ symmetry, one of the terminal thiophenes is inverted. The difference in dihedral angle between the two planes (C₅, C₁₀, C_{5'} & C_{10'} vs C₄₅, C₅₀, C_{45'} & C_{50'}) are 36.69°. In addition, the inverted edge thiophene unit in C₂ symmetry is tilted by 12.97°, whereas the middle thiophene in C₄ symmetry is deviated by 21.23° from the mean macrocyclic plane. The maximum deviation of the middle thiophene unit is reflected from the steric repulsion between the inner core hydrogen atoms (H₃₉...H₃₈). Like the planar *meso*-aryl expanded porphyrins, the *meso* aryl units in **26a** are nearly 80° deviated from the mean macrocyclic plane. The crystal analyses of **26a** revealed two different intermolecular hydrogen bonding interactions between (i) π-clouds of inner thiophene [Tp(π)] and C_{43'}-H_{43'} of C₂ symmetry molecule and (ii) π-clouds of *meso*-mesityl unit [Mes(π)] and C₁₇-H₁₇ of C₄ symmetry molecule with distances and angles of Tp(π)...C_{43'}-H_{43'} and Mes(π)...C₁₇-H₁₇ are 2.70Å & 138.08° and 2.71Å & 137.01°, respectively.

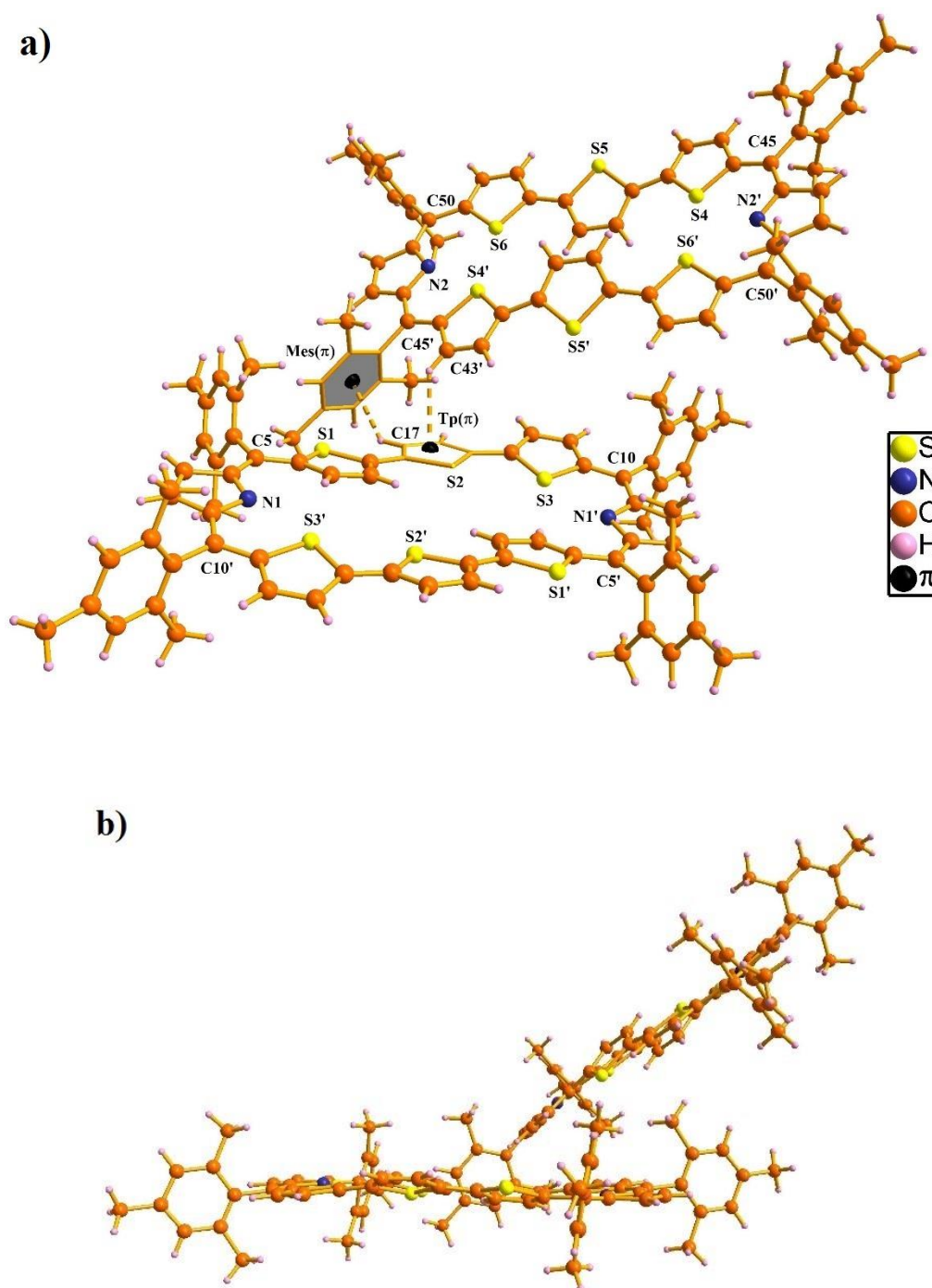
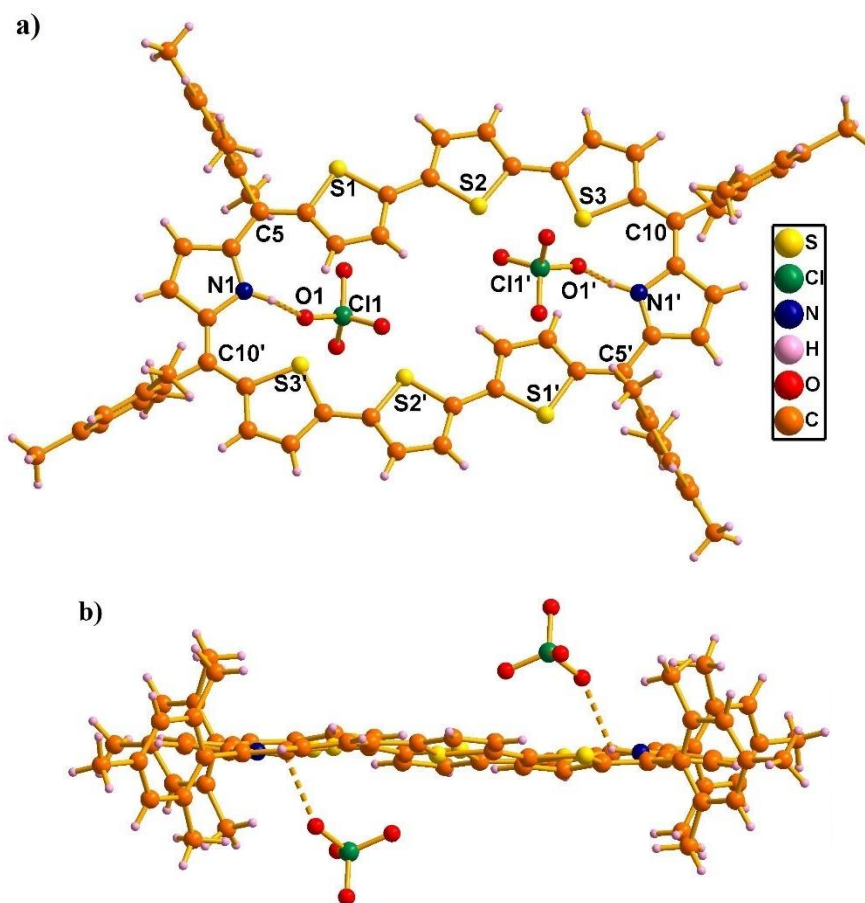


Figure 5.11: Single crystal X-ray structure of **26a** with intermolecular hydrogen bonding interaction. a) Top view and b) Side view

Table 5.1: Crystal data for **26a** and **26a.2H⁺**

	26a	2a+2H⁺
<i>T</i> , K	100 K	100K
Formula	C72 H60N2S6	C72 H62 N2 S6 Cl2 O8
Formula weight	1145.58	1455.97
Color and Habit	Dark brown	Dark green
Crystal system	Monoclinic	Triclinic
Space group	P 21/n	P -1
<i>a</i> , Å	19.747(6)	14.477(3)
<i>b</i> , Å	15.812(6)	17.107(3)
<i>c</i> , Å	22.766(7)	24.756(5)
α , deg	90	81.890(12)
β , deg	92.329(10)	79.104(12)
γ , deg	90	76.504(12)
<i>V</i> , Å ³	7103(4)	5823.8(19)
Radiation (λ , Å)	Mo K α (0.71073)	Mo K α (0.71073)
<i>Z</i>	4	1
<i>d</i> _{calcd.} , g•cm ⁻³	1.071	1.245
μ , mm ⁻¹	0.231	0.300
<i>F</i> (000)	2408	2282.0
No. of unique reflns	13018	21219
No. of params. refined	733	1352
GOF on <i>F</i> ²	0.906	0.949
<i>R</i> 1 ^a [<i>I</i> > 2 σ (<i>I</i>)]	0.0794	0.0791
<i>R</i> 1 ^a (all data)	0.1900	0.1622
<i>wR</i> 2 ^b (all data)	0.1790	0.2061

The anion bound crystal structure was unambiguously confirmed by crystal analyses and shown in Figure 5.12 (Table 5.1). The crystal was grown by slow evaporation of CHCl_3 solution in CH_3CN . The compound was crystallised in triclinic crystal lattice with P_{-1} space group. As reflected from the spectral analyses, one of the isomers with C_2 symmetry is stabilized upon protonation. In addition, two perchlorate anions are in intermolecular hydrogen bonding interaction with the protonated imine NH (N1-H1) with the bond distance and angle of N1-H1...O1 is 2.33Å and 118.41° respectively and generate zig-zag one dimensional array in the solid state. The terminal thiophene unit is hardly deviated (12.99°) from the mean plane (C5, C10, C5' and C10') and maintained the planarity as observed in freebase **26a**, whereas the *meso*-mesityl rings are maximum tilted by 81.48° from the plane.



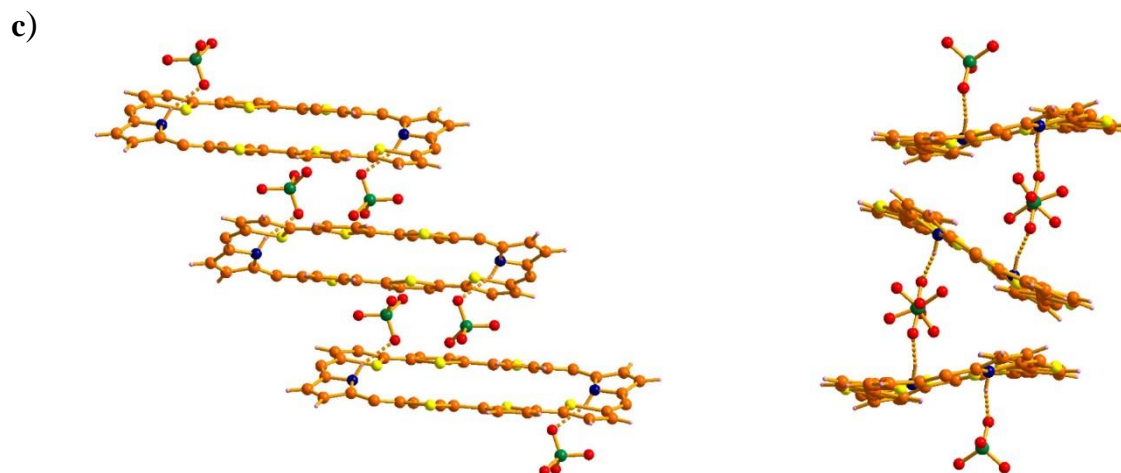
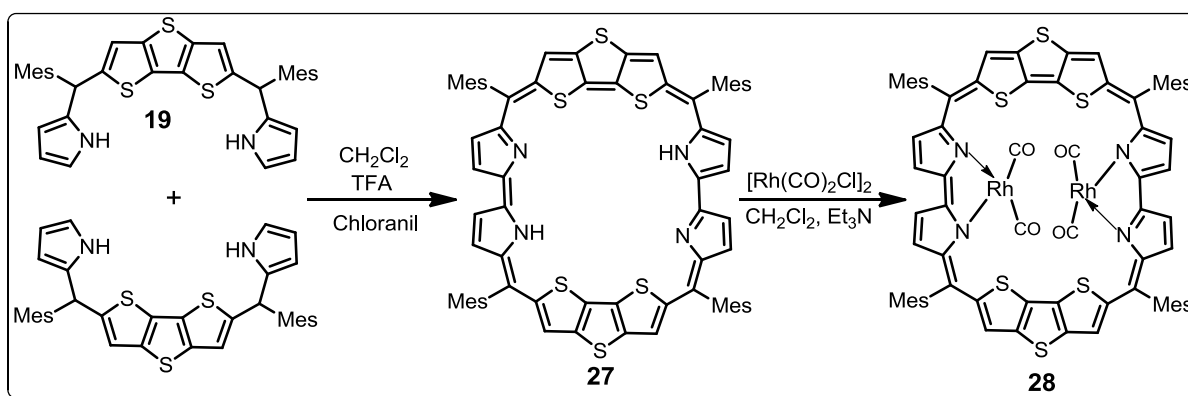


Figure 5.12: Single crystal X-ray structure of **26a.2H⁺** with intermolecular hydrogen bonding interaction with perchlorate anion. (a) Top view; (b) side view and (c) one-dimensional array.

5.4 Core-modified Fused Octaphyrin

5.4.1 Synthesis

The synthesis of core-modified fused octaphyrin (**27**) is shown in Scheme 5.12. Basically, we adopted acid-catalyzed oxidative coupling reaction. The required DTT dipyrane (**19**) precursor was synthesized as mentioned by our earlier procedure and obtained from the trifluoroacetic acid-catalyzed condensation of respective diol with excess pyrrole.^[20] In the final step, the oxidative coupling of **19** in the presence of TFA followed by chloranil oxidation afforded the crude product. After repeated column chromatographic purification by using basic alumina and silica gel (100-200 mesh), the blue color fraction was eluted with CH_2Cl_2 : *n*-hexane (85 : 15, v/v) and identified as **27** in 3% yield. The compound was further recrystallized from CH_2Cl_2 and *n*-hexane and obtained as green color crystals. The coordination chemistry was further performed by using Rh(I) salt, where the **27** was mixed with $[\text{Rh}(\text{CO})_2\text{Cl}]_2$ under basic condition for 2h at room temperature (Scheme 5.12). The color of the reaction mixture was changed from blue to cyan and monitored by TLC analyses. The crude product was purified by neutral alumina column chromatographic purification. The cyan color band was eluted with CH_2Cl_2 : CH_3OH (95 : 5, v/v) and afforded the desired Rh(I) complex (**28**) in almost quantitative yield.



Scheme 5.12: Synthesis of **27** and its bis-Rh(I) complex (**28**)

5.4.2 Spectral Characterization

5.4.2.1 Mass Spectrometric Analysis

The electron spray ionization mass spectrometric analyses of **27** and **28** were shown in Figure 5.13 and 5.14. The molecular ion signals m/z at 1171.2836 [M+1] for **27** and 1486.1174 [M+3] for **28**, thus confirms the exact composition of **27** and **28**.

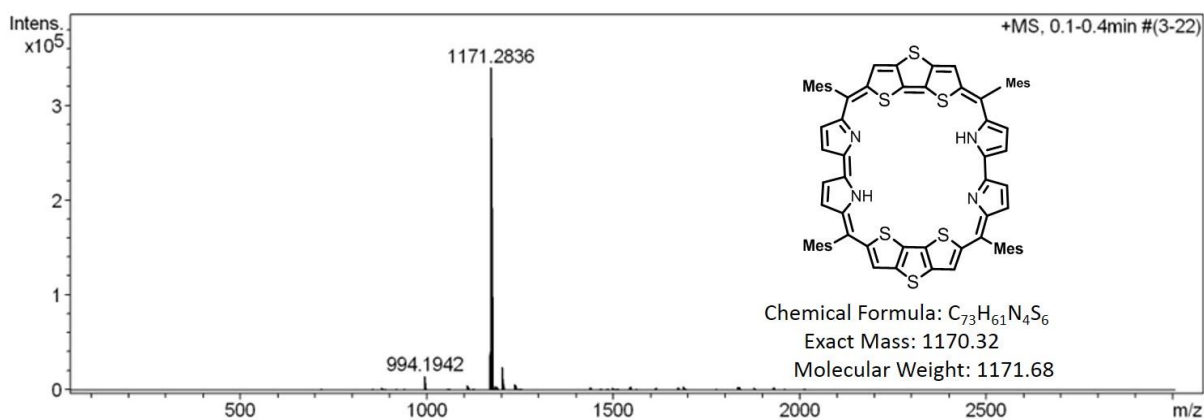


Figure 5.13: ESI-MS spectrum of **27**

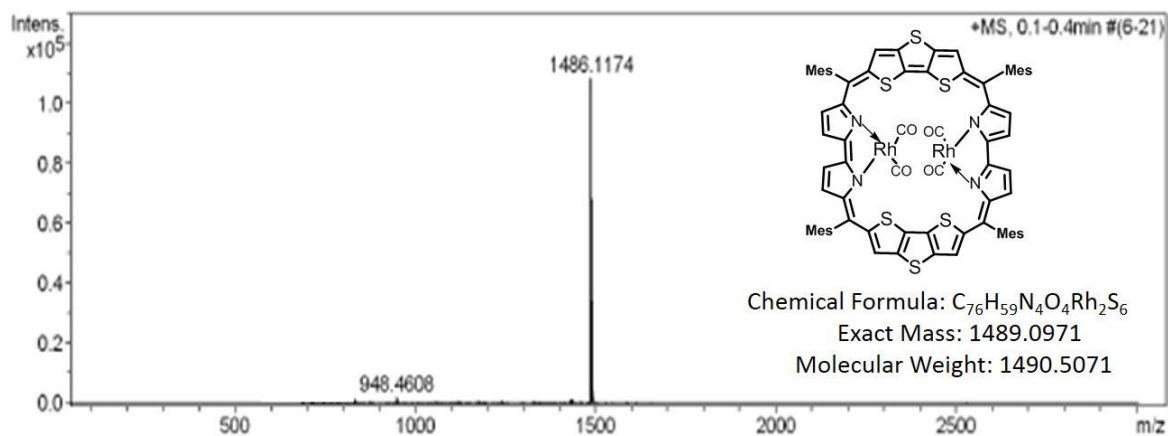


Figure 5.14: ESI-MS spectrum of **28**

5.4.2.2 NMR spectral Analysis

The ^1H NMR spectrum of **27** was recorded in CDCl_3 at 298K and shown in Figure 5.15. The molecule exists in C_4 symmetry, thus only one fourth of the signals was observed. The DTT ring β -CH protons are resonated as singlet at 12.85 ppm (a), whereas the pyrrolic β -CH protons are observed at 12.00 ppm (b) and 11.00 ppm (c) as two doublets. The inner NH signal is appeared as a broad signal at -1.83 ppm and further confirmed by D_2O exchange experiments. The *meso*-mesityl CH protons are appeared as a sharp singlet at 8.12 ppm and the mesityl methyl CH signals are from 3.75 ppm to 2.25 ppm, respectively. The chemical shift difference ($\Delta\delta$) between the inner NH and the pyrrolic β -CH protons is 13.33 ppm, thus reflects the strong diatropic ring current inside the macrocyclic framework and confirms the aromaticity.

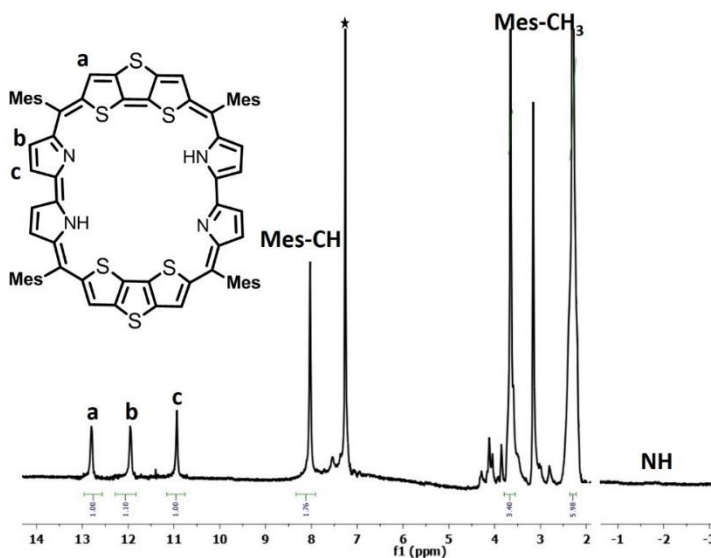


Figure 5.15: ^1H NMR spectrum of **27**

5.4.2.3 Electronic spectral Analysis

The electronic absorption spectrum of **27**, its protonated derivative (**27.2H⁺**) and **28** are shown in Figure 5.16. The freebase **27** shows a split Soret like absorption band at 573 nm and 603 nm along with weak Q-bands at 817 and 1173 nm. Upon protonation, the split Soret band in **27** merged together and appears as a sharp Soret band at 598 nm with molar absorption coefficient of 10^5 , which is 1.5 fold higher as compared to **27**, along with Q-bands at 823, 947 and 1170 nm. Upon Rh(I) metal ion insertion (**28**), the band is further red-shifted by 22 nm as compared to **27.2H⁺** and observed at 620 nm and two fold increase in molar absorption coefficient as compared to **27**. In addition, the weak Q-like bands in **28** are also red-shifted and appeared at 830, 948 and 1290 nm, respectively. Overall, the band position in **27**, **27.2H⁺** and **28** reflect the typical aromatic character.

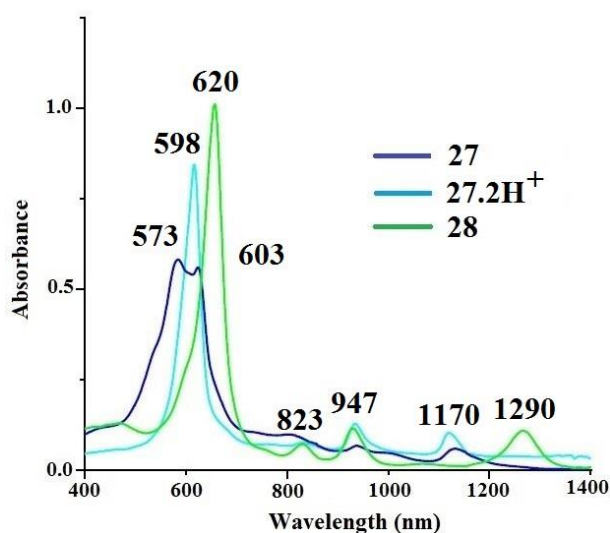


Figure 5.16: The electronic absorption spectrum of **27**, **27.2H⁺** and **28**

5.4.2.4 Single Crystal X-ray Analysis

The final confirmation has come from the single crystal X-ray analysis of **27** and the results are shown in Figure 5.17 (Table 5.2). The crystal was grown by slow diffusion of CHCl_3 over *n*-heptane. The compound was crystallized in monoclinic crystal lattice with *P21/C* space group. As reflected from the spectral analysis, the two DTT tetrapyrrole moieties are combined together to obtain the desired **27**. The heterocyclic rings are hardly deviated from the mean macrocyclic plane containing *meso*-carbon atoms (C5, C14, C5' & C14'), where the imine pyrrolic unit is maximum deviated (7.10°) from the plane. As observed in **26a**, the *meso*-aryl units in **27** are deviated by 87.83° and 77.58° , respectively. Overall, the planarity and aromaticity was maintained from the structural analysis.

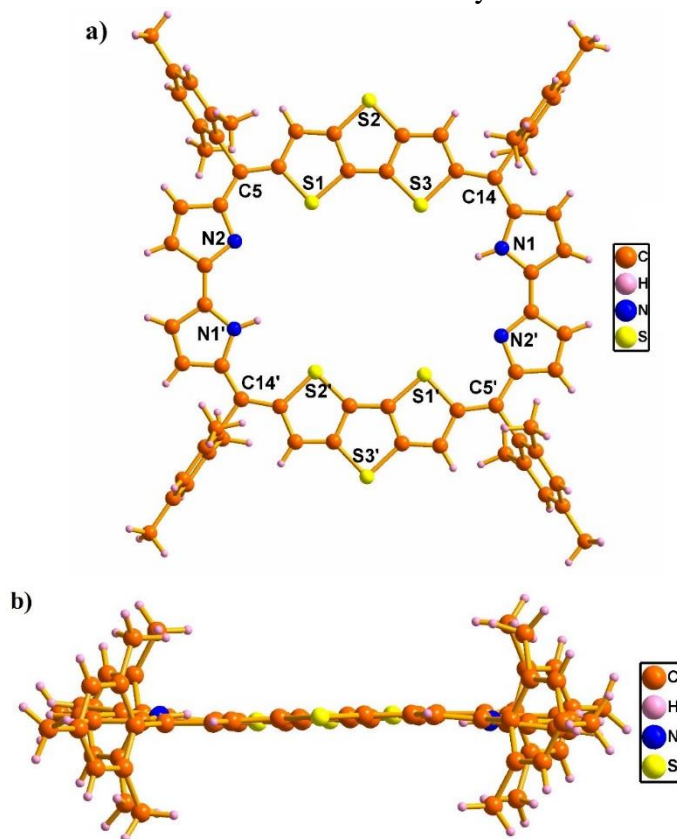


Figure 5.17: Single crystal X-ray structure of **27**. (a) Top view and (b) side view.

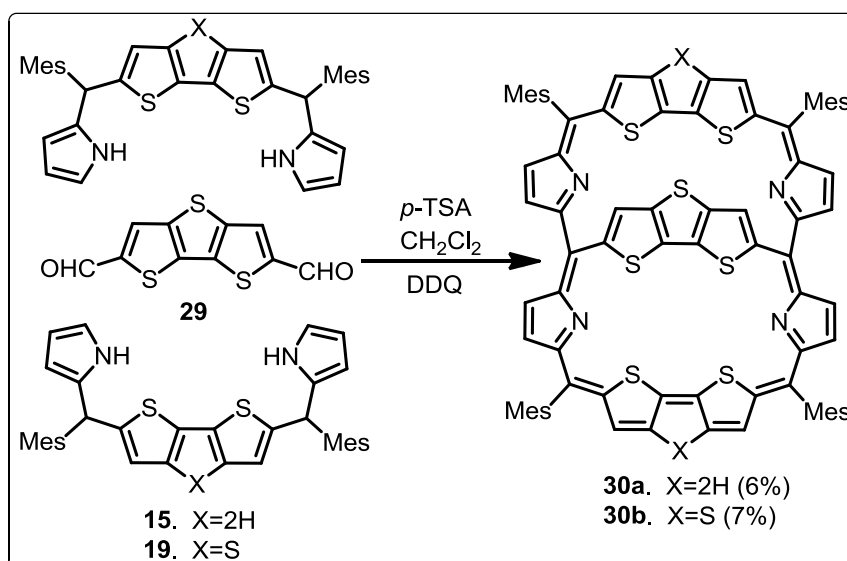
Table 5.2: Crystal data for **27**

	27
<i>T</i> , K	100 K
Formula	C ₃₆ H ₂₉ N ₂ S ₃
Formula weight	1171.58
Color and Habit	Dark brown
Crystal system	Monoclinic
Space group	<i>P</i> 21/ <i>c</i>
<i>a</i> , Å	13.929(10)
<i>b</i> , Å	16.036(11)
<i>c</i> , Å	16.308(2)
α , deg	90
β , deg	109.199(9)
γ , deg	90
<i>V</i> , Å ³	3440.0(19)
Radiation (λ , Å)	Mo K α (0.71073)
<i>Z</i>	4
d_{calcd} , g•cm ⁻³	1.131
μ , mm ⁻¹	0.240
<i>F</i> (000)	1228.0
No. of unique reflns	36210
No. of params. refined	380
GOF on <i>F</i> ²	0.932
<i>R</i> 1 ^a [<i>I</i> > 2 σ (<i>I</i>)]	0.0659
<i>R</i> 1 ^a (all data)	0.1320
<i>wR</i> 2 ^b (all data)	0.1709

5.5 Core-modified Bridged Octaphyrin

5.5.1 Synthesis

The syntheses of DTT bridged octaphyrins (**30a** and **30b**) are shown in Scheme 5.13. The required precursors for the synthesis of desired octaphyrin, such as bithiophene tetrapyrane (**15**) and DTT tetrapyrane (**19**) were adopted from our earlier reported procedure.^[40,20] The other precursor such as DTT dialdehyde (**29**) was obtained from DTT with *n*-BuLi and 1-formyl piperidine in 65% yield. In the final step, we followed acid-catalyzed condensation strategy, where 2 equiv. of bithiophene tetrapyrane (**15**) / DTT tetrapyrane (**19**) is condensed with 1 equiv. of DTT-dialdehyde (**29**) in the presence of *p*-TSA acid followed by oxidation with DDQ and afforded the desired core-modified bridged octaphyrins (**30a** and **30b**) in 6 – 7% yield.



Scheme 5.13: Synthesis of **30a** and **30b**

5.5.2 Spectral Characterization

5.5.2.1 Mass Spectrometric Analysis

Both the bridged octaphyrins (**30a** and **30b**) were confirmed through ESI mass spectrometric analysis and shown in Figure 5.18 and 5.19. The molecular ion peaks at m/z 1327.2821 $[M+H]^+$ for **30a** and 1387.2260 $[M+H]^+$ for **30b** confirm the exact composition of the expected macrocycles.

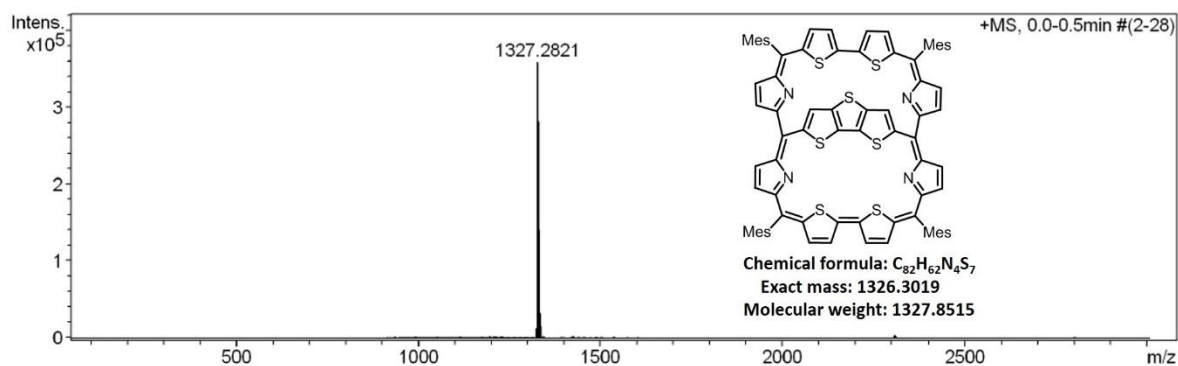


Figure 5.18: ESI-MS spectrum of **30a**

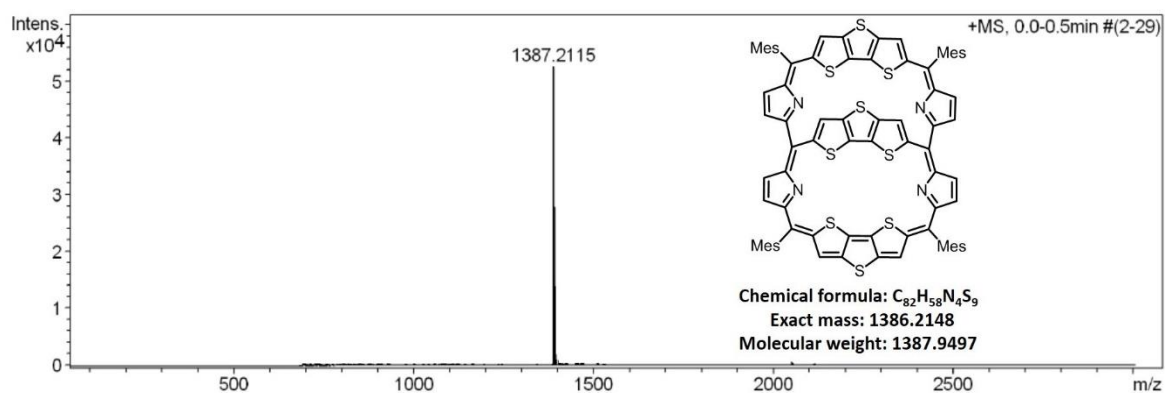


Figure 5.19: ESI-MS spectrum of **30b**

5.5.2.2 NMR Spectral Analysis

The ^1H NMR spectrum of **30a** was recorded in CD_2Cl_2 at 298 K and shown in Figure 5.20. The unsymmetrical nature of **30a** is reflected from spectral analysis, where the bithiophene (a, b, c and d) as well as pyrrolic β -CH protons (1, 2, 3 and 4) are resonated as eight doublets between 11.6 ppm and 8.25 ppm. The inner DTT β -CH protons are observed as sharp singlet at 7.20 ppm suggests the typical $[34]\pi$ aromatic circuit. The *meso*-mesityl CH signals are at 7.73 ppm and 7.36 ppm, whereas the mesityl methyl- CH_3 protons are at 2.90 to 2.52 ppm. Assignment of all the heterocyclic β -CH protons were further confirmed by ^1H - ^1H COSY spectroscopy.

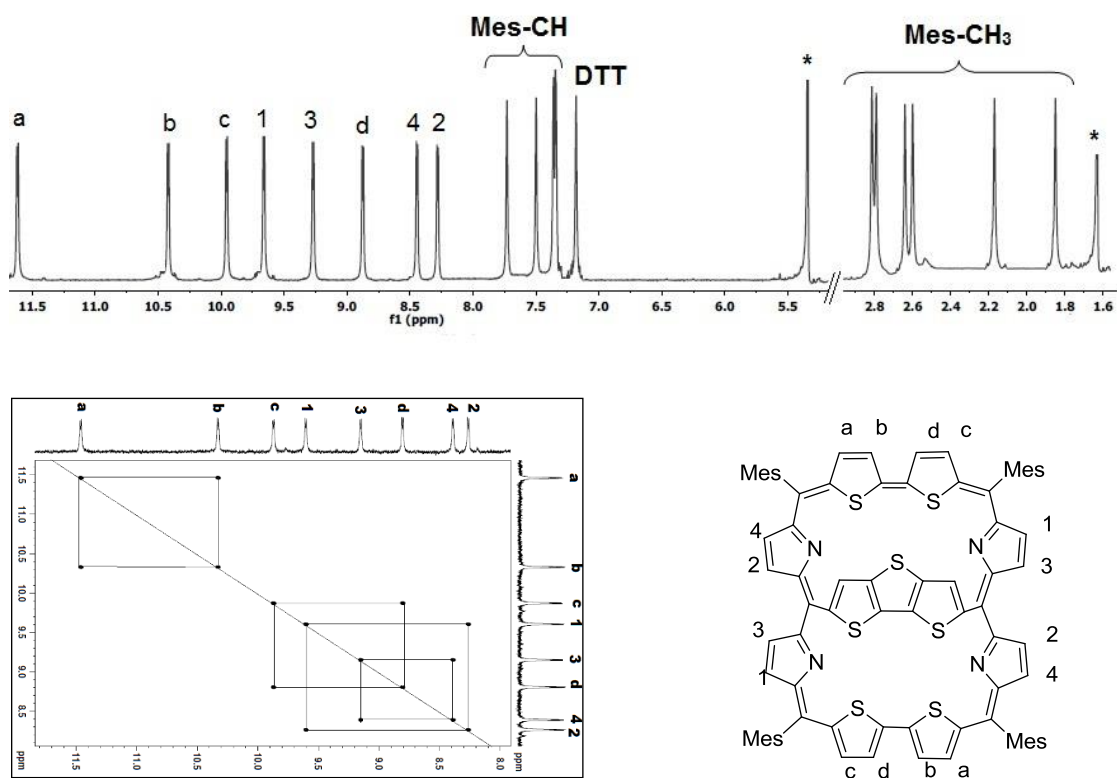


Figure 5.20: ^1H NMR and ^1H - ^1H COSY spectrum of **30a** with heterocyclic ring correlations.

The results are further compared with [26] π mono-fused ruyrin and shown in Figure 5.21. The respective macrocycle was synthesized as per our earlier reported procedure. The mono-fused DTT-CH protons in ruyrin is resonated at 10.85 ppm (H), whereas the bridged DTT-CH protons in **30a** is 3.65 ppm upfield shifted, thus suggests the shielding effect of [34] π electronic circuit and also maintains the partial [26] π aromatic character. Overall, in the freebase state **30a** adopts dual aromatic behavior.

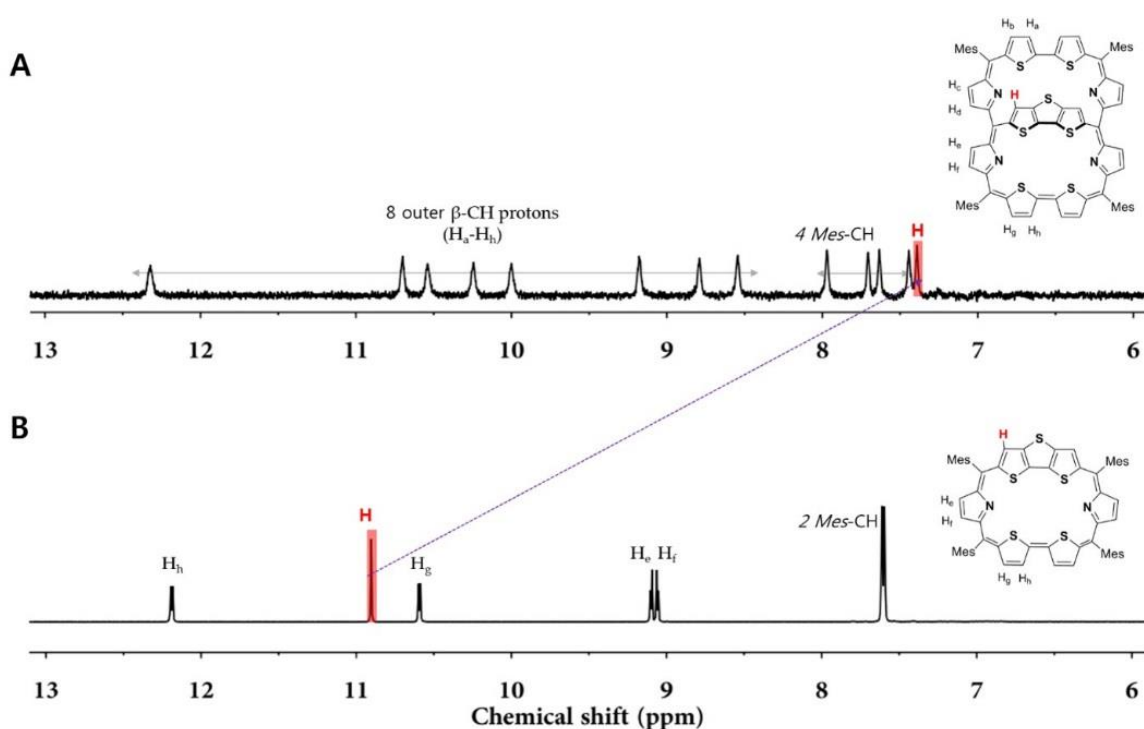


Figure 5.21: ^1H NMR spectral comparison between **30a** and monofused ruyrin.

Upon protonation of **30a** with TFA in CD_2Cl_2 at 298 K, interesting spectral changes were observed and the results were shown in Figure 5.22. Out of four pyrrolic units, two are inverted, where the respective β -CH protons are 3.65 ppm upfield shifted and resonated at 6.10 ppm (1) and 5.65 ppm (3). The normal pyrrolic β -CH protons (2, 4) and the thiophene β -CH protons (a, b, c and d) are resonated between 11.70 and 9.17 ppm. The newly

protonated inner and outer NHs are observed at -4.00 ppm and 16.00 ppm as broad singlets. These signals were further confirmed by D₂O exchange experiment. The *meso*-mesityl CH signals are at 7.70 and 6.80 ppm as four sharp singlets. Similar trend was observed in the ¹H NMR spectral analysis of **30b**, both in the freebase and protonated state.

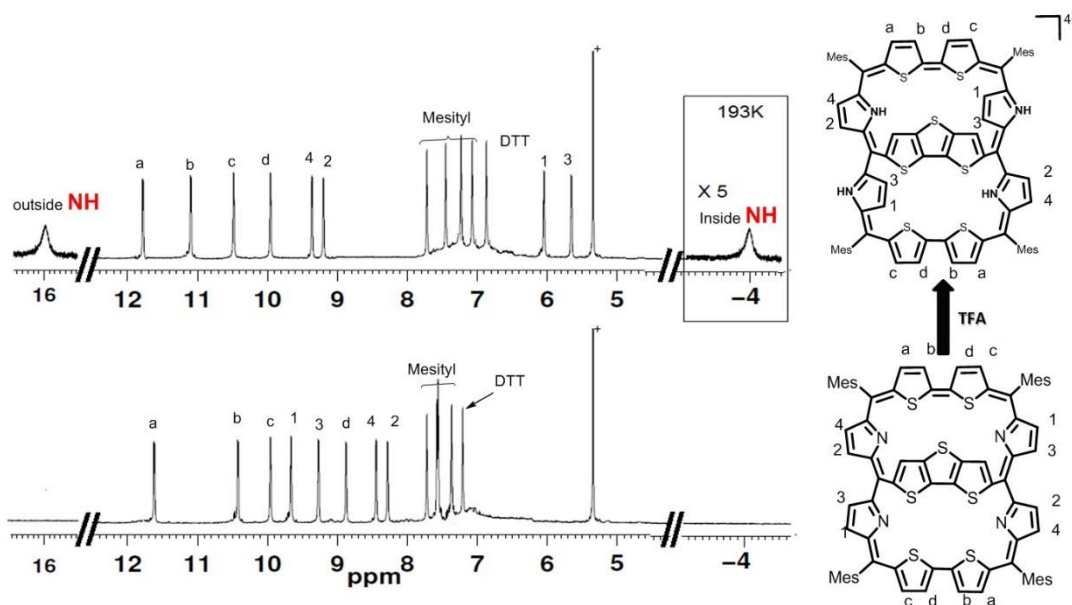


Figure 5.22: ¹H NMR spectrum of **30a** and **30a.4H⁺**

5.5.2.3 Electronic Spectral Analysis

The electronic absorption spectrum of **30a** and **30b** was recorded in CH₂Cl₂. The **30a** exhibits split Soret like band at 502 and 605 nm and two weak Q-like bands at 827 and 1004 nm, respectively (Figure 5.23). The position of the higher energy band (502 nm) has similar spectral features as that of [26] π mono-fused ruyirin, whereas the band at 605 has similar features as [34] π octaphyrin. Similar aromatic character was also reflected from the lower energy Q-bands. However, upon protonation, the higher energy bands merged together and observed as prominent Soret like band at 650 nm and Q-like band at 1021 nm. Overall, the results suggest that **30a** in the freebase state adopts dual-aromatic conformation and

protonation favours predominant [34] π octaphyrin aromatic conjugative pathway. Similar spectral trend was observed in **30b**.

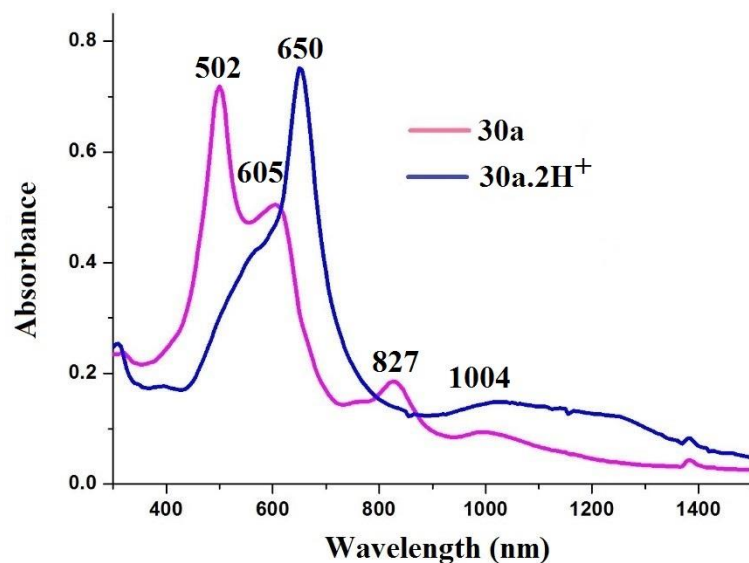


Figure 5.23: The electronic absorption spectrum of **30a** and **30a.4H⁺**

5.5.2.4 NICS Calculations and AICD Plots for [42] π Electronic System

Nucleus Independent Chemical Shift calculations were carried out in an effort to gain insight into the magnetic shielding / deshielding effects present in **30a**. Two NICS values, names - 9.51 and -13.5 ppm, were calculated for points within the two cavities present in **30a** (Figure 5.24a). These two high negative NICS values are consistent with the proposed aromatic character. However, a significant difference between the two points is seen. This difference of ca. 4 ppm is ascribed to the diatropic ring current flowing through the DTT moiety. Various control studies were carried out to provide assurance that this difference is due to local ring current differences. For instance, an imaginary [34] π octaphyrin molecule lacking the DTT moiety gives rise to paired NICS values of -13.9 and -13.7 ppm at analogous positions (Figure 5.24b). An imaginary [26] π hexaphyrin molecule that is not embedded in

a [34] π octaphyrin framework was also constructed. Related to this control, the NICS values of the DTT π -CH protons are shifted upfield by almost 7 ppm (Figure 5.24c). This difference is ascribed to the diatropic ring current of the outer [34] π octaphyrin periphery. Similar trend was observed in the NICS(0) calculations for **30b**, where the NICS values are -6.6 and -10.9 ppm and the respective imaginary [34] π octaphyrin molecule without DTT bridge are -9.8 and -10.9 ppm, respectively (Figure 5.25).

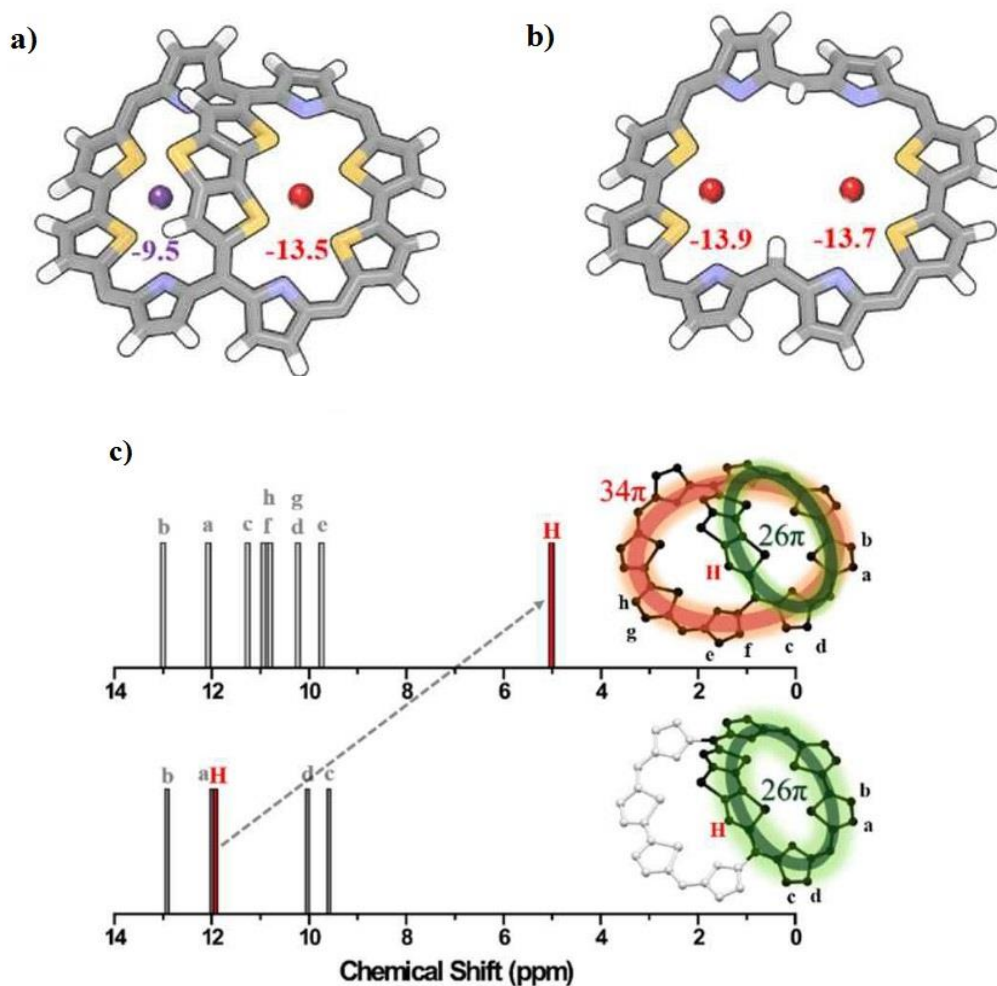


Figure 5.24: NICS(0) value of **30a** (a) and imaginary [34] π octaphyrin (b). NICS values of hydrogen atoms in **30a** and the constituent [26] π hexaphyrin. Hydrogen atoms in the DTT-bridge are shown in red (c).

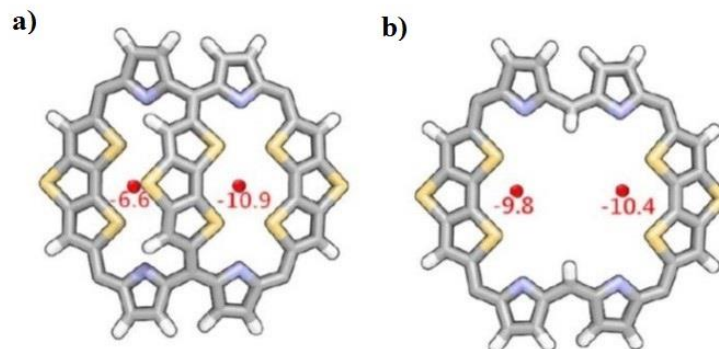


Figure 5.25: NICS(0) value of **30a** (a) and imaginary [34] π octaphyrin (b)

The Anisotropy Induced Current Density (AICD) for the inner and outer core of **30a** and **30b** shows clockwise current delocalization (Figure 5.26). The result indicates the aromatic behavior in both the macrocycle and consistent with the results observed from the spectral analyses and NICS(0) calculations.

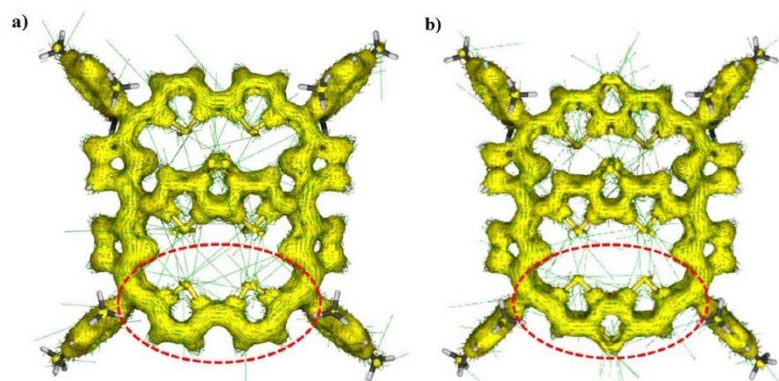


Figure 5.26: AICD plots of **30a** (a) and **30b** (b).

5.5.2.5 Single Crystal X-ray Analysis

The structures of **30a** and **30b** were unambiguously confirmed by single crystal X-ray analyses and the structures were shown in Figure 5.27 and 5.28 (Table 5.3). The crystals

were obtained by slow evaporation of CH_2Cl_2 solution in *n*-hexane. Both the molecule were crystallized in monoclinic and orthorhombic crystal system with $P21/n$ and $P2c-2ac$ space group. As reflected from spectral analysis, the compound **30a** contains two bithiophene tetrapyrane units, while **30b** consists of two DTT tetrapyrane units. Both the units are individually bridged with DTT moiety and the remaining four *meso* positions are occupied by four mesityl groups. The crystal analysis reveals that the DTT units in **30a** and **30b** are deviated by 41.05° and 40.59° , respectively, whereas *meso* mesityl rings are nearly perpendicular (87.24° , 87.41° , 83.85° , 75.29° for **30a** and 84.26° , 80.89° , 76.12° , 78.74° for **30b**) to the mean macrocyclic plane.

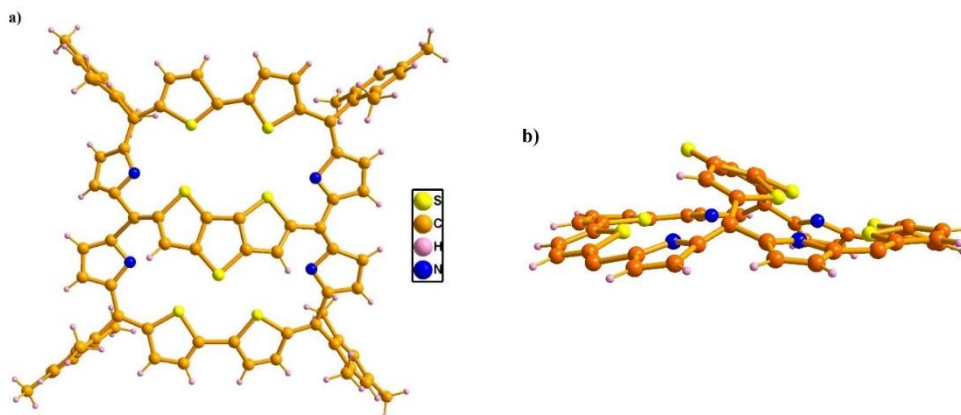


Figure 5.27: Single crystal X-ray structure of **30a**. (a) Top view and (b) side view.

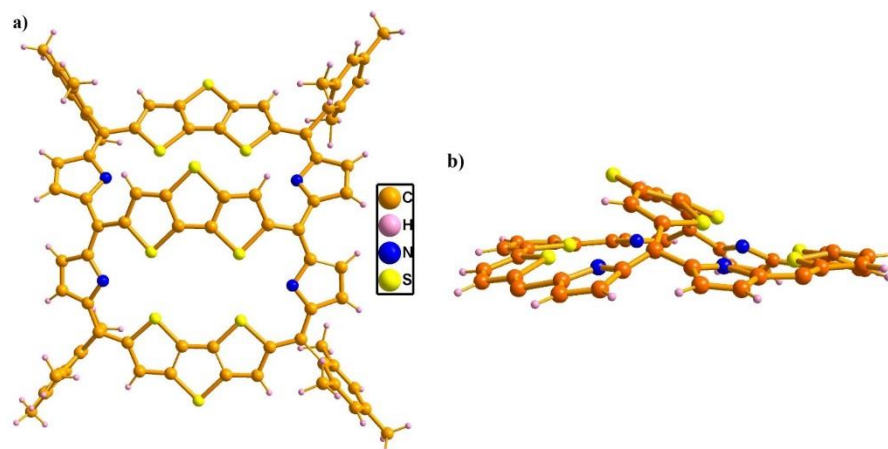


Figure 5.28: Single crystal X-ray structure of **30b**. (a) Top view and (b) side view.

Table 5.3: Crystal data for **30a** and **30b**.

	30a	30b
<i>T</i> , K	100 K	100K
Formula	C166 H120 Cl4 N8 S14	C84 H62 Cl4 N4 S9
Formula weight	2817.33	1557.71
Color and Habit	black	black
Crystal system	monoclinic	orthorhombic
Space group	<i>P</i> 21/n	<i>P</i> 2c -2ac
<i>a</i> , Å	20.2245(9)	38.0854
<i>b</i> , Å	14.9645(9)	13.6768
<i>c</i> , Å	52.604(3)	14.8701
α , deg	90	90
β , deg	95.595(5)	90
γ , deg	90	90
<i>V</i> , Å ³	14182(5)	7745
Radiation (λ , Å)	Mo K α (0.71073)	Mo K α (0.71073)
<i>Z</i>	4	4
d_{calcd} , g•cm ⁻³	1.181	1.336
μ , mm ⁻¹	0.260	0.402
<i>F</i> (000)	5856	3224
No. of unique reflns	50266	12530
No. of params. refined	17003	1352
GOF on <i>F</i> ²	1.041	1.07
<i>R</i> 1 ^a [<i>I</i> > 2 σ (<i>I</i>)]	0.1619	0.079
<i>R</i> 1 ^a (all data)	0.1949	0.091
<i>wR</i> 2 ^b (all data)	0.3678	0.217

5.5.2.6 Excited State Aromaticity

The Baird's aromaticity rule is described in the first chapter. As per the rule, the reversal of aromaticity will be reflected upon going from ground state to excited state.

In order to verify Baird prediction, we used both the octaphyrins **30a** and **30b** which contains overall 42π electrons and exhibit Hückel aromaticity in ground state. Upon two electron oxidation with NOSbF_6 or electrochemical oxidation will generate 40π electronic system. Which will show anti-aromaticity in ground state but will show Baird type aromaticity in the lowest excited triplet state. The existence of the dication was verified through triplet state ESR spectra and evaluated zero field splitting parameters D and E. The EPR parameters for the dicationic species were determined to be $g=2.003$, $D=25.3$ mT and $E=3.3$ mT. Temperature dependent EPR spectral analysis were carried out in half field region and from the evidence it is cleared that triplet state is more stable than the singlet state.

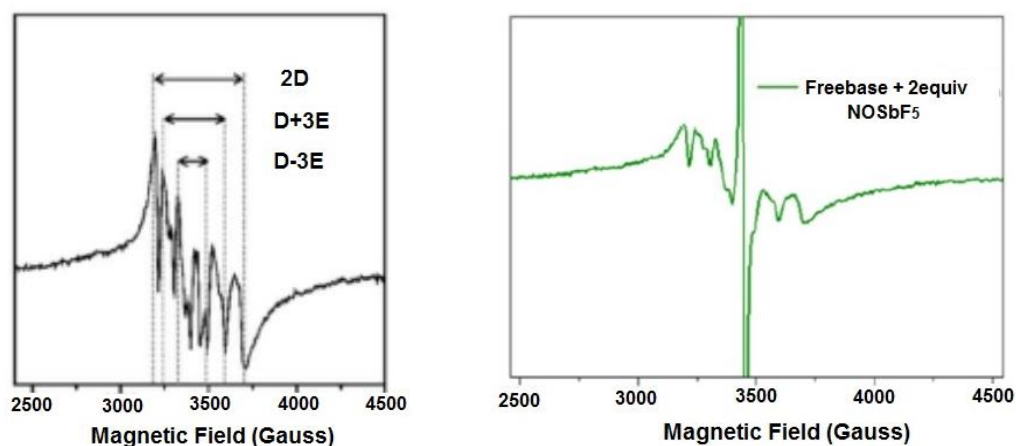


Figure 5.29: EPR spectroscopy of $2e^-$ oxidized form of **30a** and **30b**.

Same strategy we applied in our molecules. After two electron oxidation both the octaphyrin converted into $[40]\pi$ electronic system from $[42]\pi$ system (Figure 5.29). In lowest triplet excited state molecule shows Baird aromatic behaviour. Till now there is no such

experimental evidence behind the aromaticity, but theoretical calculations like NICS and AICD plots gives support behind the aromaticity of the molecule.

5.5.2.7 NICS Calculations and AICD Plots for [40] π Electronic System

The NICS values were calculated for the [40] π electronic system such as **30a**²⁺ and **30b**²⁺ and the respective values at the center of the cavity are -6.2 & -6.8 ppm for **30a**²⁺ and -5.6 & -5.9 ppm for **30b**²⁺ (Figure 5.30). The negative values indicate the aromatic behavior of the dicationic complex in the triplet excited state. The results are further supported by the AICD plots where the clockwise delocalization (Figure 5.31) of the current density are observed in the inner and outer core of the octaphyrin in triplet excited state.

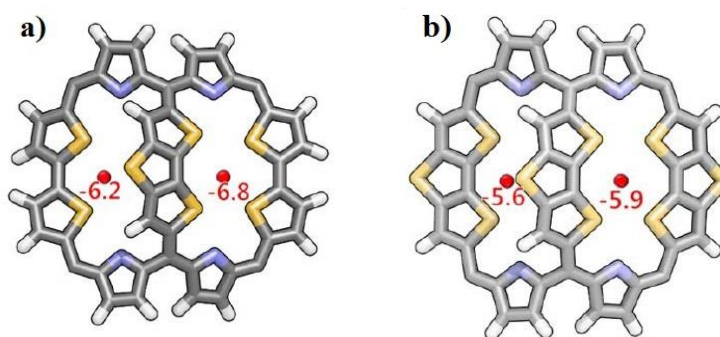


Figure 5.30: NICS(0) value of 2e⁻ oxidized form of **30a** (a) and **30b** (b)

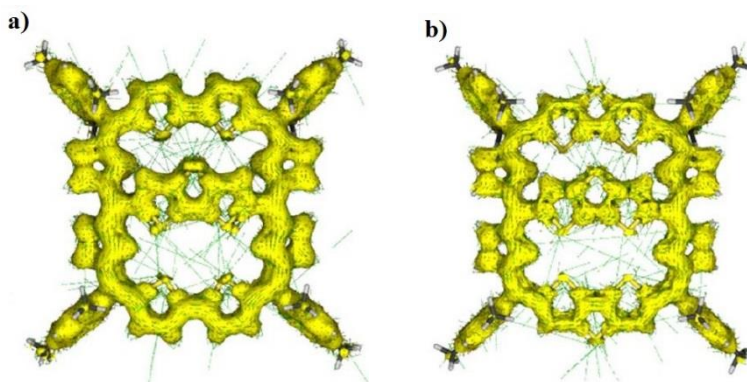


Figure 5.31: AICD plots of 2e⁻ oxidized form of **30a** (a) and **30b** (b).

5.6 Conclusions

In summary, we have successfully demonstrated the synthesis of three different types of planar octaphyrins. The acid-catalyzed condensation and oxidative coupling reactions were adopted for the synthesis of non-fused, fused and bridged aromatic octaphyrins. The non-fused derivatives were in rotational isomeric form in the freebase state and one of the isomers was stabilized upon protonation. The fused core-modified derivative was effectively utilized to stabilize Rh(I) metal ions. The core-modified bridged octaphyrin was in dual aromatic character with $[26]\pi$ and $[34]\pi$ electronic conjugation pathway in the freebase form, however, $[34]\pi$ electronic conjugation pathway was exclusively stabilized upon protonation. In addition, the overall $[42]\pi$ electrons in the aromatic core-modified bridged system was further subjected to two electron oxidation in order to achieve Hückel anti-aromatic $[40]\pi$ system. At the lowest triplet excited state, $[40]\pi$ system maintained the aromatic character as such and the results were further supported by theoretical calculations.

5.7 Experimental Procedure

5.7.1 Synthesis of 26a

A mixture of terthiophene pentapyrrane (200 mg, 0.31 mmol) (**25a**) and terthiophene aryl diol (169 mg, 0.31 mmol) (**24**) were dissolved in 200 ml of dry CH_2Cl_2 and the resulting solution was stirred under nitrogen atmosphere for 15 min. Trifluoroacetic acid (24 μl , 0.31 mmol) was added and the resulting solution was stirred for 1h. The progress of the reaction was monitored by TLC. DDQ (212 mg, 0.93 mmol) was added and the resulting solution was stirred for another 1h. The solvent was evaporated in rotary evaporator. The residue was purified by basic alumina followed by silica gel (100-200 mesh) column chromatography.

The dark blue color band was eluted with CH₂Cl₂/*n*-hexane (55:45, v/v) and identified as octaphyrin (**26a**) in 12% yield. Recrystallization with CH₂Cl₂/CH₃OH gave bronze color crystalline product.

Compound 26a: ¹H NMR (400 MHz, Toluene-d₈) δ (in ppm) = 9.85 (d, 1H), 9.83 (d, 1H), 9.76 (d, 1H), 9.21 (s, 5H), 8.58 (d, 1H), 8.5 (d, 1H), 8.06 (s, 4H), 7.39 (s, 2H), 7.25 (s, 2H), 7.16 (s, 8H), 2.60 (s, 3H), 2.53 (s, 3H), 2.46 (s, 12H), 2.34 (s, 6H), 2.16 (s, 6H), 2.12 (s, 12H), 0.37 (s, 2H), 0.38 (s, 1H), -1.26 (s, 1H); **26a**·2H⁺: ¹H NMR (400 MHz, Toluene-d₈) δ (in ppm) = 11.02 (d, 1H), 10.9 (d, 1H), 10.8 (d, 1H), 10.21 (d, 1H), 9.08 (d, 1H), 9.03 (d, 1H), 7.34 (s, 2H), 7.18 (s, 1H), 2.50 (s, 3H), 2.41 (s, 3H), 2.33 (s, 2H), 2.04 (s, 6H), 1.74 (s, 4H), -3.02 (s, 1H, NH), -4.55 (d, 1H), -4.97 (d, 1H). **26a:** UV/Vis (CH₂Cl₂): λ_{max} in nm (ε in dm³mol⁻¹cm⁻¹) = 603 (8.65×10⁴), 647 (1.10×10⁵), 905 (7.45×10⁴); **26a**·2H⁺ (TFA/CH₂Cl₂): λ_{max} in nm (ε in dm³mol⁻¹cm⁻¹) = 632 (2.10×10⁵), 1167 (9.80×10⁴).

5.7.2 Synthesis of 26b

Terthiophene tolyl pentapyrrane (200 mg, 0.34 mmol) (**25b**), terthiophene mesityl diol (185 mg, 0.34 mmol) (**24**) and Trifluoroacetic acid (26 μl, 0.34 mmol) were dissolved in 200 ml of dry CH₂Cl₂ under similar condition as mentioned in **26a**. After DDQ (232 mg, 1.02 mmol) oxidation, the crude residue was purified by basic alumina followed by silica gel (100-200 mesh) column chromatography. The dark blue color band was eluted with CH₂Cl₂/*n*-hexane (58:42, v/v) and identified as octaphyrin (**26b**) in 10% yield. Recrystallization with CH₂Cl₂/CH₃OH gave bronze color crystalline product.

Compound 26b: ¹H NMR (400 MHz, Toluene-d₈) δ (in ppm) = 9.88-9.80 (m, 3H), 9.31 (s, 2H), 9.21 (s, 2H), 8.74 (d, 1H), 8.63 (d, 1H), 8.53 (s, 1H), 8.34 (d, 1H), 8.27 (s, 2H), 8.13 (s, 3H), 7.88 (s, 4H), 7.59 (d, 2H), 7.44 (d, 3H), 7.34 (s, 4H), 7.24 (s, 4H), 2.54 (s, 6H), 2.45

(s, 6H), 2.22 (s, 12H), 2.13 (s, 25H), 0.48 (m, 4H), -1.10 (d, 1H), -1.24 (d, 1H). **26b·2H⁺**: ¹H NMR (400 MHz, Toluene-d₈) δ (in ppm) = 11.06-10.83 (m, 5H), 10.61 (s, 1H), 10.26 (d, 1H), 10.12 (d, 1H), 9.19 (d, 1H) 9.16 (d, 1H), 9.09 (d, 1H), 8.99 (d, 2H), 8.88 (d, 2H), 8.69 (d, 2H), 8.59 (d, 1H), 8.44 (d, 1H), 7.88 (d, 2H), 7.76 (d, 2H), 7.66 (s, 1H), 7.59 (s, 2H), 7.44 (s, 2H), 2.73 (s, 3H), 2.67 (s, 6H), 2.63 (s, 3H), 2.30 (s, 6H), 2.03 (s, 6H), -1.12 (s, 1H, NH), -3.12 (d, 1H), -3.27 (s, 1H, NH), -3.73 (d, 1H), -3.86 (d, 1H), -4.09 (d, 1H). **26b**: UV/Vis (CH₂Cl₂): λ_{max} in nm (ε in dm³mol⁻¹cm⁻¹) = 602 (8.58×10⁴), 650 (1.03×10⁵), 917 (7.32×10⁴); **26b·2H⁺** (TFA/CH₂Cl₂): λ_{max} in nm (ε in dm³mol⁻¹cm⁻¹) = 634 (2.07×10⁵), 1153 (8.95×10⁴).

5.7.3 Synthesis of 27

DTT-tetrapyrane (**19**) (300 mg, 0.51 mmol) was dissolved in 200 ml dry CH₂Cl₂ and resulting solution was stirred under nitrogen atmosphere for 15 min. TFA (39 μl, 0.51 mmol) was added and resulting mixture was stirred under similar condition for further 90 min. Progress of the reaction was monitored by TLC. Chloranil (375 mg, 1.53 mmol) was added and resulting mixture was refluxed under open air condition for 1h. Solvent was evaporated in rotary evaporator. The crude product was purified through basic alumina column followed by silica gel (100 – 200 mesh) column chromatography. A dark blue color band was eluted with CH₂Cl₂: *n*-hexane (80:20, v/v) and identified as octaphyrin (**27**) in 3% yield.

Compound 27: ¹H NMR (400 MHz, CH₂Cl₂) δ (in ppm) = 12.87 (s, 1H), 12.00 (d, 1H), 11.00 (s, 1H), 8.21 (s, 2H), 3.81 (s, 3H), 2.42 (s, 6H). UV/Vis (CH₂Cl₂) λ_{max} in nm (ε in dm³mol⁻¹cm⁻¹) = 573 (9.74×10⁴), 603 (9.63×10⁴), 1173 nm (1.91×10³); **27·2H⁺** (TFA/CH₂Cl₂): λ_{max} in nm (ε in dm³mol⁻¹cm⁻¹) = 598 (1.48×10⁵), 947 (1.96×10³), 1170 (1.87×10³); **28**: (CH₂Cl₂): λ_{max} in nm (ε in dm³mol⁻¹cm⁻¹) = 620 (1.963×10⁵), 947 (1.94×10³), 1290 (1.94×10⁵).

5.7.4 Synthesis of **30a**

To a degassed solution of **15** (400 mg, 0.714 mmol) and 2,2-dithienothiophene carboxaldehyde **29** (90 mg, 0.357 mmol) in 200 mL distilled CH₂Cl₂ under a nitrogen atmosphere, *p*-TSA acid (27 mg, 0.14 mmol) was added and the reaction mixture stirred overnight at room temperature. Subsequently, DDQ (483 mg, 2.13 mmol) was added and stirring was continued for 90 min at the same temperature under open air conditions. The reaction was monitored by TLC. The reaction mixture was quenched via the addition of triethylamine (1 mL). Solvent was evaporated in rotary evaporator. The residue was purified by silica gel (100 – 200 mesh) column chromatography (1:6, EtOAc: *n*-hexanes, eluent) to give the expected product **30a** as a bluish solid (75 mg, 13% yield).

Compound 30a: ¹H NMR (400 MHz, CH₂Cl₂) δ (in ppm) = 12.08 (d, 2H), 10.41 (d, 2H), 10.27 (d, 2H), 9.97 (d, 2H), 9.76 (d, 2H), 8.89 (d, 2H), 8.49 (d, 2H), 8.25 (d, 2H), 7.69 (s, 2H), 7.40 (s, 2H), 7.33 (s, 2H), 7.14 (s, 2H) 7.12 (s, 2H), 2.78 (s, 6H), 2.76 (s, 6H), 2.62 (s, 6H), 2.58 (s, 6H), 2.17 (s, 6H), 1.81 (s, 6H); **30a·4H⁺**: ¹H NMR (400 MHz, CH₂Cl₂) δ (in ppm) = 16.00 (s, 1H, NH), 11.79 (d, 1H), 11.10 (d, 1H), 10.50 (d, 1H), 9.94 (d, 1H), 9.41 (d, 1H), 9.20 (d, 1H), 7.70 (s, 1H), 7.52 (s, 1H), 7.31 (s, 1H), 7.13 (s, 1H), 6.85 (s, 1H, DTT-CH), 6.10 (d, 1H), 5.65 (d, 1H), -3.92 (s, 1H, NH).

30a: UV/Vis (CH₂Cl₂): λ_{max} in nm (ε in dm³mol⁻¹cm⁻¹) = 502 (1.05×10⁵), 605 (8.54×10⁴), 827 (1.31×10³), 1004 (1.03×10³); **30a·4H⁺** (TFA/CH₂Cl₂): λ_{max} in nm (ε in dm³mol⁻¹cm⁻¹) = 650 (1.14×10⁵), 1021 (2.55×10³).

5.7.5 Synthesis of **30b**

To a degassed solution of **19** (390 mg, 0.661 mmol) and 2,2-dithienothiophene carboxaldehyde **29** (83 mg, 0.330 mmol) in 300 ml distilled CH₂Cl₂ under an argon atmosphere, *p*-TSA acid (25 mg, 0.13 mmol) was added and the reaction mixture stirred for overnight at room temperature. Subsequently, DDQ (449 mg, 1.98 mmol) was added and stirring was continued for 90 min at the same temperature under open air conditions. At the conclusion of the reaction, the reaction mixture was quenched with triethylamine (1 ml). The solvent was evaporated under reduced pressure. The residue was purified by silica gel column chromatography (1:7, EtOAc: *n*-hexane) to afford the desired product as a bluish solid **30b** (128 mg, 27% yield).

Compound 30b: ¹H NMR (400 MHz, CH₂Cl₂) δ (in ppm) = 10.47 (d, 4H, β-CH), 10.05 (s, 4H), 8.99 (d, 4H, β-CH), 7.65 (s, 4H), 7.35 (s, 4H), 6.27 (s, 2H), 2.75 (s, 12H), 2.73 (s, 12H), 2.49 (s, 12H); **30b·4H⁺**: ¹H NMR (400 MHz, CH₂Cl₂) δ (in ppm) = 10.91 (d, 1H), 10.75 (d, 1H), 9.30 (s, 1H), 7.54 (s, 1H), 7.46 (s, 1H), 7.10 (s, 1H), 2.85 (s, 6H), 2.73 (s, 6H), 2.58 (s, 6H), 2.37 (s, 6H), -4.71 (s, 1H, NH).

30b: UV/Vis (CH₂Cl₂): λ_{max} in nm (ε in dm³mol⁻¹cm⁻¹) = 498 (1.17×10⁵), 634 (8.94×10⁴), 835 (2.31×10³); **30b·4H⁺** (TFA/CH₂Cl₂): λ_{max} in nm (ε in dm³mol⁻¹cm⁻¹) = 654 (2.08×10⁵), 1090 (1.57×10³), 1174 (2.58×10³).

5.8 References:

- 1) Saito, S.; Osuka, A. *Angew. Chem. Int. Ed.* **2011**, *50*, 4342-4373.
- 2) Sessler, J. L.; Seidel, D. *Angew. Chem. Int. Ed.* **2003**, *42*, 5134-5175.
- 3) Stępień, M.; Sprutta, N.; Latos-Grażyński, L. *Angew. Chem. Int. Ed.* **2011**, *50*, 4288-4340.
- 4) Umetani, M.; Tanaka, T.; Kim, T.; Kim, D.; Osuka, A. *Angew. Chem. Int. Ed.* **2016**, *55*, 8095-8099.
- 5) Osuka, A.; Saito, S. *Chem. Commun.* **2011**, *47*, 4330-4339.
- 6) Shimizu, S.; Aratani, N.; Osuka, A. *Chem. Eur. J.* **2006**, *12*, 4909-4918.
- 7) Tanaka, Y.; Shin, J.-Y.; Osuka, A. *Eur. J. Org. Chem.* **2008**, 1341-1349.
- 8) Chatterjee, T.; Theophall, G. G.; Silva, K. I.; Lakshmi, K. V.; Ravikanth, M. *Inorg. Chem.* **2016**, *55*, 6873-6881.
- 9) Zhang, Z.; Cha, W.-Y.; Williams, N. J.; Rush, E. L.; Ishida, M.; Lynch, V.; Kim, D.; Sessler, J. L. *J. Am. Chem. Soc.* **2014**, *136*, 7591-7549.
- 10) Kamimura, Y.; Shimizu, S.; Osuka, A. *Chem. Eur. J.* **2007**, *13*, 1620-1628.
- 11) Saito, S.; Osuka, A. *Chem. Eur. J.* **2006**, *12*, 9095-9102.
- 12) Soya, T.; Kim, W.; Kim, D.; Osuka, A. *Chem. Eur. J.* **2015**, *21*, 8341-8346.
- 13) Kumar, R.; Misra, R.; Chandrashekar, T. K.; Nag, A.; Goswami, D.; Suresh, E.; Suresh, C. H. *Eur. J. Org. Chem.* **2007**, 4552-4562.
- 14) Shin, J.-Y.; Furuta, H.; Yoza, K.; Igarashi, S.; Osuka, A. *J. Am. Chem. Soc.* **2001**, *123*, 7190-7191.
- 15) Chandrashekar, T. K.; Venkatraman, S. *Acc. Chem. Res.* **2003**, *36*, 676-691.

-
- 16) Srinivasan, A.; Anand, V. G.; Pushpan, S. K.; Chandrashekar, T. K.; Sugiura, K.-i.; Sakata, Y. *J. Chem. Soc. Perkin Trans. 2* **2000**, 1788-1793.
- 17) Jeong, S.-D.; Sessler, J. L.; Lynch, V.; Lee, C.-H. *J. Am. Chem. Soc.* **2008**, *130*, 390-391.
- 18) Karthik, G.; Srinivasan, A.; Chandrashekar, T. K. *Org. Lett.* **2014**, *16*, 3472-3475.
- 19) Gokulnath, S.; Chandrashekar, T. K. *Org. Lett.* **2008**, *10*, 637-640.
- 20) Chandrashekar, T. K.; Prabhuraja, V.; Gokulnath, S.; Sabarinathan, R.; Srinivasan, A. *Chem. Commun.* **2010**, *46*, 5915-5917.
- 21) a) Karthik, G.; Lim, J. M.; Srinivasan, A.; Suresh, C. H.; Kim, D.; Chandrashekar, T. K. *Chem. Eur. J.* **2013**, *19*, 17011-17020. b) Hata, H.; Kamimura, Y.; Shinokubo, H.; Osuka, A. *Org. Lett.* **2006**, *8*, 1169-1172. c) Mori, H.; Aratani, N.; Osuka, A. *Chem. Asian J.* **2012**, *7*, 1340-1346.
- 22) Karthik, G.; Srinivasan, A.; Suresh, C. H.; Chandrashekar, T. K. *Chem. Commun.* **2014**, *50*, 12127-12130.
- 23) Anand, V. G.; Saito, S.; Shimizu, S.; Osuka, A. *Angew. Chem. Int. Ed.* **2005**, *44*, 7244-7248.
- 24) Suzuki, M.; Osuka, A. *J. Am. Chem. Soc.* **2007**, *129*, 464-465.
- 25) Karthik, G.; Sneha, M.; Prabhuraja, V.; Lim, J. M.; Kim, D.; Srinivasan, A.; Chandrashekar, T. K. *Chem. Eur. J.* **2013**, *19*, 1886-1890.
- 26) Karthik, G.; Cha, W.-Y.; Ghosh, A.; Kim, T.; Srinivasan, A.; Kim, D.; Chandrashekar, T. K. *Chem. Asian J.* **2016**, *11*, 1447-1453.
- 27) Ajami, D.; Oeckler, O.; Simon, A.; Herges, R. *Nature* **2003**, *426*, 819-821.
-

-
- 28) Stępień, M.; Latos-Grażyński, L.; Sprutta, N.; Chwalisz, P.; Szterenber, L. *Angew. Chem. Int. Ed.* **2007**, *46*, 7869-7873.
- 29) Saito, S.; Shin, J.-Y.; Lim, J. M.; Kim, K. S.; Kim, D.; Osuka, A. *Angew. Chem. Int. Ed.* **2008**, *47*, 9657-9660.
- 30) Lim, J. M.; Shin, J.-Y.; Tanaka, Y.; Saito, S.; Osuka, A.; Kim, D. *J. Am. Chem. Soc.* **2010**, *132*, 3105-3114.
- 31) Marcos, E.; Anglada, J. M.; Torrent-Sucarrat, M. *J. Org. Chem.* **2014**, *79*, 5036-5046.
- 32) a) Higashino, T.; Soya, T.; Kim, W.; Kim, D.; Osuka, A. *Angew. Chem., Int. Ed.* **2015**, *54*, 5456-5459. b) Tanaka, Y.; Mori, H.; Koide, T.; Yorimitsu, H.; Aratani, N.; Osuka, A. *Angew. Chem. Int. Ed.* **2011**, *50*, 11460-11464. c) Cha, W.-Y.; Soya, T.; Tanaka, T.; Mori, H.; Hong, Y.; Lee, S.; Park, K. H.; Osuka, A.; Kim, D. *Chem. Commun.* **2016**, *52*, 6076-6078.
- 33) Vogel, E.; Bröring, M.; Fink, J.; Rosen, D.; Schmickler, H.; Lex, J.; Chan, K. W. K.; Wu, Y.-D.; Plattner, D. A.; Nendel, M.; Houk, K. N. *Angew. Chem., Int. Ed. Engl.* **1995**, *34*, 2511-2514.
- 34) Bröring, M.; Jendry, J.; Zander, L.; Schmickler, H.; Lex, J.; Wu, Y.-D.; Nendel, M.; Chen, J.; Plattner, D. A.; Houk, K. N.; Vogel, E. *Angew. Chem. Int. Ed. Engl.* **1995**, *34*, 2515-2517.
- 35) Seidel, D.; Lynch, V.; Sessler, J. L. *Angew. Chem. Int. Ed.* **2002**, *41*, 1422-1425.
- 36) Sprutta, N.; Latos-Grażyński, L. *Chem. Eur. J.* **2001**, *7*, 5099-5112.
- 37) Anand, V. G.; Pushpan, S. K.; Venkatraman, S.; Dey, A.; Chandrashekar, T. K.; Joshi, B. S.; Roy, R.; Teng, W.; Senge, K. R. *J. Am. Chem. Soc.* **2001**, *123*, 8620-8621.
-

- 38) Kumar, R.; Misra, R.; Chandrashekar, T. K.; Suresh, E. *Chem. Commun.* **2007**, 43-45.
- 39) Rath, H.; Prabhuraja, V.; Chandrashekar, T. K.; Nag, A.; Goswami, D.; Joshi, B. S. *Org. Lett.* **2006**, 8, 2325-2328.
- 40) Rath, H.; Sankar, J.; Prabhuraja, V.; Chandrashekar, T. K.; Joshi, B. S.; Roy, R. *Chem. Commun.* **2005**, 3343-3345.

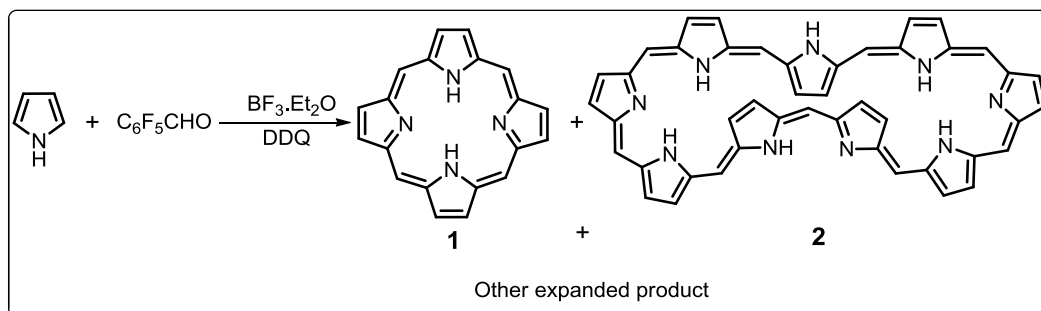
CHAPTER 6

Core-modified Nonaphyrins with Structural Diversity

6.1	Introduction	183-187
6.2	Object of the work	187-188
6.3	Result and discussion	188-207
	6.3.1 Syntheses	188-190
	6.3.2 Spectral Characterization	190-207
	6.3.2.1 Mass Spectrometric Analysis	190-191
	6.3.2.2 Electronic spectral analysis	191-193
	6.3.2.3 NMR Analysis	193-201
	6.3.2.4 Single crystal X-ray analysis	202-204
	6.3.2.5 Nucleus Independent Chemical Shift (NICS)	205-207
6.4	Conclusions	208
6.5	Experimental Procedures	208-211
	6.5.1 Synthesis of 17	208-210
	6.5.2 Synthesis of 18	210-211
6.6	References	211-214

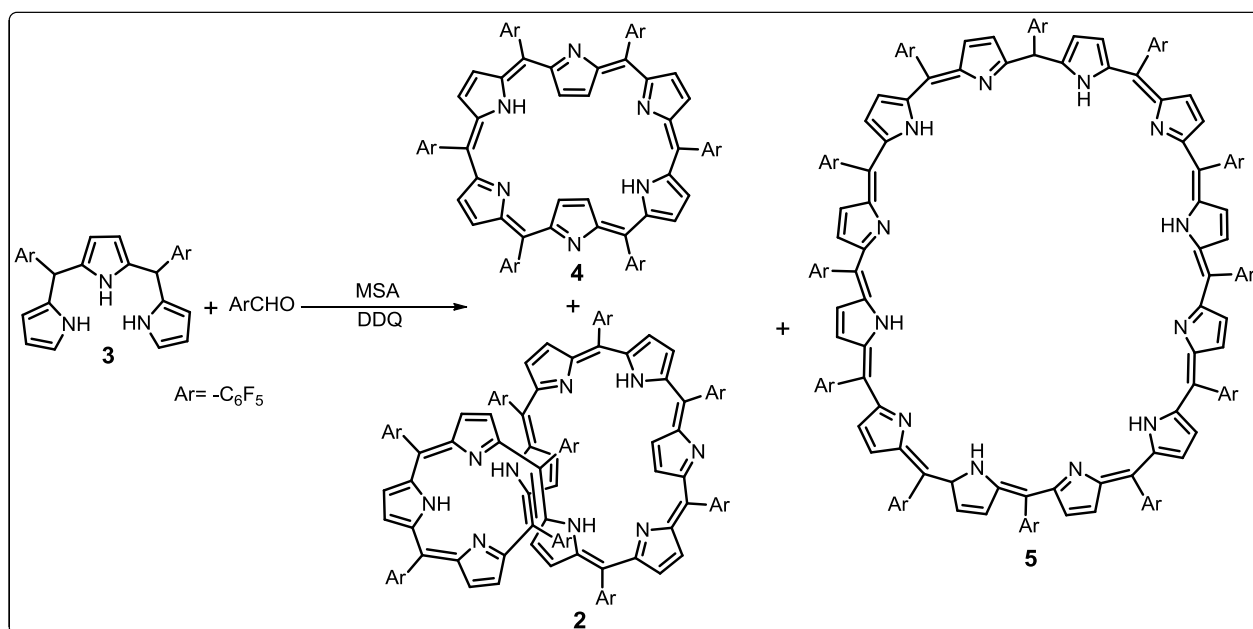
6.1 Introduction

Chemistry of expanded porphyrins^[1-3] are not only interesting from a structural perspective but also attract attention due to their applications in various field.^[4-24] Expanded porphyrins containing five, six, seven and eight heterocyclic rings mentioned in previous chapters are well studied and their chemistry has been exploited for various applications such as anion,^[4-7] cation complexing agents,^[8-12] NLO materials^[13-16] and as Möbius-Hückel aromatic switch.^[17-24] However, there are only few reports on the next higher analogue, such as nonaphyrin,^[25-31] where nine pyrrolic or heterocyclic rings are connected through nine or less number of *meso* carbon atoms. Due to synthetic difficulties, very low yield, less stability and conformational flexibility of the macrocycles, these analogues are weakly explored in the literature. Thus, development of nonaphyrin chemistry to its full potential demands easy and efficient synthetic methods to synthesize them in decent yields. The first nonaphyrin (**2**) with nine *meso*-carbon bridges was reported by Osuka and co-workers by Rothmund type condensation of pyrrole and pentafluorobenzaldehyde in the presence of BF₃.Et₂O as acid-catalyst followed by oxidation with DDQ to afford the [40] π nonaphyrin(1.1.1.1.1.1.1.1.1) (**2**) in 2-3% yield along with porphyrin (**1**) and other expanded porphyrinoids (Scheme 6.1).^[25,26] The crystal analysis of **2** proved that the molecule was in highly twisted conformation with helically arranged porphyrin like tetrapyrrolic core and hexapyrrolic core with two pyrrole rings were inverted. The **2** was further reduced with sodium borohydride (NaBH₄) to form the 42 π nonaphyrin in almost quantitative yield. The distorted asymmetric butterfly-like structure of reduced derivative was reflected from the solid state analyses. Upon protonation, the **2** was bound effectively with TFA and adopted a helical twisted conformation as observed in the reduced nonaphyrin.



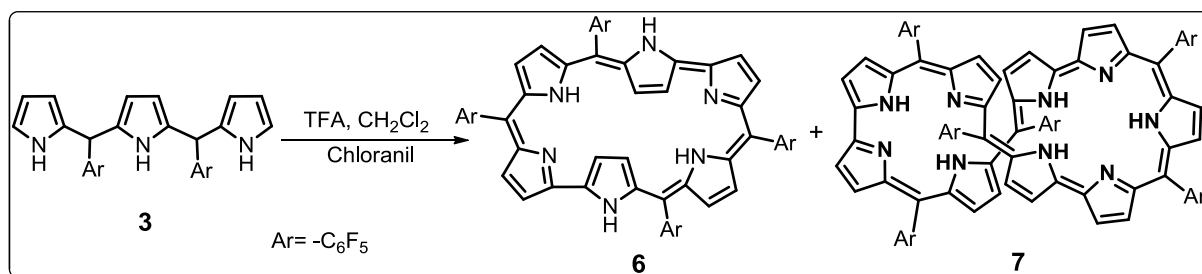
Scheme 6.1: Synthesis of **2**

In order to improve the yield of **2**, the reaction was further performed by ring-size-selective synthetic protocol by same group.^[27] The *meso*-pentafluorophenyl substituted tripyrrane (**3**) was condensed with pentafluorobenzaldehyde by using Lewis acid such as $\text{BF}_3 \cdot \text{Et}_2\text{O}$ or protic acid such as methanesulfonic acid (MSA) followed by DDQ oxidation. In the presence of protic acid, in addition to hexaphyrin (30%) (**4**) and dodecaphyrin (2%) (**5**), **2** was obtained in 15% yield (Scheme 6.2). The core was further effectively utilized to stabilize the hetero-trinuclear metal complexes.^[27]



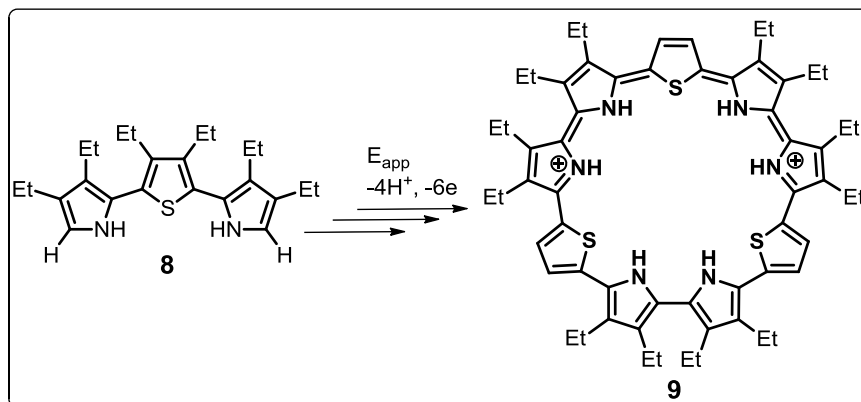
Scheme 6.2: Synthesis of **2** by [3 + 1] methodology

In 2005, Osuka and co-workers were also reported the synthesis of $[38]\pi$ nonaphyrin(1.1.0.1.1.0.1.1.0) with six *meso*-carbon bridges and three direct pyrrole-pyrrole links (**7**).^[28] TFA acid-catalyzed oxidative coupling reaction of tripyrromethane (**3**) followed by chloranil oxidation afforded rubyrin (**6**) along with 38π nonaphyrin (**7**) in 9% yield (Scheme 6.3). The structure was confirmed by crystallographic analysis and revealed a twisted figure-eight conformation with larger $[38]\pi$ conjugated electronic circuit.



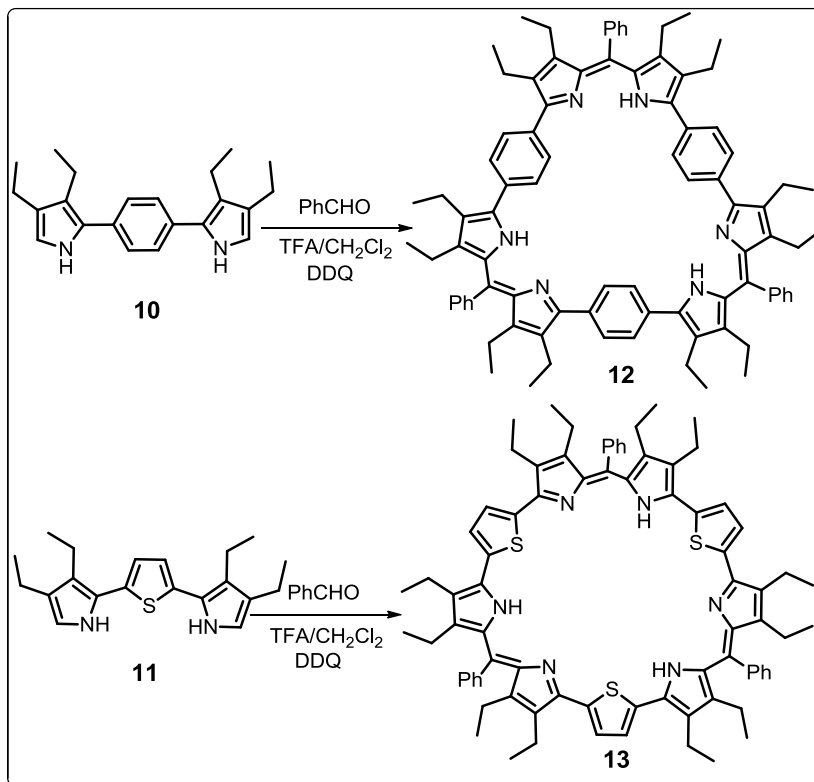
Scheme 6.3: Synthesis of **7**

In 2011, Sessler and co-workers have demonstrated the synthesis of thiophene-containing cyclo[9]pyrrole (**9**) without any *meso*-linkages by electrochemical oxidative methodology using thiophene-containing terpyrrole precursor (**8**) (Scheme 6.4).^[29] The nine pyrrole units were connected through their α,α' -positions to form 34π electronic circuit. The aromatic nature was reflected from the electronic absorption and NMR spectral analysis. The structural analysis revealed that the molecule was in dicationic form and a sulphate ion was trapped inside the macrocyclic core.



Scheme 6.4: Synthesis of **9**

In 2015, Setsune and co-workers have synthesized the nonaphyrins (**12** and **13**), where the pyrrole / heterocyclic rings (thiophene / phenyl) were connected through three *meso*-carbon bridges.^[30] The synthesis was adopted by TFA acid-catalyzed condensation followed by DDQ oxidation of 1,4-bis(2-pyrryl)benzene (**10**) / 2,5-bis(2-pyrryl)thiophene (**11**) with benzaldehyde afforded the phenyl ring based nonaphyrin (**12**) in 61% and thiophene incorporated macrocycle (**13**) in 21% yield, respectively (Scheme 6.5). The structural analyses revealed that both the molecule were in triangular shape, where in **12**, the phenyl rings were deviated from the mean plane, on the other hand, in **13**, all the thiophene rings were inverted. The coordination chemistry was further performed and the ligand was suitable to stabilize the Rh(I) metal ion with square planar geometry around the metal center.^[31]



Scheme 6.5: Synthesis of **12** and **13**

6.2 Objective of the work:

The main objective of this chapter is to introduce fusion in the macrocyclic framework, which is hitherto unknown in nonaphyrin chemistry and explore its characteristic properties. Hence, in this chapter, we wish to report the synthesis of two kinds of nonaphyrins (**17** and **18**) by an acid-catalysed condensation of appropriate precursors. The rigidity in the macrocycle was brought by introducing a fused dithienothiophene in **17** and the results were further compared with non-fused nonaphyrin (**18**) derivative.

The crystal analysis of **17** and **18** and crystal analysis of **17b** (figure 6.4) reveal a twisted figure-eight conformation in the freebase form and is non-aromatic. The structural changes occur from figure-eight to open extended conformation upon protonation and adopts $4n\pi$

Hückel anti-aromatic character, which is reflected from spectral and theoretical studies. Such a structural change also induces ring inversions of specific heterocyclic rings by 180° .

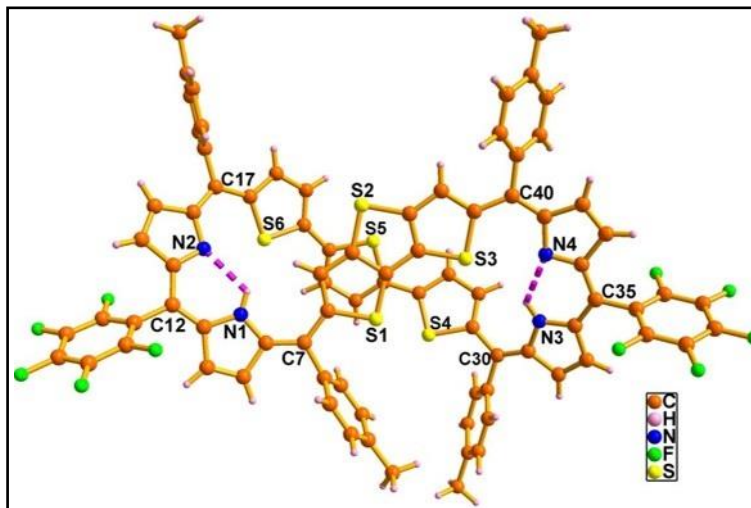


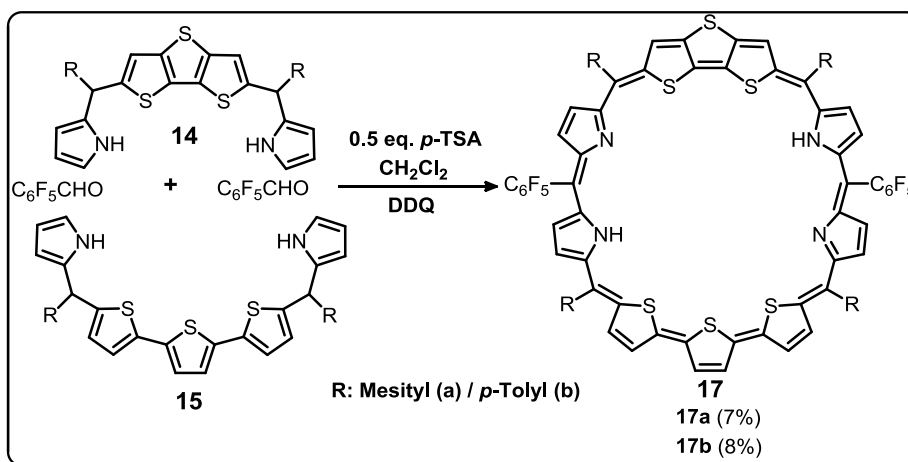
Figure 6.1: Crystal structure of **17b**

6.3 Results and Discussion

6.3.1 Syntheses

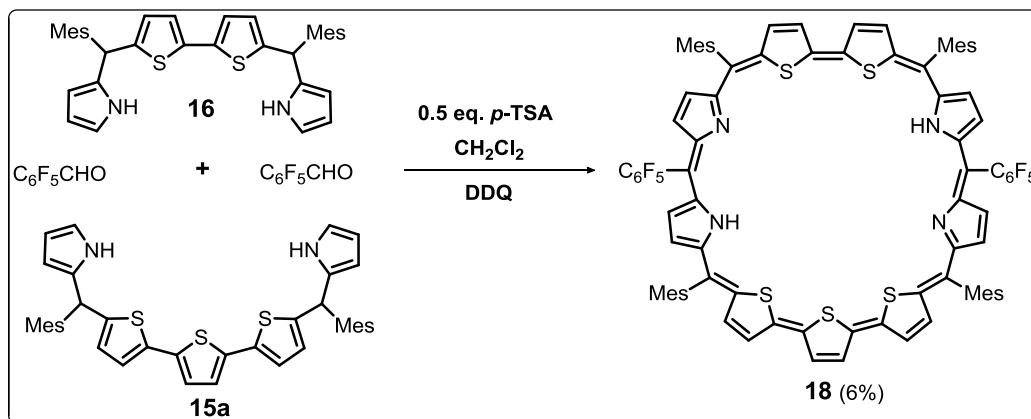
To synthesize fused nonaphyrin (**17**), we adopted [5+4] Mac-Donald type condensation pathways. The required precursors *meso*-mesityl terthiophene pentapyrrane (**15a**) and fused DTT-tetrapyrane (**14**) were synthesized as mentioned in the previous chapters. Thus condensation of non-fused precursor **15a** and fused derivative **14** in presence of pentafluorobenzaldehyde with 0.5 equiv. of *p*-toluenesulphonic acid (*p*-TSA) in dry CH_2Cl_2 followed by DDQ oxidation afforded monofused $[40]\pi$ nonaphyrin (**17a**) with six *meso* linkages in 7% yield (Scheme 6.6). Along with nonaphyrin, a trace amount of self-condensed doubly fused octaphyrin ^[36] and decaphyrin ^[38] were also isolated upon column

chromatographic purification. Under similar reaction condition, the respective *meso-p*-tolyl incorporated nonaphyrin (**17b**) was synthesized in 8% yield.



Scheme 6.6: Synthesis of **17**

In order to understand the effect of fusion on the macrocyclic conformation, a non-fused nonaphyrin involving bithiophene moiety was synthesized. For synthesis of bithiophene linked non-fused nonaphyrin (**18**), the required precursor bithiophene tetrapyrane (**16**) was synthesized by our earlier procedure. Thus condensation of **16** with **15a** in the presence of pentafluorobenzaldehyde with 0.5 equiv. of *p*-TSA followed by DDQ oxidation afforded non-fused nonaphyrin (**18**) with six *meso* links in 6% yield (Scheme 6.7). Here also we isolated trace amount of self-condensed bithiophene containing octaphyrin^[39] and decaphyrin^[38] upon purification by column chromatography.

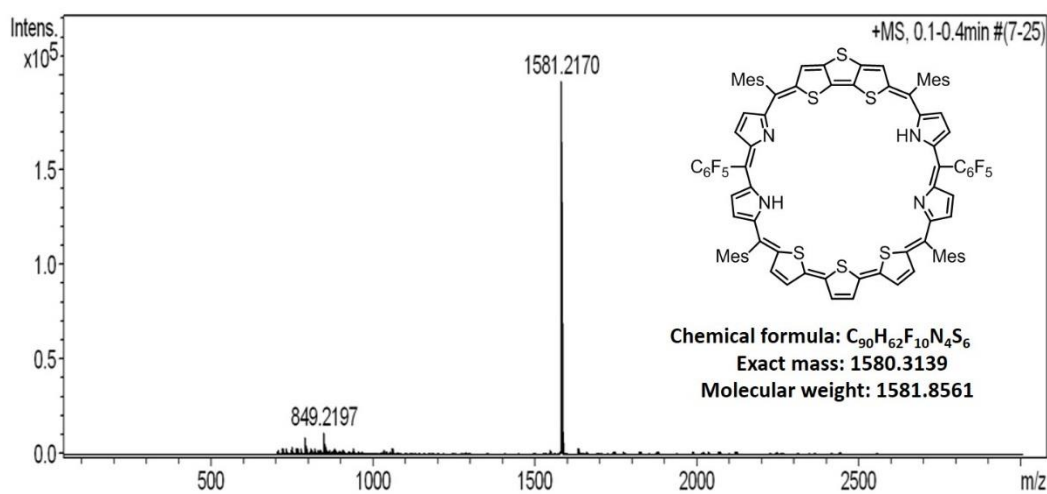


Scheme 6.7: Synthesis of 18

6.3.2 Spectral Characterization

6.3.2.1 Mass spectrometric analysis

The electron spray ionization (ESI) mass spectrometric analysis of **17a**, **17b** and **18** were showed the molecular ion signal m/z at 1581.2170 [M+1] (**17a**), 1469.2073 [M+1] (**17b**) and 1551.9742 [M+1] (**20**) and confirmed the exact composition of the macrocyclic ligand (Figure 6.2-6.4).



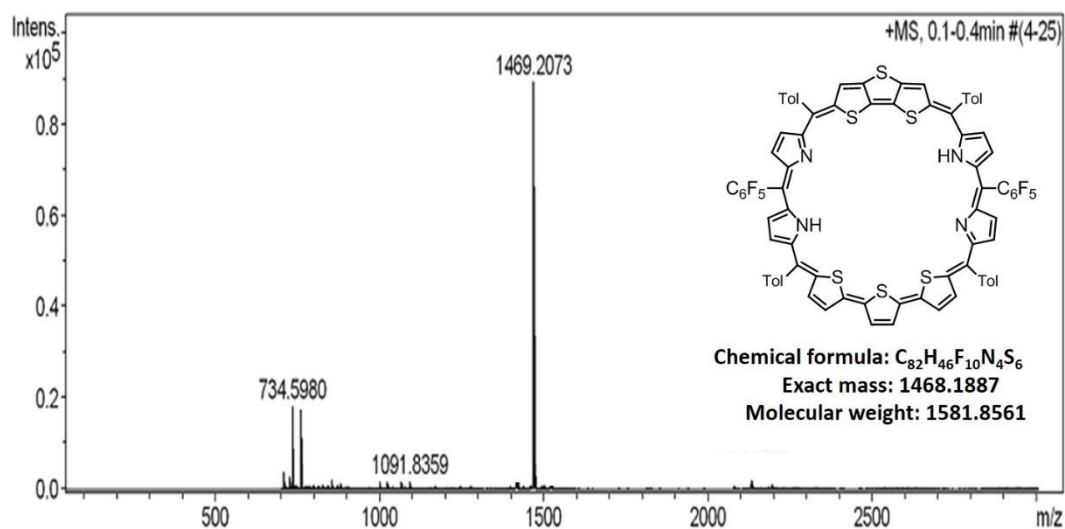


Figure 6.3: ESI-Mass spectrum of **17b**

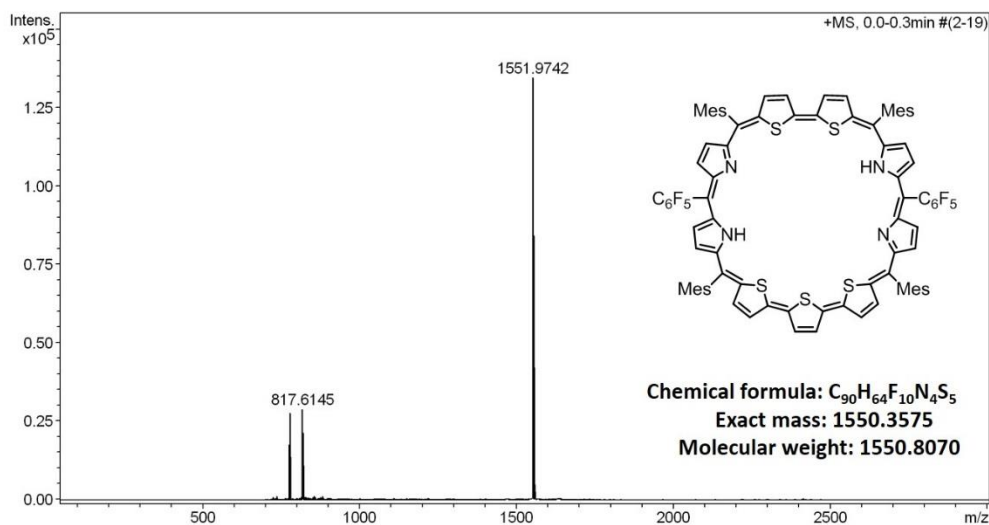


Figure 6.4: ESI-Mass spectrum of **18**

6.3.2.2 Electronic spectral analysis

The electronic absorption spectrum of mono-fused nonaphyrin **17a** in CH₂Cl₂ at room temperature shows broad and ill-defined peaks, with bands at 390 nm, 519 nm and a weak shoulder at 722 nm with molar extinction coefficient (ϵ) value of 10^4 for intense band, which is typical of expected for a $4n\pi$ Hückel non-aromatic macrocycle (Figure 6.5). However, upon stepwise protonation with a dilute solution of TFA significant changes occur; (a)

absorption bands become sharper and intense with more than two fold increase in molar absorptivity. (b) Large red shift of the bands (306 nm and 219 nm) and (c) addition of excess of TFA leads to further red shift of band and appear at 696 nm and 738 nm with ϵ value of 10^5 . Similar electronic spectral analysis was reflected from mono-fused nonaphyrin **17b**. Here, the intense band is appeared at 527 nm and broad Q band at 728 nm suggests Hückel non-aromatic behavior. However upon protonation, the major intense band is appeared at 689 nm and 746 nm with similar ϵ value as observed in **17a** (Figure 6.6)

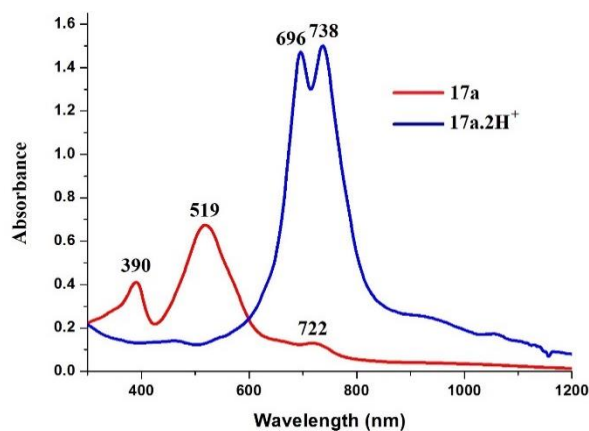


Figure 6.5: The electronic absorption spectrum of **17a** and **17a.2H⁺** in CH₂Cl₂.

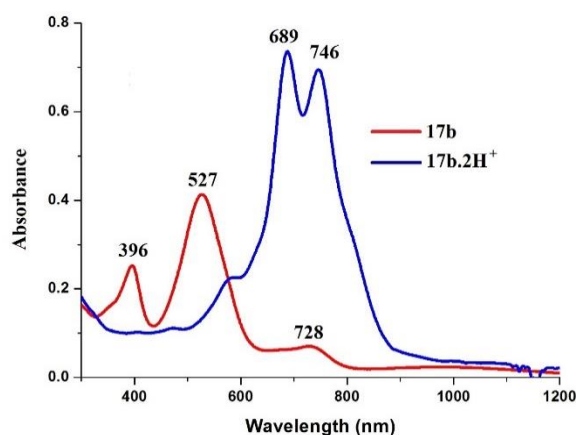


Figure 6.6: The electronic absorption spectrum of **17b** and **17b.2H⁺** in CH₂Cl₂.

In the case of non-fused nonaphyrin **18**, similar trend was observed as reflected in the absorption spectral analysis of mono-fused nonaphyrin **17**. A broad intense band is observed at 534 nm and Q band at 719 nm with ϵ value of 10^4 . Upon protonation, the intense band is red shifted and observed at 699 and 735 nm with one fold increase in molar extinction value (Figure 6.7). Overall, the electronic spectral analyses of **17** and **18** suggest a major structural change from Hückel non-aromatic to anti-aromatic character upon protonation as well as binding of TFA anion to the macrocycle through N-H...O hydrogen bonding interaction.

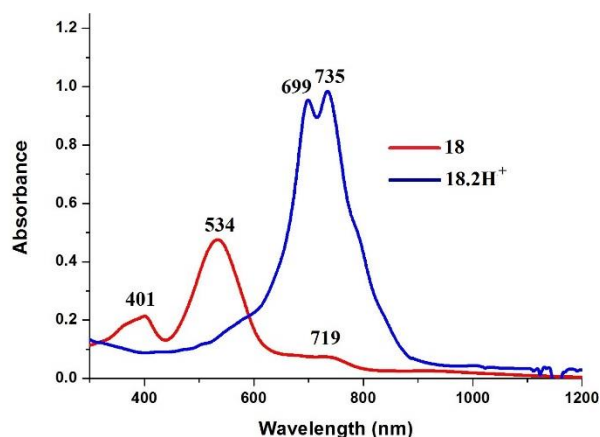


Figure 6.7: The electronic absorption spectrum of **18** and **18.2H⁺** in CH₂Cl₂.

6.3.2.3 NMR analysis

The solution structure of **17a** and **17b** were confirmed by ¹H and 2D NMR analysis by recording in CDCl₃ and CD₂Cl₂. The unsymmetrical nature of **17** was perceptible in ¹H NMR analysis where each and every proton exhibit their identical signals. For example, for **17a** (Figure 6.8), the β -CH of DTT moiety is observed at 10.13 (a) and 6.61 (a') ppm as two sharp singlets. Eight *meso* mesityl-CH protons appear between 6.76 and 7.03 ppm. The β -CH protons of thiophene and pyrrolic rings appear as 14 signals (b, b'), (c, c'), (d, d'), (e, e'), (f, f'), (g, g') and (h, h') between 5.67-7.27 ppm. These assignments were done by ¹H-¹H

COSY correlation spectroscopy (Figure 6.9). The NH protons of pyrrole rings appear as broad signals at 13.7 and 11.05 ppm. D₂O exchange experiment was done to confirm this assignment. The methyl groups of *meso*-mesityl rings appear as 12 signals between 1.79 and 2.95 ppm. Upon lowering temperature from 298 K to 203 K, only the two pyrrole NH signals shifts to 14.1 ppm and 10.5 ppm, while the other heterocyclic proton signals become broaden. Increasing temperature upto 323K had no significant spectral change. The chemical shift of NH protons suggests the presence of large paratropic ring current. Overall, the molecule **17a** adopts in figure-eight conformation.

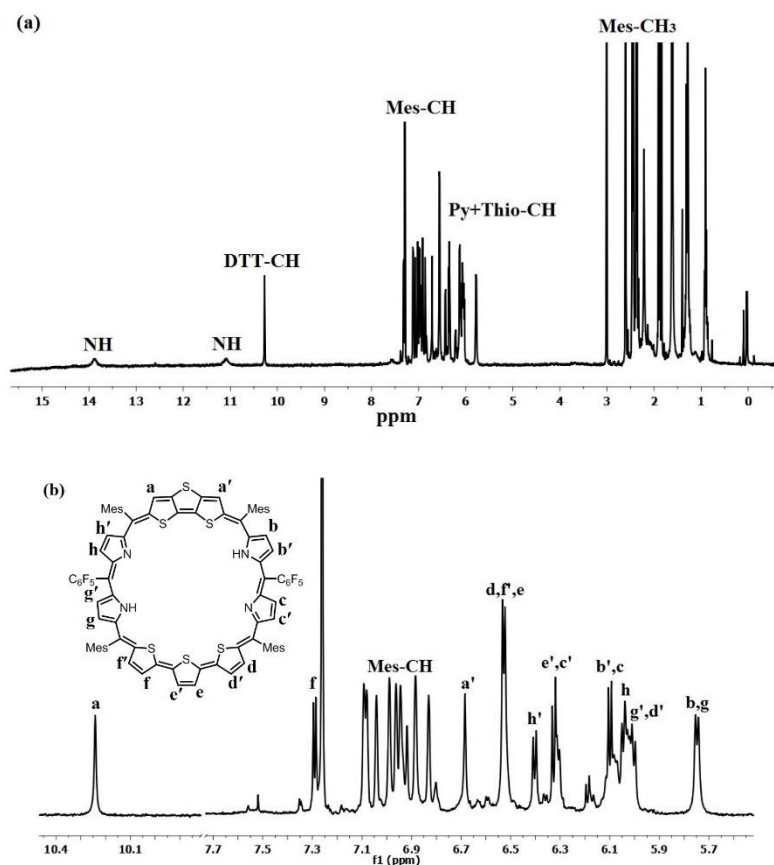


Figure 6.8: ¹H NMR spectrum of **17a** in CDCl₃ (a). The expansion in aromatic ring protons (b)

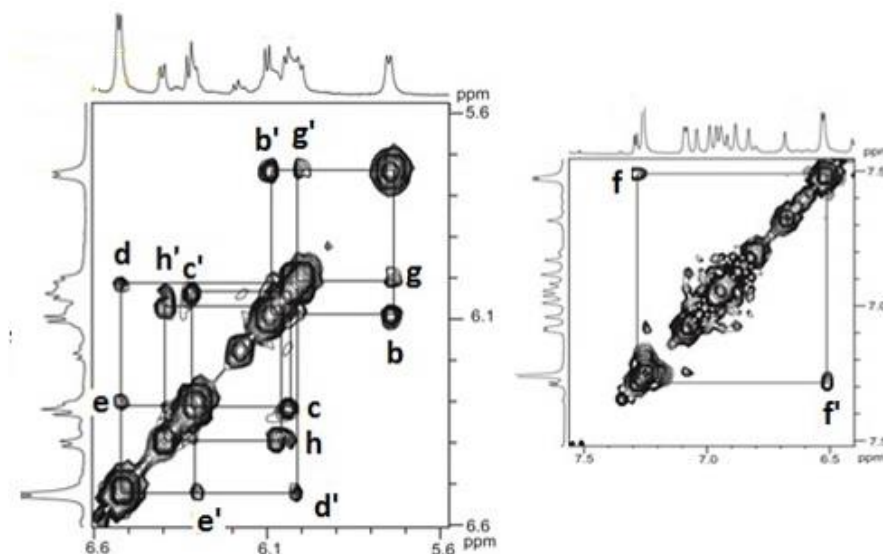


Figure 6.9: ^1H - ^1H COSY spectrum of **17a** heterocyclic ring protons in CDCl_3 .

Significant changes occur upon diprotonation of **17a** to generate dication **17a.2H⁺** (Figure 6.10). One of the pyrrole rings in each of dipyrane unit undergoes inversion of ring and the four β -CH protons of the inverted ring appear as two sets of doublets at 13.14 to 12.30 ppm (cc' , hh'). The DTT β -CH protons experience a large upfield shift relative to freebase form and appear at 4.95 and 4.86 ppm (aa'). The β -CH protons of normal pyrrole rings observed between 4.89 and 5.38 ppm (gg' , bb'). The three thiophene β -CH protons appear at 5.20-5.35 ppm (dd' , ee' , ff'). The *meso*-mesityl-CH protons do not experience much shift. The two NH protons inside the ring experience further downfield shift to 16.56 and 14.89 ppm, while other two NH protons of inverted rings appear at 3.26 and 2.71 ppm. All the proton signal assignments were confirmed by ^1H - ^1H COSY correlations spectroscopy (Figure 6.11). Overall, the spectral analyses reveal that the molecule **17a** is in figure-eight conformation and adopt open conformation upon protonation.

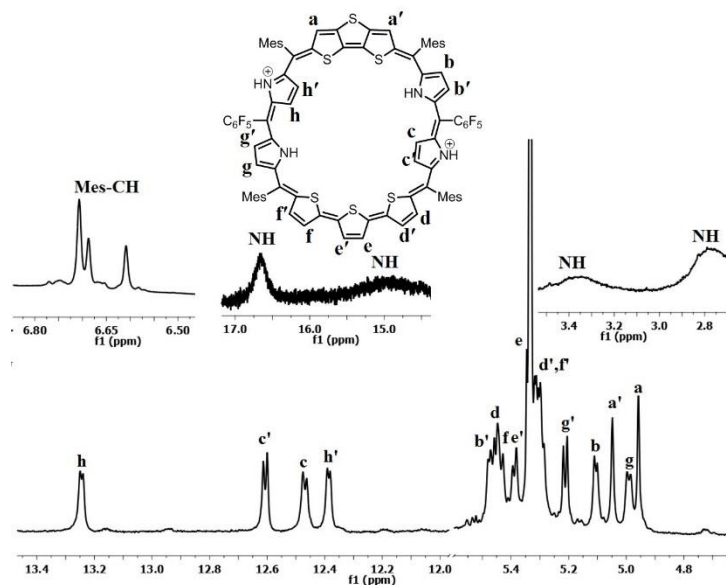


Figure 6.10: ^1H NMR spectrum of $17\text{a}.2\text{H}^+$ in CD_2Cl_2 . The inset shows the NH and *meso* mesityl-CH signals

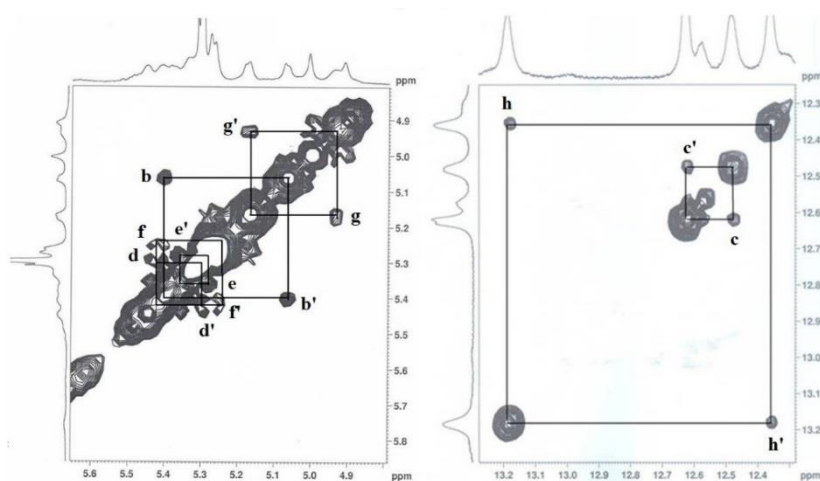


Figure 6.11: ^1H - ^1H COSY spectrum of $17\text{a}.2\text{H}^+$ heterocyclic rings in CD_2Cl_2 .

Similar trend was observed in *meso*-tolyl incorporated nonaphyrin **17b** and maintained the asymmetric nature as such. Therefore, each protons in the figure-eight conformation shows their individual peak positions (Figure 6.12). The DTT β -CH resonates at 9.57 (a) and 6.91

(a') ppm as two sharp singlets and the *meso*-tolyl-CH signals appear between 7.68-7.04 ppm. The β -CH protons of heterocyclic moiety (including pyrrolic and thiophene) appear as 14 doublets (bb', cc', dd', ee', ff', gg', hh') between 6.93-5.80 ppm. Two different pyrrolic NH signals are observed between 13.49 and 12.06 ppm. Assignment of all the aromatic proton signals were confirmed by ^1H - ^1H COSY spectroscopy and shown in Figure 6.13. The methyl signals of the *meso*-tolyl groups are observed between 2.47-2.36 ppm as four sharp singlets.

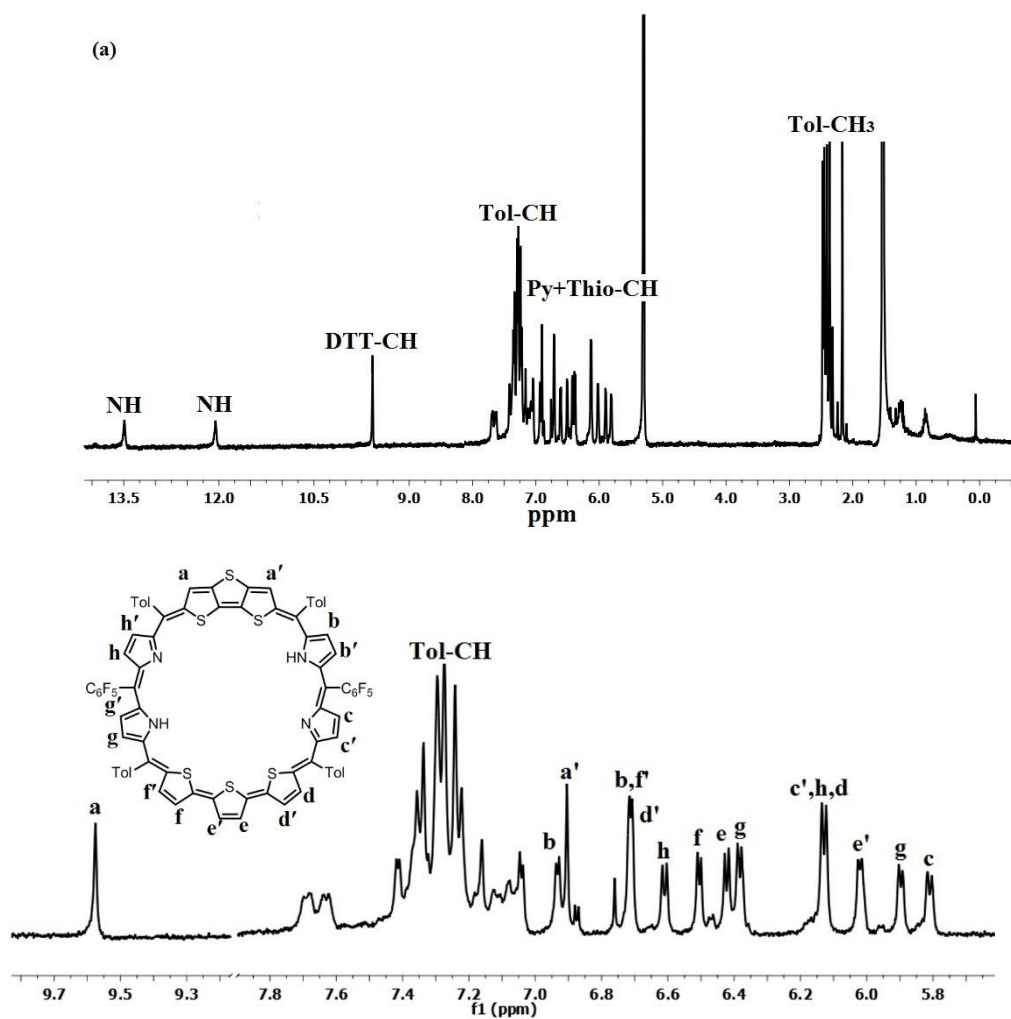


Figure 6.12: ^1H NMR spectrum of **17b** in CD_2Cl_2 (a). The expansion in aromatic ring protons (b)

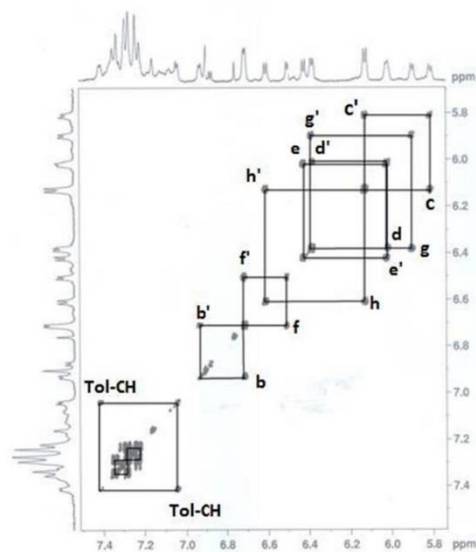


Figure 6.13: ^1H - ^1H COSY spectrum of **17b** aromatic ring protons in CD_2Cl_2 .

As observed in **17a.2H⁺**, similar trend was observed upon protonation of **17b** to obtain **17b.2H⁺** by using TFA. This leads to inversion of one the pyrrolic moieties of each dipyrromethane and shows strong paratropic ring current inside the molecule. Thus, two sets of inverted pyrrolic β -CH which are experiencing paratropic ring currents and appear at 11.17-10.56 ppm as four doublets (cc' and hh') (Figure 6.14). The *meso*-tolyl-CH signals resonate at 7.03-6.68 ppm. The pyrrolic and thiophene β -CH are at 6.28-5.45 ppm (aa', bb', dd', ee', ff' and gg'). Assignment of the heterocyclic signals were justified through ^1H - ^1H COSY correlation spectroscopy and shown in Figure 6.15. The normal pyrrolic NH with paratropic ring currents resonates at 13.88 and 13.37 ppm. The inverted pyrrolic NHs resonate at 3.59 and 3.28 ppm. The methyl signal of *meso*-tolyl units appear at 2.27-2.17 ppm respectively.

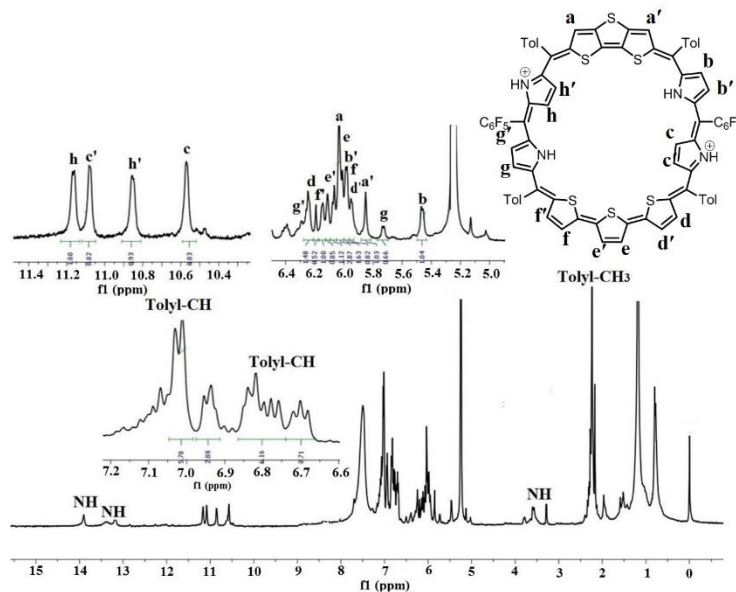


Figure 6.14: ^1H NMR spectrum of **17b.2H⁺** in CD_2Cl_2 . (Inset shows the expansion in aromatic protons)

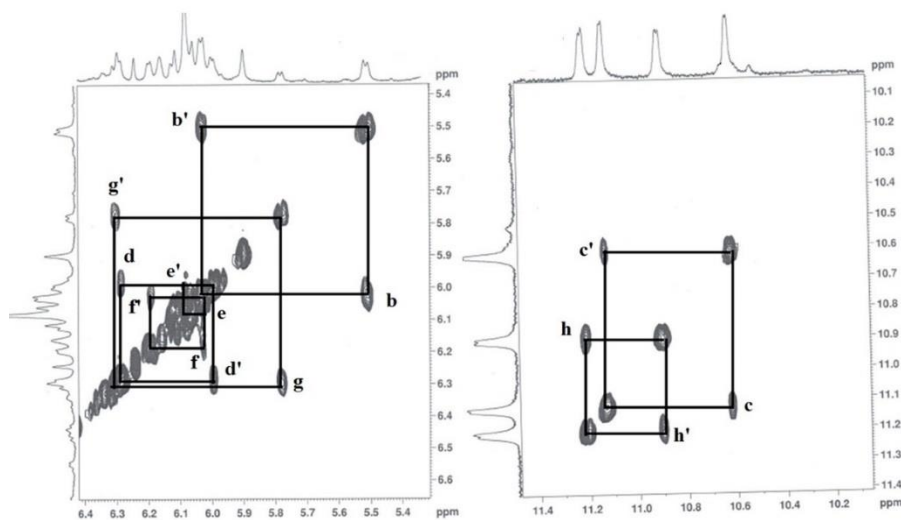


Figure 6.15: ^1H - ^1H COSY spectrum of **17b.2H⁺** aromatic ring protons in CD_2Cl_2 .

On the other hand, a notable ^1H NMR spectral change was observed on going from singly fused nonaphyrin **17** to non-fused nonaphyrin **18**. Interestingly, the freebase form of **18** exhibits simple NMR spectrum due to C_2 symmetry (Figure 6.16). The broad signal observed

around 13.9 ppm is assigned to two pyrrole NH protons. Disappearance of the NH signals by D₂O experiment signifies the assignment. Eight doublets (a, b, c, d, e, f, g and h) observed between 9.14 and 5.87 ppm and a singlet (i) at 7.18 ppm corresponds to heterocyclic β-CH protons. The *meso* mesityl-CH resonates at 6.96-7.02 ppm, while methyl groups in mesityl rings appears between 2.21 and 2.39 ppm, respectively.

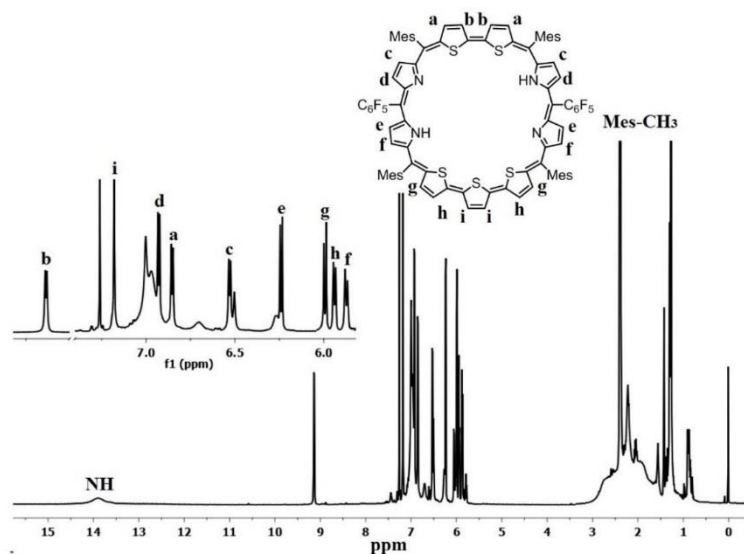


Figure 6.16: ¹H NMR spectrum of **18** in CDCl₃

Upon protonation of **18** also leads to significant changes in the ¹H NMR spectrum and shows in (Figure 6.17). Interestingly one of the thiophene rings of bithiophene moiety is inverted and the β-CH protons resonate between 11.12-11.34 ppm (a', b', c, d, e' and f'). As observed in **17**, out of four pyrrole rings two of them are inverted. The β-CH of inverted pyrrole resonates at 12.1 ppm to 12.8 ppm as four doublets and normal pyrrole rings appear at 5.12-5.45 ppm (a, b, c', d', e, f, g, h, i, i', g' and h'). The four thiophene β-CH protons display at 4.92-5.51 ppm. The inner NH proton observed at 16.2 and 14.45 ppm clearly indicating the paratropic ring current, whereas the inverted pyrrolic NH proton resonate at 2.52 and 2.6

6.3.2.4 Single Crystal X-ray analysis

The figure-eight conformation of **17b** in its freebase form was confirmed from single crystal X-ray structure of **17b** (Figure 6.19) (Table 6.1). The crystal was obtained by slow evaporation of CHCl₃ solution in CH₃CN and the compound crystallized in triclinic crystal lattice with a *P2(1)2* space group. The crystal structure contains terthiophene, DTT rings, two dipyrromethene units and are connected by six *meso* carbons which are occupied by four tolyl and two pentafluorophenyl rings and maintained figure-eight conformation (Figure 6.19a). As predicted from the NMR analysis, the dipyrromethene unit contains both amine and imine pyrrole nitrogens with intramolecular hydrogen bonding interactions with the distances and angles of N1-H1...N2 and N3-H3...N4 are 2.24, 2.29 Å and 121.24°, 122.38° respectively. In addition, the middle thiophene (S5) ring which is part of terthiophene unit is inverted and both the β-CH protons are inside the macrocyclic framework. The DTT ring as well as the terthiophene units are nearly parallel to each other with the dihedral angle of 17.66° and exist in bowl like conformation (Figure 6.19b). As compared to DTT unit (5.28°), the pyrrole rings (18.51° to 32.25°) and terthiophene ring (20°) are maximum deviated from the mean macrocyclic plane containing C7, C12, C17, C30, C35 and C40 atoms, while the *meso*-aryl units are tilted between 45.37° and 83.46°, respectively. The crystal analysis of **17b** generates two types of self-assembled dimers by intermolecular hydrogen bonding interactions between; (i) *meso*-tolyl unit (C45-H45) and pyrrolic π-cloud and (ii) the pyrrolic β-CH (C9-H9) and fluorine (F6) with the distances and angles of C45-H45...Py(π) and C9-H9...F6 are 2.84, 2.68 Å and 129.17°, 164.23° respectively (Figure 6.20).

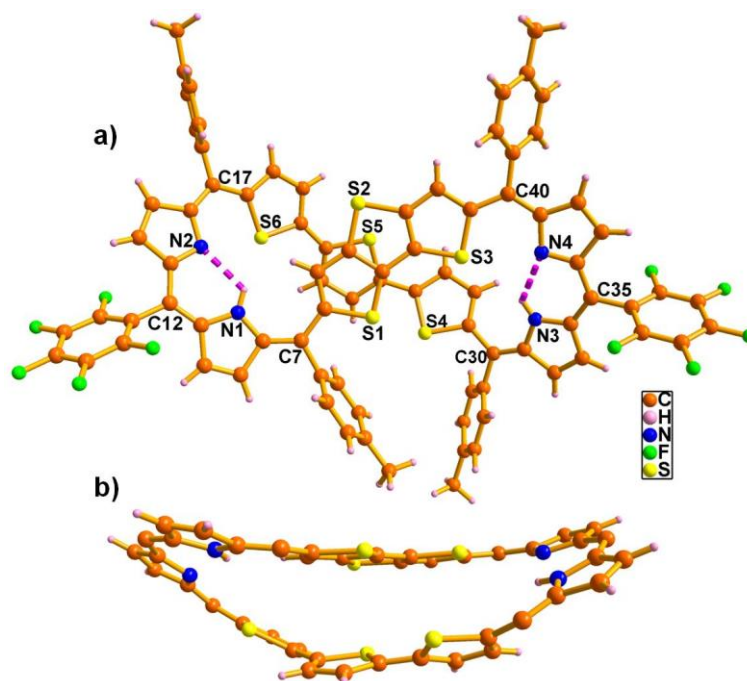


Figure 6.19: Single crystal X-ray structure of **17b**. a) Top view and b) side view. The *meso*-aryl groups are omitted for clarity in the side view.

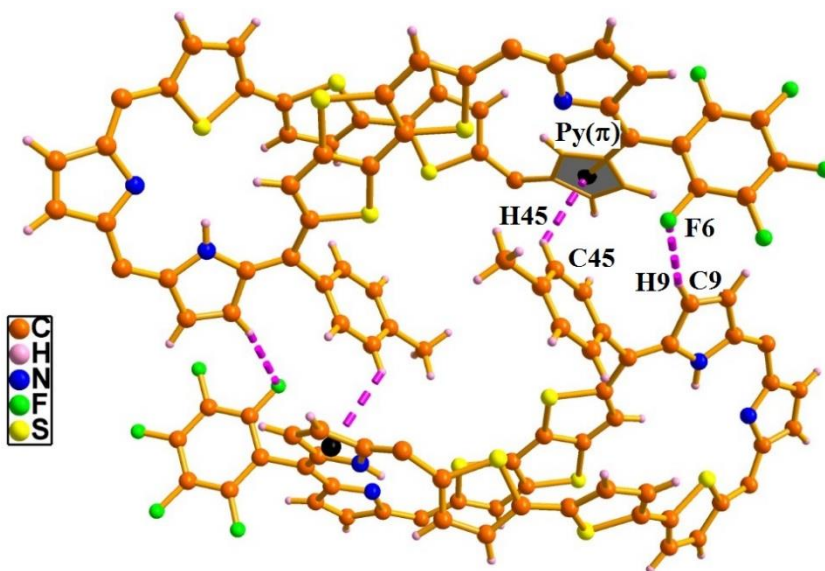


Figure 6.20: Self-assembled dimer in **17b** with intermolecular hydrogen bonding interactions.

Table 6.1: Crystallographic data for **17b**

	17b
<i>T</i> , K	100 K
Formula	C82 H46 F10 N4 S6
Formula weight	1469.59
Color and Habit	Dark brown
Crystal system	Monoclinic
Space group	P 21/n
<i>a</i> , Å	18.415(4)
<i>b</i> , Å	19.471(4)
<i>c</i> , Å	21.665(4)
α , deg	90
β , deg	98.344(13)
γ , deg	90
<i>V</i> , Å ³	7686(3)
Radiation (λ , Å)	Mo K α (0.71073)
<i>Z</i>	4
d_{calcd} , g•cm ⁻³	1.270
μ , mm ⁻¹	0.248
<i>F</i> (000)	3008
No. of unique reflns	14275
No. of params. refined	877
GOF on <i>F</i> ²	1.042
<i>R</i> 1 ^a [<i>I</i> > 2 σ (<i>I</i>)]	0.0809
<i>R</i> 1 ^a (all data)	0.1462
<i>wR</i> 2 ^b (all data)	0.2485

6.3.2.5 Nucleus Independent Chemical Shift (NICS)

Nucleus Independent Chemical Shift is the best indication to assess aromaticity of the molecules. The NICS(0) values are calculated for **17b** at various geometrical position of pyrrolic rings containing amino nitrogen, which have large negative values of -3.7 and -4.5 ppm as compared to imino nitrogen at -1.8 and -2.0 ppm. The two terminal thiophene units of DTT moiety have high negative NICS(0) values at -7.3 and -9.9 ppm as compared to core thiophene unit (-6.8 ppm). In case of terthiophene moiety, the NICS(0) values of two terminal thiophene atoms are -9.7 and -7.1 ppm, whereas the value of inverted middle thiophene is -8.8 ppm. Overall the NICS (0) value at the center of macrocycle is 0.01 ppm, which reveals typical non-aromatic behavior of the macrocycle (Figure 6.21a).

However upon protonation, two of the four pyrrolic nitrogens are inverted and these two pyrrolic units show NICS(0) values at -3.5 and -2.9 ppm, whereas normal pyrrolic units appear at 1.0 and 1.1 ppm. The NICS(0) values of two terminal thiophene atoms of DTT moieties are 1.2 and 1.5 ppm whereas inverted one is at -10.5 ppm. The respective value of two terminal thiophene of terthiophene moiety are 0.4 and 1.2 ppm, whereas middle inverted thiophene is -10.9 ppm. Overall the NICS(0) value at the center of the macrocycle is 9.9 ppm. This reveals the typical anti-aromatic behavior of the macrocycle upon protonation (Figure 6.21b).

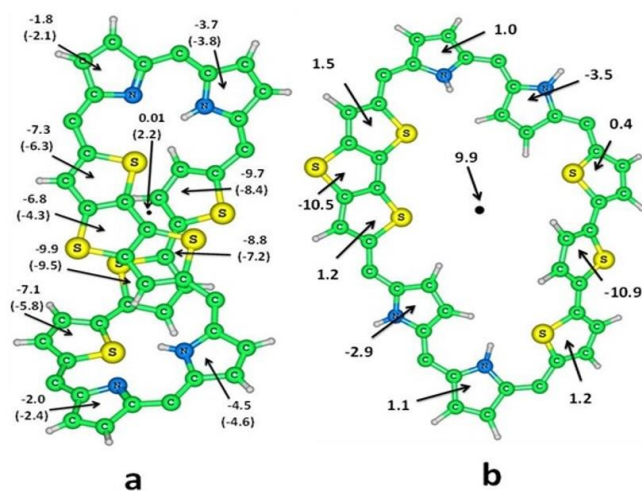


Figure 6.21: NICS (0) value of **17b**. a) Freebase form and b) Diprotonated state.

Similar trend was observed in non-fused nonaphyrin **18**. In this case, NICS(0) value at center of the freebase macrocycle is at 1.0 ppm, which indicates moderate Hückel anti-aromatic behavior (Figure 6.22a). However upon protonation, both the imine nitrogens of the molecule and one thiophene atom of bithiophene units are inverted. Thus overall NICS(0) values of the center of macrocycle is at 6.8 ppm and confirms anti-aromatic behavior upon protonation (Figure 6.22b).

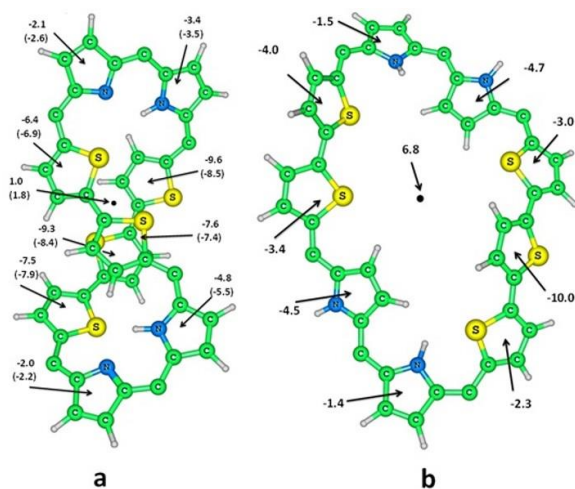
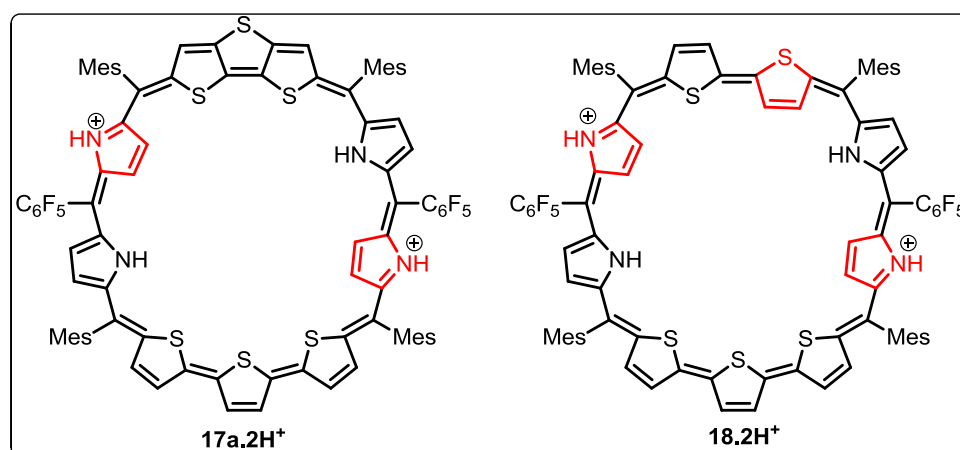


Figure 6.22: NICS (0) value of **18**. a) Freebase form and b) Diprotonated state.

Overall, the spectral analyses and theoretical studies reveals; (a) a significant upfield shift of DTT protons, (b) a large red shift of absorption bands and one fold increase in the ϵ values and (c) positive NICS(0) value upon protonation, thus confirms a major structural change. A similar observation was reported very recently for doubly fused octaphyrin^{9c} and 36π octaphyrin by Osuka et al¹³ upon diprotonation. Based on the ¹H NMR chemical shift changes, the changes in the electronic spectra and our earlier observation, we propose a change from figure-eight conformation in freebase form to an open conformation in diprotonated state for both **17a** and **18** (Scheme 6.8). This observation clearly suggests the fusion of the rings in nonaphyrin is not necessarily required for change over from figure-eight to open conformation.



Scheme 6.8: Open conformation of **17a.2H⁺** and **18.2H⁺**. Inverted rings are shown in colored.

6.4 Conclusions

In conclusion, we have synthesized two new core-modified nonaphyrins by an efficient methodology which exhibit a figure-eight conformation in its freebase form and are non-aromatic. However, protonation of pyrrole nitrogens induces a structural change where figure-eight conformation changes to an open conformation with inversion of the pyrrole rings in **17** and pyrrole rings and one of thiophene rings of bithiophene units in **18**. Both the dications, **17.2H⁺** and **18.2H⁺** exhibit $4n\pi$ Hückel anti-aromatic character in spite of open conformation.

6.5 Experimental Procedure

6.5.1 Synthesis of **17**

A mixture of fused DTT tetrapyrane (**14**) (0.3 g, 0.51 mmol), terthiophene pentapyrane (**15a**) (0.327 g, 0.51 mmol) and pentafluorobenzaldehyde (0.1 g, 0.51 mmol) were dissolved in dry CH_2Cl_2 (200 ml) and stirred under nitrogen atmosphere for 10 min. *p*-Toluenesulfonic acid (*p*-TSA) (0.032 g, 0.17 mmol) was added and the resulting solution was stirred for 90 min. The progress of the reaction was monitored by TLC. DDQ (0.432 g, 2.5 mmol) was added and the resulting solution was stirred for further 90 min in open air. The solvent was evaporated in rotary evaporator. The residue was purified by column chromatography, basic alumina column followed by silica gel (100-200 mesh) column chromatography. Three consecutive pink color bands were separated. First band was identified as octaphyrin (4%), second pink band eluted with $\text{CH}_2\text{Cl}_2/n$ -hexane (35:65, v/v) was characterized as decaphyrin (9%) and the last pink fraction eluted with $\text{CH}_2\text{Cl}_2/n$ -hexane (45:55, v/v) was the desired

nonaphyrin (**17**). After repeated purification by column chromatography and recrystallization from CH₂Cl₂/CH₃OH, **17** was obtained as greenish crystal in 7% yield.

Compound 17a: ¹H NMR (400 MHz, CD₂Cl₂) δ (in ppm) = 13.7 (brs, 1H, NH), 11.7 (brs, 1H, NH), 10.22 (s, 2H), 7.27 (d, *J* = 3.7 Hz, 1H), 7.07 (s, 1H), 7.06 (1H), 7.02 (1H), 6.97 (1H), 6.94 (1H), 6.92 (1H), 6.86 (1H), 6.81 (1H), 6.72 (s, 1H), 6.60 (d, *J* = 3.7 Hz, 1H), 6.56 (d, *J* = 3.8 Hz, 1H), 6.55 (d, *J* = 3.8 Hz, 1H), 6.45 (d, *J* = 4.1 Hz, 1H), 6.38 (d, *J* = 4.3 Hz, 1H), 6.35 (d, *J* = 3.8 Hz, 1H), 6.17 (*J* = 3.8 Hz, 1H), 6.15 (d, *J* = 3.7 Hz, 1H), 6.14 (d, *J* = 4.3 Hz, 1H), 6.12 (d, *J* = 4.3 Hz, 1H), 6.1 (d, *J* = 4.1 Hz, 1H) 6.05 (d, *J* = 4.5 Hz, 1H), 5.58 (d, *J* = 4.5 Hz, 1H), 5.57 (d, *J* = 4.5 Hz, 1H), 2.95 (s, 3H, Mes-CH₃), 2.56 (s, 3H, Mes-CH₃), 2.55 (s, 3H, Mes-CH₃), 2.41 (s, 3H, Mes-CH₃), 2.4 (s, 3H, Mes-CH₃), 2.39 (s, 3H, Mes-CH₃), 2.33 (s, 3H, Mes-CH₃), 2.31 (s, 3H, Mes-CH₃), 1.85 (s, 6H, Mes-CH₃), 1.82 (s, 3H, Mes-CH₃), 1.79 (s, 3H, Mes-CH₃). **17a·2H⁺**: ¹H NMR (400 MHz, CD₂Cl₂) δ (in ppm) = 16.56 (brs, 1H, NH), 14.89 (brs, 1H, NH), 13.14 (d, *J* = 4.7 Hz, 1H), 12.55 (d, *J* = 4.9 Hz, 1H), 12.41 (d, *J* = 4.9 Hz, 1H), 12.30 (d, *J* = 4.7 Hz, 1H), 6.61 (s, 4H), 6.59 (s, 2H), 6.51 (s, 2H), 5.38 (d, 1H), 5.36 (d, 1H), 5.34 (d, 1H), 5.29 (d, 1H), 5.21 (d, 1H), 5.20 (d, 1H), 5.19 (d, 1H), 5.11 (d, 1H), 5.01 (d, 1H), 4.95 (s, 1H), 4.89 (d, 1H), 4.86 (s, 1H), 3.26 (brs, 1H, NH), 2.03 (s, 6H, Mes-CH₃), 1.97 (s, 6H, Mes-CH₃), 1.96 (s, 6H, Mes-CH₃), 1.93 (s, 6H, Mes-CH₃), 1.92 (s, 6H, Mes-CH₃), 1.89 (s, 6H, Mes-CH₃). **17a:** UV/Vis (CH₂Cl₂): λ_{max} in nm (ε in dm³mol⁻¹cm⁻¹) = 390 (6.29×10³), 518 (1.03×10⁴), 717 (1.91×10³); **17a·2H⁺** (TFA/CH₂Cl₂): λ_{max} in nm (ε in dm³mol⁻¹cm⁻¹) = 696 (1.963×10⁵), 738 (1.9995×10⁵).

Compound 17b: ¹H NMR (400 MHz, CD₂Cl₂) δ (in ppm) = 13.42 (brs, 1H, NH), 11.98 (brs, 1H, NH), 9.51 (s, 1H), 7.59 (d, 1H), 7.35 (d, *J* = 3.8 Hz, 1H), 7.28 (d, 3H), 7.22 (d, 4H), 7.17 (d, 3H), 7.1 (d, 1H), 6.98 (d, *J* = 3.8 Hz, 1H), 6.87 (d, *J* = 3.7 Hz, 1H), 6.84 (s, 1H), 6.81 (d,

1H), 6.7 (s, 1H), 6.65 (d, $J = 3.7$ Hz, 2H), 6.54 (d, $J = 5.0$ Hz, 1H), 6.44 (d, $J = 3.7$ Hz, 1H), 6.36 (d, $J = 4.5$ Hz, 1H), 6.31 (d, $J = 4.5$ Hz, 1H), 6.06 (d, $J = 5.0$ Hz, 2H), 5.95 (d, $J = 4.5$ Hz, 1H), 5.83 (d, $J = 4.5$ Hz, 1H), 5.75 (d, $J = 5.0$ Hz, 1H), 2.41 (s, 3H, Tol-CH₃), 2.39 (s, 3H, Tol-CH₃), 2.35 (s, 3H, Tol-CH₃), 2.30 (s, 3H, Tol-CH₃); **17b**·**2H**⁺ : ¹H NMR (400 MHz, CD₂Cl₂) δ (in ppm) = 13.90 (brs, 1H, NH), 13.37 (brs, 1H, NH), 11.16 (d, $J = 4.5$ Hz, 1H), 11.07 (d, $J = 4.3$ Hz, 1H), 10.86 (d, $J = 4.5$ Hz, 1H), 10.56 (d, $J = 4.3$ Hz, 1H), 7.06-6.68 (m, 16H, tolyl-CH), 6.24 (d, 1H), 6.19 (s, 1H), 6.15 (d, 1H), 6.11 (d, 1H), 6.07 (d, 1H), 6.03 (s, 1H), 6.02 (d, 2H), 5.97 (d, 2H), 5.95 (d, 1H), 5.85 (s, 1H), 5.73 (d, 1H), 5.46 (d, 1H), 3.57 (brs, 1H, NH), 3.28 (brs, 1H, NH), 2.24-2.17 (s, 12H, tolyl-CH₃). **17b**: UV/Vis (CH₂Cl₂): λ_{\max} in nm (ϵ in dm³mol⁻¹cm⁻¹) = 396 (5.70×10^4), 527 (9.33×10^4), 728 (1.599×10^4); **17b**·**2H**⁺ (TFA/CH₂Cl₂): λ_{\max} in nm (ϵ in dm³mol⁻¹cm⁻¹) = 689 (1.66×10^5), 746 (1.57×10^5);

6.5.2 Synthesis of 18

A mixture of terthiophene pentapyrrane (**15a**), bithiophene tetrapyrane (**16**) (0.285 g, 0.51 mmol), and pentafluorobenzaldehyde (0.1 g, 0.51 mmol) were dissolved in dry CH₂Cl₂ (200 ml) and stirred under nitrogen atmosphere for 10 min. *p*-Toluenesulfonic acid (*p*-TSA) (0.032 g, 0.17 mmol) was added and the resulting solution was stirred for 90 min. The progress of the reaction was monitored by TLC. DDQ (0.432 g, 2.5 mmol) was added and the resulting solution was stirred for further 90 min in open air. The solvent was evaporated in rotary evaporator. The residue was purified by column chromatography, initially by basic alumina column followed by silica gel (100-200 mesh) column chromatography. Three consecutive pink color bands were separated. First band contains trace amount of octaphyrin (1%). The second pink band was eluted with CH₂Cl₂/*n*-hexane (37:63, v/v) and characterized as decaphyrin (9%). The last pink fraction was eluted with CH₂Cl₂/*n*-hexane (48:52, v/v)

and identified as nonaphyrin (**18**). After repeated purification by column chromatography and recrystallization from CH₂Cl₂/CH₃OH, **18** was obtained as greenish crystal in 6% yield.

Compound 18: ¹H NMR (400 MHz, CDCl₃) δ (in ppm) = 13.9 (brs, 2H, NH), 9.14 (d, J = 4.1 Hz, 2H), 7.18 (s, 2H), 6.93 (d, J = 4.1 Hz, 2H), 6.85 (d, J = 4.1 Hz, 2H), 6.53 (d, J = 4.1 Hz, 2H), 6.24 (d, J = 4.8 Hz, 2H), 5.99 (d, J = 5.3 Hz, 2H), 5.94 (d, J = 4.8 Hz, 2H), 5.87 (d, J = 5.3 Hz, 2H), 2.39 (s, 6H), 2.38 (s, 12H), 2.37 (s, 12H), 2.21 (s, 6H).

18·2H⁺: ¹H NMR (400 MHz, CDCl₃) δ (in ppm) = 16.20 (brs, 1H, NH), 14.45 (brs, 1H, NH) 12.84 (d, J = 4.3 Hz, 1H), 12.62 (d, J = 4.3 Hz, 1H), 12.36 (d, J = 3.8 Hz, 1H), 12.15 (d, J = 3.8 Hz, 1H), 11.34 (d, J = 4.1 Hz, 1H), 11.12 (d, J = 4.1 Hz, 1H), 6.65-6.77 (s, 8H), 5.51 (d, 1H), 5.46 (d, 1H), 5.41 (d, 1H), 5.36 (d, 1H), 5.33 (d, 1H), 5.27 (d, 1H), 5.25 (d, 1H), 5.16 (d, 1H), 5.14 (d, 1H), 5.02 (d, 1H), 5.00 (d, 1H), 4.92 (d, 1H), 2.60 (brs, 1H, NH), 2.52 (brs, 1H, NH), 1.92-2.41 (s, 36H). **18**: UV/Vis (CH₂Cl₂): λ_{\max} in nm (ϵ in dm³mol⁻¹cm⁻¹) = 401 (3.905×10⁴), 534 (8.725×10⁴), 730 (1.366×10⁴); **18·2H⁺** (TFA/CH₂Cl₂): λ_{\max} in nm (ϵ in dm³mol⁻¹cm⁻¹) = 699 (1.75×10⁵), 735 (1.807 ×10⁵).

6.6 References:

1. Saito, S.; Osuka, A. *Angew. Chem. Int. Ed.* **2011**, *50*, 4342-4373.
2. Sessler, J. L.; Seidel, D. *Angew. Chem. Int. Ed.* **2003**, *42*, 5134-5175.
3. Misra, R.; Chandrashekar, T. K. *Acc. Chem. Res.* **2008**, *41*, 265-279.
4. Rambo, B. M.; Sessler, J. L. *Chem. Eur. J.* **2011**, *17*, 4946-4959.
5. Pareek, Y.; Ravikanth, M. *Eur. J. Org. Chem.* **2011**, 5390-5399.
6. Sessler, J. L.; Camiolo, S.; Gale, P. A. *Coord. Chem. Rev.* **2003**, *240*, 17-55.
7. Sessler, J. L.; Furuta, H.; Král, V. *Supramol. Chem.* **1993**, *1*, 209-220.

-
8. Kido, H.; Shin, J.-Y.; Shinokubo, H. *Angew. Chem. Int. Ed.* **2013**, *52*, 13727-13730.
 9. Blusch, L. K.; Mitevski, O.; Martin-Diaconescu, V.; Pröpper, K.; DeBeer, S.; Dechert, S.; Meyer, F. *Inorg. Chem.* **2014**, *53*, 7876-7885.
 10. Ho, I. T.; Zhang, Z.; Ishida, M.; Lynch, V. M.; Cha, W.-Y.; Sung, Y. M.; Kim, D.; Sessler, J. L. *J. Am. Chem. Soc.* **2014**, *136*, 4281-4286.
 11. Ishida, S.-i.; Osuka, A. *Chem. Asian. J.* **2015**, *10*, 2200-2206.
 12. Mori, H.; Tanaka, T.; Lee, S.; Lim, J. M.; Kim D.; Osuka, A. *J. Am. Chem. Soc.* **2015**, *137*, 2097-2106.
 13. Chaudhary, A.; Srinivasan, A.; Chandrashekar, T. K. *The Handbook of Porphyrin Science*, Kadish, K. M.; Smith, K. M.; Guillard, R. World scientific Ltd, **2014**, *32*, 271-366.
 14. Shin, J.-Y.; Kim, K. S.; Yoon, M.-C.; Lim, J. M.; Yoon, Z. S.; Osuka, A.; Kim, D. *Chem. Soc. Rev.* **2010**, *39*, 2751-2767.
 15. Lim, J. M.; Yoon, Z. S.; Shin, J.-Y.; Kim, K. S.; Yoon, M.-C.; Kim, D. *Chem. Commun.* **2009**, 261-273.
 16. Senge, M. O.; Fazekas, M.; Notaras, E. G. A.; Blau, W. J.; Zawadzka, M.; Locos, O. B.; Ni Mhuircheartaigh, E. M. *Adv. Mater.* **2007**, *19*, 2737-2774.
 17. Ghosh, A.; Chaudhary, A.; Srinivasan, A.; Suresh, C. H.; Chandrashekar, T. K. *Chem. Eur. J.* **2016**, *22*, 3942-3946.
 18. Soya, T.; Kim, W.; Kim, D.; Osuka, A. *Chem. Eur. J.* **2015**, *21*, 8341-8346.
 19. Möbius, K.; Plato, M.; Klihm, G.; Laurich, C.; Savitsky, A.; Lubitz, W.; Szyszko, B.; Stępień, M.; Latos-Grażyński, L. *Phys. Chem. Chem. Phys.* **2015**, *17*, 6644-6652.

-
20. Naoda, K.; Mori, H.; Oh, J.; Park, K. H.; Kim, D.; Osuka, A. *J. Org. Chem.* **2015**, *80*, 11726-11733.
 21. Marcos, E.; Anglada, J. M.; Torrent-Sucarrat, M. *J. Org. Chem.* **2014**, *79*, 5036-5046.
 22. Saito, S.; Shin, J.-Y.; Lim, J. M.; Kim, K. S.; Kim, D.; Osuka, A. *Angew. Chem. Int. Ed.* **2008**, *47*, 9657-9660.
 23. Stępień, M.; Latos-Grażyński, L.; Sprutta, N.; Chwalisz, P.; Szterenber, L. *Angew. Chem. Int. Ed.* **2007**, *46*, 7869-7873.
 24. Ajami, D.; Oeckler, O.; Simon, A.; Herges, R. *Nature* **2003**, *426*, 819-821.
 25. Shin, J.-Y.; Furuta, H.; Yoza, K.; Igarashi, S.; Osuka, A. *J. Am. Chem. Soc.* **2001**, *123*, 7190-7191.
 26. Taniguchi, R.; Shimizu, S.; Suzuki, M.; Shin, J.-Y.; Furuta, H.; Osuka, A. *Tetrahedron Lett.* **2003**, *44*, 2505-2507.
 27. Kamimura, Y.; Shimizu, S.; Osuka, A. *Chem. Eur. J.* **2007**, *13*, 1620-1628.
 28. Shimizu, S.; Taniguchi, R.; Osuka, A. *Angew. Chem. Int. Ed.* **2005**, *44*, 2225-2229.
 29. Bui, T.-T.; Iordache, A.; Chen, Z.; Roznyatovskiy, V. V.; Saint-Aman, E.; Lim, J. M.; Lee, B. S.; Ghosh, S.; Moutet, J.-C.; Sessler, J. L.; Kim, D.; Bucher, C. *Chem. Eur. J.* **2012**, *18*, 5853-5859.
 30. Setsune, J.-i.; Toda, M.; Yoshida, T.; Imamura, K.; Watanabe, K. *Chem. Eur. J.* **2015**, *21*, 12715-12727.
 31. Setsune, J.-i.; Toda, M.; Yoshida, T. *Chem. Commun.*, **2008**, 1425-1427.
 32. Zeng, W.; Lee, S.; Son, M.; Ishida, M.; Furukawa, K.; Hu, P.; Sun, Z.; Kim, D.; Wu, J. *Chem. Sci.* **2015**, *6*, 2427-2433.
-

33. Tanaka, T.; Osuka, A. *Chem. Soc. Rev.* **2015**, *44*, 943-969.
34. Ota, K.; Tanaka, T.; Osuka, A. *Org. Lett.* **2014**, *16*, 2974-2977.
35. Chandrashekar, T. K.; Prabhuraja, V.; Gokulnath, S.; Sabarinathan, R.; Srinivasan, A. *Chem. Commun.* **2010**, *46*, 5915-5917.
36. Karthik, G.; Lim, J. M.; Srinivasan, A.; Suresh, C. H.; Kim, D.; Chandrashekar, T. K. *Chem. Eur. J.* **2013**, *19*, 17011-17020.
37. Karthik, G.; Srinivasan, A.; Chandrashekar, T. K. *Org. Lett.* **2014**, *16*, 3472-3475.
38. Rath, H.; Prabhuraja, V.; Chandrashekar, T. K.; Nag, A.; Goswami, D.; Joshi, B. S. *Org. Lett.* **2006**, *8*, 2325-2328.
39. Rath, H.; Sankar, J.; Prabhuraja, V.; Chandrashekar, T. K.; Joshi, B. S.; Roy, R. *Chem. Commun.* **2005**, 3343-3345.

Summary

